5-2016

# Application of Computational Fluid Dynamics in Flow Measurement and Meter Design

Zachary B. Sharp
*Utah State University*

# APPLICATIONS OF COMPUTATIONAL FLUID DYNAMICS IN FLOW MEASURMENT AND METER DESIGN

by

Zachary B. Sharp

A dissertation proposal submitted in partial fulfillment
of the requirements for the degree

of

DOCTOR OF PHILOSOPHY

in

Civil and Environmental Engineering

Approved:

| | |
|---|---|
| Dr. Michael C. Johnson<br>Major Professor | Dr. Mac McKee<br>Committee Member |
| Dr. Blake P. Tullis<br>Committee Member | Dr. Robert E. Spall<br>Committee Member |
| Steven L. Barfuss<br>Committee Member | Dr. Mark R. McLellan<br>Vice President for Research and<br>Dean of the School of Graduate Studies |

UTAH STATE UNIVERSITY
Logan, Utah

2016

# ABSTRACT

Application of Computational Fluid Dynamics in Flow Measurement and Meter Design

by

Zachary B. Sharp, Doctor of Philosophy

Utah State University, 2016

Major Professor: Dr. Michael C. Johnson
Department: Civil and Environmental Engineering

Computational Fluid Dynamics is a very effective tool for understanding fluid flow and predicting how flow will respond to different boundary conditions. With this knowledge, the focus of this research is applying computational fluid dynamics to problems dealing with flow measurement in closed conduits using differential producing flow meters like Venturis. After discussion with many meter manufactures and a thorough literature review, specific areas of research were determined which will contribute to better understanding of differential producers and will add to the limited literature available on such meters. This research will present the findings of computational fluid dynamics coupled with laboratory data in the following areas:

1. Determine the effects of sudden pipe wall offsets on Venturi flow meters. This research includes both the effects of the pipe wall offset on the meter discharge coefficient as well as determining the minimum distance between the offset and the Venturi so that there is no longer any effect on meter performance. It also

shows how well computational fluid dynamics can predict Venturi discharge coefficients via comparison to laboratory data.

2. Investigate the design of pressure recovery cones on different Venturi flow meter designs including determining the optimal angle of recover cone required to minimize permanent pressure loss.
3. Investigate truncated recovery cones such that a meter can be manufactured using a shorter length. This research also includes determining the best way to truncate the meter to minimize head loss while not changing the flow metering capability of the flow meter.

This research will be CFD based with laboratory data used to calibrate and validate the CFD results.

(199 pages)

# PUBLIC ABSTRACT

Application of Computational Fluid Dynamics in Flow Measurement and Meter Design

Zachary B. Sharp

Flow measurement has been an important part of society for hundreds of years. For this reason there are many methods to measure flow rates both in open channel scenarios like irrigation canals and also in closed conduits like pipelines that supply water for human use. This research focused on Venturi flow meters which have been used to measure flow since the 1890's. The object of this research was to use computational fluid dynamics and laboratory data to provide industry with applicable answers to some under researched areas in flow measurement. The areas chosen for this research include areas requested by meter manufacturers. This fact helps the readers to understand how valuable this information will be to the flow measurement industry.

The results include guidelines for manufacturers and meter users to utilize regarding how close a Venturi can be installed to a change in pipe diameter so its flow metering capabilities are not compromised. This information will help with proper installation of flow meters in the field and the laboratory for flow meter calibrations. The research also provides details on how to design the recovery cone for various Venturi designs to minimize the energy loss from fluid passing through the meter. The results are valuable to many including meter manufactures, industry where the meters get used, and academia alike as the results are very applicable and were previously not available.

CONTENTS

# LIST OF TABLES

# LIST OF FIGURES

# NOTATIONS

$A$ = Cross sectional area of the pipe ($in^2$)

$D$ = Inlet pipe diameter (in)

$d$ = Venturi throat diameter (in)

$E$ = Total head at specified location in the pipe (psi)

$g$ = Acceleration due to gravity ($ft/s^2$)

$P$ = Pressure at some location in the pipe (psi)

$\Delta P$ = Differential pressure between the high taps and low taps (psi)

$Q$ = Total flow rate (lb/s)

$V$ = Average pipe velocity (ft/s)

$C_d$ = Venturi Discharge Coefficient

$\rho$ = density of water ($lb/ft^3$)

# CHAPTER 1

## INTRODUCTION

Computational Fluid Dynamics (CFD) is a numerical approach to analyze a system involving fluid flow. It is a method that has been used since the 1960's by the aerospace industry but has been more widely used for the last 30 years. CFD can be used to analyze aerodynamics, hydrodynamics, chemical processing, and turbo machinery to name just a few. The strengths of CFD are vast with specific strengths beneficial to this research including flexibility in problem solving, nearly unlimited data from simulations and the ease of changing or adjusting certain elements of a simulation. Often times it is difficult to set up a physical experiment where there is unlimited adjustability of one or more parameters. Doing so is both expensive and at times difficult to manufacture. CFD however, has no problems with this approach to research and is very effective at assisting in determining the differences in results even if the absolute answer varies from laboratory data.

Some of the strengths of CFD make it an obvious tool to use for this research. Excessive fabrication costs and the time consuming nature and challenge of obtaining laboratory data result in CFD being the most economical as well as the most informative with regard to flow patterns and understanding fluid behavior. Using CFD simulations in flow measurement applications is not new, however using it to help develop meter designs and to review and understand past designs is a good application for this powerful tool. This research exposes some great applications for CFD and effective ways to use it for design and analysis.

## Problem Introduction

Venturi Discharge Coefficients with Sudden Offsets

Although accurate flow measurement is a requirement in many applications, flow meters are often installed in non-favorable conditions. Ideally, a flow meter should be installed per manufacturer prescribed conditions; however in some cases, this does not happen. Any time a flow meter is installed in close proximity to a flow disturbance, such as a pipe fitting or a valve, the installation should be investigated to ensure there will be no negative effects on the meter's performance. A favorable circumstance would be to have at least 20 diameters of straight pipe with the same inside diameter as the meter's inlet installed upstream of the flow meter. However, this does not always happen nor is it always possible. This portion of the research used both Computational Fluid Dynamics and laboratory data to determine the effects that sudden changes in pipe diameter can have on the discharge coefficients of Venturi flow meters. This part of the study was two-fold; first, to determine how accurately Computational Fluid Dynamics can match laboratory data in predicting pipe fitting effects on discharge coefficients of Venturi flow meters, and second, to use Computational Fluid Dynamics to determine how much distance is needed following a sudden change in pipe diameter before the Venturi discharge coefficient is no longer affected by the sudden diameter change. Figure 1 shows an image of a Venturi design with no offset upstream of it (ideal conditions), a sudden contraction upstream of it, and a sudden expansion upstream of the meter respectively.

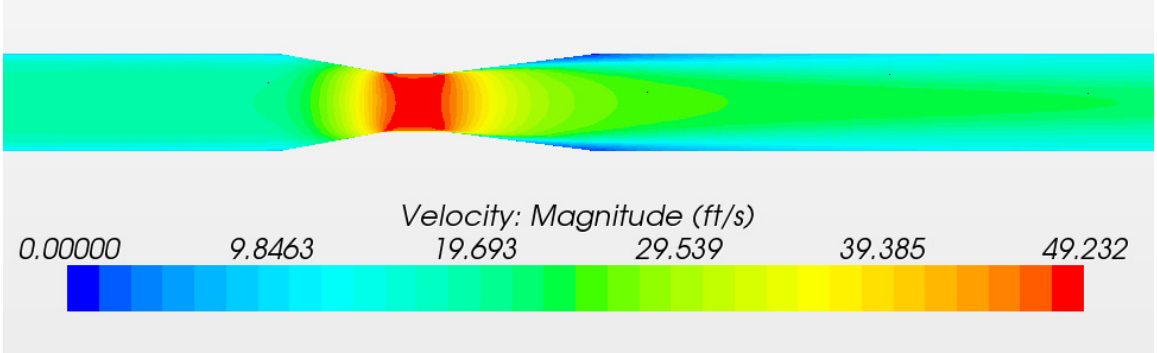


**A) No offset upstream of a Venturi**

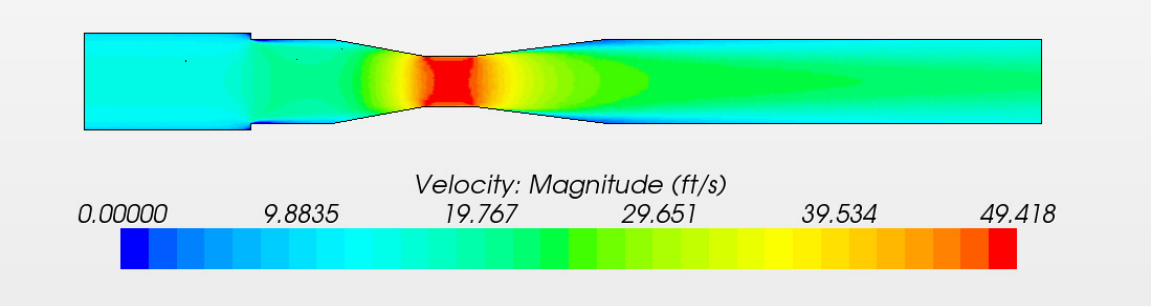


**B) A sudden contraction upstream of a Venturi**

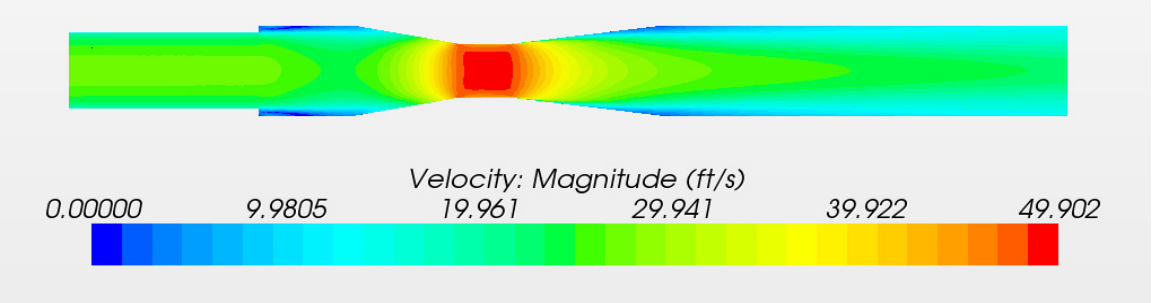


**C) A sudden expansion upstream of a Venturi**

**Fig. 1. Velocity plots with Different offsets upstream of Venturis**

Recovery Cone Angle Optimization

There are many varying applications for flow meters. Many of them require very accurate flow measurement (within 0.25% of actual) while other applications accept flow measurements with uncertainties better than 2%. Some applications attempt to minimize head loss while others rely on the flow meter to produce head loss in the system. There are also applications where there are limits on head loss imposed that a flow meter cannot exceed. In many instances where highly accurate flow measurement and low head loss are required, Venturi flow meters are a viable option. The accuracy of a Venturi in flow measurement is well established and documented, however the design of recovery cones and their associated head loss is not.

One case in point is a project where a meter manufacturer was given design criteria for a choking Venturi to be used in a nuclear application. The Venturi ended up needing to be near a 0.2 beta ratio (defined as the ratio of the Venturi throat diameter to the inlet diameter) to choke under the conditions given and have a permanent pressure loss of less than 7% of the corresponding meter differential pressure. While the Utah Water Research Laboratory was employed to help optimize the recovery cone design, the manufacturer was very interested in research that would help solve problems like this in the future.

This portion of the research uses Computational Fluid Dynamics and laboratory data to show how changing the angle of the recovery cone on a Venturi can change the head loss characteristics. Results show that to minimize head loss the optimum recovery cone angle is a function of meter design, beta ratio, and Reynolds number. This research

will focus on how sensitive recovery cone design can be to pressure recovery and not only present the optimum angles for minimizing pressure but what parameters make the biggest difference in pressure loss and how much change in permanent pressure loss to expect with different recovery cone designs

Recovery Cone Truncation

While information regarding optimal recovery cone angles is informative it does not help in cases where there are length requirements for the meter. Little information is available that gives insight to the head loss added for different levels of a truncated recovery cone on a Venturi flow meter. This portion of the research will provide insight so that Venturi flow meters can be shortened without compromising flow metering performance. It will also provide information on head loss for different levels of recovery cone truncation. As can be expected this kind of research can be very costly without CFD. Both the cost to build so many incremental variations of different flow meters and laboratory accessibility prohibit this type of data from being collected. While Figure 1 shows a classical Venturi design with a full recovery cone, Figure 2 shows a Halmi Venturi design with a truncated recovery cone.

## Literature Review

Venturi flow meters have been used to measure flow rate for more than 100 years (Finnemore and Franzini 2006). Over that time period, many variations of the Venturi

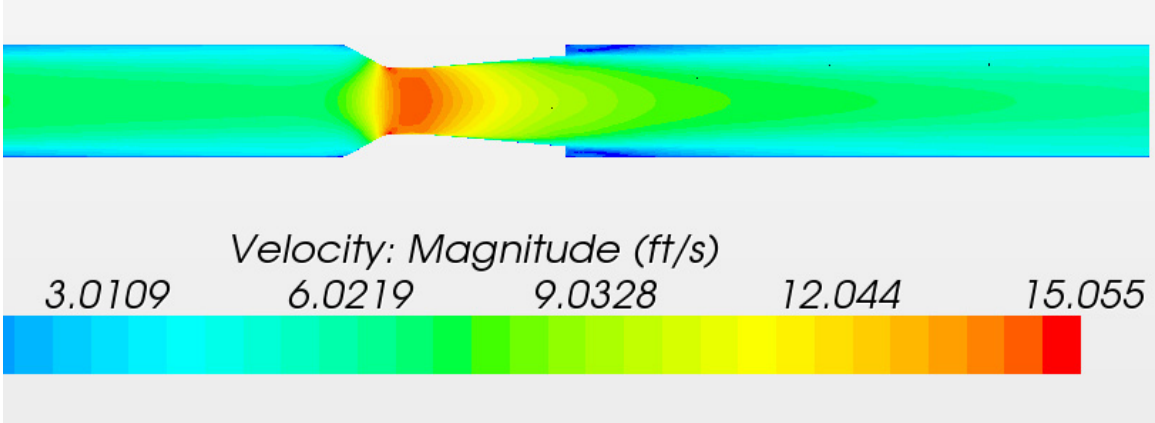


**Fig. 2. Venturi with truncated recovery cone**

flow meter have been developed, and a large amount of discharge coefficient and head loss data have been collected. There has also been substantial effort spent to determine the required pipe diameters needed between various pipe fittings and the Venturi flow meter to maintain the accuracy of the meter. The American Society of Mechanical Engineers (ASME 2005, ASME 2007) reports the distance of straight pipe needed before a Venturi after an elbow, two elbows in plane, two elbows out of plane, various fully open and partially throttled valves, pipe reducers and pipe expanders. All of the recommended distances are relative to the beta ratio of the Venturi. Others have reported straight pipe requirements for all types of flow meters which include most of the same flow disturbances as reported by the ASME (Baker 2000, ISO 2003). Many meter manufacturers have also performed research on their own designs to determine the distances needed between their meter and various pipe fittings (BIF 2016). One pipe disturbance, however, that is not found in the literature is a sudden change in pipe diameter adjacent to or relatively close to the meter, although most research recommends

matching the meter and pipe diameters on the inlet end of the meter (ASME 2005). Ideally a meter should always be built to match the pipe, however, in some cases the pipe is in service and the exact pipe diameter is unknown until the time of meter installation. In other instances, a calibration laboratory may not have the exact pipe the meter will be installed in. As water continues to become more and more of precious resource, accuracy in flow measurement will also become more important. Understanding the effects caused by pipe wall offsets will help improve meter accuracy under the right circumstances.

There has been research performed on Venturi flow meters with Computational Fluid Dynamics (CFD) for various reasons over the years. One study used CFD to analyze the trend of discharge coefficients on multiple differential pressure flow meters ranging from very low Reynolds numbers to very high Reynolds numbers (Hollingshead et al. 2011). Hollingshead showed success in calculating discharge coefficients using CFD compared to laboratory data. This particular research also showed the great flexibility researchers can have using CFD. Hydraulic laboratories have limits in flow rates and pressure that prevent them from testing over the vast Reynolds number ranges that were investigated by Hollingshead with CFD. While CFD is not a replacement for a laboratory calibration, it is a useful tool for identifying trends or relative differences associated with changes in the installation.

Prajapati (Prajapati et al. 2010) also showed good success using CFD in flow metering applications. Their research used CFD to determine the permanent pressure loss of various differential producing flow meters including a Venturi, Wedge, V-Cone, and concentric Orifice plate flow meters. In 1908, Gibson showed experimental data for

expansions in circular, square and rectangular conduits that showed the angle in which the head loss is minimized through the expansion (Gibson 1908). His results showed that for circular and square conduits, regardless of the ratio of pipe diameters, the inclusive angle for which head loss is minimized to be 5.5 degrees. Gibson also showed that for different area ratios of rectangular pipe the expansion angle in which the head loss was minimized was near 10 degrees. This information is often referred to in literature as the Gibson method for Venturi recovery cone design. The research lacks important information such as how long the pipe was prior to the expansion leaving the development of the flow profile in question. It is also uncertain if these data can be applied to Venturi recovery cone designs as the flow profile will be different in straight pipe versus the throat of a Venturi. The ASME MFC code (ASME 2007) on fluid flow measurement in pipes lists acceptable ranges of the recovery cone for a classical or AMSE (name changes with different codes) Venturi flow meter as between 7 and 15 degrees inclusive. It also lists head loss information for a meter with the 7 degree cone and a 15 degree cone but nothing in between. This code also gives the design information for a nozzle Venturi in which the recommended inclusive recovery cone angle is limited to less than 30 degrees. For both meter designs, the code says that the recovery cone can be truncated up to 35% of its length. This refers to a sudden truncation such that the resulting diameter at the end of the recovery cone is less than the diameter of the pipe downstream of the flow meter. The code indicates this will increase the head loss of the device but does not list how much increase to expect. All of these generalized factors leave holes in the literature pertaining to recovery cone design.

Using CFD and laboratory data together provides an effective tool for determining the effect of various flow disturbances on flow meter performance or the design of a recovery cone. CFD provides a cost effective way of extending laboratory data and offers a complete set of pressure and velocity data whereas the laboratory data only gives pressure data at the pressure tap locations. With CFD however, pressure or velocity data can be calculated at any location in the flow domain at any time during or after the simulation, which can add insight to analysis that laboratory data does not.

# CHAPTER 2

## EXPERIMENTAL PROCEEDURE AND SCOPE OF WORK

All data for this dissertation were collected at the Utah Water Research Laboratory (UWRL). For any laboratory data, water was supplied to the test setup from First Dam, a small impoundment located on the Logan River near the UWRL. The approach to each research topic presented herein was procedurally similar apart from the uniqueness of the topics. Baseline tests were performed in the laboratory for a classical Venturi tube and a Halmi Venturi tube with more than 40 diameters of straight pipe matching the meter inlet diameters were installed upstream from the meter. The meters were tested over inlet Reynolds numbers ranging from 60,000 to 1,200,000. The flow meters were provided to the UWRL by meter manufacturers for experimental and research use and each had a beta ratio of approximately 0.60. The straight pipe flow meter data included discharge coefficients and permanent pressure loss for each Venturi. To assist with the pipe offset problem, various schedules of 12-inch diameter pipe were then tested upstream of the sample Venturi meters to simulate sudden pipe expansions and contractions. The changes in $C_d$ from the baseline tests over the same Reynolds number range were determined. To assist with the recovery cone problems each flow meter had a removable portion of the recovery cone so the pressure loss was collected for both meters with a full and truncated recovery cone.

The same tests were then reproduced using CFD. The CFD data were collected at the UWRL using STAR-CCM+, a commercially available CFD solver. The CFD

simulations were set up to match, as close as possible, the experimental setup from the physical data. The CFD results were then compared to the results of the experimental data. All mesh convergence, and CFD model calibration were completed at this time in the research. Once the comparison of CFD and physical data were satisfactory the CFD simulations were expanded to complete the research as explained for each topic.

**Venturi Discharge Coefficients with Sudden Offsets**

To show the effects of pipe wall offsets on Venturi's as a whole, CFD was used. In order to do this effectively the research was expanded to different line sizes (to see if size scale effects exist), Venturi designs, beta ratios, and a wider range of Reynolds numbers for both sudden pipe contractions and sudden pipe expansions upstream of the flow meters. CFD was also used to determine the minimum distance required between a sudden pipe offset and Venturi to remove any effect that offset has on the discharge coefficient. This was done by moving the offset in the CFD model farther upstream from the meter inlet until the Venturi discharge coefficient matched that of the baseline data. It should be noted that the CFD results were compared to laboratory data for a wide range of installations to verify the validity of the results.

**Recovery Cone Angle Optimization**

To determine the effect recovery cone angles have on the permanent head loss of Venturis various Venturi designs were tested. The classical (ASME) Venturi, Halmi Venturi, Universal Venturi, Nozzle Venturi and the as-cast classical Venturi Tube were

included in the study. The study not only determined the effect of the meter design on the optimal recovery cone angle but of the beta ratio and Reynolds number as well. The CFD models were used to develop curves of head loss versus recovery cone angles for the different meter designs and beta ratios. These curves were then used to predict the angle of recovery cone with the lowest head loss.

**Recovery Cone Truncation**

To determine the head loss from truncating recovery cones the same Venturi designs evaluated in the recovery cone optimization study were analyzed. The ASME (classical) Venturi, Halmi Venturi, Universal Venturi, Nozzle Venturi and the as-cast classical Venturi Tube were tested for each recovery cone design. The tests included various beta ratios and recovery cone angles coupled with different truncations to discover the most efficient way, in terms of pressure loss, to truncate a recovery cone.

**Scope of Work**

More than 1000 CFD runs were produced to complete the proposed tasks. CFD was used to evaluate the effects of incrementally changing the distance between the offset and Venturi, the angle of recovery cones, and the level of truncation. As mentioned, CFD coupled with laboratory data were used throughout the testing to determine the following:

1. The effect various pipe wall offsets have on the discharge coefficients of several Venturi flow meter designs.

2. The minimum distance required between pipe wall offsets and the Venturi such that there is no longer any effect on the discharge coefficients of different Venturi designs.
3. The optimum angle of the recovery cone on different Venturi flow meters to minimize head loss.
4. The sensitivity of varying angles of recovery cones and the effect it has on permanent pressure loss for different Venturi designs.
5. The most efficient way to truncate Venturi recovery cones such that meters can be manufactured at shorter lengths while continuing to minimize head loss.
6. The head loss associated with different levels of truncated recovery cones for various Venturi designs.

While the main points of the research are listed above there were more key findings from the research that are discussed in detail in the reports. This dissertation is in a multi paper format. The first paper (chapter 3) will be published in the August 2016 edition of Journal AWWA and the papers in chapters 4 and 5 have been submitted to journals and are in the review process. It is also noteworthy to reiterate the input from industry in these research topics leading one to believe the contribution to the literature will be noticed providing useful guidance for future Venturi mater designs.

# CHAPTER 3

## EFFECTS OF ABRUPT PIPE DIAMETER CHANGES ON VENTURI FLOW METERS

**Abstract**

Although accurate flow measurement is a requirement in many applications, flow meters are often installed in less-favorable conditions. Ideally, a flow meter should be installed per the manufacturer prescribed conditions; however in some cases, for a number of reasons this does not happen. Any time a flow meter is installed in close proximity to a flow disturbance, such as a pipe fitting or a valve, the installation should be investigated to ensure there will be no negative effects on the meter's performance. A favorable circumstance would be to have at least 20 diameters of straight pipe with the same inside diameter as the meter's inlet installed upstream of the flow meter. However, this does not always happen nor is it always possible. This study uses both Computational Fluid Dynamics and laboratory data to determine the effects that sudden changes in pipe diameter can have on the discharge coefficients of Venturi flow meters. The study was twofold; first, to determine how accurately Computational Fluid Dynamics can match laboratory data in predicting pipe fitting effects on discharge coefficients of Venturi flow meters, and second, to use Computational Fluid Dynamics to determine how much distance is needed following a sudden change in pipe diameter before the Venturi discharge coefficient is no longer affected by the sudden diameter change.

---

Coauthored by Michael C. Johnson[2] P.E., Member AWWA, Steven L. Barfuss[3] P.E., Member AWWA

**Background**

Venturi flow meters have been used to measure flow rate for more than 100 years (Finnemore 2006). Over that time period, many variations of the Venturi flow meter have been developed, and a large amount of discharge coefficient and head loss data has been collected. There has also been substantial effort spent to determine the required pipe diameters needed between various pipe fittings and the Venturi flow meter to maintain the accuracy of the meter. The American Society of Mechanical Engineers (ASME 2005) reports the distance of straight pipe needed before a Venturi after an elbow, two elbows in plane, two elbows out of plane, various fully open and partially throttled valves, pipe reducers and pipe expanders. All of the recommended distances are relative to the beta ratio of the Venturi. Others have reported straight pipe requirements (Baker 2000), which include most of the same flow disturbances as reported by ASME. One pipe disturbance, however, that is not found in the literature is a sudden change in pipe diameter adjacent to or relatively close to the meter, although most research recommends matching the meter and pipe diameters on the inlet end of the meter (ASME 2004). Ideally a meter should always be built to match the pipe, however, in some cases the pipe is in service and the exact pipe diameter is unknown until the time of meter installation.

There has been research performed on Venturi flow meters with Computational Fluid Dynamics (CFD) for various reasons over the years. One study used CFD to analyze the trend of discharge coefficients on multiple differential pressure flow meters ranging from very low Reynolds numbers to very high Reynolds numbers (Hollingshead

et al. 2011). Hollingshead showed success in calculating discharge coefficients using CFD compared to laboratory data. This particular research also showed the great flexibility researchers can have using CFD. Hydraulic laboratories have limits in flow rates and pressure that prevent them from taking data over the vast Reynolds number ranges that were investigated by Hollingshead with CFD. While CFD is not a replacement for a laboratory calibration, it is a useful tool for identifying trends or relative differences associated with changes in the installation.

Using CFD and laboratory data together provide an effective tool for solving hydraulic problems like the effect of various flow disturbances on flow meter performance. CFD provides a cost effective way of extending laboratory data and offers a complete set of pressure and velocity data whereas the laboratory data only gives pressure data at the pressure taps. With CFD however, pressure or velocity data can be calculated at any location in the flow domain at any time during or after the simulation, which can add insight to analysis that laboratory data does not.

**Theoretical Background**

The equation used to calculate the discharge coefficient ($C_d$) for a Venturi is derived from the Bernoulli energy equation. To generalize the equation such that it can be used for compressible and incompressible fluids, conservation of mass must be maintained. A general equation to determine the discharge coefficient ($C_d$) for a Venturi is given by:

$$C_d = \frac{Q}{Y\frac{\pi}{4}d_f^2\sqrt{\frac{2g}{1-\left[\left(d_f/D_f\right)^4\right]}}*\sqrt{\Delta P\rho_f}} \quad (1)$$

where $Q$ is the mass flow rate, $C_d$ is the discharge coefficient, $d_f$ is the flowing diameter of the throat, $D_f$ is the flowing diameter of the meter inlet, $g$ is the acceleration due to gravity, $\Delta P$ is the difference in piezometric pressure from the inlet to the throat, $\rho_f$ is the flowing density of the fluid, and $Y$ is the gas expansion coefficient for gasses or 1 for liquids.

As can be seen in Eq. 1, $C_d$ is directly proportional to $Q$. If then, $C_d$ is determined incorrectly and is inaccurate by 2% then the resulting flow calculation will also be off by 2%. Every differential-based flow meter has a discharge coefficient that can be calculated using different variations of Eq. 1. While it is possible to predict the discharge coefficient, especially for some well documented meter designs, the best results are found when the meter is calibrated in a laboratory setting and assigned its discharge coefficient which corresponds to the specific set of pressure taps used. When the meter is calibrated in a laboratory setting, it should be calibrated in a pipe configuration that is representative of the conditions in the field to achieve the highest degree of accuracy when installed. When a laboratory calibration is not possible, it becomes necessary for the manufacturer's predicted performance data to be used to determine how a meter will perform in piping that deviates from recommended installations. If there is no recommendation or experience from the manufacturer, CFD can act as an alternative to physically modeling the pipe in a laboratory to assess the differences to be expected as

compared to an ideal installation. CFD is well suited for determining both the relative differences in $C_d$ from pipe installation effects and the distances required after pipe disturbances such that $C_d$ is no longer affected.

**Experimental Procedure**

All data for this study were collected at the Utah Water Research Laboratory (UWRL). For the physical data, water was supplied to the test setup from First Dam, a small impoundment located on the Logan River near the UWRL. This study was designed to show the change in $C_d$ as a result of sudden changes in pipe diameter upstream from the meter. A baseline test was performed in the laboratory for a classical Venturi tube and a Halmi Venturi tube where more than 40 diameters of straight pipe matching the meter inlet diameters were installed upstream from the meter. The meters were tested over inlet Reynolds numbers ranging from 60,000 to 1,200,000. The flow meters were provided to the UWRL for experimental and research use and each had a beta ratio of approximately 0.60. Various schedules of 12-inch diameter pipe were then tested upstream of the sample Venturi meters to simulate sudden pipe expansions and contractions. The changes in $C_d$ from the baseline tests over the same Reynolds number range were determined.

The same tests were then reproduced using CFD. The CFD data were collected at the UWRL using Star-CCM+, a commercially available CFD solver (CD-adapco 2016). The CFD simulations were set up to match as close as possible the experimental setup from the physical data. The CFD results were then compared to the results of the

experimental data for a specific pipe offset. This was completed for three pipe configurations where the offset was 0.5, 2 and 4 diameters upstream from the meter inlet pressure taps.

As shown in the experimental results section, the CFD and physical data compared well. The CFD simulations were then expanded to show the effects of pipe wall offsets on Venturi's in different line sizes, with different Venturi designs, beta ratios, and a wider range of Reynolds numbers for both sudden contractions and sudden expansions. CFD was also used to determine the distance required after a sudden pipe offset to remove any effect that offset has on the Venturi discharge coefficient. This was done by moving the offset further upstream from the meter inlet until the Venturi discharge coefficient matched that of the baseline data. It should be noted that the CFD results were compared to laboratory data for a wide range of installations to verify the validity of the results. This will be shown later in the paper.

**Experimental Results**

During this study, over 200 CFD data runs were completed. As mentioned previously, the primary objectives for the study were to determine how well CFD could predict the discharge coefficient ($C_d$) of various Venturi designs and to predict how $C_d$ is affected by pipe diameter offsets as well as using CFD to determine the distance a Venturi needs to be installed from an offset to no longer be affected. Noteworthy is that all CFD runs were simulated using progressively finer meshes and simulated until the

solution was mesh independent and grid convergence occurred. Furthermore, the laboratory discharge coefficient data has a maximum experimental uncertainty of 0.25%.

Comparison of CFD to Experimental Data

In order to gain understanding of the CFD results, they were first compared to the results from the experimental data. One of the reasons CFD was used to determine the distance downstream of a sudden change in pipe diameter a meter should be installed is because it is expensive to acquire different lengths of varying pipe diameters for so many laboratory setups. The UWRL did purchase lengths of all of the 12-inch pipe schedules for the study, but CFD was used to vary the standard wall pipe lengths between the offset and the meter. With this in mind, the UWRL did have a few pipe spools that were used to increase the distance from the offset to the meter so the confidence in the CFD model could be increased. The experimental data that the CFD were compared to were for the Halmi Venturi Tube and the Classical Venturi Tube with 0.5, 2.0 and 4 pipe diameters between the Venturi's pressure taps and the pipe wall offset.

The offset tested in the laboratory was from a 12-inch schedule 160 pipe with an I.D. of 10.126 inches to 12-inch standard pipe with an I.D. of 12.00 inches. This offset was defined as a 15.6% sudden expansion upstream from the meter. For clarity, an expansion is defined as a sudden increase in diameter experienced by the flow as it approaches the meter. Figures 3 and 4 show the discharge coefficient for each meter plotted against the Reynolds number. The plots show the discharge coefficient with

different meter inlet pipe diameters between the sudden pipe expansion and the meters for both the experimental and numerical data.

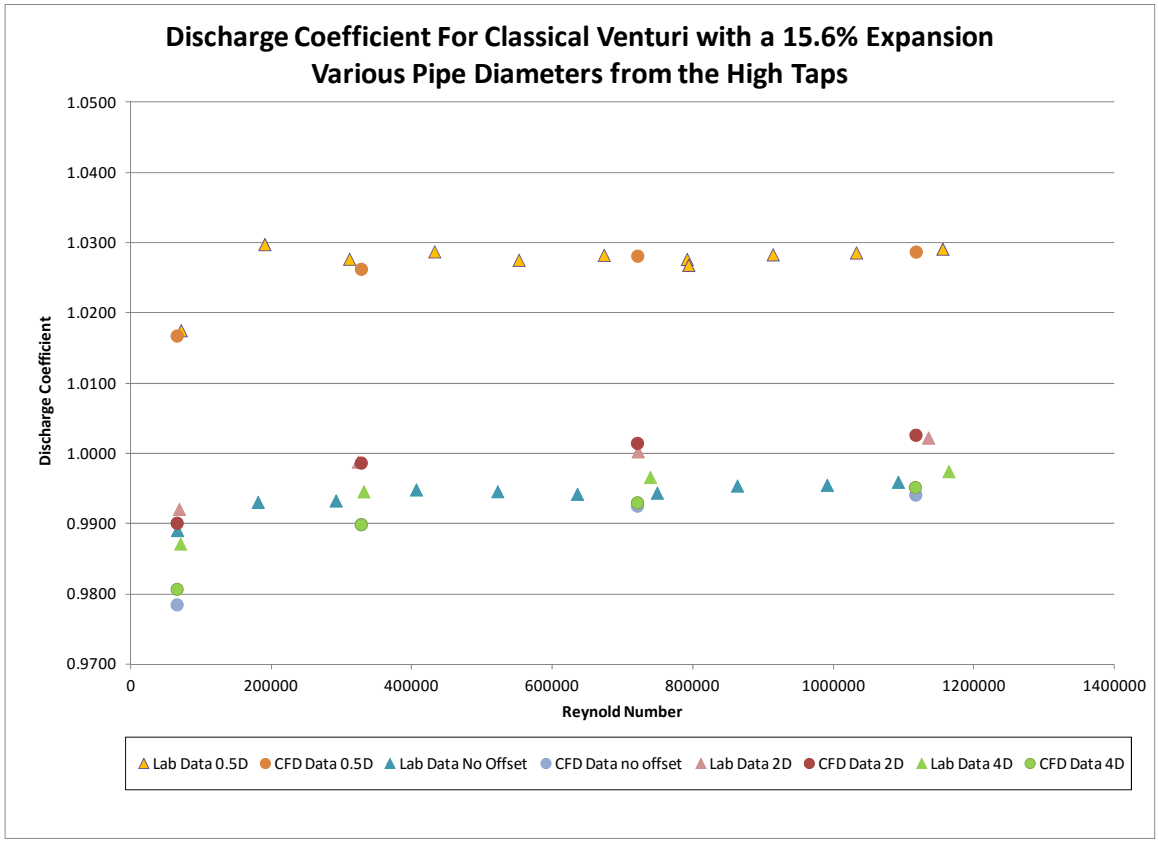


**Fig. 3. Classical Venturi discharge coefficients with a 15.6% expansion for both physical and numerical data**

As shown in Figures 3 and 4 the agreement between the CFD and experimental data is very good when a 15.6% expansion occurs upstream from a Classical or Halmi Venturi meter. It should be noted that although the value of the discharge coefficient matches well with these Venturis, this was not a critical part of this study. The critical part of this study was how well CFD can predict the change in the $C_d$ caused by the

sudden change in pipe diameter. Figures 3 and 4 indicate that the CFD captures the change rather well.

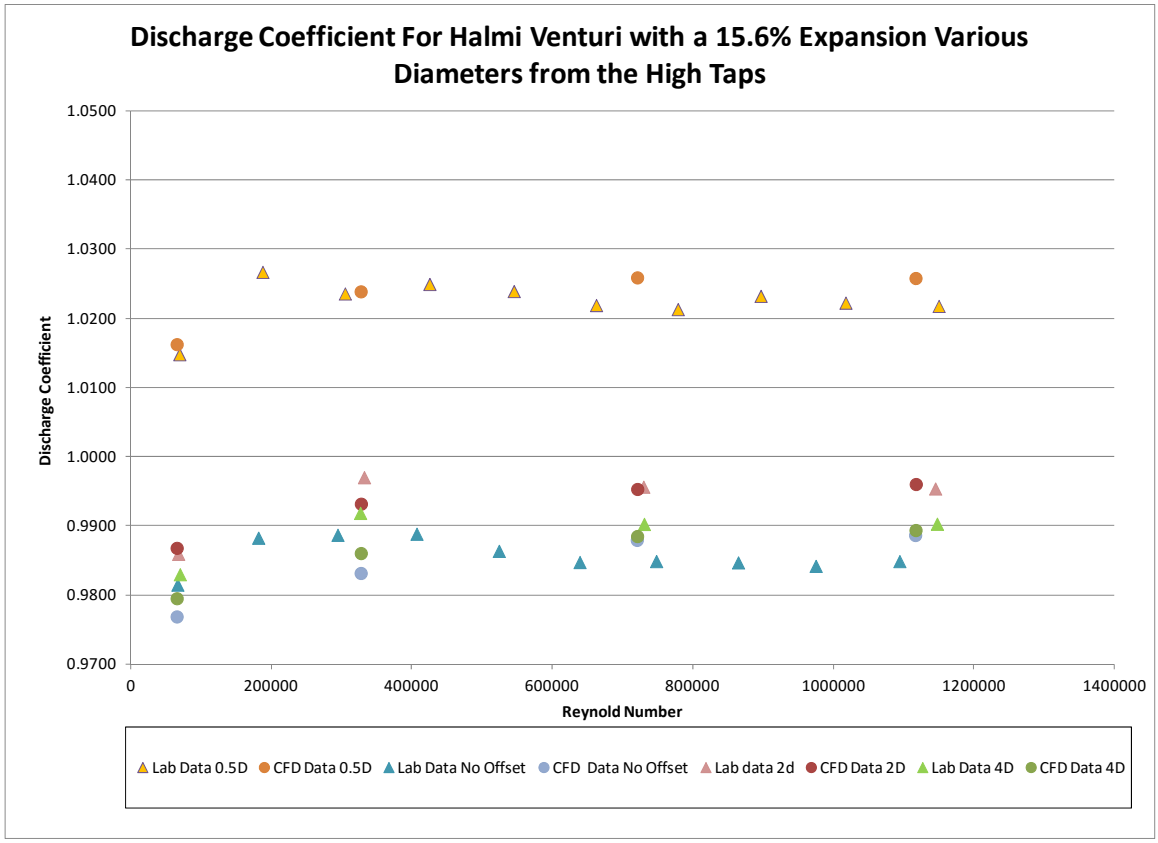


**Fig. 4. Halmi Venturi discharge coefficients with a 15.6% expansion for both physical and numerical data**

After the CFD model was proven reliable, it could then be used to determine the required distances between an offset and Venturi flow meter. As mentioned previously, the experimental laboratory data that were collected for this study were used to document the effects of installing various differential pressure flow meters in different pipe schedules so that a pipe wall offset was created immediately upstream of the meter.

These experiments were performed in varying schedules of 12-inch pipe and all of the meters tested were standard wall (12-inch I.D.). All differential producing meters had a beta ratio of approximately 0.6. The full results of the experimental data for this research were published in Journal AWWA (Pope et al. 2015) and show that $C_d$ is most certainly affected by the pipe wall offsets.

It would take many more CFD simulations to test the entire range of pipe schedules investigated in Pope's research so only two were chosen for proof of concept. The two upstream pipe schedules that were tested with the CFD simulations were 12-inch schedule 100 (11.064 inch I.D.) and schedule 160 (10.126 inch I.D.). These schedules equate to a 7.8% and 15.6% change in diameter from the standard wall (12.00 inch I.D) pipe. These schedules were chosen for use in the CFD simulations because the 7.8% change in diameter is where the change in $C_d$ was consistently greater than the meter's published accuracy and the 15.6% change was the largest diameter change tested during the experimental work, which accordingly resulted in the largest change in $C_d$.

One limitation of the experimental data was that the sudden expansions that were tested had a larger change in diameter than the sudden contractions that were tested. It is feasible however, to have the same magnitude of sudden contraction as the sudden expansion in the experimental data. This would mean a 12-inch schedule 100 or 160 meter would be installed in a larger standard schedule 12-inch pipe. A full background on pipe schedules and sizes available can help one see this picture clearly and can be found in literature (Nayyar 2000). The CFD simulations therefore also include a 7.8% and a 15.6% sudden contraction prior to the meters. Figure 5 shows velocity contour

plots from the CFD of a Classical Venturi with a 7.8% expansion and contraction as well as a 15.6% expansion and contraction. The images in Figure 5 are all with the offset close coupled to the flow meter such that the offset was 0.5 pipe diameters from the high pressure tap location.

As previously stated, each of the differential flow meters tested experimentally in the laboratory were 12-inch meters and had a beta ratio of approximately 0.6. To determine how the same meter designs with different beta ratios are affected by the sudden expansion and contractions the various Venturi meters were tested in the CFD simulations with beta ratios of 0.4, 0.6, and 0.75. These are all common beta ratios available in commercial Venturi meters and provided enough information to predict how meters with other beta ratios than those tested should respond. Figure 6 shows a CFD velocity contour plot of each beta ratio of a Classical Venturi with no pipe wall offset upstream of the meter.

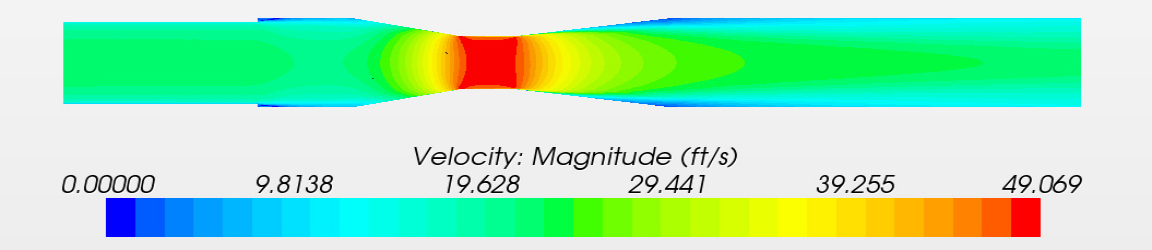


A) 7.8% expansion

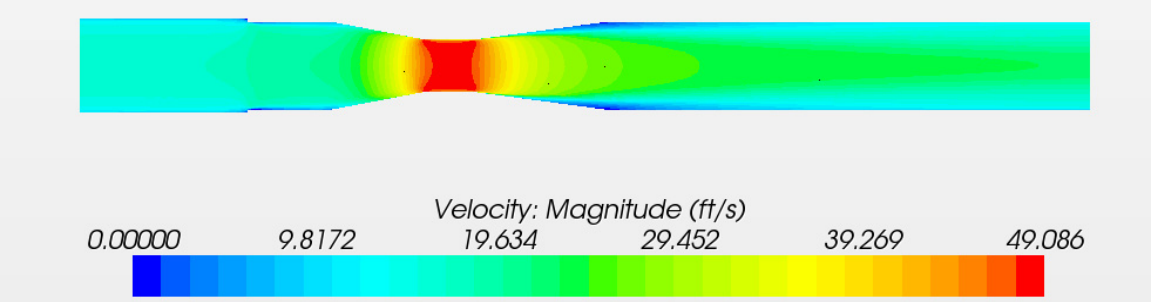


B) 7.8% Contraction

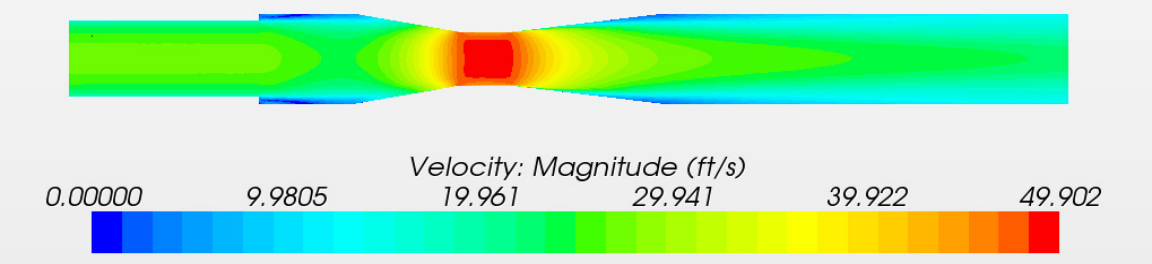


C) 15.6% Expansion

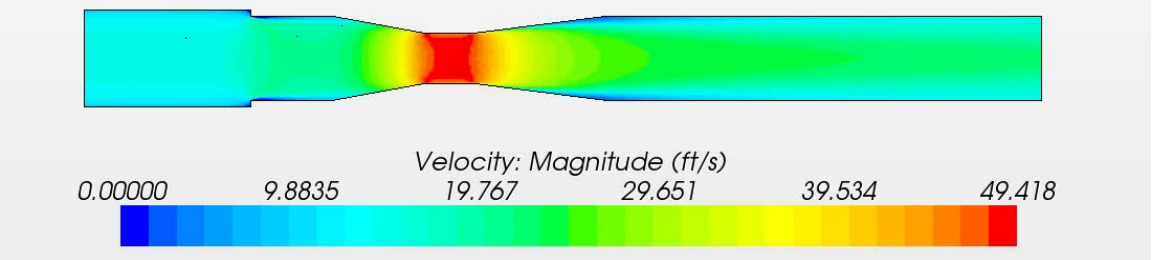


D) 15.6% Contraction

**Fig. 5. CFD Velocity contour plots showing different offsets tested with CFD**

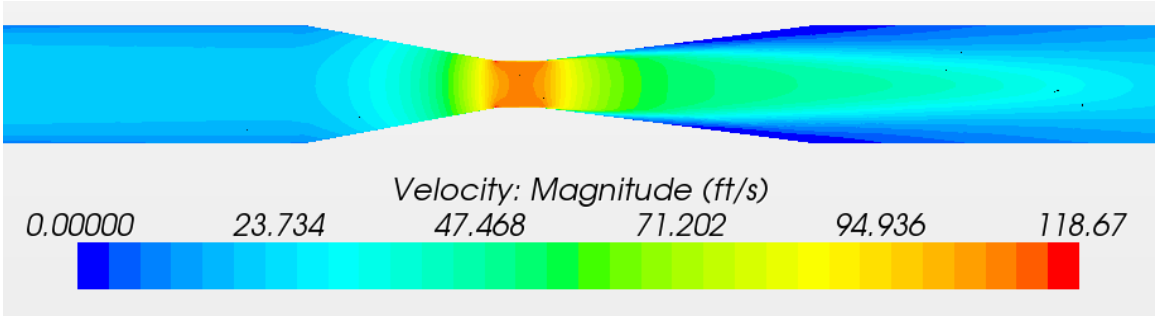


A) 0.4 beta ratio

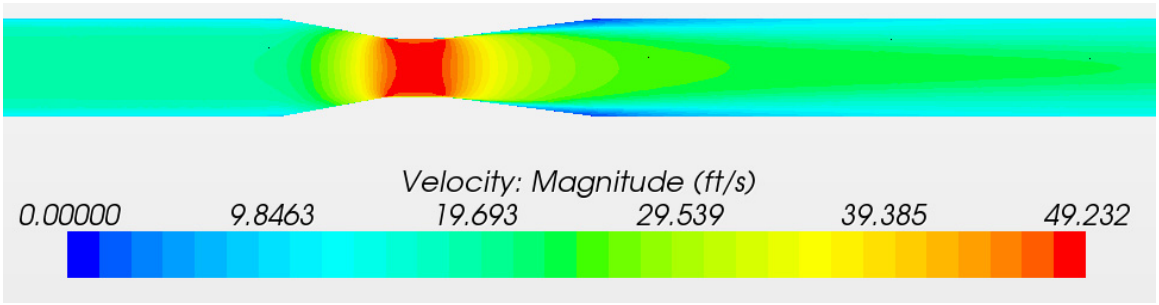


B) 0.6 beta ratio

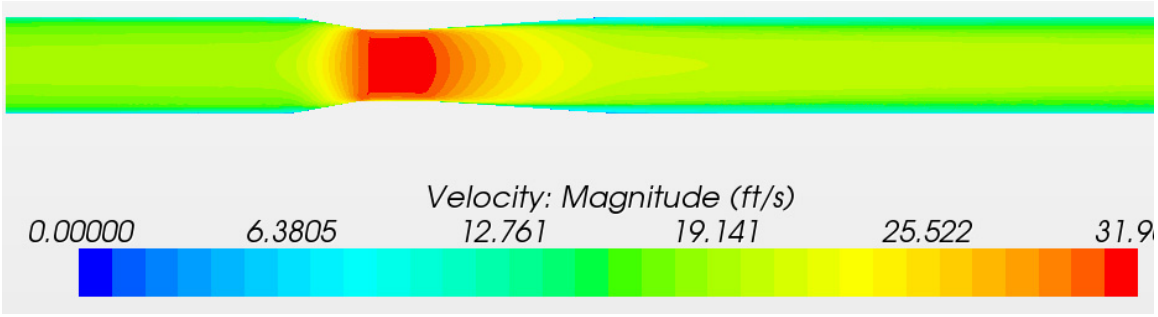


C) 0.75 beta ratio

**Fig. 6. CFD velocity contour plots of 0.4, 0.6, and 0.75 beta ratio Classical Venturi**

For completeness both 4-inch and 48-inch Venturi meters were also tested with CFD simulations in addition to the 12-inch meters to show how meters in different line sizes respond to pipe wall offsets. Also, higher Reynolds numbers were tested using

CFD to make sure no Reynolds number effects were present. The data were also expanded to include a few runs with the Universal Venturi Tube (UVT) with CFD.

Determining Required Distance from Offset

To determine the distance the Venturi meter needs to be installed from the offset such that $C_d$ is no longer affected, the offset was moved farther upstream from the Venturi meter until the change in $C_d$ was less than the 0.25% calibrated accuracy (PFS 2014) of the meter. Figure 7 shows a 0.6 beta ratio HVT with a 15.6% expansion at varying distances from the meter. This figure is helpful to visually see the changes in velocity near the meter resulting from the offset. The figures that follow show plots of the change in discharge coefficient from the baseline runs plotted against the distance from the offset to the inlet pressure taps in step heights, where a step height is the difference in radius from the offset pipe to the meter inlet.

Figures 8 through 11 show plots of the change in $C_d$ for a 12-inch Halmi Venturi Tube (HVT) with different beta ratios versus the distance from the offset to the meter inlet taps in step heights. Figure 7 also shows data for a 4-inch HVT, a 4-inch UVT, and laboratory data for a 12-inch HVT. Figures 12 through 15 show plots of the change in $C_d$ for the Classical Venturi with different beta ratios versus the distance from the offset to the meter inlet taps in step heights. Figure 10 also shows data from a 48-inch Classical Venturi and Figure 11 includes data from a 4-inch Classical Venturi and laboratory data from a 12-inch Classical Venturi.

Table 1 shows a summary of the distances required between the offset and the high-pressure meter taps for $C_d$ to be changed by 0.25% or less as compared to ideal conditions.

It should be noted that the data presented in Figures 3 through 10 and Table 1 represent the average change in $C_d$ over the Reynolds number range tested. Reynolds number effects will be discussed later in the paper. It should also be noted that in some cases the offset had no effect on $C_d$ when tested at the shortest feasible distance. In these cases the required distance could be less than shown in Table 1, however the values shown would be conservative.

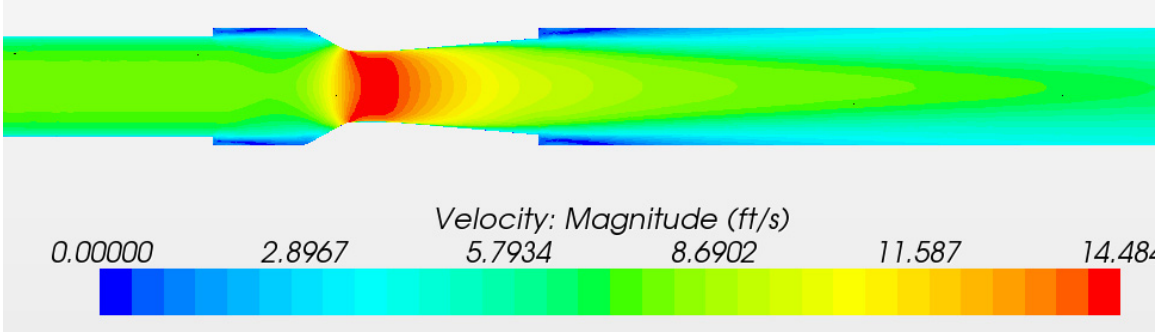


A) HVT with 6.4 step heights (0.5 pipe diameters) from offset to meter inlet taps.

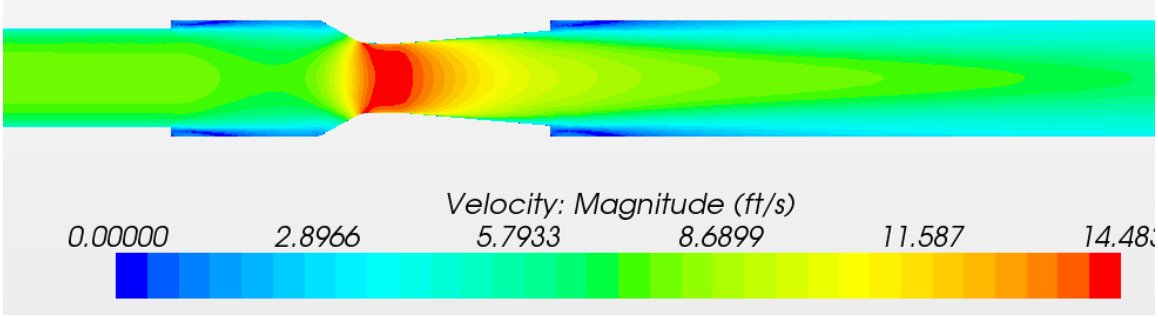


B) HVT with 12.8 step heights (1 pipe diameters) from offset to meter inlet taps.

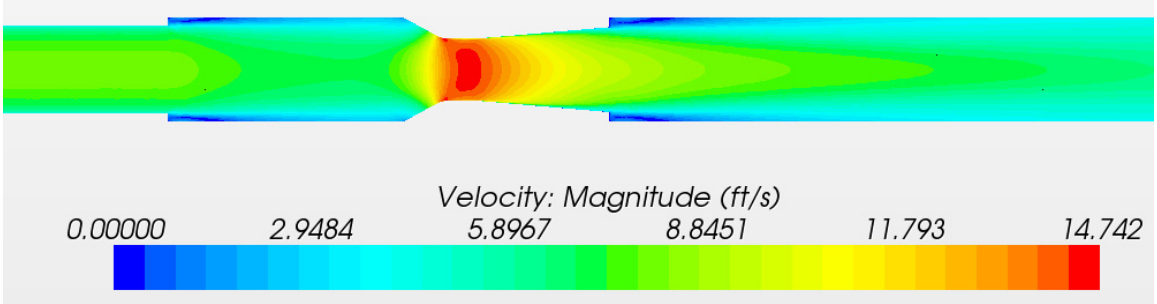


C) HVT with 25.6 step heights (2 pipe diameters) from offset to meter inlet taps.

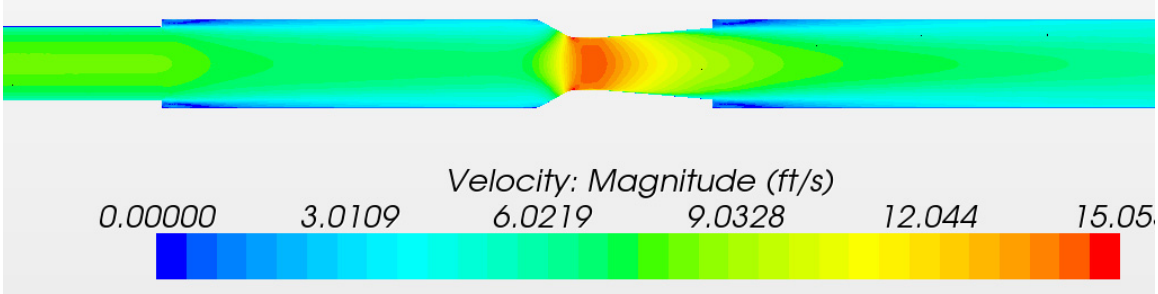


D) HVT with 51.2 step heights (4 pipe diameters) from offset to meter inlet taps.

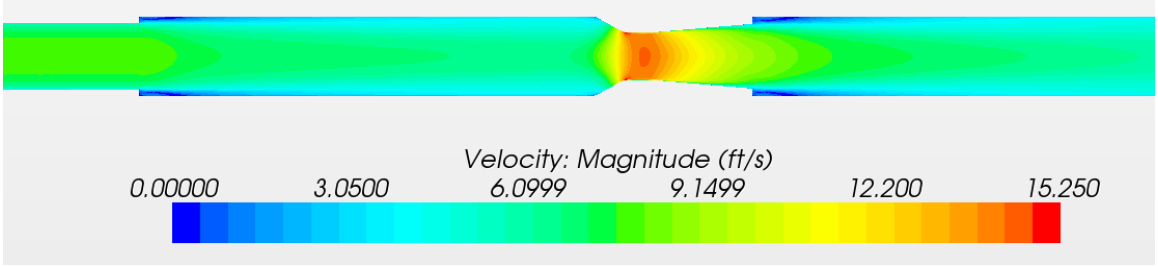


E) HVT with 64 step heights (5 pipe diameters) from offset to meter inlet taps.

**Fig. 7. Contour velocity plots of a 0.6 beta ratio HVT with varying distances between a 15.6% expansion and the meter inlet taps**

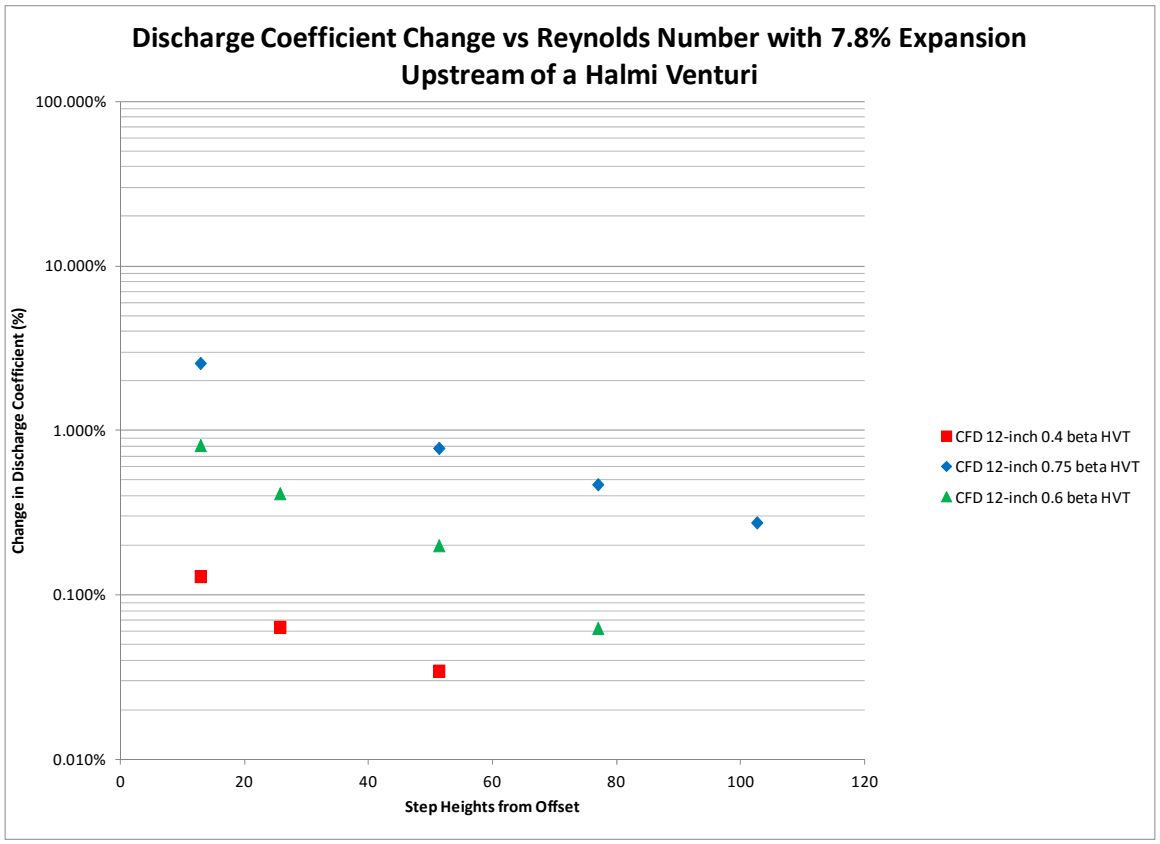


**Fig. 8. Change in discharge coefficient vs. Reynolds number for the Halmi Venturi Tube with a 7.8% pipe wall expansion at various distances upstream**

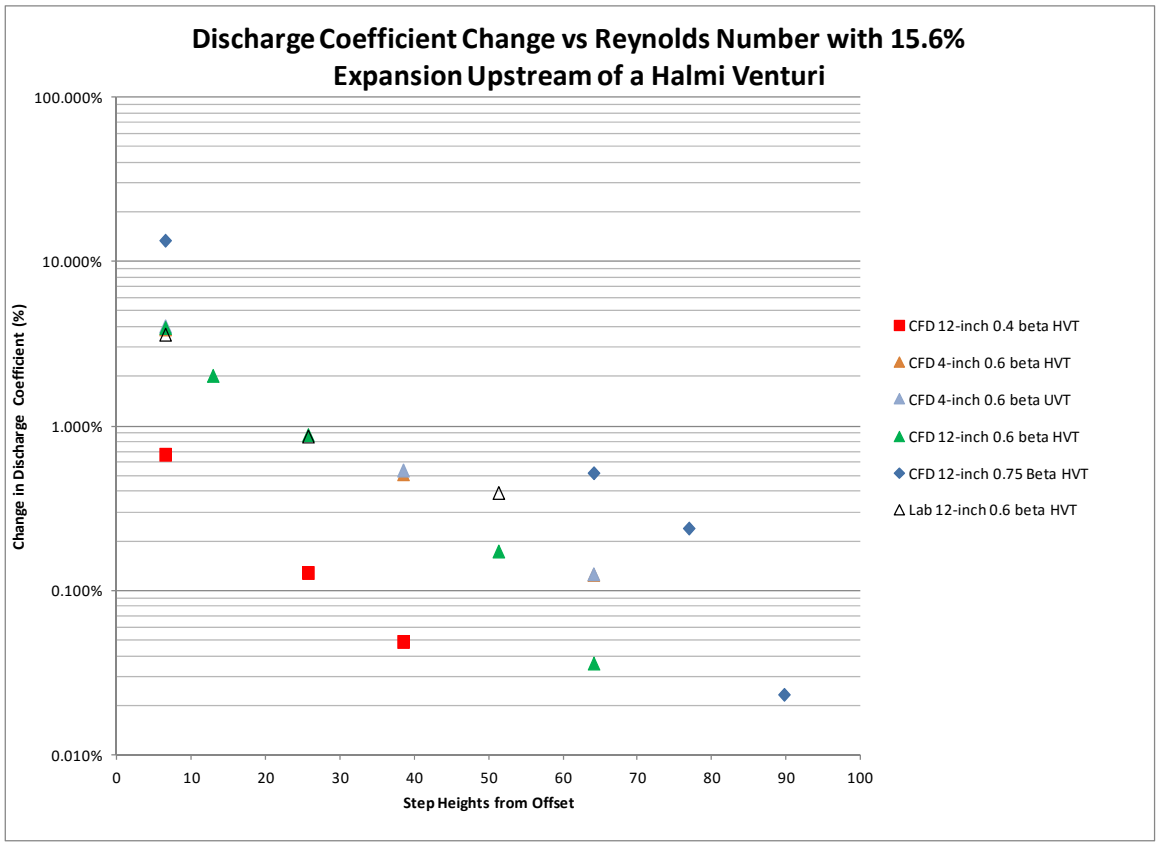


**Fig. 9. Change in discharge coefficient vs. Reynolds number for the Halmi Venturi Tube with a 15.6% pipe wall expansion at various distances upstream**

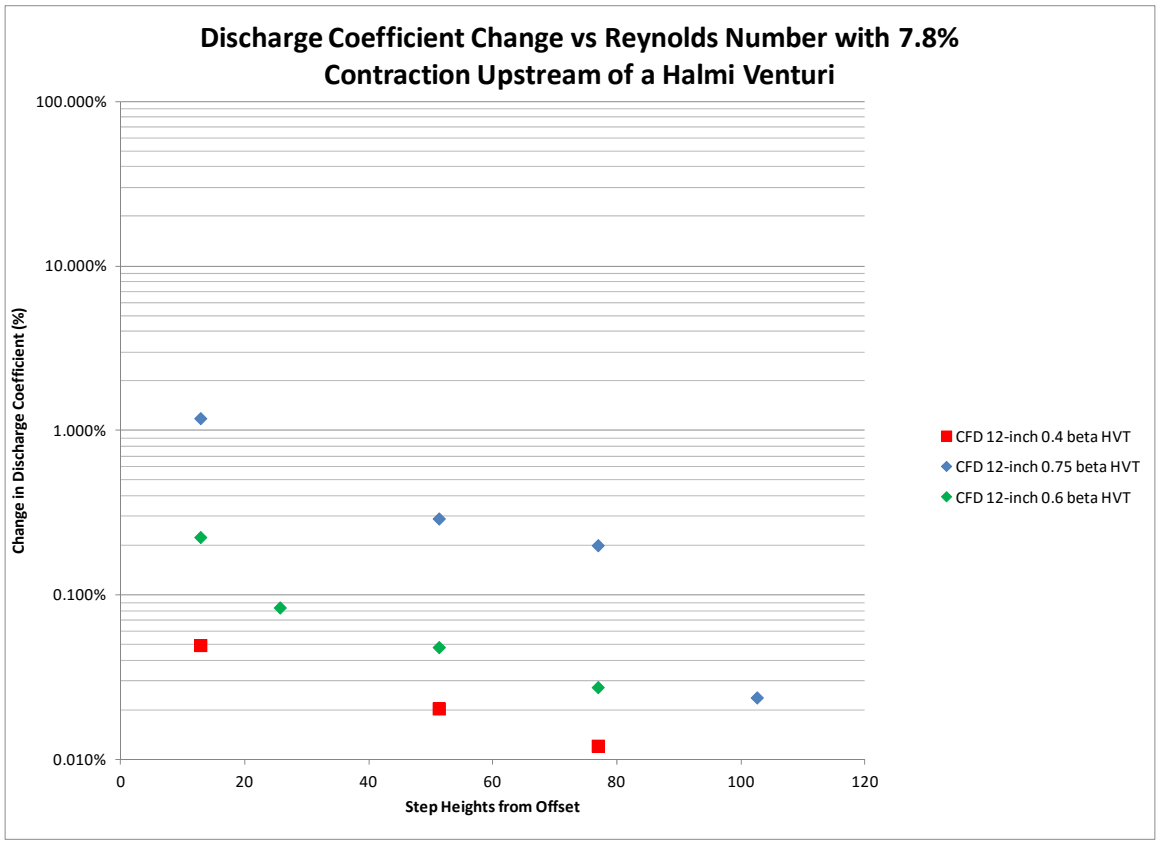


**Fig. 10. Change in discharge coefficient vs. Reynolds number for the Halmi Venturi Tube with a 7.8% pipe wall contraction at various distances upstream**

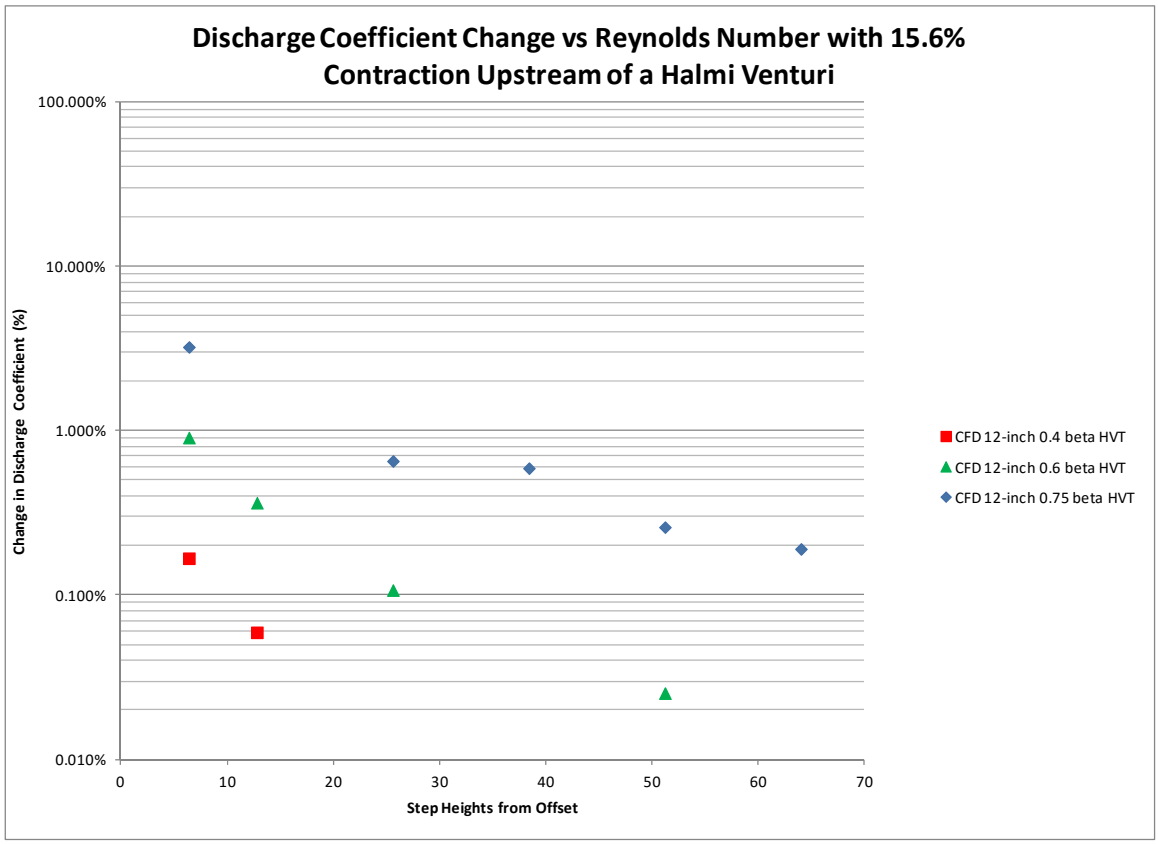


**Fig. 11. Change in discharge coefficient vs. Reynolds number for the Halmi Venturi Tube with a 15.6% pipe wall contraction at various distances upstream**

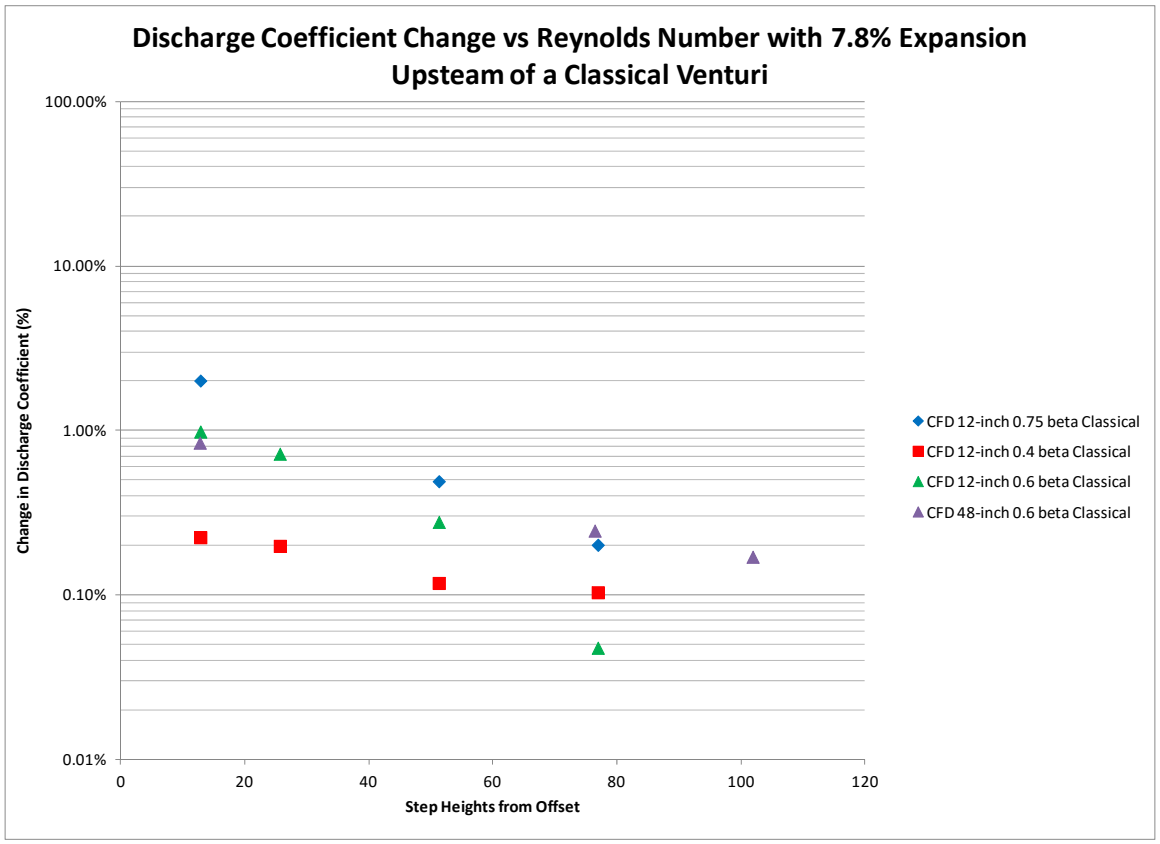


**Fig. 12. Change in discharge coefficient vs. Reynolds number for the Classical Venturi Tube with a 7.8% pipe wall expansion at various distances upstream**

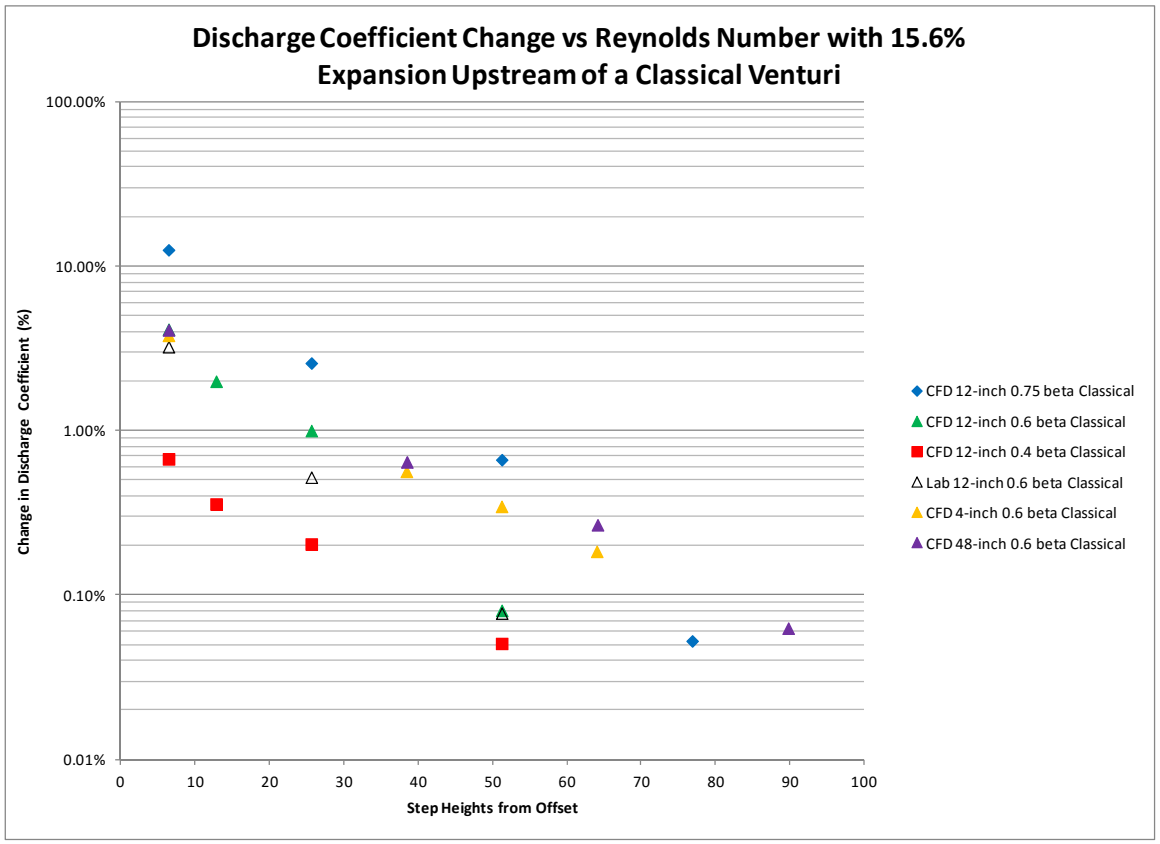


**Fig. 13. Change in discharge coefficient vs. Reynolds number for the Classical Venturi Tube with a 15.6% pipe wall expansion at various distances upstream**

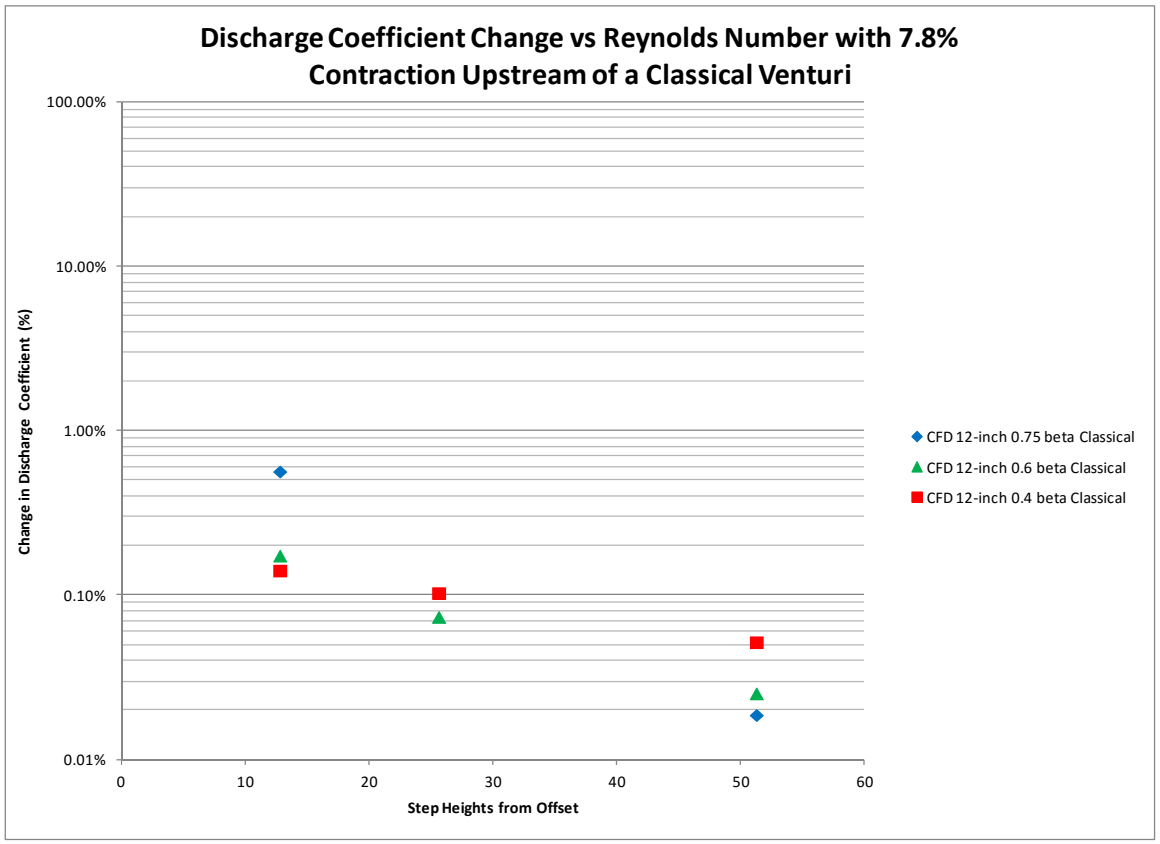


**Fig. 14. Change in discharge coefficient vs. Reynolds number for the Classical Venturi Tube with a 7.8% pipe wall contraction at various distances upstream**

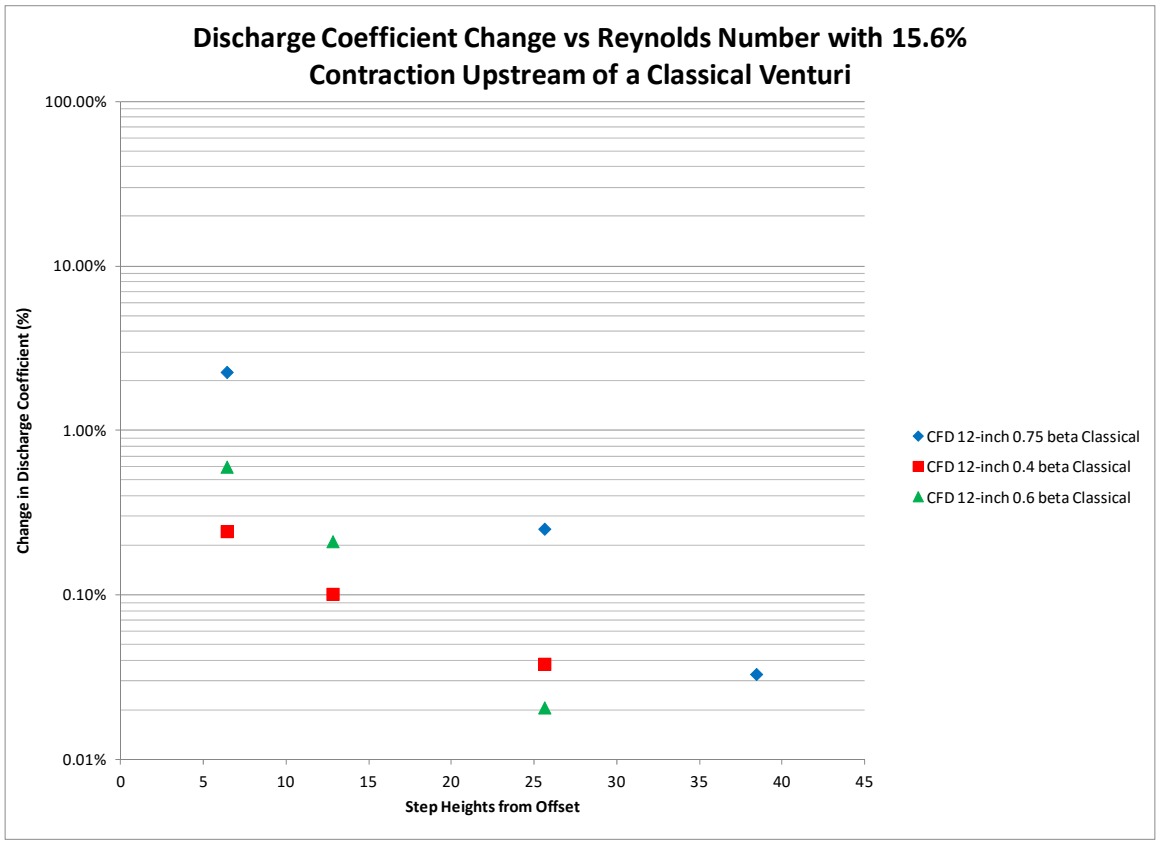


**Fig. 15. Change in discharge coefficient vs. Reynolds number for the Classical Venturi Tube with a 15.6% pipe wall contraction at various distances upstream**

In general, the data demonstrate that the smaller the beta ratio the more resilient and less affected the meter is to upstream disturbances. It appears from Figure 12 and 13 that both the 4-inch and 48-inch meter sizes require slightly more step heights than the 12-inch meter to minimize the effect of the offset on $C_d$ although there is no laboratory data for comparison in these two sizes. As compared to laboratory data, the CFD accurately predicted the effect of the offset on $C_d$ and the required distance to remove that

effect. It is the author's opinion that CFD can be a helpful tool in predicting how different piping arrangements can affect the performance of flow meters.

**Understanding the Results**

In an effort to discover why the coefficient is changed with a pipe wall offset upstream of the meter, plots were created with the CFD software showing the total energy distribution in the test domain. Figures 16 through 21 show these plots, with the total energy on the y-axis and the position in the meter on the x-axis. In essence, these plots show the energy grade line from upstream to downstream along the wall of the pipe and meter and down the centerline of the domain. The reason there is a difference in the total head along the wall and the centerline is of course because there is no velocity at the wall (no-slip boundary condition) leaving the wall pressure representing the hydraulic grade line, or just the piezometric head. All of the plots are for a 0.6 beta HVT, but each plot has a different offset scenario upstream of the meter. Figure 16 shows a baseline run with no pipe offset upstream of the meter and demonstrates the hydraulic and energy grade lines without an offset. Figures 17 through 21 show the energy plots for the scenarios showed in the contour plots of Figure 7 with a 15.6% expansion located 6.4, 12.8, 25.6, 51.2, and 64 step heights (0.5, 1, 2, 4, and 5 pipe diameters) upstream of the high pressure taps respectively. The plots also indicate the location of the high and low pressure taps.

The plots show that if there is not sufficient room for the pressure drop that occurs after the expansion to recover, the offset will affect the meter discharge coefficient.

**Table 1. A summary of the required distance between an offset and the high pressure taps such that the discharge coefficient of a Venturi is changed by less than 0.25%**

| Meter Size (inches) | Venturi Meter Type | Beta Ratio | Offset Description | Step Height (inches) | Distance from Offset To High Taps (step heights) | Distance from Offset To High Taps (pipe diameters) | Average Change in Coefficient (%) |
|---|---|---|---|---|---|---|---|
| | | | | | | | |
| 12 | HVT | 0.40 | 7.8% Expansion | 0.47 | 12.8 | 0.5 | 0.13% |
| 12 | HVT | 0.40 | 15.6% Expansion | 0.94 | 25.6 | 2 | 0.13% |
| 12 | HVT | 0.40 | 7.8% Contraction | 0.47 | 12.8 | 0.5 | 0.05% |
| 12 | HVT | 0.40 | 15.6% Contraction | 0.94 | 6.4 | 0.5 | 0.17% |
| 12 | HVT | 0.60 | 7.8% Expansion | 0.47 | 51.3 | 2 | 0.20% |
| 12 | HVT | 0.60 | 15.6% Expansion | 0.94 | 51.2 | 4 | 0.17% |
| 12 | HVT | 0.60 | 15.6% Contraction | 0.94 | 25.6 | 2 | 0.11% |
| 12 | HVT | 0.60 | 7.8% Contraction | 0.47 | 12.8 | 0.5 | 0.23% |
| 4.026 | HVT | 0.60 | 15.6% Expansion | 0.31 | 64.0 | 5 | 0.12% |
| 4.026 | UVT | 0.60 | 15.6% Expansion | 0.31 | 64.0 | 5 | 0.13% |
| 12 | HVT | 0.75 | 7.8% Expansion | 0.47 | 128.2 | 5 | 0.17% |
| 12 | HVT | 0.75 | 15.6% Expansion | 0.94 | 76.8 | 6 | 0.24% |
| 12 | HVT | 0.75 | 7.8% Contraction | 0.47 | 76.9 | 3 | 0.20% |
| 12 | HVT | 0.75 | 15.6% Contraction | 0.94 | 64.0 | 5 | 0.19% |
| 12 | Classical | 0.40 | 7.8% Expansion | 0.47 | 12.8 | 0.5 | 0.22% |
| 12 | Classical | 0.40 | 15.6% Expansion | 0.94 | 25.6 | 2 | 0.20% |
| 12 | Classical | 0.40 | 7.8% Contraction | 0.47 | 12.8 | 0.5 | 0.14% |
| 12 | Classical | 0.40 | 15.6% Contraction | 0.94 | 6.4 | 0.5 | 0.24% |
| 12 | Classical | 0.60 | 7.8% Expansion | 0.47 | 76.9 | 3 | 0.05% |
| 12 | Classical | 0.60 | 15.6% Expansion | 0.94 | 51.2 | 4 | 0.08% |
| 12 | Classical | 0.60 | 15.6% Contraction | 0.94 | 25.6 | 2 | 0.02% |
| 12 | Classical | 0.60 | 7.8% Contraction | 0.47 | 12.8 | 0.5 | 0.17% |
| 4.026 | Classical | 0.60 | 15.6% Expansion | 0.31 | 64.0 | 5 | 0.18% |
| 47.25 | Classical | 0.60 | 2.6% Expansion | 0.63 | 37.8 | 0.5 | 0.18% |
| 47.25 | Classical | 0.60 | 7.8% Expansion | 1.86 | 101.9 | 4 | 0.17% |
| 47.25 | Classical | 0.60 | 15.6% Expansion | 3.69 | 89.8 | 7 | 0.06% |
| 12 | Classical | 0.75 | 7.8% Expansion | 0.47 | 76.9 | 3 | 0.20% |
| 12 | Classical | 0.75 | 15.6% Expansion | 0.94 | 76.8 | 6 | 0.05% |
| 12 | Classical | 0.75 | 7.8% Contraction | 0.47 | 51.3 | 2 | 0.02% |
| 12 | Classical | 0.75 | 15.6% Contraction | 0.94 | 38.4 | 3 | 0.03% |

Noteworthy is the fact that all offsets, both contractions and expansions resulted in an increase of the discharge coefficient from the ideal installation. All of the CFD runs were made using a pressure boundary condition for the outlet of the model where the pressure was held to 30 psi. As there is no difference in any of these models from the low pressure taps to the outlet, the low-pressure reading of all of these scenarios remains very close to the same. The high-pressure readings on the other hand, vary as the pressure drop caused by the offset attempts to recover. These plots show that the change in $C_d$ comes from a change in the high tap pressure reading and not the low tap pressure reading.

Reynolds Number Effects

To say that there are Reynolds number effects, or Reynolds number dependency, means that a result of interest changes with Reynolds number. In this study, Reynolds number dependency would mean one of two things. It could mean that the change in $C_d$ from an offset installation to the ideal installation varied with Reynolds number or that the required distance between the offset and the meter inlet taps such that $C_d$ was no longer affected would again vary with Reynolds number. It turns out that the former is true in some flow scenarios for this study, but the required distance to have no change in $C_d$ does not depend on the Reynolds Number. For this study, the closer the offset to the meter the larger the resulting changes in $C_d$, and the more noticeable the Reynolds number effects are. However, both the CFD and laboratory data showed that as the

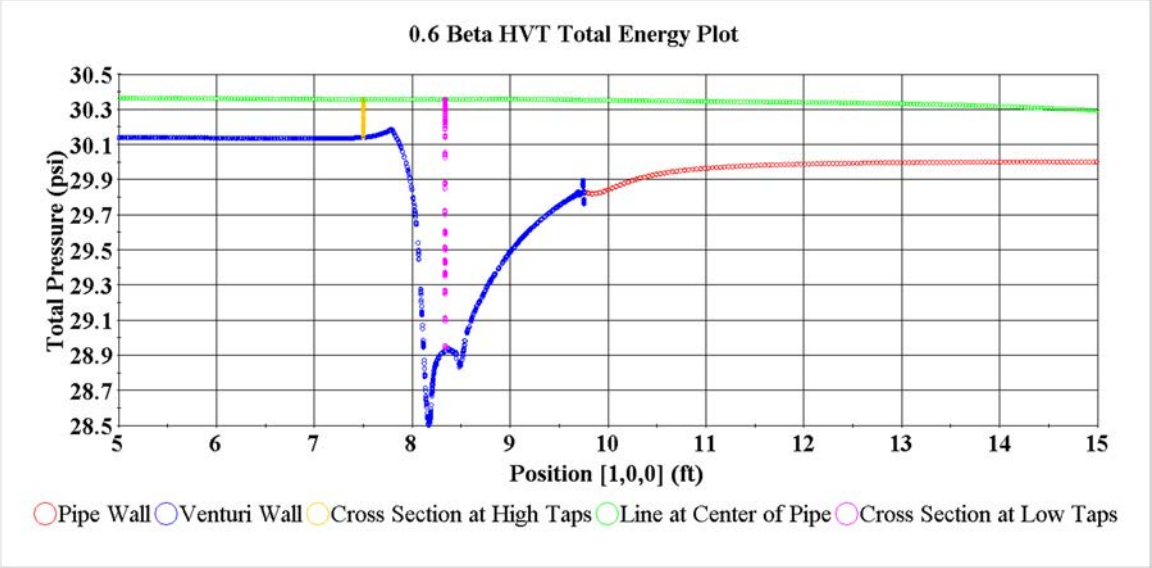


**Fig. 16. Total energy distribution for a 12-inch 0.6 beta HVT with no offset**

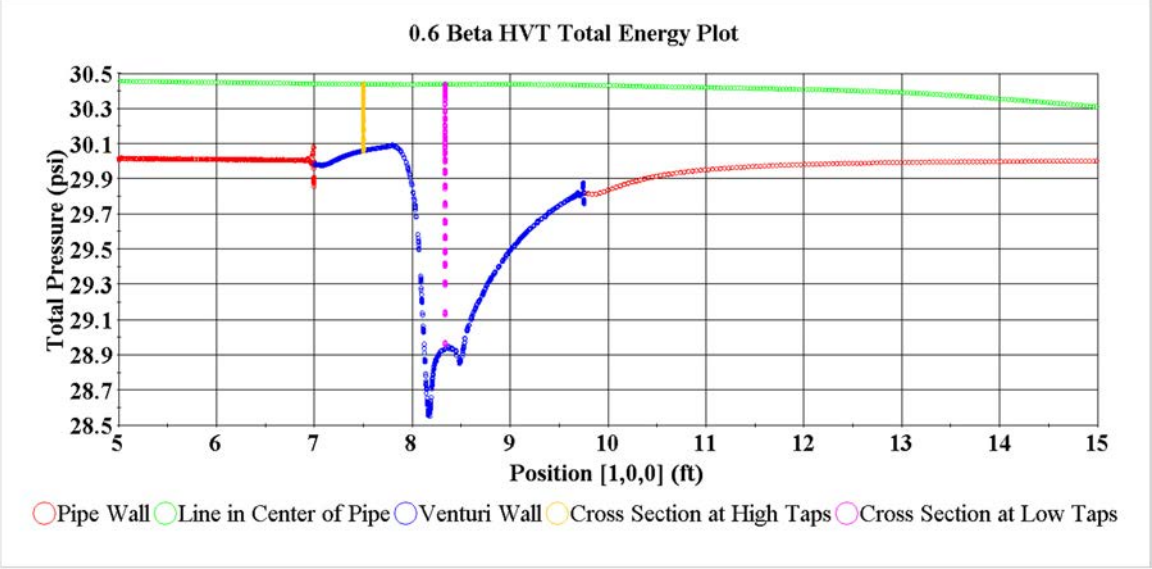


**Fig. 17. Total energy distribution for a 12-inch 0.6 beta HVT with a 15.6% expansion 6.4 step heights upstream of the high taps**

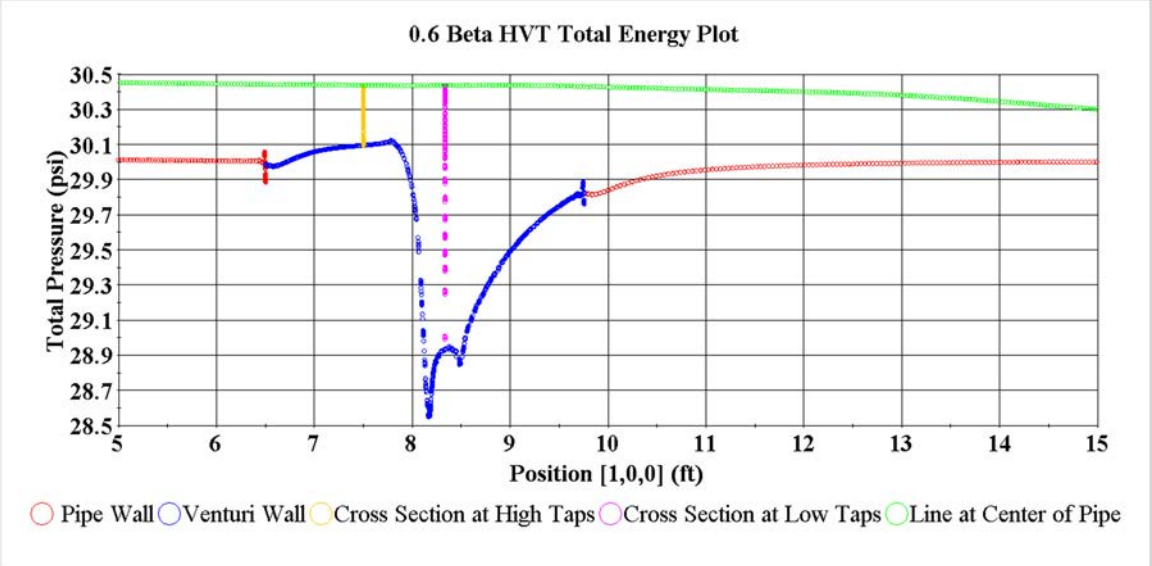


**Fig. 18. Total energy distribution for a 12-inch 0.6 beta HVT with a 15.6% expansion 12.8 step heights upstream of the high taps**

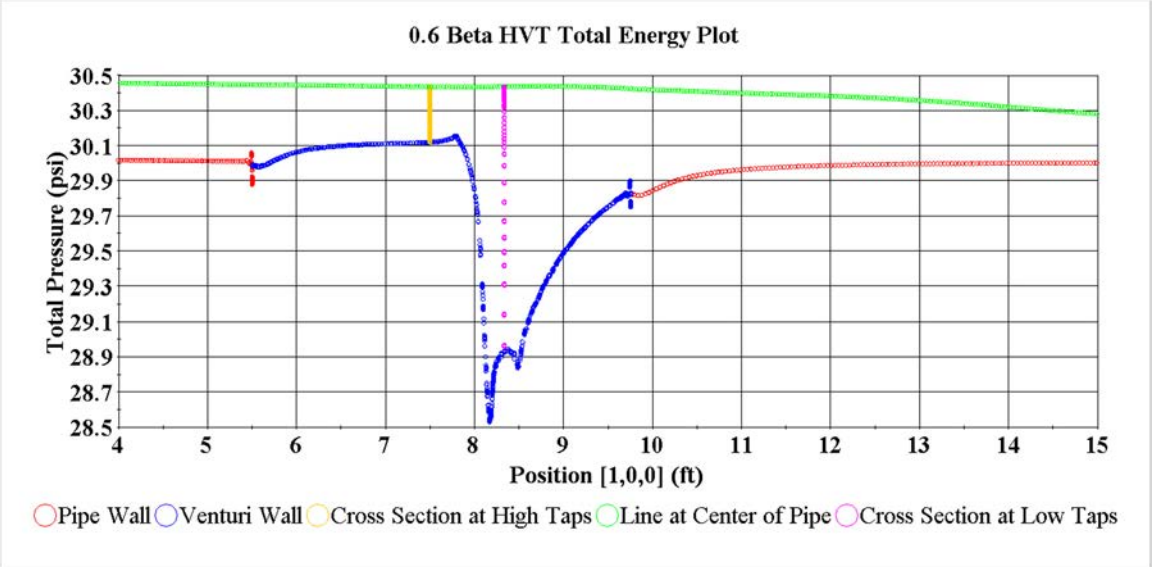


**Fig. 19. Total energy distribution for a 12-inch 0.6 beta HVT with a 15.6% expansion 25.6 step heights upstream of the high taps**

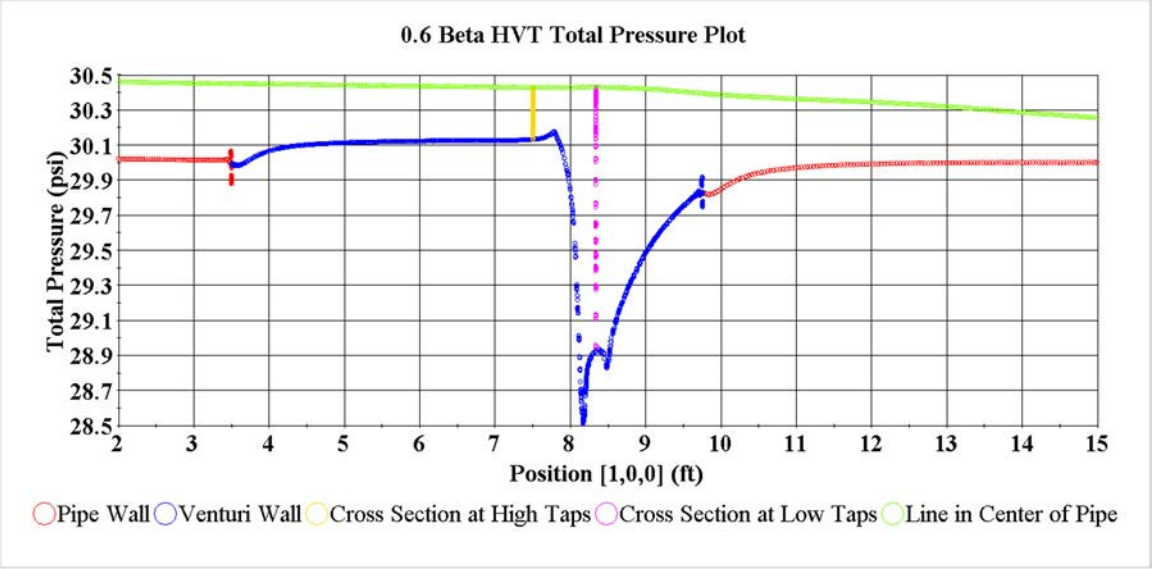


**Fig. 20. Total energy distribution for a 12-inch 0.6 beta HVT with a 15.6% expansion 51.2 step heights upstream of the high taps**

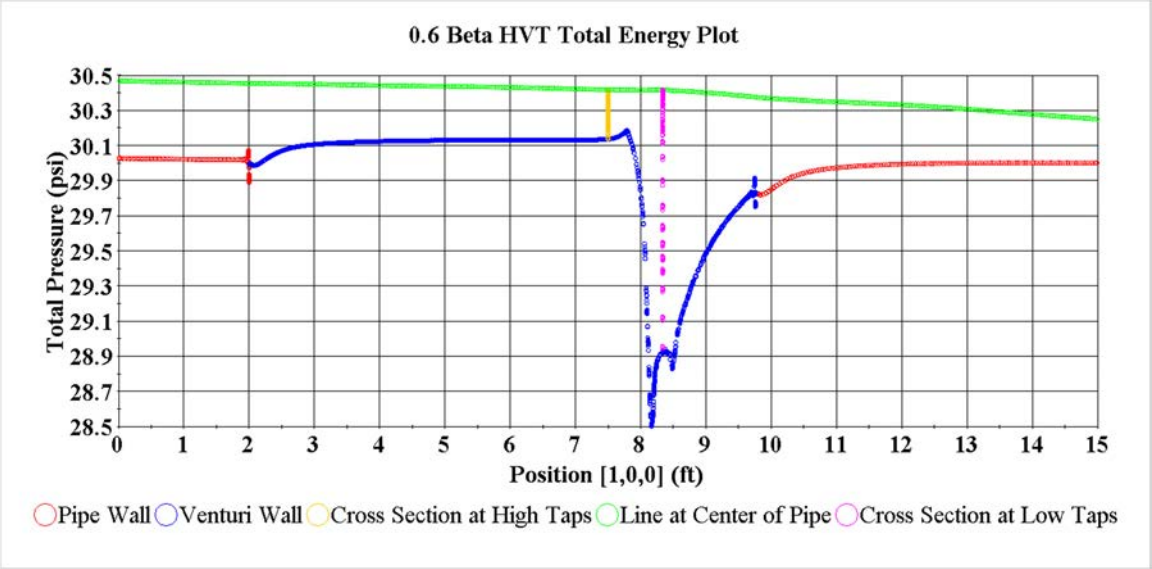


**Fig. 21. Total energy distribution for a 12-inch 0.6 beta HVT with a 15.6% expansion 64 step heights upstream of the high taps**

distance between the offset and the meter increase, the Reynolds number effects decrease. Figure 22 shows the change in $C_d$ plotted versus Reynolds number for a 0.75 beta ratio HVT for three different distances from the offset to the meter. The offset is a 15.6% contraction, so the step height is 0.937-inches, and the plot shows data with the offset at 6.4, 25.6 and 51.2 step heights away from the meter inlet taps.

As shown in the figure the change in $C_d$ varies over the Reynolds number range when the offset is 6.4 step heights away but once the offset is 25.6 or 51.2 step heights away there are no longer Reynolds number effects. It should be noted that the Reynolds number effects were the most severe with larger beta ratio meters and with sudden contractions instead of expansions. It should also be noted that the required distance where there is no longer any change in $C_d$ does not depend on Reynolds number.

**Using the Results**

The results of this study predict the change in the discharge coefficient $C_d$ for sudden changes in pipe diameter at different distances upstream of a Venturi. This paper can act both as a guide for how far a Venturi meter needs to be installed to minimize or even remove the effect of the offset and gives guidance to the affect the offset can have on the $C_d$ of the meter if the meter installation is closer to an offset than desired.
This study also provides more assurance of the capabilities of CFD. For example, if a meter installation has to be less than ideal, a CFD investigation could safely predict to within 1%, the affect the installation could have on the meter $C_d$. This could be an alternative to modeling the piping scenario in a laboratory setting which can be more costly and time consuming than the CFD analysis.

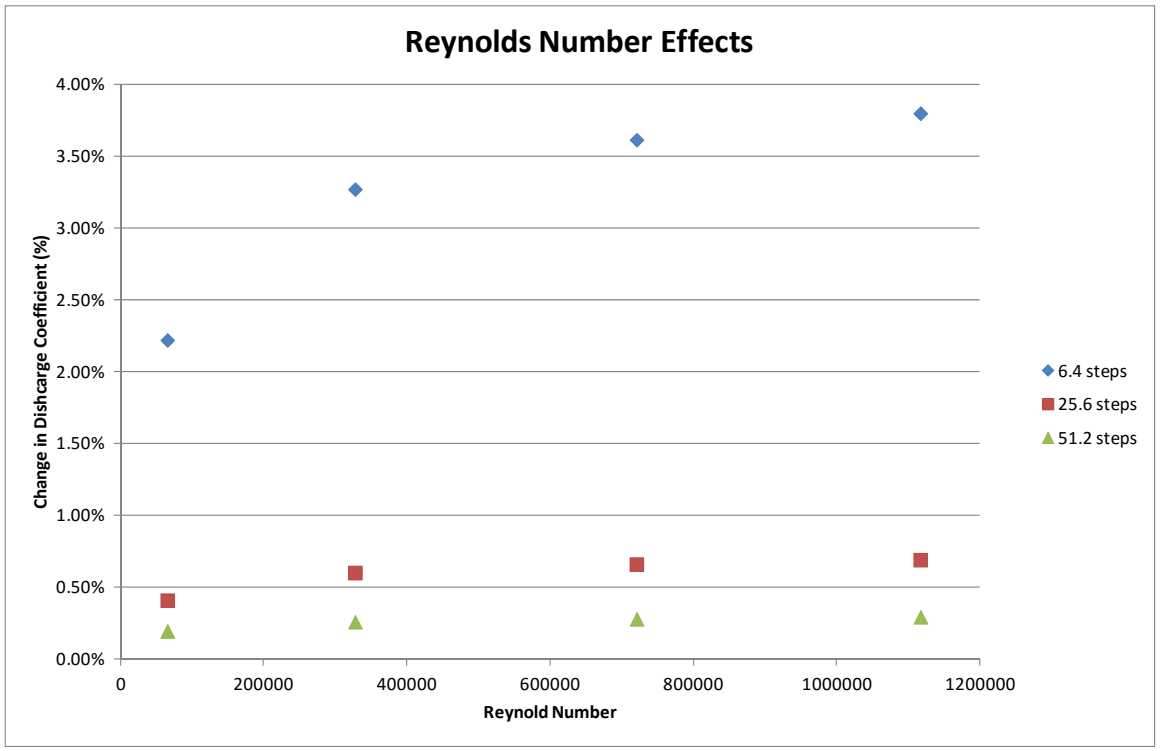


**Fig. 22. Reynolds number effects on the discharge coefficient of a 0.75 beta ratio HVT with varying distances between the offset and the meter**

## Discussion and Conclusions

This study used physical and numerical data to determine the distance required from a sudden pipe expansion or contraction to the inlet taps on a Venturi flow meter so the Venturi discharge coefficient ($C_d$) is no longer affected by the offset. Three different beta ratios of 0.4, 0.6, and 0.75 were analyzed on 2 different types of Venturi flow meters including the Classical Venturi tube, the Halmi Venturi Tube. A beta ratio of 0.6 was also tested on the Universal Venturi Tube design for comparison. Line sizes of 4-inches, 12-inches, and 48-inches were investigated to determine if line size can change the results for a given offset or for a given relative offset. A broad Reynolds number range was

investigated to determine if the required distance between a pipe diameter offset and a flow meter was Reynolds number dependant. The following list describes the key findings of this study.

- A competent CFD analysis can accurately predict both the affect a pipe offset can have on the $C_d$ of a Venturi Flow meter and the required distance between the offset and the meter such that there is no longer any affect on $C_d$.
- While each Venturi design is generally similar, the required distance from the offset to the inlet taps does slightly vary based on design.
- The smaller the beta ratio the less susceptible the Venturi is to upstream disturbances like the offset.
- When the offset is close coupled to the meter such that there was 0.5 pipe diameters from the offset to the meter inlet taps the change in $C_d$ varied slightly over a high Reynolds number range. However, the distance where $C_d$ was no longer affected was the same regardless of the Reynolds number.
- Line size has minimal affect the distance required for a relative offset to stop affecting $C_d$.
- An offset of the same size has different effects in different line sizes. In other words an offset of 0.5 inches has a more extreme effect on $C_d$ in a 4-inch line than a 12-inch line and the same offset may not have any effect in a 48-inch line.

In order to better understand the use of CFD in predicting piping effect on flow meters future research could include testing different pipe fittings upstream of meters both physically and numerically to determine if CFD can accurately predict the effect. Some pipe fittings could include elbows, two elbows, Tee's, or combinations of other pipe fittings.

It is also important to mention that CFD is not a tool to replace laboratory calibrations. One reason is that it is difficult to detect and model slight manufacturing changes from meter to meter including pressure taps and surface finish to name a few. For these reasons CFD should not be used to replace Laboratory calibrations but can be used as an effective tool for determining changes to a meter's performance based on installation effects.

# CHAPTER 4

## USING CFD TO OPTIMIZE VENTURI RECOVERY CONE ANGLES

**Abstract**

There are various applications for flow meters and often they require accurate flow measurement (0.25% of actual flow or better) while other applications accept flow measurements that are not as accurate. Some applications attempt to minimize head loss while others have ample energy such that a flow meter with higher head loss is preferred. There are also applications where there are limits on head loss imposed that a flow meter cannot exceed. In many instances where highly accurate flow measurement and low head loss are required, Venturi flow meters are a viable option. The accuracy of a Venturi for flow measurement is well established and documented, however the design of recovery cones and their associated head loss is not. This study uses Computational Fluid Dynamics and laboratory data to demonstrate the relationship between the angle of the recovery cone on common Venturi meter designs and the associated head loss. Results from this study show that to minimize head loss, the optimum recovery cone angle is a function of meter design, beta ratio, and Reynolds number. This research provides the optimal recovery cone angle to minimize pressure loss for many Venturi designs and beta ratios.

---

Coauthored by Michael C. Johnson[2] PhD, P.E., Steven L. Barfuss[3] P.E.

**Background and Literature Review**

There are many different Venturi flow meter designs with some of the designs being widely used while others are or at least started proprietary (BIF 2016, PFS 2014). The most common Venturi designs include the American Society of Mechanical Engineers (ASME) Venturi (or classical by some codes), Halmi Venturi Tube (HVT), Universal Venturi Tube (UVT), nozzle Venturi, low loss Venturi, and the Dahl Tube. This research will include the first 4 meters listed, which are the ASME, HVT, UVT, and nozzle Venturi because the Dahl tube is not used as commonly. Design details for the ASME Venturi and nozzle Venturi are covered in design Code Manuals while the other two are, or began as proprietary designs (ISO 2003, ASME 2007). In the ASME code, the design for the ASME Venturi includes a design for a machined, fabricated, and as-cast Venturi. In the code, the machined and fabricated designs have the same specifications for radii entering and exiting the throat, the as-cast design is different however, and was also used in this research.

There has been research performed on Venturi flow meters to determine installation effects on discharge coefficients including several pipe fittings and valves. The literature is laden with information providing guidance on Venturi installation (Baker 2000, Baker 2003, Miller 1996, Rapier 1981, ASME 2005). Research on Venturis has also been performed using Computational Fluid Dynamics (CFD) for various reasons in recent years due to the proliferation of commercially available CFD solvers and modern computing power. One study used CFD to analyze the trend of discharge coefficients on

multiple differential pressure flow meters over a wide Reynolds number range (Hollingshead et al. 2011). Hollingshead showed success in calculating discharge coefficients using CFD compared to laboratory data then used CFD to extend the Reynolds number range of the flow meters. This particular research also showed the great flexibility researchers could have using CFD. Hydraulic laboratories are often limited in flow rates and pressure, which correspondingly prevents them from taking data over the Reynolds number ranges that were investigated by Hollingshead with CFD. While CFD is not a replacement for a laboratory calibration, it is a useful tool for identifying performance trends or relative differences associated with changes in meter design. Prajapati also showed good success using CFD in flow metering applications (Prajapati et al. 2010). Their research used CFD to determine the permanent pressure loss of different differential producing flow meters including a Venturi meter, Wedge meter, V-Cone meter, and concentric Orifice plate. CFD has also been used to study flow characteristics in multiple pipe fittings including elbows, valves, and tees (Ramamurthy et al. 2006).

Lacking CFD, Gibson showed experimental data for gradual expansions in circular, square and rectangular conduits that showed the angle in which the head loss is minimized through the expansion (Gibson 1908). His results showed that for circular and square conduits, regardless of the ratio of pipe diameters, the inclusive angle in which head loss was minimized was 5.5 degrees. Gibson also showed that for different area ratios of rectangular pipe the expansion angle in which the head loss was minimized was near 10 degrees. This information is often referred to in literature as the Gibson method

for Venturi recovery cone design. The research lacks important information such as how long the pipe was prior to the expansion leaving the development of the flow profile in question. It is also uncertain if this data can be applied to Venturi recovery cone designs as the flow profile will be different in straight pipe versus the relatively short length in the throat of a Venturi.

The ASME MFC code on fluid flow measurement in pipes lists acceptable ranges for the recovery cone of the ASME Venturi flow meter being between 7 and 15 degrees inclusive (ASME 2007). It also lists head loss information for a meter with the 7-degree cone and a 15-degree cone but nothing in between. This code also gives the design information for a nozzle Venturi in which the recommended inclusive recovery cone angle (RCA) is less than or equal to 30 degrees.

Fluid mechanics text books also provide information on this topic and show similar curves to that of Gibson (Finnemore and Franzini 2006). The head loss in a gradually expanding cone comes from two sources. First is the friction of the fluid along the wall of the cone and the second is the head loss associated with the turbulence of the fluid. Relatively, the head loss associated with the turbulence is usually the greater loss. With that understanding, to reduce the pressure loss in Venturis there needs to be a balance between the two sources of loss. If there is too much friction loss then the length of the meter is too long so the friction is the predominant source of loss. If there is too much turbulent loss the angle of the recovery cone is too large leading to separation of the flow and no wall friction in the recovery cone. The optimal RCA occurs when each

source of loss is optimized such that when combined the pressure loss of the meter is minimized.

There are many applications where minimizing the head loss is of interest. One case in point was a recent project at the Utah Water Research Laboratory where design criteria for a choking Venturi to be used in a nuclear application was supplied. The Venturi needed to be near a 0.24 beta ratio (defined as the ratio of the throat diameter to the inlet diameter) to choke under the conditions given and have a permanent pressure loss not exceeding 7% of the corresponding meter differential pressure. A combination of CFD and laboratory testing was employed to optimize the recovery cone design to meet the requirements.

The present research used Computational Fluid Dynamics along with laboratory data to show the relationship between the RCA on a Venturi and the head loss characteristics. Study results show that to minimize head loss the optimum RCA is a function of meter design, beta ratio, and Reynolds number. The focus of the research was on how sensitive recovery cone design can be to pressure recovery and not only presents the optimum cone angles for minimizing pressure loss but also what design parameters effect the optimum RCA and the change in permanent pressure loss to expect with different recovery cone designs.

**Theoretical Background**

The equation used to calculate the discharge coefficient ($C_d$) for a Venturi is derived from the Bernoulli energy equation. To generalize the equation such that it can be used for compressible and incompressible fluids, conservation of mass must be maintained. A general equation to determine the discharge coefficient ($C_d$) for a Venturi is given by (Crane 2010, Miller 1996):

$$C_d = \frac{Q}{Y\frac{\pi}{4}d_f\sqrt{\frac{2g}{1-\left[\left(d_f/D_f\right)^4\right]}}*\sqrt{\Delta P\rho_f}} \tag{1}$$

where $Q$ is the mass flow rate, $C_d$ is the discharge coefficient, $d_f$ is the flowing diameter of the throat, $D_f$ is the flowing diameter of the meter inlet, $g$ is the acceleration due to gravity, $\Delta P$ is the difference in piezometric pressure between the inlet to the throat pressure tap locations, $\rho_f$ is the flowing density of the fluid, and $Y$ is the gas expansion coefficient for gasses and is 1.000 for liquids.

For meters included in code manuals, the shape of the meter profile and the location of pressure taps where $\Delta P$ is measured are clearly dictated. For other meters, manufacturers have design conditions as to the shape of the meter profile and the location of the pressure taps. For determining the permanent pressure loss caused by a Venturi, current codes state that pressure taps at least one pipe diameter upstream and six pipe diameters downstream of the Venturi should be used. The measured value obtained from these pressure tap locations becomes the gross permanent pressure loss of the meter. The

net pressure loss is then determined by removing the Venturi from the line and testing the same pipe and same pressure taps with no meter in the line. The difference in the readings becomes the net permanent pressure loss which is often related to the $\Delta P$ by dividing the pressure loss by the $\Delta P$ so the loss is reported as a percentage of the meter's differential pressure as measured between the high and low pressure taps (ISA 2008, ISO 2003, ASME 2007).

**Experimental Procedure**

All data for this study were collected at the Utah Water Research Laboratory (UWRL). This study was designed to determine the optimum RCA for different Venturi designs. Laboratory data were collected on a 12-inch ASME Venturi and a 12-inch HVT. The meters were tested over inlet Reynolds numbers ranging from 60,000 to 1,200,000. The flow meters were provided to the UWRL for experimental and research use and each had a beta ratio of approximately 0.60.

Once the permanent pressure loss of the meters was determined, CFD was used to reproduce the experiment. The meters were modeled per manufacturing drawings provided by the meter manufacturer. The pipe in the CFD model was meshed such that a surface roughness could be included in the model to produce the same pressure loss as was found for the laboratory steel piping. Since the meters that were tested were fabricated, the same roughness was then used in the meter body as the pipe with the throats of the meters being modeled much smoother than the meter body. For

comparison, the CFD models were also run with the wall of the whole Venturi modeled as a smooth surface to assess how the optimum recovery cone was affected by surface roughness. The CFD models were tested over the same Reynolds number range as the laboratory tests and the results were compared.

As shown in the experimental results section, the CFD and physical data for the 12-inch meters compared well. To gain more confidence in the CFD, additional laboratory data were collected for different meters and beta ratios and again CFD was used to simulate the same tests. Once confidence in the CFD was achieved the CFD simulations were then expanded for different Venturi designs, beta ratios, and a wider range of Reynolds numbers. Multiple RCAs were then tested for each combination of meter design, beta ratio, and Reynolds number.

**Experimental Results**

At the conclusion of this study, over 500 CFD data runs had been completed. Each of the five Venturi designs was tested with two surface finishes, at least four RCAs, and the Reynolds number and beta ratio information shown in Table 2. It is understood that some of the beta ratios tested fall outside of some of the recommended limits indicated by code and/or manufacturer, however because the intent of the testing was to provide guidelines for cone design, the authors felt it important to cover a wide beta ratio range for all meter designs.

**Table 2. The beta ratio and Reynolds numbers tested with CFD for each Venturi design**

| Beta Ratio | Inlet Reynolds Number | | | | |
|---|---|---|---|---|---|
| | 60,000 | 300,000 | 1,000,000 | 3,000,000 | 5,000,000 |
| 0.2 | X | X | X | | |
| 0.4 | X | | X | X | |
| 0.6 | X | | X | | X |
| 0.75 | X | | X | | X |

The primary objective for the study was to determine the optimum RCA required to minimize permanent pressure loss for different Venturi designs with varying beta ratios. Noteworthy is that prior to completing all of the CFD runs, some were simulated using progressively finer meshes until the solution was mesh independent and grid convergence occurred. As stated earlier, in order to match the laboratory data, friction had to properly be accounted for in the mesh. Therefore, for the rough runs, while each mesh was finer, the wall treatment was adjusted accordingly such that each mesh had the same fiction factor as the laboratory piping.

Grid Convergence and Model Parameters

In order to determine the numerical uncertainty due to the mesh a procedure from the AMSE Journal of Fluids Engineering was followed (Celik et al. 2008). In general the procedure states that at least three meshes should be tested each with an average cell size at least 1.3 times greater than the next mesh. During this study, four independent meshes were used to determine the Grid convergence index (GCI) for gross loss on an ASME Venturi. This was done both for 0.20 beta ratio and 0.60 beta ratio designs, and the GCI for the discretization error did not exceed 0.5%. Table 3 shows a summary of the mesh

convergence exercise performed on these two Venturi meters where ϕ is the gross loss of the different Venturi designs and other variables are defined by Celik.

**Table 3. Shows GCI for two numerical runs where GCI is less than 0.5%**

| Grid Convergence Index Runs | | |
|---|---|---|
| Parameter | 0.2 Beta | 0.6 Beta |
| $R_{21}$ | 1.400 | 1.429 |
| $R_{32}$ | 1.429 | 1.400 |
| ϕ1 | 189.098 | 27.747 |
| ϕ2 | 192.358 | 29.048 |
| ϕ3 | 192.557 | 28.962 |
| P | 8.879 | 7.188 |
| Q(p) | -0.188 | 0.144 |
| S | 1 | 0 |
| $\phi^{21}_{ext}$ | 188.92 | 27.64 |
| $\phi^{32}_{ext}$ | 192.35 | 29.06 |
| $e^{21}_{a}$ | 1.724% | 4.689% |
| $e^{21}_{ext}$ | 0.092% | 0.393% |
| $GCI^{21}_{fine}$ | 0.11% | 0.49% |

While the full grid convergence procedure was not completed on all 500 runs of this study, it was assumed that due to the commonality of each run, the baseline grid convergence tests that were performed were sufficiently applicable to all other similar geometries that were tested. The CFD code used for this research was STAR-CCM+ version 10.06 by CD-adapco which is a double precision code using the finite volume method (CD-adapco 2016). All numerical methods used were at least 2$^{nd}$ order accurate and all residuals were reduced by at least four orders of magnitude prior to stopping the

solutions. The differential pressure and gross loss of the Venturi were also monitored prior to stopping the simulations.

The inlet boundary condition for all CFD runs was taken from a fully developed flow profile in which the velocity, turbulent kinetic energy, and turbulent dissipation rate were used and input at the inlet of each model. As previously stated, the wall boundary condition was modeled both as smooth and rough surfaces and when modeled rough, the roughness height was set such that the numerical pipe friction matched that of laboratory piping. When the wall was modeled as smooth the wall Y+ values were targeted to be one and varied between 0.5 and 3 when there was flow separation. When the wall was modeled as rough the wall Y+ values were targeted between 30 and 50 but varied as low as 20 and high as 100 which is acceptable per STAR-CCM+ literature. The outlet boundary condition was set as a pressure boundary in which an appropriate pressure was maintained in which the pressure throughout the domain always remained positive. The inlet and outlet boundaries were located at least two pipe diameters upstream or downstream of any measurement point in the computational domain.

In addition to the numerical uncertainties, and perhaps more important, is the fact the numerical data were compared to physical laboratory data. This comparison is shown in the next section. The uncertainty of the physical data were also performed following the ASME PTC 19.1 2005 test uncertainty standard in which all physical data had uncertainties less than 0.25% with 95 percent confidence (ASME 2006).

Comparison of CFD to Experimental Data

One of the reasons CFD was used for this research was due to the ease of incrementally changing the angle of the recovery cone and the strength of CFD for comparing differences in solutions with differing geometries. However, to gain additional confidence in the CFD results and approach, actual laboratory test data were used to compare with CFD results and to verify its accuracies. Laboratory experimental data (to which the CFD was directly compared) were collected on a 12-inch HVT with a 10-degree recovery cone, a 12-inch ASME Venturi tube with a 14.66-degree recovery cone, a 4-inch ASME Venturi with a 7-degree recovery cone, a 4-inch nozzle Venturi with a 7-degree recovery cone, and a 48-inch HVT with a 10-degree truncated recovery cone.

Because the majority of this study was done with CFD using different 12-inch meter designs, more CFD to laboratory comparisons were done for this line size. The validation done with the 4-inch and 48-inch meter sizes were a spot check of one flow condition, which compared well. Figure 23 shows the comparison of the CFD and laboratory data for the 12-inch meters in a plot of pressure loss versus Reynolds number. Figure 23 shows how well CFD tracks the permanent pressure loss over a wide Reynolds number range.

As shown in Figure 23, the agreement between the CFD and experimental data is good. It should be noted that CFD also shows good comparison of discharge coefficients for these Venturis; however this was not a critical part of this study. In fact, the absolute

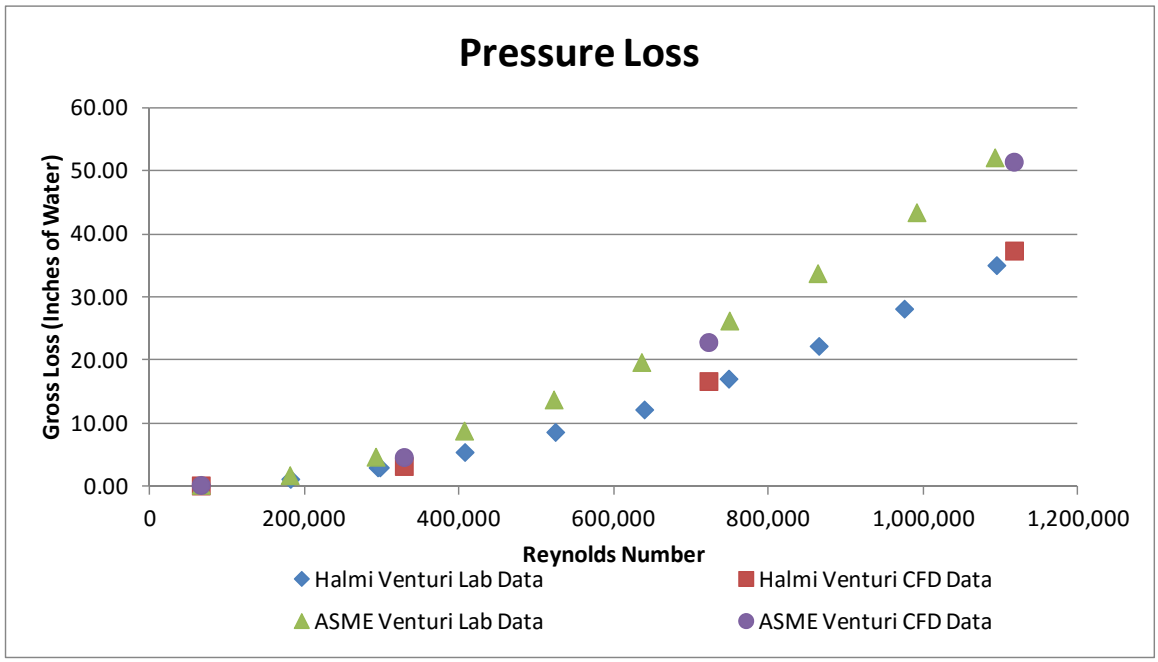


**Fig. 23. Gross loss comparison for laboratory and CFD data**

value of pressure losses is not near as important to the results of this study as the difference in pressure loss from one RCA to the other. Since no lab data were available where pressure loss is recorded for identical Venturis with different recovery cones, the ability CFD has to track both 12-inch meters, one with a 14.66-degree cone and one with a 10-degree cone, is very important to the results of the study. After the CFD model was proven reliable in doing this, it was then used to test identical Venturis with identical flow conditions while varying only the angle of the recovery cone.

CFD Results

As mentioned previously, the objective of the CFD work was to determine the optimum RCA to minimize head loss through various Venturi flow meter designs. As it

turn out this angle varies widely with different meter designs, beta ratios, Reynolds number ranges, and also with wall roughness. Optimum included RCAs were found to vary from 4.2 degrees to 14.3 degrees over all of the tests performed and as much as 8.2 degrees for one meter design. The results of this study were definitely different than the authors expected and the optimum RCAs had enough variation to be surprising. Noteworthy is the fact that the optimal RCAs do not always agree with the manufacturer or the code recommendations for the meter tested. For example, the optimum RCA for an ASME Venturi is less than 7 degrees for smaller beta ratios. Also the optimal RCA for the HVT and UVT varies from the 10 degree recommendation down to 6 degrees for the HVT and down to nearly 4 degrees for the UVT. It should be noted that the RCA directly affects the overall length of the Venturi flow meter with smaller angles lengthening a given meter design.

To determine the optimum angle, CFD data were used to develop plots of pressure loss versus RCA to be able to determine what angle would have the least head loss. In order to see what angle resulted in the minimum head loss, angles both above and below the optimum angle needed to be tested. It took some trial and error to determine what RCAs to test, so early on in the study more angles were tested than needed. Figure 24 shows velocity contour plots from the CFD of a 0.6 beta ASME Venturi for recover cones having inclusive angles of 5.5, 7, 10, and 14.66 degrees. The data from the models that produced the images in Figure 24 were then used to create Figure 25 and Figure 26. Figure 25 is a plot of the permanent pressure loss versus the RCA for a 0.6 beta ASME Venturi at an inlet Reynolds number of 1,100,000 with wall

surface roughness modeled and Figure 26 shows the same plot for the same Venturi and flow conditions with a smooth wall surface. It should be noted that Figures 25 and 26 are a small sample of the plots created for this study. On those plots, each point represents one CFD run and 24 plots were created for each of the five meters tested totaling 120 plots which are all shown in Appendix A.

In the development of these head loss versus cone angle curves, the angles tested were arbitrary since the goal was to determine the angle with the minimum pressure loss. With curves developed for each meter design, beta ratio and Reynolds number tested, the optimum RCA for each condition was determined using the developed curves. The same curves were then used to determine how much the cone angle could be increased and keep the head loss within 2% and 5% of the minimum head loss which occurs at the optimum angle of the recovery cone. Table 4 provides a summary of the results and shows the meter design, beta ratio, Reynolds number, optimum RCA for the smooth and rough Venturi, and the RCA in which the permanent head loss across the meter will increase by 2% and 5% from the optimum angle for the rough version of the full recovery cone Venturi design. Noteworthy is the fact that while the surface roughness increased the permanent pressure loss of the Venturis, the optimum RCA was not dramatically affected. For the 0.60 and 0.75 beta ratio Venturis the optimum cone angle was decreased with the rough Venturi, but not by enough to be outside of angle where the head loss would increase by more than 2%. This helps the user have confidence in the recovery cone information presented regardless of the surface finish of the meter being used.

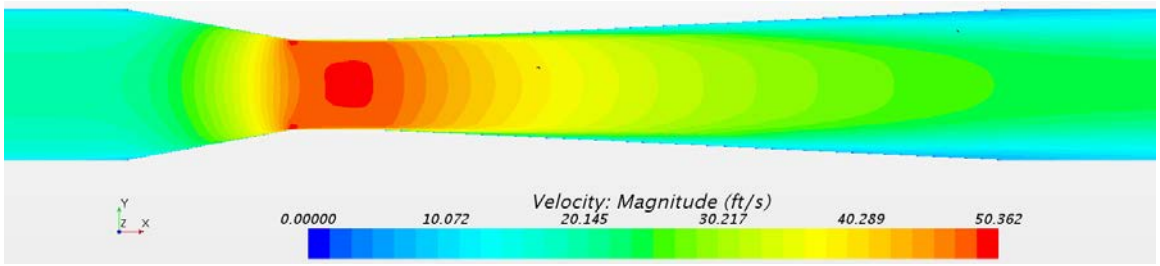


A) 5.5 Degree Inclusive Recovery Cone

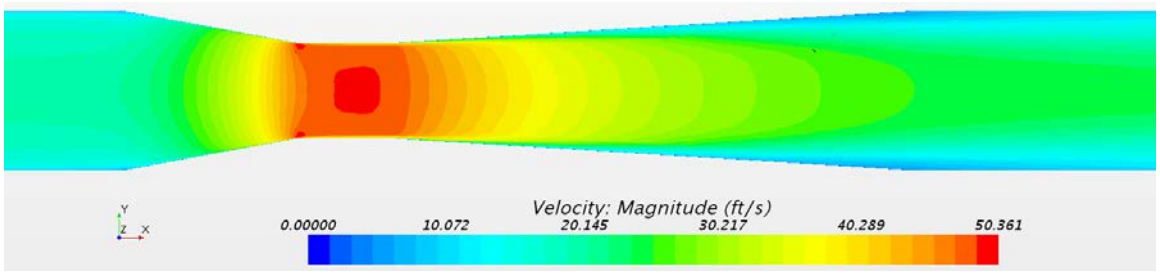


B) 7 Degree Inclusive Recovery Cone

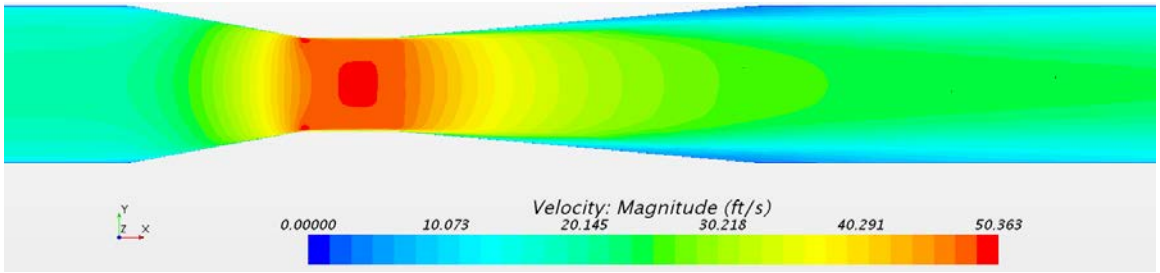


C) 10 Degree Inclusive Recovery Cone

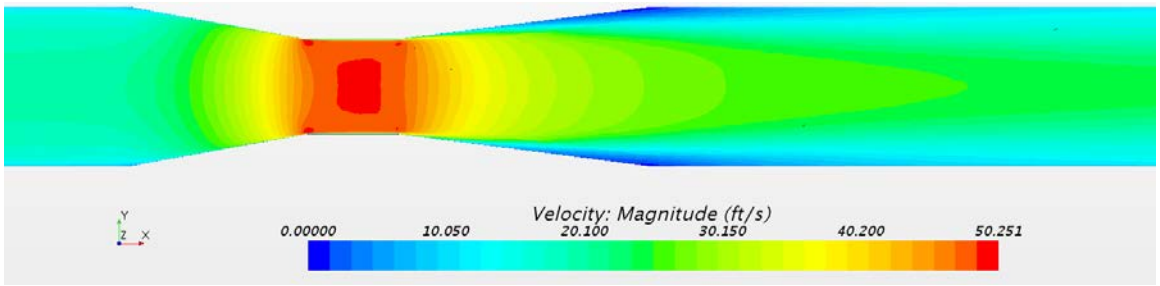


D) 14.66 Degree Inclusive Recovery Cone

**Fig. 24. CFD Velocity contour plots showing some different recovery cone angles**

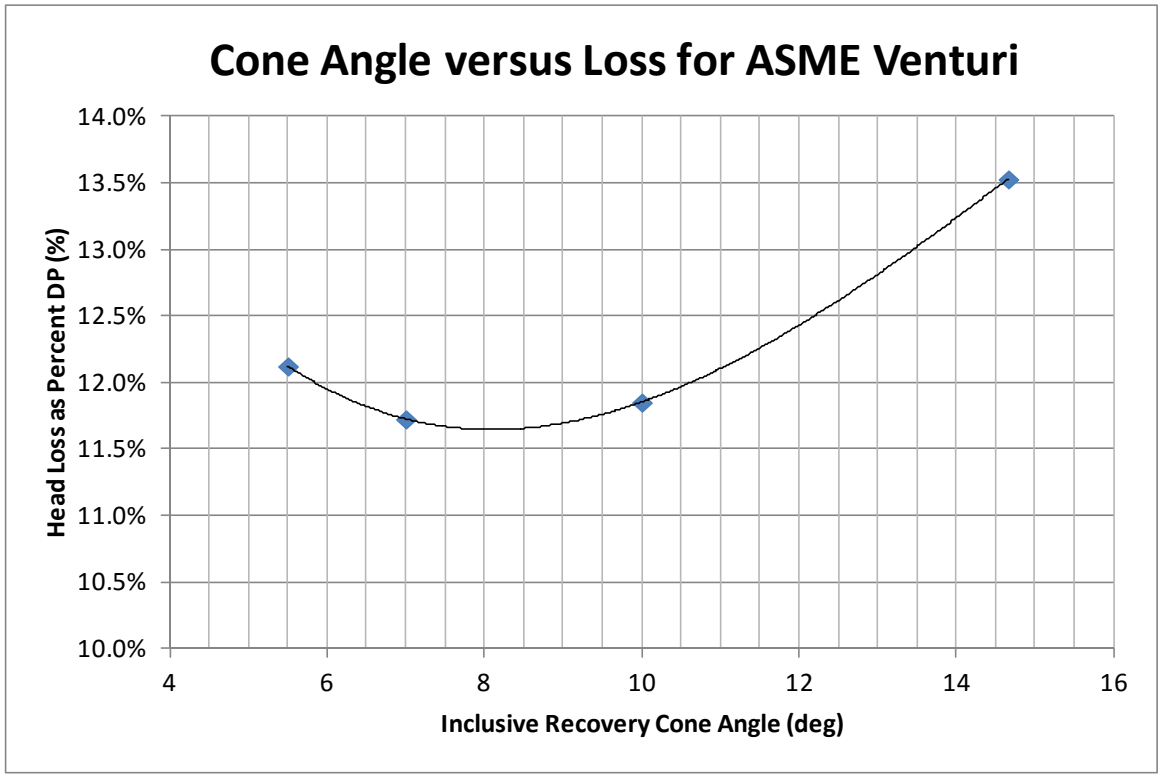


**Fig. 25. Head loss versus cone angle for a 0.6 beta ASME Venturi with surface roughness**

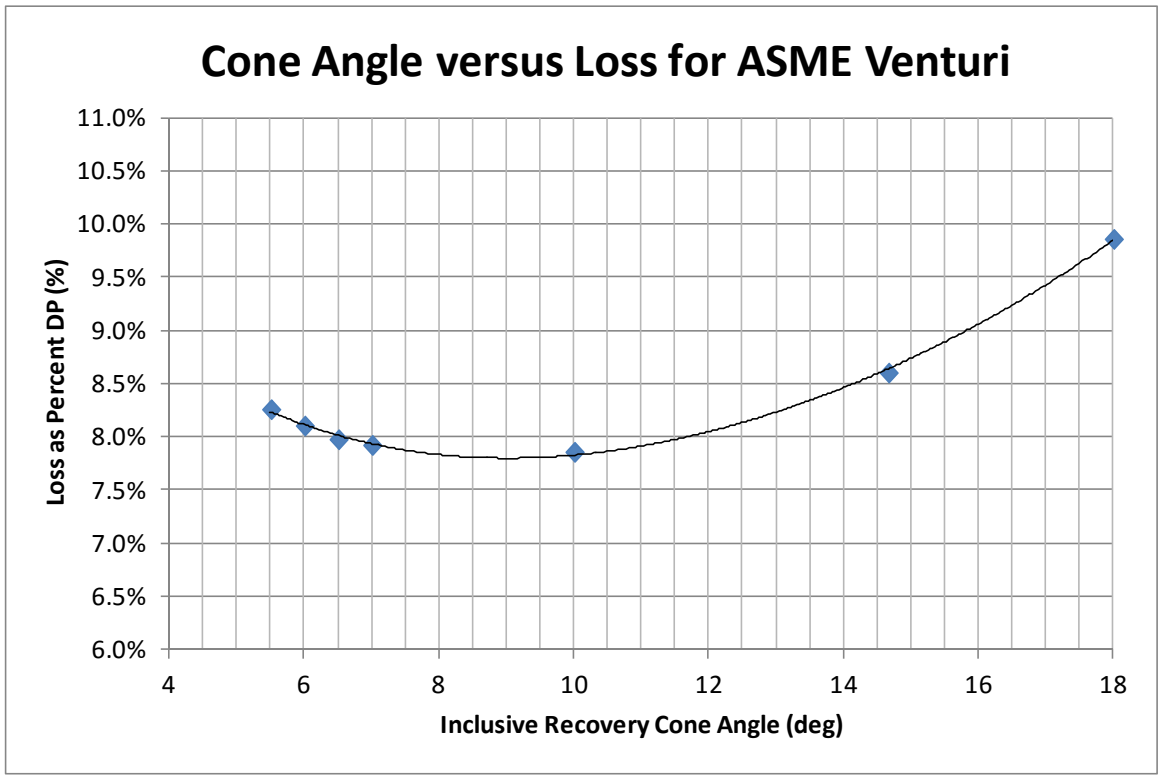


**Fig. 26. Head loss versus cone angle for a 0.6 beta ASME Venturi with smooth surface**

## Table 4. Summary of results for full recovery cone Venturi designs

| Venturi Meter Design | Meter Beta Ratio | Inlet Reynolds Number | Throat Reynolds Number | Smooth Optimum Cone Angle (degrees) | Rough Optimum Cone Angle (degrees) | Cone Angle for 2% more Loss (degrees) | Cone Angle for 5% more Loss (degrees) |
|---|---|---|---|---|---|---|---|
| | | | | | | | |
| ASME | 0.2 | 65904 | 331288 | 5.2 | 5.3 | 6.5 | 7.2 |
| ASME | 0.2 | 328240 | 1650018 | 5.3 | 5.2 | 6.4 | 7.2 |
| ASME | 0.2 | 1116665 | 5613320 | 5.1 | 5.1 | 6.2 | 7.0 |
| ASME | 0.4 | 65803 | 164654 | 5.2 | 6 | 7.4 | 8.3 |
| ASME | 0.4 | 1118327 | 2798238 | 5.8 | 5.8 | 7.0 | 7.8 |
| ASME | 0.4 | 3342164 | 8362956 | 5.8 | 5.8 | 7.0 | 7.8 |
| ASME | 0.6 | 65827 | 109971 | 7.1 | 7 | 9.0 | 10.2 |
| ASME | 0.6 | 1117207 | 1866422 | 8.7 | 8.1 | 10.1 | 11.4 |
| ASME | 0.6 | 5070032 | 8469800 | 9.7 | 7.9 | 9.9 | 11.2 |
| ASME | 0.75 | 65908 | 87890 | 10.9 | 7.2 | 9.5 | 11.4 |
| ASME | 0.75 | 1116941 | 1490592 | 12.1 | 10.8 | 14.4 | 16.9 |
| ASME | 0.75 | 5066185 | 6755900 | 12.2 | 11.9 | 16.8 | 21.6 |
| | | | | | | | |
| HVT | 0.2 | 65904 | 330540 | 5.8 | 6 | 7.2 | 8.0 |
| HVT | 0.2 | 327883 | 1644500 | 5.9 | 6.1 | 7.4 | 8.2 |
| HVT | 0.2 | 1116594 | 5599124 | 5.9 | 5.8 | 7.0 | 7.8 |
| HVT | 0.4 | 65818 | 164681 | 6.9 | 8.3 | 6.3 | 13.4 |
| HVT | 0.4 | 1118378 | 2798244 | 7.9 | 7 | 8.7 | 9.7 |
| HVT | 0.4 | 3342351 | 8362852 | 8.2 | 6.7 | 8.6 | 9.6 |
| HVT | 0.6 | 65894 | 109982 | 8.9 | 8.9 | 11.2 | 13.0 |
| HVT | 0.6 | 1117128 | 1864541 | 10.7 | 9 | 11.2 | 12.7 |
| HVT | 0.6 | 5065238 | 6340869 | 12 | 9.6 | 11.9 | 13.3 |
| HVT | 0.75 | 65892 | 87861 | 11.6 | 8.5 | 12.3 | 15.3 |
| HVT | 0.75 | 1117162 | 1489637 | 13.5 | 12.1 | 16.0 | 18.5 |
| HVT | 0.75 | 5076693 | 6774443 | 14 | 12.2 | 16.2 | 19.0 |
| | | | | | | | |
| UVT | 0.2 | 65905 | 331307 | 4.8 | 5.5 | 6.7 | 7.4 |
| UVT | 0.2 | 327815 | 1646968 | 4.6 | 4.7 | 5.9 | 6.7 |
| UVT | 0.2 | 1116551 | 5609633 | 4.2 | 4.6 | 5.8 | 6.5 |
| UVT | 0.4 | 65821 | 164682 | 5.8 | 6.3 | 7.9 | 9.2 |
| UVT | 0.4 | 1118418 | 2798267 | 5.6 | 5.6 | 7.0 | 7.9 |
| UVT | 0.4 | 3342414 | 8362678 | 5.7 | 5.7 | 7.0 | 8.0 |
| UVT | 0.6 | 65853 | 109945 | 7.5 | 7.6 | 9.8 | 11.4 |
| UVT | 0.6 | 1117479 | 1865702 | 7.7 | 7.3 | 9.4 | 11.0 |
| UVT | 0.6 | 5067082 | 8459816 | 7.5 | 7.5 | 9.6 | 11.2 |
| UVT | 0.75 | 65921 | 87916 | 10.7 | 8.1 | 11.2 | 13.5 |
| UVT | 0.75 | 1117215 | 1489972 | 11.6 | 10.7 | 14.5 | 17.3 |
| UVT | 0.75 | 5066399 | 6756800 | 12.3 | 10.9 | 14.8 | 17.6 |
| | | | | | | | |
| Nozzle | 0.2 | 65905 | 332381 | 5.8 | 5.8 | 7.0 | 7.8 |
| Nozzle | 0.2 | 327872 | 1653564 | 6.1 | 5.9 | 7.2 | 8.0 |
| Nozzle | 0.2 | 1116655 | 5592269 | 5.9 | 5.7 | 7.0 | 7.8 |
| Nozzle | 0.4 | 65810 | 164669 | 6.5 | 7.6 | 9.5 | 10.7 |
| Nozzle | 0.4 | 1119067 | 2800763 | 7.3 | 7 | 8.9 | 10.0 |
| Nozzle | 0.4 | 3341281 | 8362324 | 7.7 | 7.2 | 9.2 | 10.2 |
| Nozzle | 0.6 | 65830 | 1398521 | 8.3 | 8 | 10.2 | 12.0 |
| Nozzle | 0.6 | 1121450 | 109950 | 9.6 | 9 | 11.5 | 13.0 |
| Nozzle | 0.6 | 5086853 | 6343931 | 10 | 8.9 | 11.3 | 12.9 |
| Nozzle | 0.75 | 65891 | 87868 | 12.5 | 9.3 | 13.3 | 16.9 |
| Nozzle | 0.75 | 1123195 | 1497817 | 14 | 12.5 | 16.5 | 19.0 |
| Nozzle | 0.75 | 5087025 | 6783716 | 14.3 | 12.6 | 16.5 | 19.1 |
| | | | | | | | |
| As Cast ASME | 0.2 | 65905 | 331255 | 4.9 | 5.1 | 6.2 | 6.9 |
| As Cast ASME | 0.2 | 327853 | 1647884 | 5 | 5.1 | 6.3 | 7.1 |
| As Cast ASME | 0.2 | 1116532 | 5612011 | 4.9 | 5 | 6.2 | 7.0 |
| As Cast ASME | 0.4 | 65789 | 164767 | 5 | 5.4 | 6.6 | 7.4 |
| As Cast ASME | 0.4 | 1122592 | 2809783 | 5.7 | 5.4 | 6.7 | 7.6 |
| As Cast ASME | 0.4 | 3341906 | 8365692 | 5.6 | 5.4 | 6.8 | 7.7 |
| As Cast ASME | 0.6 | 65907 | 109829 | 6.5 | 6.2 | 8.0 | 9.1 |
| As Cast ASME | 0.6 | 1117067 | 1861491 | 7.4 | 7.1 | 9.1 | 10.5 |
| As Cast ASME | 0.6 | 5066381 | 8442786 | 7.7 | 7.3 | 9.2 | 10.7 |
| As Cast ASME | 0.75 | 65893 | 87855 | 8.3 | 6.4 | 8.6 | 9.9 |
| As Cast ASME | 0.75 | 1117135 | 1489467 | 10.5 | 9 | 12.7 | 15.0 |
| As Cast ASME | 0.75 | 5065776 | 6754157 | 11.2 | 9.8 | 14.1 | 16.5 |

**Understanding the Results**

There are many factors that contribute to the optimum angle of the recovery cone. All of the variables tested in this research ended up having some contribution to the resulting optimum angle, including; the meter design, beta ratio, Reynolds number and wall roughness of the Venturi. Each of these will be briefly discussed to show its contribution to the optimum RCA.

Meter Design: The meter design had a surprising effect on the RCA. For example, for the rough wall 0.60 beta ratio runs with the inlet Reynolds number near 5,000,000, the optimum RCA varies from 7.5 degrees for the UVT to 9.6 degrees for the HVT with all of the other designs in between. For the smooth wall 0.40 beta ratio runs with an inlet Reynolds number of 3,300,000 the optimum RCA varies from 5.6 degrees for the as-cast ASME Venturi to 8.2 degrees for the HVT with the angle for the other designs again being in between. One observation made as to why the difference from one meter to the next was the velocity profile entering and exiting the throat of the Venturi. Figure 27 shows velocity contour plots for the smooth wall 0.40 beta ratio runs with a 3,300,000 inlet Reynolds number. Note the high velocity recorded by CFD in each meter throat and the location of the reading. It appears that the meter designs with shorter inlets and smooth transitions to the throat have a high velocity near the wall at the inlet of the throat, which appears to affect the optimum RCA.

Beta Ratio: The beta ratio has the largest effect on the optimum angle of the recovery cone. For each meter design, from a 0.2 beta ratio to a 0.75 beta ratio, the smallest change in the optimum RCA was 5 degrees for the rough wall model of the

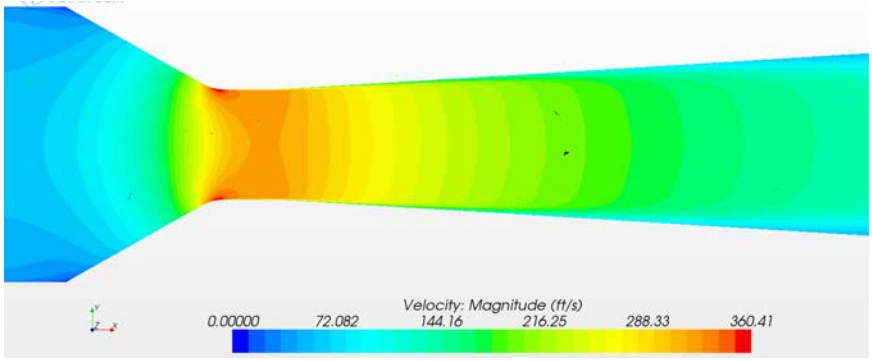


A) HVT with the optimum recovery cone being 8.2 degrees

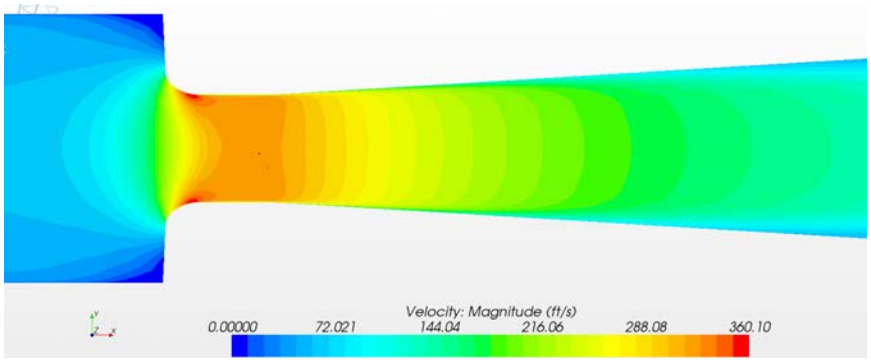


B) Nozzle Venturi with the optimum recovery cone being 7.7 degrees

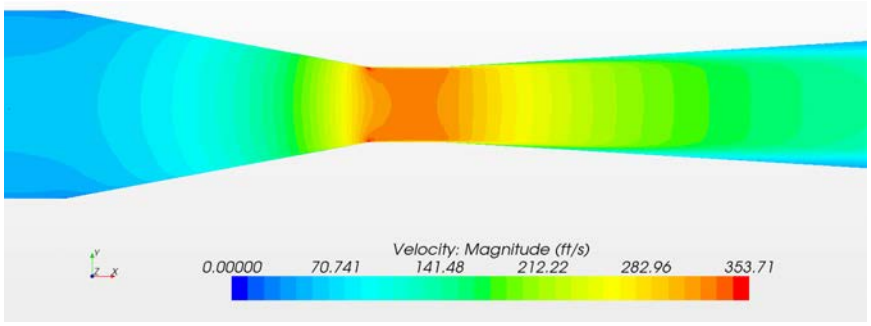


C) ASME Venturi with the optimum recovery cone being 5.8 degrees

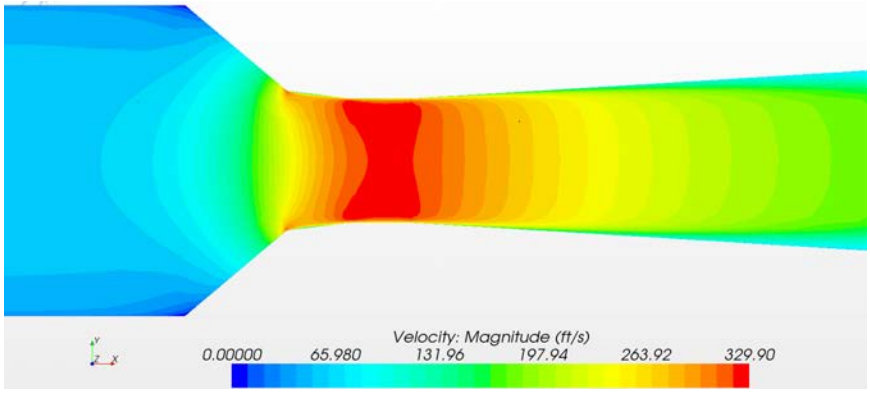


D) UVT with the optimum recovery cone being 5.7 degrees

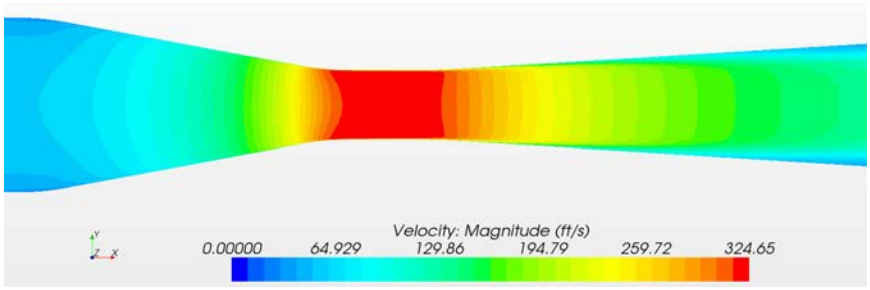


E) As-cast ASME Venturi with the optimum recovery cone being 5.6 degrees

**Fig. 27. CFD Velocity contour plots showing some different recovery cone angles**

as-cast ASME Venturi and the largest change was 8.2 degrees for the smooth wall model of the Nozzle Venturi. While there are many reasons to why there is such a large change in the optimum RCA from the beta ratio a few key ones will be discussed. One major reason as to why the RCA is different is simply due to the difference in acceleration from the inlet to the throat of meters with different beta ratios. The velocity in the throat of a 0.20 beta ratio Venturi is 25.3 times that at the inlet, a 0.40 beta is 6.3 times larger, a 0.60 beta is 2.8 times larger, and the 0.75 beta ratio meter has a throat velocity 1.8 times larger than the inlet. This may not make the difference in the optimum RCA obvious, however

when this acceleration is investigated further the CFD models show more acceleration happens near the wall then at the center line of the meters. Figure 28 shows the velocity profile at the exit of the throat of an ASME Venturi with a 0.20, 0.40, 0.60, and 0.75 beta ratio meter design respectively. As can be seen in the figure the velocity profile from one beta ratio to the next is drastically different which results is large changes of the optimal RCA. If the same velocity profiles are compared for the same beta ratio but different meter designs or different Reynolds numbers, the velocity profiles are noticeably different most of the time but the difference is not near as drastic as with different beta ratios. Figure 29 shows a plot of the optimum RCA versus the throat Reynolds number for a HVT. This plot shows how the optimal RCA changes both with beta ratio and Reynolds number and shows a much larger variation in RCA from beta ratio changes than Reynolds number changes.

Reynolds Number: Reynolds number effects on the optimum RCA exist but are small compared to the other two factors especially when the lowest Reynolds numbers tested are not included in the comparison. This is reasonable since large beta ratio meter will not be designed for Reynolds numbers less than 100,000. The largest effect from Reynolds number was for the 0.60 beta HVT where the optimum RCA changed by 1.3 degrees between inlet Reynolds numbers of 1,000,000 and 5,000,000 (throat Reynolds numbers of 1,870,000 and 8,460,000) where the smallest effect was no change in the optimum angle. It is noteworthy that the Reynolds number effects are more significant with larger beta ratio meters while with smaller beta ratio meters (0.40 and smaller) the effect was not more than 0.5 degrees.

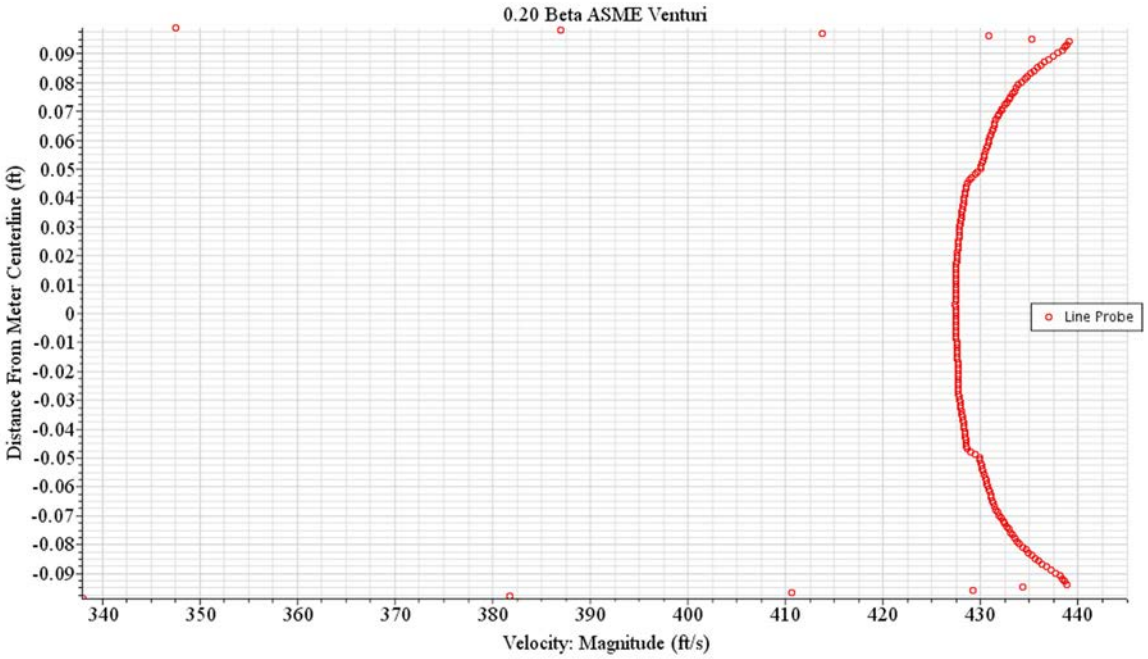


A) Velocity profile exiting the throat of a 0.20 Beta ASME Venturi

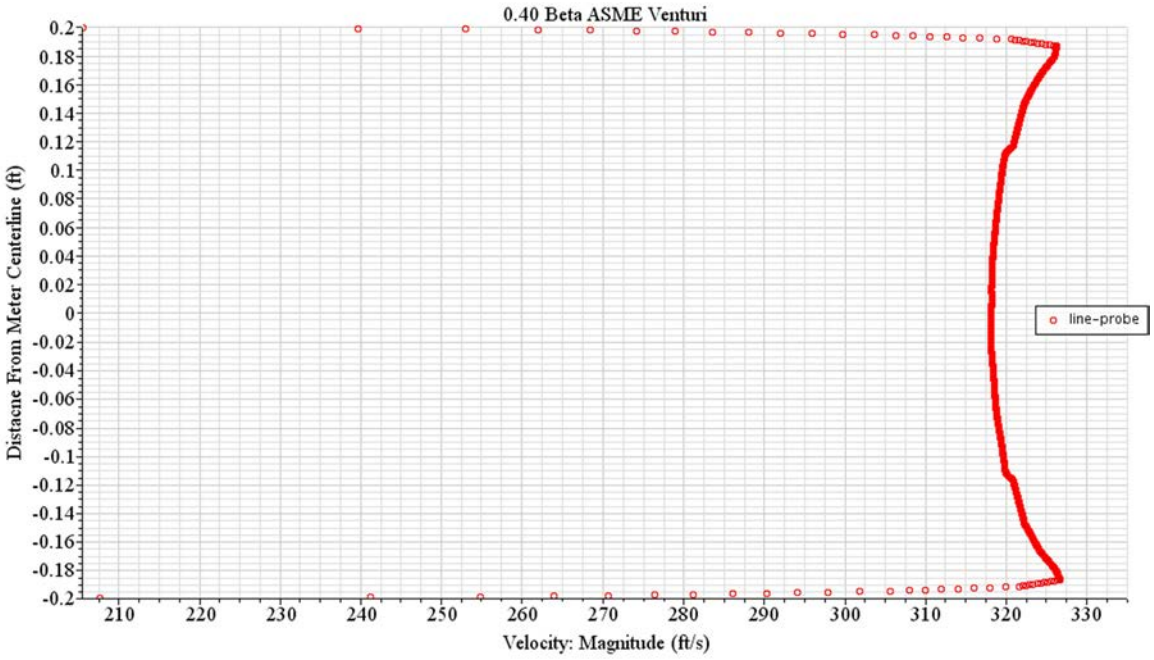


B) Velocity profile exiting the throat of a 0.40 Beta ASME Venturi

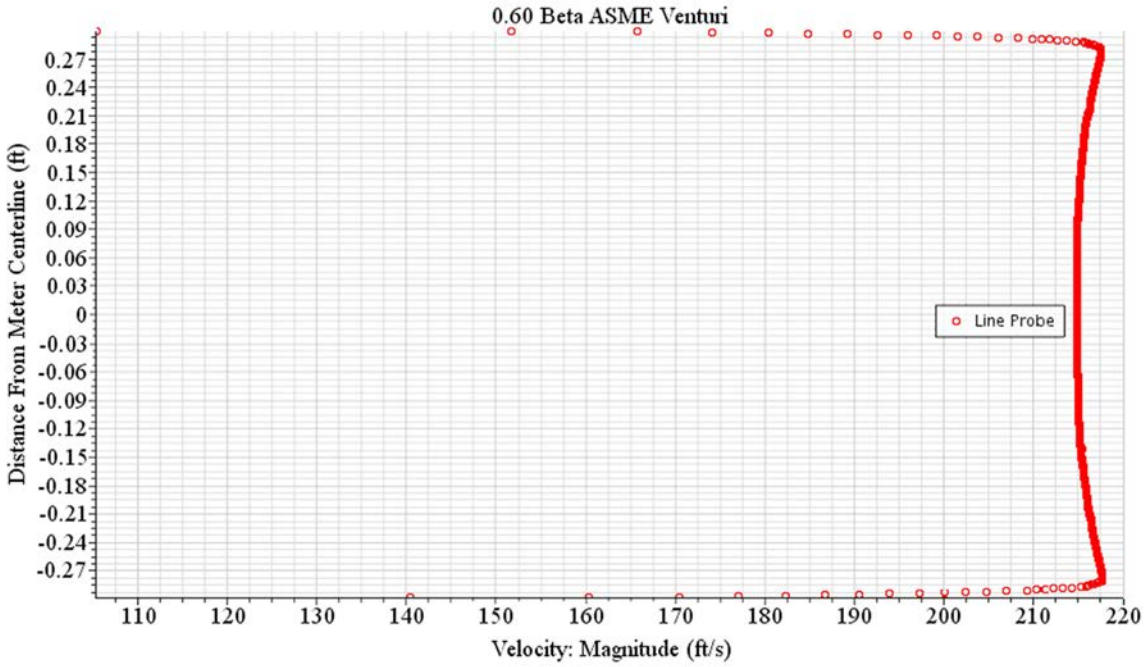


C) Velocity profile exiting the throat of a 0.60 Beta ASME Venturi

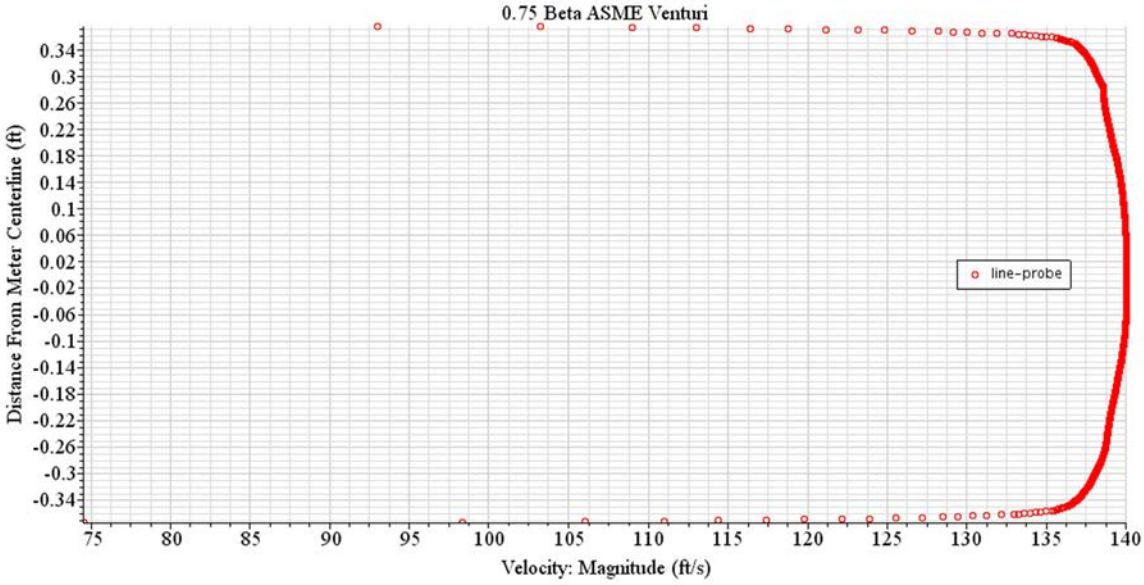


D) Velocity profile exiting the throat of a 0.75 Beta ASME Venturi

**Fig. 28. Velocity profile at the exit of the throat of an ASME Venturi**

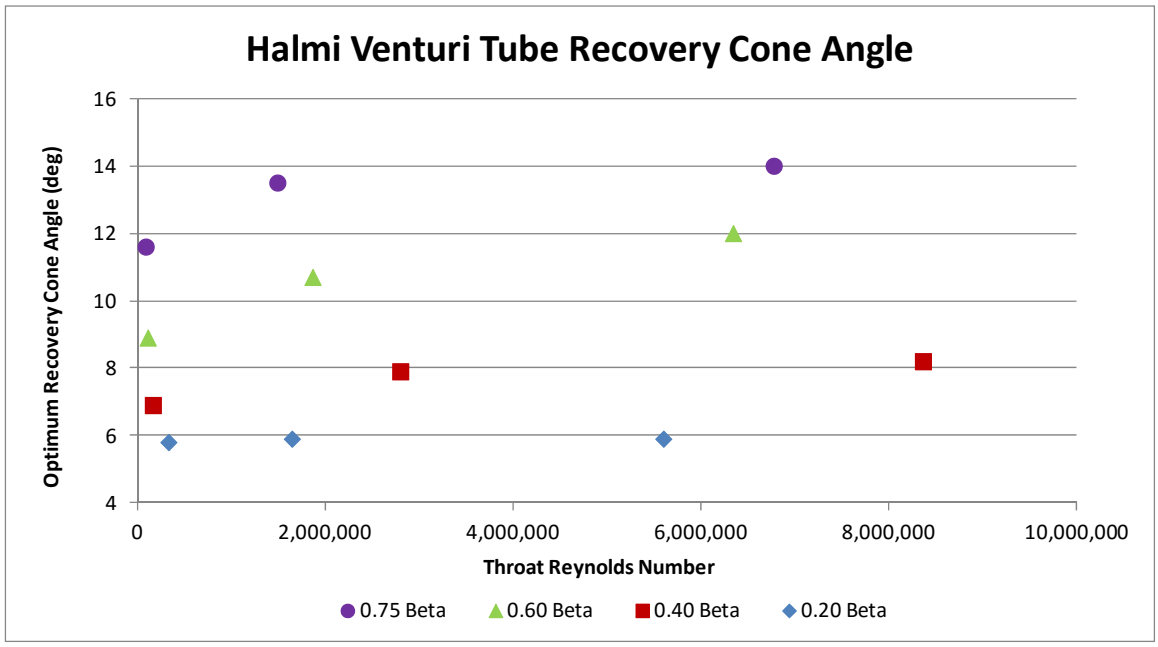


**Fig. 29. The effect that beta ratio and Reynolds number have on the recovery cone angle**

Wall Roughness: There were also wall roughness effects on the optimum RCA. These were also small and did not result in more than a 2-degree change in the optimum RCA when the beta ratio was 0.75. For beta ratios less than 0.40 there was no significant change in the optimum RCA implying that friction losses become negligible in determining the optimum RCAs for small beta ratio Venturis.

In general, the data demonstrate that the smaller the beta ratio, the smaller the optimum RCA is and the less it can be affected by Reynolds number, wall roughness and meter design. On the contrary the smoother the meter inlet and the larger the beta ratio, the larger and more susceptible to change the optimum RCA is.

**Using the Results**

This study produced optimum RCAs for a broad range of Venturi designs that can be used for most instances of various Venturi meter designs. There is no implication that the results need to be used in all recovery cone designs; however in any instance where head loss is of sufficient concern, the data can provide design guidance that was nonexistent prior to this study. The study also confirms that CFD, coupled with experimental testing, is a useful tool in optimizing the cone angle of other unique Venturi designs.

It has been stated that the ASME code calls for recovery cones angles to fall between 7 and 15 degrees inclusive. These angles work fine and result in accurate flow measurement. The CFD however, predicted optimum RCAs of 7.9 degrees for a rough wall and 9.7 degrees for a smooth wall 0.60 beta ratio ASME Venturi. If a 15-degree cone were to be used instead of either of these, the head loss would be between 9% and 15% higher. For a 0.40 beta ratio ASME Venturi the optimum recover cone angle was determined to be 5.8 degrees. In this case if a 15-degree recovery cone were to be used, the head loss would be 80% higher. In the case of a 0.20 beta ASME venturi the loss would be 150% higher if a 15-degree recovery cone were used instead of the optimal 5.1-degree included cone angle.

Each meter has a signature curve for the optimum RCA versus the recovery cone length. This is a convenient way to determine the optimum RCA for beta ratios that were not tested in this study. Figures 30 through 34 show these plots in the following order of Venturi design; ASME Venturi, HVT, UVT, Nozzle Venturi, and the as-cast ASME

Venturi. The plots include a formula to calculate the trend line for the optimum RCA curve. The plots also include a second series that shows how much the RCA can be increased (which would decrease the recovery cone length) while only increasing the head loss by 2% of the minimum, which occurs at the optimum RCA. Note that each of the plots represents the summary of least 96 data points.

Noteworthy is the fact that these plots do not indicate how much of a decrease in pressure loss one can expect by using the optimum RCA versus some other angle. This is something difficult to present in one plot however, using the plots coupled with Table 4 can provide the reader some insight (though not exact) as to how much increase in pressure loss to expect from different RCAs. For example, if one wanted to use a 10-degree included RCA on 0.4 beta UVT where the optimal angle is 5.7 degrees the following can be assumed. Since a 7-degree angle gives a 2% increase in pressure loss there is 2% in 1.3 degrees of angle increase or approximately 1.5% per degree. A 9-degree angle gives a 5% increase from the optimal recovery cone, or a 3% increase in pressure loss from the 7-degree recovery cone. That means there was a 3% increase in pressure loss over a 2-degree increase in recovery which again equates to approximately a 1.5% pressure loss increase per degree of RCA increase. One can then assume that a 4.3-degree increase in RCA from 5.7 to 10 degrees would then produce a 6.5% (1.5 x 4.3) increase in pressure loss. This type of procedure can be used for any meter with the table or simply by using the plot and assuming a linear increase in head loss past the 2% pressure loss increase line.

It should also be mentioned that in order to determine the exact optimal angle of the recovery cone, an iterative solution will be required. In other words, one can look at the plot and get a good idea of the recovery cone length and angle needed; however after designing the meter the length and angle should then be plotted to see how the design compares to the optimal angle. If it plots above the line there will be an increase in head loss, if it plots below the line the meter is being built too long and there will also be an increase in head loss. It is also well understood by the authors that recovery cones as long as ten inlet diameters can be difficult and very costly to build. In some of those cases these data still provide some design criteria as to how much increase in head loss will result from shortening the meter and allow the meter designer the ability to optimize the meter design to minimize head loss and manufacturing costs.

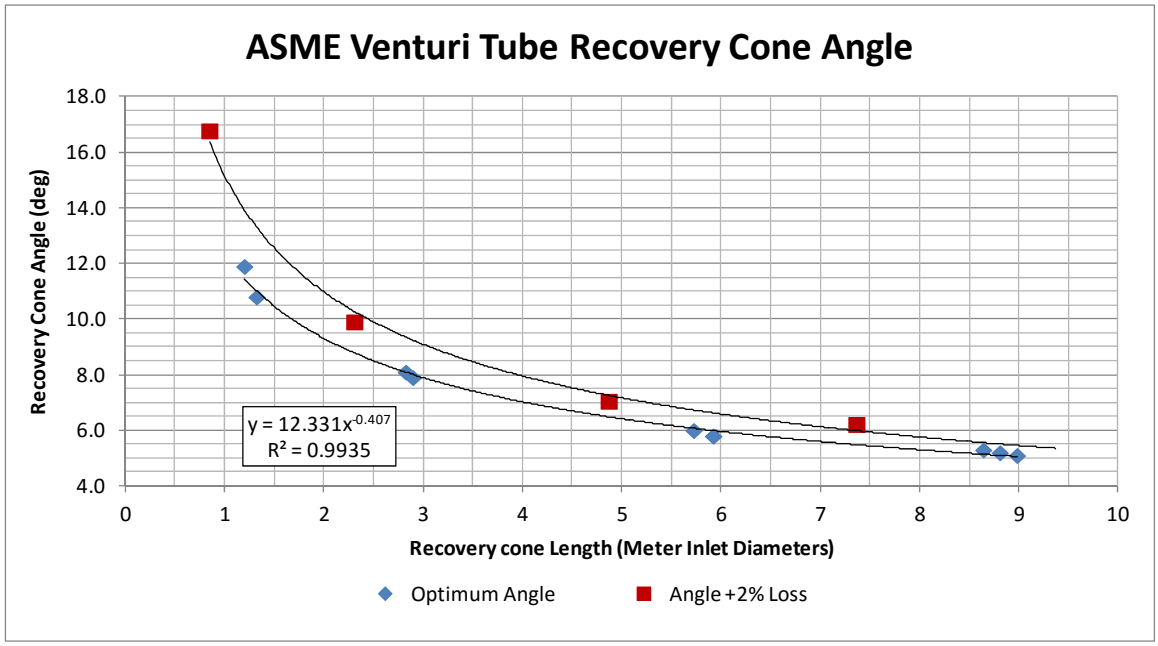


**Fig. 30. Optimum recovery cone angle versus recovery cone length for ASME Venturi**

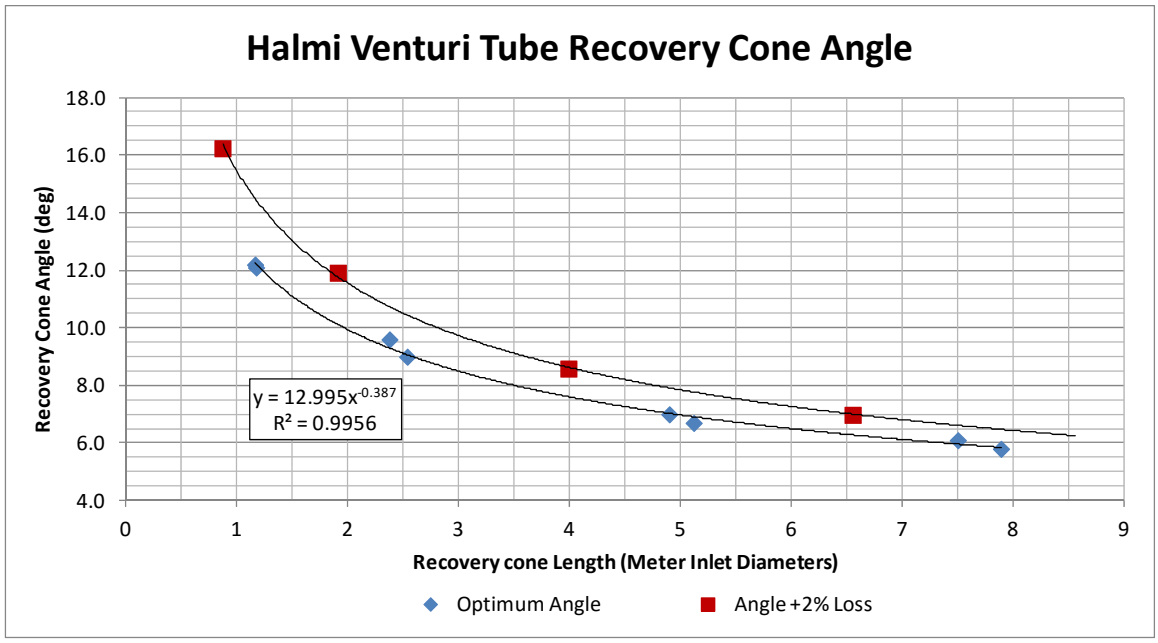


**Fig. 31. Optimum recovery cone angle versus recovery cone length for HVT**

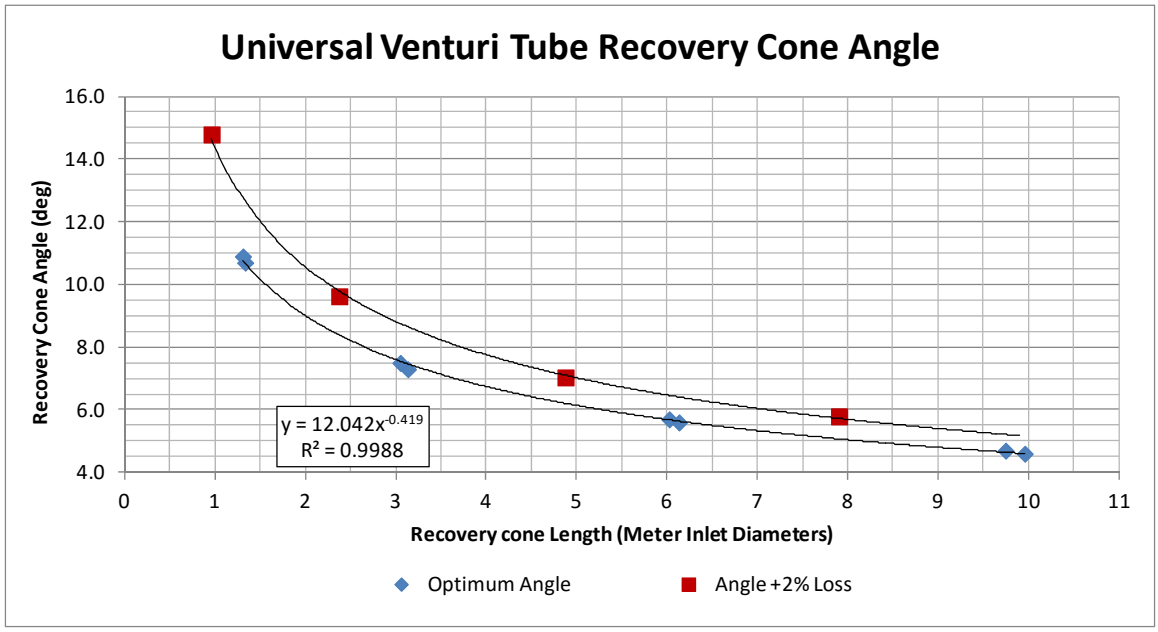


**Fig. 32. Optimum recovery cone angle versus recovery cone length for UVT**

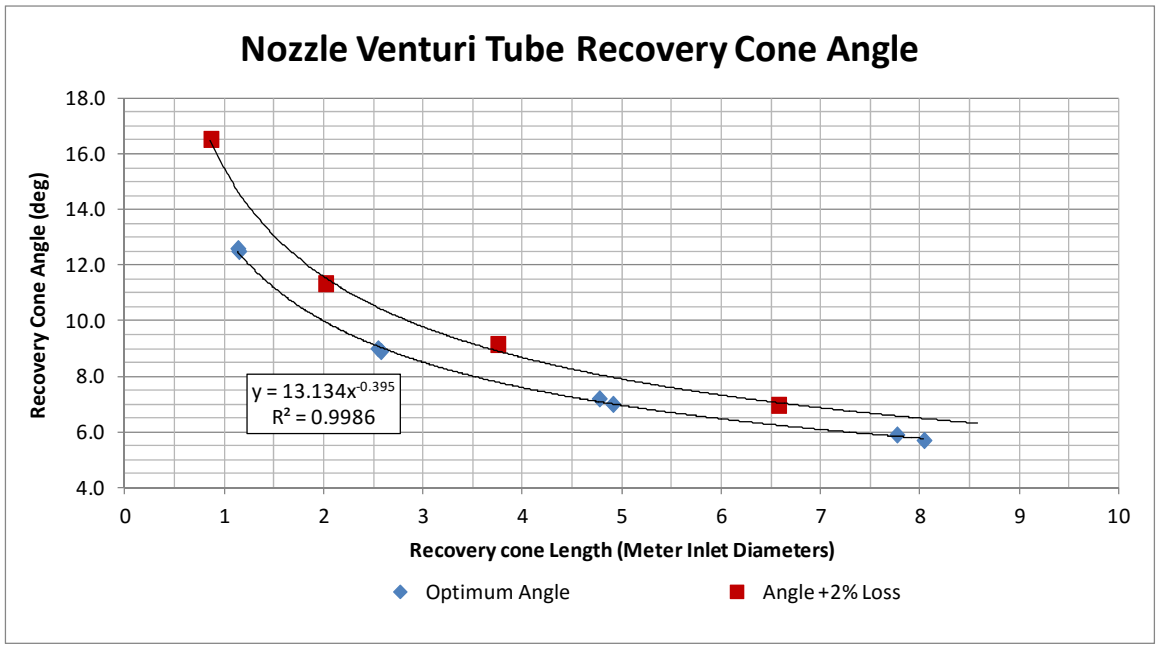


**Fig. 33. Optimum recovery cone angle versus recovery cone length for Nozzle Venturi**

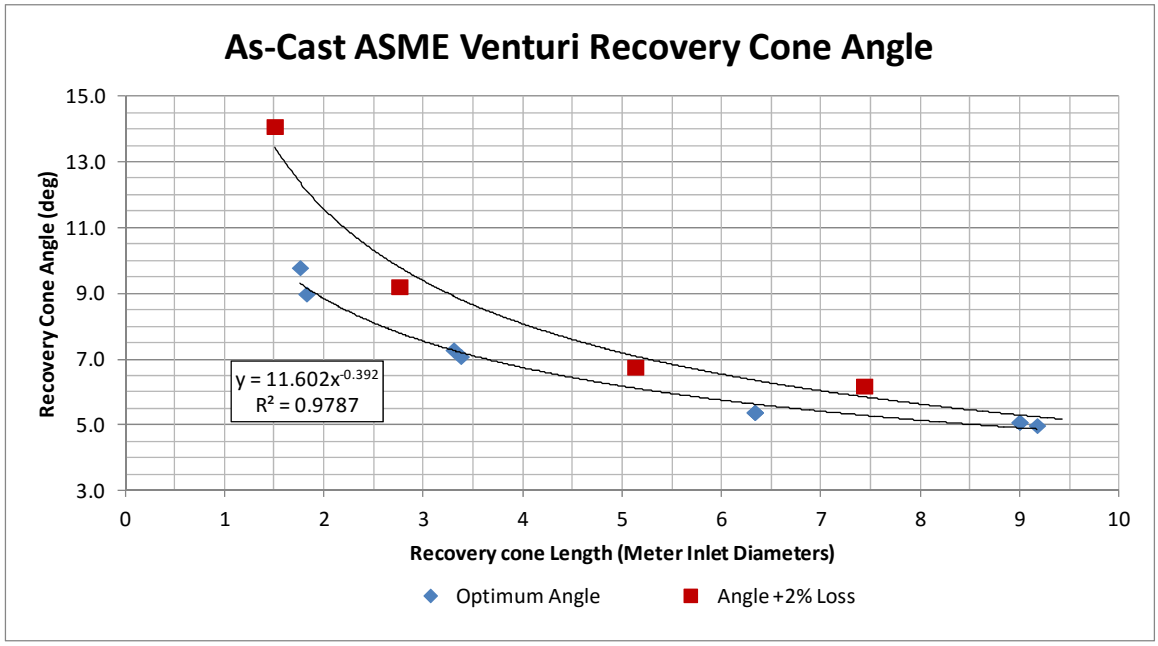


**Fig. 34. Optimum recovery cone angle versus recovery cone length for as-cast ASME Venturi**

**Discussion and Conclusions**

This study used physical and numerical data to determine optimum RCAs for five different Venturi designs. Four different beta ratios of 0.20, 0.40, 0.60, and 0.75 were analyzed with two different Venturi wall roughnesses, three different Reynolds numbers and multiple RCAs. The following describes some key findings of this study.

- CFD is capable of producing data predicting permanent pressure loss for many different Venturi designs.
- Head loss measurements are sensitive to the recovery cone angle. In other words, slight changes in the recovery cone angle can result is large increases in permanent pressure loss.
- Smaller beta ratio meter designs result in smaller optimal recovery cone angles. They also make the optimal cone angle less susceptible to change from factors including meter design, wall roughness and Reynolds number change the optimal angle.
- The change in the optimal recovery cone angle can vary widely for the same meter design with different beta ratios. The optimum angle in some meters changed as much as 8.2 degrees from a 0.20 beta ratio to a 0.75 beta ratio.
- The optimal recovery cone angle can change as much as 3 degrees from one meter design to another.

- Changes in recovery cone angle from one meter to another are greater for larger beta ratios. Changes in the optimal angle due to Reynolds number and meter roughness are also greater with larger beta ratio meters.
- The optimal recovery cone angles found are not always included in code or manufacturers specifications for the design recovery cone angle.

It is the author's opinion that CFD needs to be coupled with laboratory data in order to best utilize this powerful tool. It is very easy to believe the results of any CFD simulation, however there are many ways to feed the model inaccurate information that will always produce poor results. When properly used and verified however, CFD can be used to extend the range of laboratory data, especially when it is not feasible to collect the incrementally varying data in a laboratory. While it is not implied that all of the data in this study is absolute, it should be understood that there are numerical uncertainties, however the many instances shown of good data comparison with laboratory data gives confidence in the results of this study.

# CHAPTER 5

## USING CFD TO OPTIMIZE THE TRUNCATION OF VENTURI RECOVERY CONES

**Abstract**

Venturi flow meters are one of the most commonly used devices for flow measurement. The Venturi flow meter was introduced as a flow measurement technology in the 1890s. Accuracy in flow measurement for many Venturi designs is well established and documented; however, acceptable methods for optimizing the recovery cone design, including recovery cone truncation, have not been thoroughly investigated. This study uses Computational Fluid Dynamics coupled with laboratory data to demonstrate the relationship between the truncation of recovery cones on common Venturi meter designs and the associated head loss. The goal of the research is to present a method for determining the appropriate angle to minimize head loss for a known recovery cone length. For example, if the site installation requires that the length of a Venturi be shorter than the standard meter design, the question arises as to whether there will be more head loss if one were to increase the recovery cone angle to shorten the meter, or to truncate the recovery cone. This study answers this question and also presents the recovery cone angle which results in the least amount of permanent pressure loss for Venturi meters with truncated recovery cones.

---

Coauthored by Michael C. Johnson[2] PhD, P.E., Steven L. Barfuss[3] P.E.

**Background and Literature Review**

The most common Venturi designs presently used include the American Society of Mechanical Engineers (ASME) Venturi (or classical by some codes), the Halmi Venturi Tube (HVT) (PFS 2014), the Universal Venturi Tube (UVT) (BIF 2016), the nozzle Venturi, the Low Loss Venturi, and the Dahl Tube. This research will include the first 4 meters listed, which are the ASME, HVT, UVT, and nozzle Venturi because the Dahl tube and Low Loss Venturi designs are not as common. Design details for the ASME Venturi and nozzle Venturi are covered in ASME design Code Manuals (ISO 2003, ASME 2007) while the other two are, or began as proprietary designs. In the ASME code, the design for the ASME Venturi includes a design for machined, fabricated, and as-cast Venturi meters. In the code, the machined and fabricated designs have the same specifications for radii entering and exiting the throat, the as-cast design is different however, and was also used in this research totaling five meters that were tested in this research.

With Venturi flow meters being such an old flow measurement technology there has been great deals of research performed on them. Most to the research has been focused on flow measurement performance and as a result there are guidelines for Venturi installations downstream of many pipe fittings and valves (Baker 2000, Baker 2003, Rapier 1981, ASME 2005). There has been research performed on Venturi flow meters using Computational Fluid Dynamics (CFD) for various reasons during the past few years. One study used CFD to analyze the trend of discharge coefficients on multiple differential pressure flow meters over a wide Reynolds number range (Hollingshead et al.

2011). Another study used CFD to determine the permanent pressure loss in a wide range of differential flow meters (Prajapati et al. 2010). CFD has also been used to study flow characteristics in multiple pipe fittings including elbows, valves, and tees (Ramamurthy et al. 2006). While CFD is not a replacement for a laboratory calibration, it is a useful tool for identifying performance trends or relative differences associated with changes in meter design. CFD was also used to determine the optimal recovery cone angle for Venturi flow meters where the lowest total head loss through the meter occurs.

The ASME MFC code (ASME 2007) on fluid flow measurement in pipes lists acceptable ranges for the recovery cone of the ASME Venturi flow meter being between 7 and 15 degrees inclusive. This code also gives the design information for a nozzle Venturi in which the recommended inclusive recovery cone angle (RCA) is less than or equal to 30 degrees. The code also gives one detail applicable to this research, which states that the recovery cone of a Venturi can be truncated up to 35% of its length without affecting the discharge coefficient. It also states that this will increase the head loss through the Venturi but does not state by how much.

Fluid mechanics text books (Finnemore and Franzini 2006, Gibson 1908) also provide information on this topic and show curves that indicate the optimal cone angle in an expansion to minimize head loss. It has been found that the head loss in a gradually expanding cone comes from two sources. First is the friction of the fluid along the wall of the cone and the second is the head loss associated with the turbulence of the fluid. Relatively, the head loss associated with the turbulence is usually the greater loss.

The head loss in a truncated expansion cone comes from the friction in the cone, the turbulence caused by the gradual expansion, as well as the added turbulence caused by the sudden expansion at the location of the cone truncation. In this instance, the head loss from the turbulence is also the larger pressure loss. While the head loss caused by a sudden expansions is known and documented in textbooks, the loss associated with a sudden expansion from a gradual expansion is likely different depending on the angle of the gradually expanding cone. It is also unknown how the losses from the contraction of the Venturi inlet cone, the gradual expansion in the recovery cone, and the sudden expansion of the recovery cone truncation interact with each other.

To minimize the pressure loss in Venturis with truncated recovery cones there needs to be a balance between the sources of pressure loss. If there is too much friction loss then the length of the gradually expanding portion of the meter is too long. If there is too much turbulent loss then the angle of the recovery cone is too large leading to separation of the flow. This case also produces conditions in which the higher velocities separate from wall boundaries which reduce wall friction losses. On the other hand, as recovery cone angle is reduced the sudden expansion occurring at the truncation increases, which creates more head loss. In this study, to determine the optimal recovery cone angle for Venturis with truncated recovery cones, it was determined that each source of loss needed to be adjusted by holding the recovery cone the same length and adjusting the recovery cone angle, which in turn adjusts the size of the sudden expansion.

In practice, there are many applications where minimizing the head loss is of interest and there are also many applications where there are restrictions on the length of

a meter due to space constraints. Even if minimizing head loss in not a top priority, a meter design with less head loss than another will often be preferred. The present research used Computational Fluid Dynamics along with laboratory data to show the relationship between the recovery cone angle (RCA) in a Venturi with a truncated cone and the head loss characteristics. Study results show that to minimize head loss, the optimum RCA in a truncated recovery cone is mainly a function of meter design, and beta ratio. It should be noted that Reynolds number effects and surface roughness become insignificant due to the increase in head loss caused by the truncations.

**Theoretical Background**

The equation used to calculate the discharge coefficient ($C_d$) for a Venturi is derived from the Bernoulli equation and the conservation of mass. To generalize the equation such that it can be used for compressible and incompressible fluids, conservation of mass must be maintained. A general equation to determine the discharge coefficient ($C_d$) for a Venturi is given by (Crane 2010, Miller 1978, Miller 1996):

$$C_d = \frac{Q}{Y\frac{\pi}{4}d_f\sqrt{\frac{2g}{1-\left[\left(d_f/D_f\right)^4\right]}}*\sqrt{\Delta P\rho_f}} \tag{1}$$

where $Q$ is the mass flow rate, $C_d$ is the discharge coefficient, $d_f$ is the flowing diameter of the throat, $D_f$ is the flowing diameter of the meter inlet, $g$ is the acceleration due to gravity, $\Delta P$ is the difference in piezometric pressure between the inlet to the throat

pressure tap locations, $\rho_f$ is the flowing density of the fluid, and $Y$ is the gas expansion coefficient and is unity for liquids.

For meters included in code manuals, the shape of the meter profile and the location of pressure taps where $\Delta P$ is measured are clearly dictated. For other meters, manufacturers have design guidelines for the meter profile and the location of the pressure taps. For determining the permanent pressure loss caused by a Venturi, current codes state that pressure taps at least one pipe diameter upstream and six pipe diameters downstream of the Venturi should be used. The measured value obtained from these pressure tap locations becomes the gross permanent pressure loss of the meter (ISA 2008, ASME 2007). The net pressure loss is then determined by removing the Venturi from the line and testing the same pipe and same pressure taps with no meter in the line. The difference in the readings from when the meter is in to when it is removed becomes the net permanent pressure loss which is often related to $\Delta P$ across the meter's pressure taps by dividing the pressure loss by $\Delta P$ so the loss is reported as a percentage of the meter's differential pressure measured between the high and low pressure taps.

**Experimental Procedure**

All data for this study were collected at the Utah Water Research Laboratory (UWRL). This study was designed to determine the optimum RCA for different Venturi designs for cases where the recovery cone needs to be truncated. Laboratory data were collected on a 12-inch ASME Venturi and a 12-inch HVT. Both meters had a section of the recovery cone that could be removed such that there was a full recovery cone and a

truncated recovery cone. The meters were tested over inlet Reynolds numbers ranging from 60,000 to 1,200,000.

Once the permanent pressure loss of the meters with a full recovery cone and a truncated recovery cone was determined, CFD was used to reproduce the experiments. The meters were modeled in CFD using drawings provided by the meter manufacturer. The pipe in the CFD model was meshed such that a surface roughness could be included in the model to produce the same pressure loss as was found experimentally for the laboratory steel piping. Since the meters tested in the laboratory were fabricated and not machined, the roughness of the meters, other than the throat, were similar to that of steel pipe. Therefore in the CFD model, the same roughness was used in the meter body as the pipe with the throats of the meters being modeled smoother than the meter body. The CFD models were tested over the same Reynolds number range as the laboratory tests and the results were compared. It was very important that CFD was able to predict the absolute value of the permanent pressure loss, but perhaps even more important that CFD was able to predict the increase in pressure loss due to different truncations and RCAs.

One of the reasons CFD was used for this research is that laboratory setups with identical meters with different recovery cones are not common. Therefore, the ability to compare the CFD head loss results with two different meter designs tested in the laboratory, both of which had truncated and full recovery cones, was important. The ASME Venturi, which had a 14.6-degree recovery cone, was truncated by 34.5% of its length, leaving a sudden expansion with diameter ratio of 85.9% from the exit of the recovery cone to the nominal pipe diameter. The HVT Venturi had a 10-degree recovery

cone and was truncated by 46.5% of its length, leaving a sudden expansion with a diameter ratio of 81.9% from the exit of the recovery cone to the nominal pipe diameter. Therefore, two meter designs with different recovery cone angles and truncation levels were tested both in the laboratory and with CFD giving confidence in how well CFD is able to match laboratory data under the changing circumstances this study would require.

In the experimental results section, the CFD and physical data for the 12-inch meters are compared and agree well. Once confidence in the CFD was achieved the CFD simulations were then expanded to different Venturi designs, recovery cone lengths, and beta ratios. Reynolds number effects were also investigated and found to be minimal as they were in previous research performed on optimizing RCAs for full recovery cones as shown in the previous chapter. Multiple RCAs were then tested for each combination of meter design, recovery cone length, and beta ratio to be able to characterize the relationship between the optimal RCA and the length of the recovery cone. Once a meter design, recovery cone length, and beta ratio combination was tested a new recovery cone length was implemented. Once enough recovery cone lengths were tested for one meter design and beta ratio combination, the beta ratio was changed and the process repeated.

**Experimental Results**

At the conclusion of this study, over 300 CFD data runs had been completed. Each of the five Venturi designs was tested with four to five beta ratios, an average of three recovery cone lengths (often more), and at least four RCAs. The beta ratios tested include 0.20, 0.40, 0.60, and 0.75 for all of the meter designs and a 0.30 beta ratio for

some of the designs. It is understood that some of the beta ratios tested fall outside design codes and manufacturer recommendations, however to provide guidelines for cone design a wide beta ratio range was necessary.

The primary objective for the study was to determine the optimum RCA required to minimize permanent pressure loss for different Venturi designs with varying beta ratios and recovery cone lengths. Prior to completing all of the CFD runs, some were simulated using progressively finer meshes until the solution was mesh independent and grid convergence occurred. As stated earlier, in order to match the laboratory data, friction had to properly be accounted for in the mesh. Therefore, while each mesh was finer, the wall treatment was adjusted accordingly so that each mesh had the same friction factor as the laboratory piping. It should also be noted that prior to completing the CFD runs various turbulence models including K-epsilon, K-omega, Large eddy simulation, Detached eddy simulation, and Reynolds stress models were each used to determine which model most closely agreed with the laboratory data. It was determined that the K-epsilon model yielded the best results and this model was used for the remainder of the testing. The following section describes more details about the numerical model.

Grid Convergence and Model Parameters

In order to determine the numerical uncertainty due to the mesh, a procedure from the AMSE Journal of Fluids Engineering (Celik et al. 2008) was followed. In general the procedure states that at least three meshes should be tested each with an average cell size at least 1.3 times greater than the next mesh. During this study, three independent

meshes were used to determine the Grid convergence index (GCI) for gross loss on an ASME Venturi. This was done for both 0.20 beta ratio and 0.60 beta ratio designs, and the GCI for the discretization error was typically less than 1%. It should be noted that GCI values this high never occurred near optimal recovery cone design conditions in the sample of runs where grid convergence was performed. Table 5 shows a sample of the mesh convergence exercise performed on these two Venturi meters where $\phi$ is the gross loss of the different Venturi designs and other variables are defined by Celik.

**Table 5. Shows GCI for two numerical runs where GCI is less than 1.0%**

| Grid Convergence Index Runs | | |
|---|---|---|
| Parameter | 0.2 Beta | 0.6 Beta |
| $R_{21}$ | 1.400 | 1.400 |
| $R_{32}$ | 1.429 | 1.429 |
| $\phi 1$ | 205.07 | 1.738 |
| $\phi 2$ | 204.84 | 1.757 |
| $\phi 3$ | 203.93 | 1.808 |
| P | 3.710 | 2.749 |
| Q(p) | -0.104 | -0.090 |
| S | 1 | 1 |
| $\phi^{21}_{ext}$ | 205.16 | 1.73 |
| $\phi^{32}_{ext}$ | 205.16 | 1.73 |
| $e^{21}_{a}$ | 0.115% | 1.060% |
| $e^{21}_{ext}$ | 0.046% | 0.702% |
| $GCI^{21}_{fine}$ | 0.06% | 0.87% |

While the full grid convergence procedure was not completed on all of the runs of this study, it was performed on a wide range of runs having a variety of RCAs, truncation levels, beta ratios, and meter designs, such that the grid convergence tests that were

performed were sufficiently applicable to all other similar geometries that were tested. The CFD code used for this research was STAR-CCM+ version 10.06 by CD-adapco, which is a double precision code using the finite volume method (CD-adapco 2016). All numerical methods used were at least 2nd order accurate and all residuals were reduced by at least four orders of magnitude prior to stopping the solutions. The differential pressure and gross loss of the Venturi were also monitored prior to stopping the simulations.

The inlet boundary condition for all CFD runs was taken from a fully developed flow profile in which the velocity, turbulent kinetic energy (K), and turbulent dissipation rate (epsilon) were used and input at the inlet of each model. As previously stated, the wall boundary condition was modeled both as a rough surface where the roughness height was set such that the numerical pipe friction matched that of laboratory piping. The wall Y+ values were targeted between 30 and 50 but varied as low as 20 and high as 100 or slightly higher which is acceptable per STAR-CCM+ literature. The outlet boundary condition was set as a pressure boundary in which an appropriate pressure was maintained such that the pressure throughout the domain always remained positive. The inlet and outlet boundaries were located at least two pipe diameters upstream or downstream of any measurement location in the computational domain.

In addition to the numerical uncertainties, and perhaps more important, the numerical data were compared to physical laboratory data. This comparison is shown in the next section. All physical data has also had an uncertainty analysis performed following the ASME PTC 19.1 2005 test uncertainty standard in which all physical data had uncertainties of less than 0.25% with 95 percent confidence (ASME 2006). As

previously stated, all of the numerical simulations used a three-dimensional model and employed the K-epsilon turbulence model.

Comparison of CFD to Experimental Data

Three principal reasons CFD was used for this research included 1) the ease of incrementally changing the angle and truncation location of the recovery cone, 2) the ease of extracting data at any location in the numerical domain from each modeling run and 3) the strength of CFD for comparing differences in solutions with differing geometries. In order to have confidence in the CFD results and approach, actual laboratory test data were used to compare with CFD results as previously discussed. Laboratory experimental data (to which the CFD was directly compared) were collected on a 12-inch HVT with a full 10-degree recovery cone and a truncated 10-degree recovery cone, a 12-inch ASME Venturi tube with a full 14.6-degree recovery cone and a truncated 14.6-degree recovery cone.

Figures 35 and 36 show the comparison of the CFD and laboratory data for the 12-inch meters in a plot of pressure loss versus Reynolds number. The reason Reynolds number was used for comparison when head loss is more directly tied to pipe velocity is because the optimum recovery cone angle is more closely tied to Reynolds number than velocity. For the comparison shown, the CFD and laboratory fluids had the same density and viscosity so the comparison would not change with regard to Reynolds number or velocity. Figure 35 shows the comparison of laboratory to CFD data for the ASME Venturi with a full and truncated recovery cone. Figure 36 shows the laboratory to CFD

comparison of the HVT with a full and truncated recovery cone. These Figures show how well CFD is able to track the permanent pressure loss over a wide Reynolds number (velocity) range. As illustrated in the figures, CFD slightly under predicts the head loss associated with the ASME Venturi and slightly over predicts the head loss associated with the HVT. The absolute values of pressure loss produced by CFD were typically within 2% of the laboratory data, but varied by nearly 5% in a few cases.

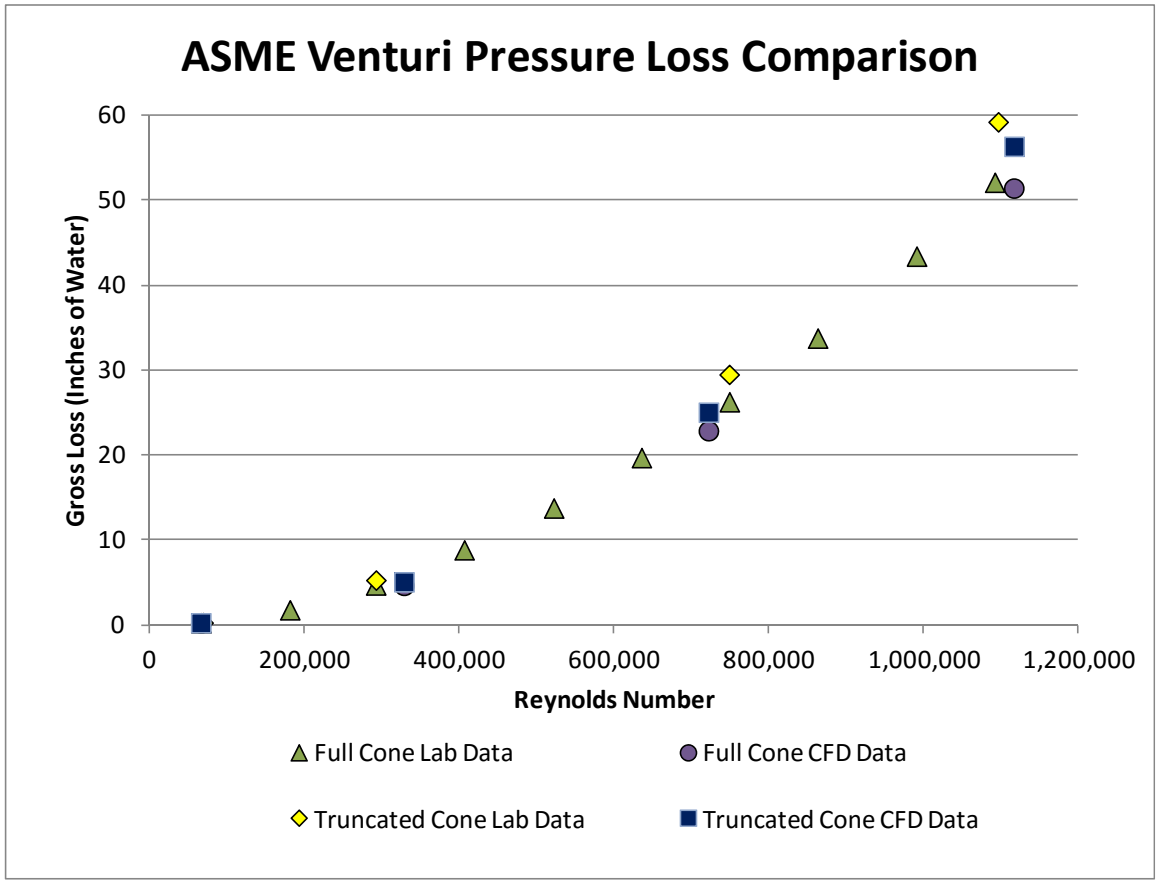


**Fig. 35. Gross loss comparison for laboratory and CFD data of an ASME Venturi**

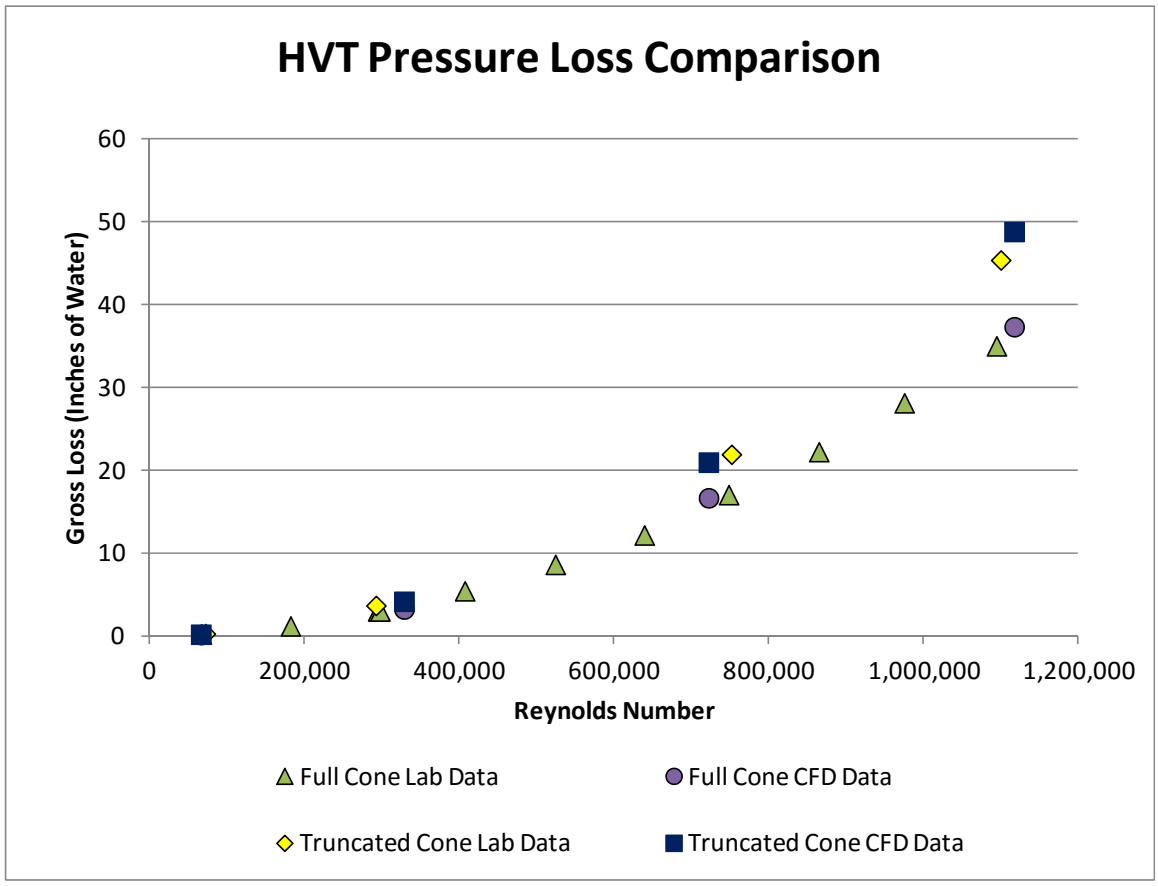


**Fig. 36. Gross loss comparison for laboratory and CFD data of an HVT**

While Figures 35 and 36 show good agreement in the comparison between the CFD and laboratory data, it is important to note how well CFD predicts the increase in pressure loss from the full recovery cone to the truncated recovery cone. In fact, the absolute value of pressure losses are not as important to the results of this study as the difference in pressure loss caused by changing the RCA and the truncation location in the recovery cone. The plots show how well the CFD matches the absolute values of pressure loss found with laboratory data. Table 6 summarizes the increase in pressure

loss caused by the truncation in the recovery cone for both the laboratory and CFD data for both the ASME Venturi and the HVT. This Table shows that at an inlet Reynolds number of approximately one million (18 feet/second) the laboratory data showed a 29.6% increase in pressure loss for the HVT while the CFD showed a 30.7% increase. The CFD matched the pressure increase due to the recovery cone truncation to within 1%. In addition, the CFD and experimental comparison was within 3% of matching the pressure loss increase due to the truncation for the ASME Venturi.

**Table 6. Pressure loss increase caused by recovery cone truncation**

| | | Truncation | Laboratory Data | | CFD Data | |
|---|---|---|---|---|---|---|
| Meter Type | Recovery Cone Angle (deg) | Length Change (%) | Reynolds Number | Increase in Loss (%) | Reynolds Number | Increase in Loss (%) |
| ASME | 14.6 | 46.5% | 292,000 | 12.0% | 328,000 | 9.1% |
| ASME | 14.6 | 46.5% | 750,000 | 12.2% | 722,000 | 9.5% |
| ASME | 14.6 | 46.5% | 1,100,000 | 13.1% | 1,120,000 | 9.5% |
| HVT | 10 | 34.5% | 292,000 | 22.0% | 328,000 | 28.9% |
| HVT | 10 | 34.5% | 751,000 | 28.5% | 722,000 | 25.8% |
| HVT | 10 | 34.5% | 1,100,000 | 29.6% | 1,120,000 | 30.7% |

After the CFD model was proven reliable it was used to test many identical Venturis with identical flow conditions and recovery cone truncations while varying only the angle of the recovery cone. Approximately 300 numerical runs were performed to determine the anticipated pressure loss increase resulting from different combinations of RCAs and truncation locations. The results are described in detail in the following sections.

CFD Results

As mentioned previously, the objective of the CFD work was to determine the optimum RCA to minimize head loss through various Venturi flow meter designs with truncated recovery cones. The optimal RCA varies widely with different meter designs, beta ratios, and of course the location of the recovery cone truncation. It should be noted that while the surface roughness of the meter and Reynolds number were not investigated for every Venturi design tested in this study, they were used as a variable in a few cases where results showed these parameters did not have an appreciable effect on the optimal RCA. This is because the increase in pressure loss often added from truncating the RCA limits the effect some variables are able to have on the permanent pressure loss through the Venturi. Previous research (found in previous chapter) showed these two variables had an effect on the optimal RCA for Venturis with full recovery cones, but did not have as much of an effect as meter design and beta ratio. Therefore, the principle variables for the CFD models in this study became meter design, beta ratio, RCA, and recovery cone truncation location. All data presented in this study had a throat Reynolds number greater than 5,000,000 and the same calibrated wall surface roughness (to match laboratory piping) through the meter.

One main finding of the study is that a full recovery cone will always have less head loss than a truncated recovery cone when the same RCA is used. If the RCA is different however, this is not always the case and often truncating the recovery cone, while keeping the cone length the same, coupled with reducing the RCA results in a lower head loss. To state how much less the pressure loss is from a Venturi with a full

recovery cone than the same Venturi and RCA with a truncated recovery cone is difficult since there are many contributing factors. Some factors that affect the permanent pressure loss through a Venturi are Reynolds number (velocity), Venturi design, beta ratio, recovery cone design, and wall surface roughness. Not all of these factors have large impacts on the optimal RCAs or the increase in pressure loss due to a truncation however, they do have appreciable impacts on the total head lost though a Venturi flow meter and all were considered when making meter to meter comparisons.

In order to specifically compare all of meters, the increase in head loss for each beta ratio was plotted against the ratio of the diameter at the exit of the recovery cone to the pipe diameter (referred herein as diameter ratio). The plots include data from all five meter designs in the study and also include multiple RCAs for each meter. The reason the data is plotted versus the diameter ratio is because there are multiple RCAs for each meter included in these plots. This means the location of the truncation for a given diameter ratio is different with each RCA. It should be noted that the increase in pressure loss is calculated based on head loss for the given Venturi design with a full recovery cone of the same recovery cone angle. Figures 37 through 40 show these plots for beta ratios of 0.20, 0.40, 0.60, and 0.75 respectively. Each figure includes different recovery cone angles, indicating that the increase in head loss for a given beta ratio and truncation is not RCA dependent.

The plots show a few things of interest; one of which being how closely the different meter designs respond to the same truncations. Another is how much more the head loss of a larger beta ratio meter is affected by truncating the recovery cone than a

small beta ratio design. For example, for beta ratios of 0.20, 0.30, 0.40, 0.60 and 0.75 the diameter ratios at which the head loss is increased by 10%, is 50%, 77%, 89% and 93% respectively. This means a truncation can be more than five times as extreme for a 0.20 beta ratio meter as a 0.75 beta ratio meter and still cause the same pressure loss increase by percentage. Note that one main reason the percent pressure loss increase is less for smaller beta ratio meters is simply because the pressure loss is much greater than in larger beta ratio meters. In addition, the plots also show that the smaller the diameter ratio, or the shorter the recovery cone, the more unique the increase in head loss to each meter becomes. This shows that the closer the truncation gets to the meter throat, the more the meter design starts to influence the change in head loss caused by the truncations.

Another finding of interest is that the optimum included RCA was found to vary drastically as the length of a recovery cone for a given meter design changes. The shorter the recovery cone, the larger the optimal recovery cone angle needs to be. Therefore, the common practice of truncating a recovery cone without changing the RCA will produce a recovery cone that is not optimal for reducing head loss. In order to determine the optimum angle for a given recovery cone, CFD data were used to develop plots of pressure loss versus RCA to determine the angle that would have the least head loss for a given recovery cone length. In order to see what angle resulted in the minimum head loss, angles both above and below the optimum angle needed to be tested. Figure 41 shows velocity contour plots from the CFD of a 0.6 beta UVT for recovery cones having the same length, which was the length of a 13-degree full recovery cone or, 1.76 pipe

diameters. The data from the CFD models that produced the images in Figure 41 were then used to create one data set for Figure 42. Figure 42 is a plot of the permanent pressure loss versus the RCA for a 0.40 beta UVT with for different recovery cone lengths including a full recovery cone. Figure 43 shows the same plot for a 0.60 beta UVT. These plots not only show how the optimal angle for different recovery cone lengths was determined, but they also show how the head loss increases from the full recovery cone to truncated recovery cones. The plots also provide a good representation of how the optimal recovery cone angle changes with the length of the recovery cone.

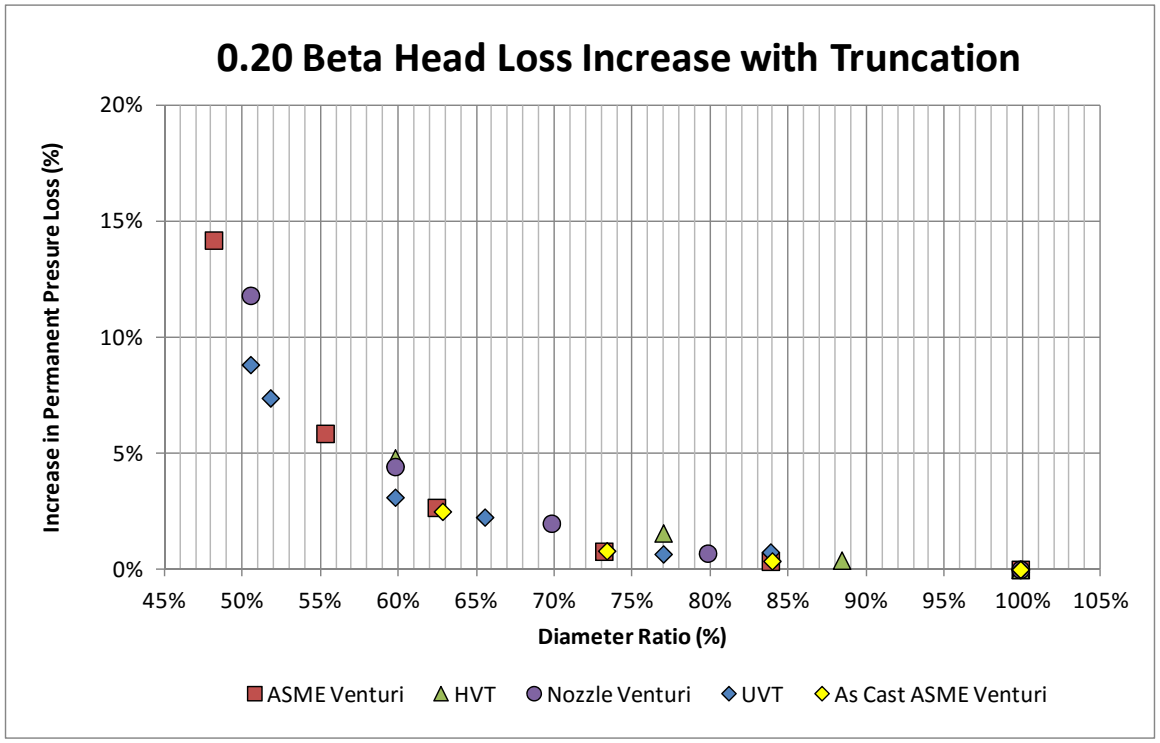


**Fig. 37. The increase in head loss caused by various truncations on 0.20 beta Venturis**

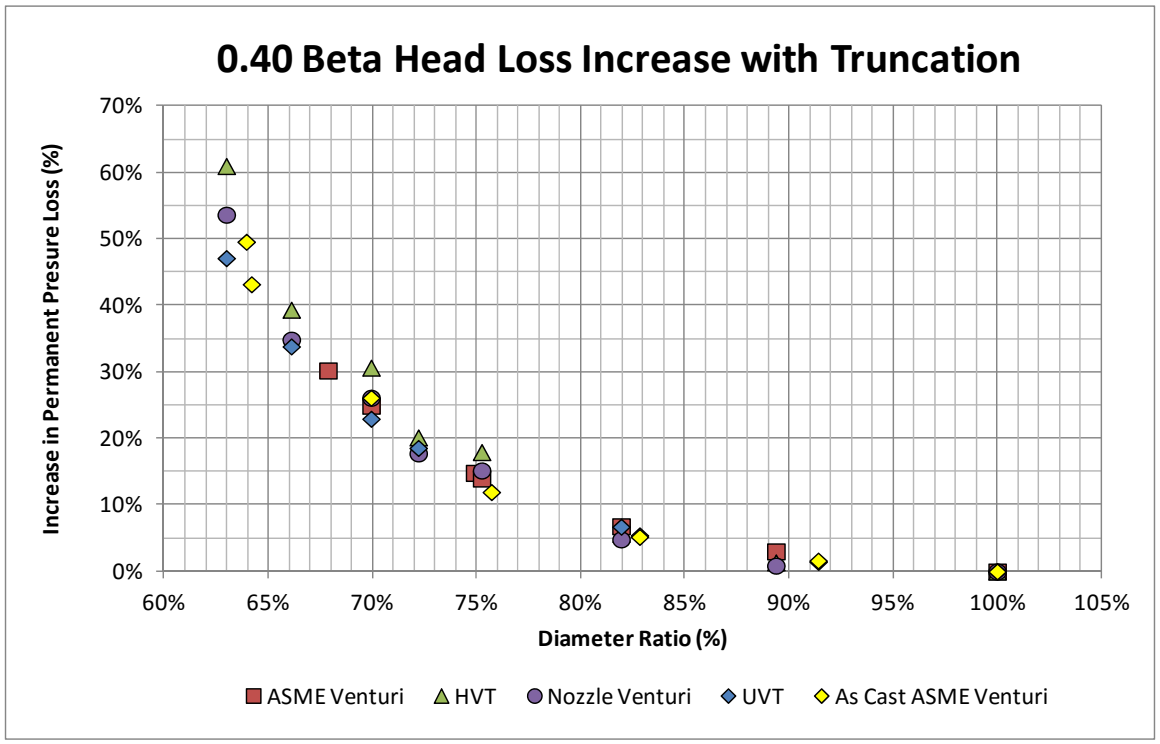


**Fig. 38. The increase in head loss caused by various truncations on 0.40 beta Venturis**

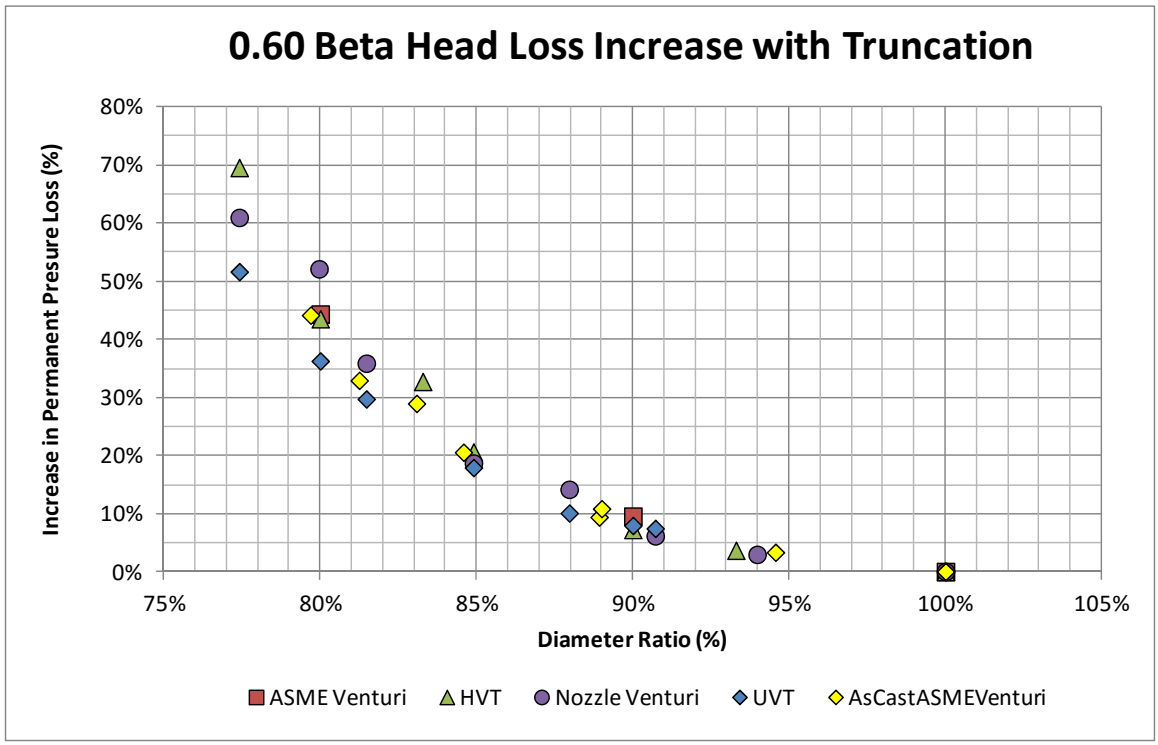


**Fig. 39. The increase in head loss caused by various truncations on 0.60 beta Venturis**

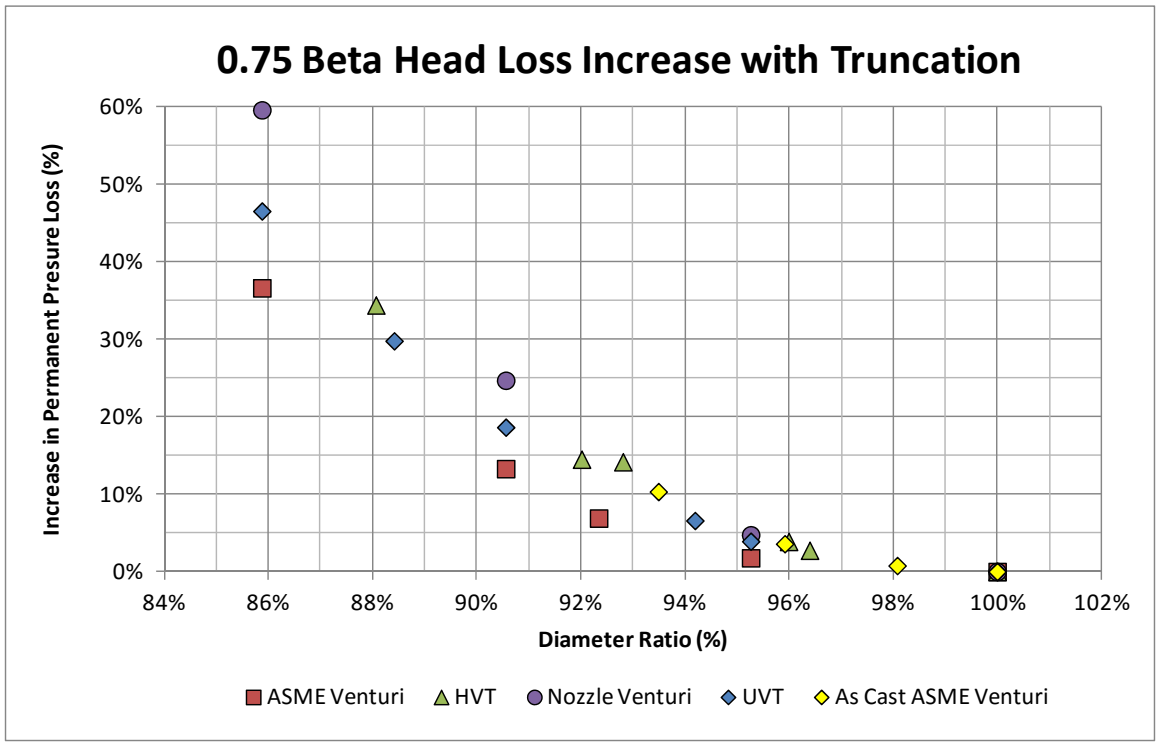


**Fig. 40. The increase in head loss caused by various truncations on 0.75 beta Venturis**

It should be noted that Figures 42 and 43 are a very small sample of the plots produced from this study. Each point in the figure represents one CFD run and four, or sometimes five plots (depending on if the 0.30 beta ratio designs were tested) were created for each of the five meters tested totaling 22 plots which are shown in Appendix B.

With head loss versus RCA curves developed for each meter design, beta ratio, and recovery cone length, the optimum RCA for each condition was determined. Table 7 provides a summary of the results and shows the meter design, beta ratio, diameter ratio, the recovery cone length reduction (in percent), and the optimum RCA for the conditions listed. This table provides the reader insight to the amount of data used for the analysis as each row in the table represents the results of at least four CFD runs. It also shows

another finding of the study, which is, that the larger the beta ratio, the larger the optimal recovery cone angle. This is shown in Table 7 with the ASME meter when for a similar diameter ratio, in the 60 to 70% range, the optimal recovery cone angle for a 0.20 beta ratio is 5.6 degrees, for a 0.30 beta the optimal angle is 8.2 degrees, and for the 0.40 beta meter the optimal angle jumps to 11.4 degrees. This trend is clearly shown in Figure 44, which shows a plot of the recovery cone angle versus the diameter ratio for different beta ratios of the ASME Venturi. This plot not only shows how the optimal recovery cone angle varies with beta ratio, but also how the optimal angle changes, as the recovery cone gets shorter.

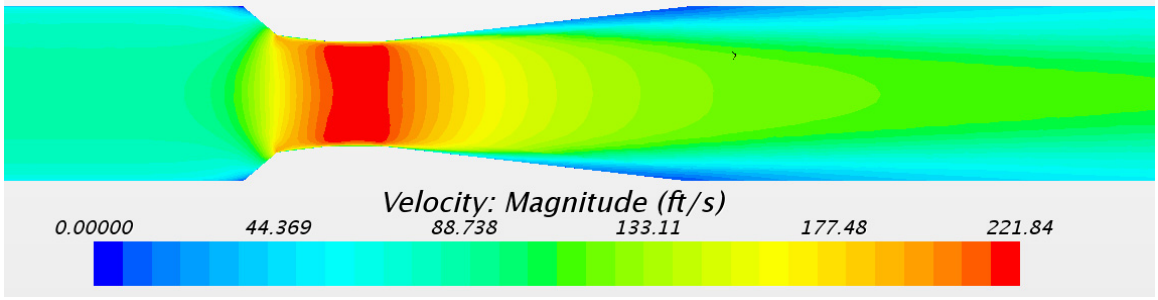


A) 13-degree inclusive recovery cone length (1.76D) with full 13-degree recovery cone.

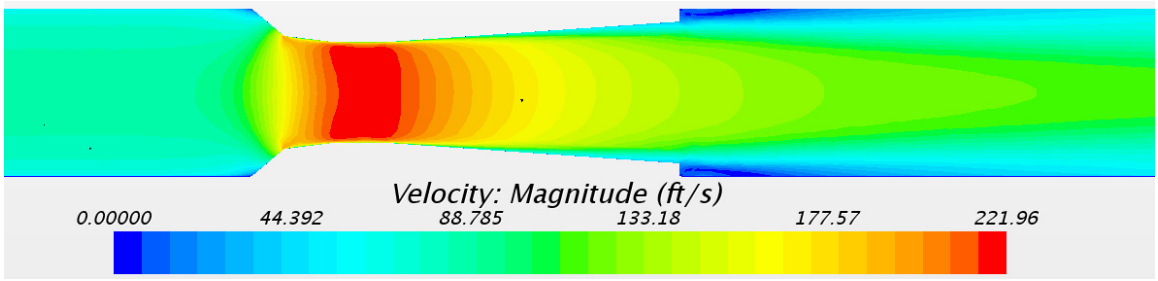


B) 13-degree inclusive recovery cone length (1.76D) with 10-degree recovery cone.

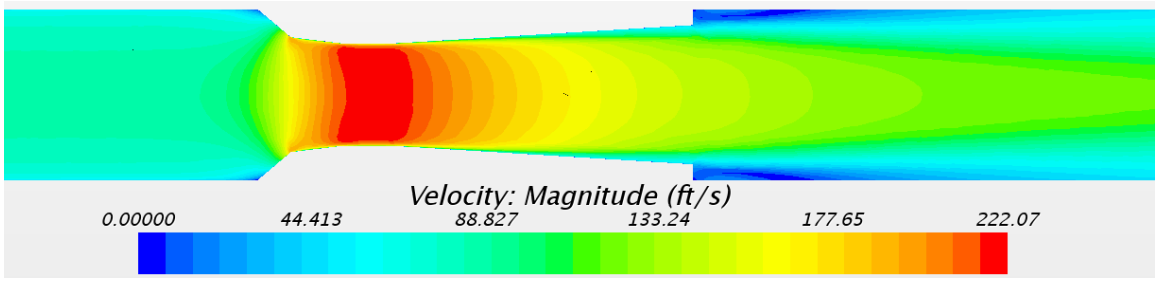


C) 13-degree inclusive recovery cone length (1.76D) with 7-degree recovery cone.

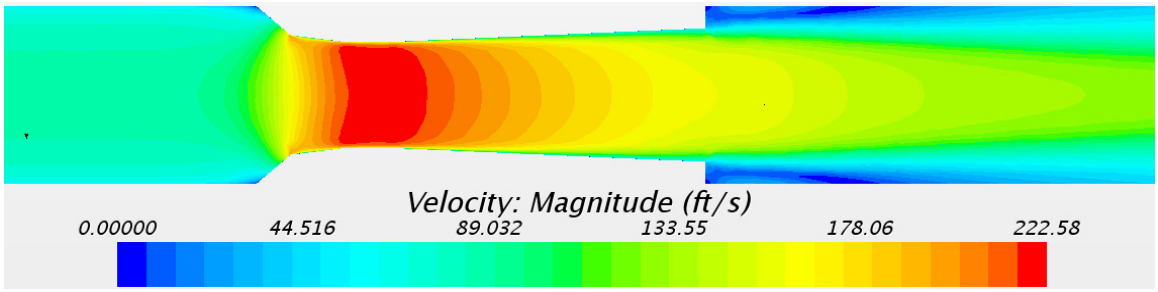


D) 13-degree inclusive recovery cone length (1.76D) with 5-degree recovery cone.

**Fig. 41. CFD Velocity contour plots showing different recovery cone truncations**

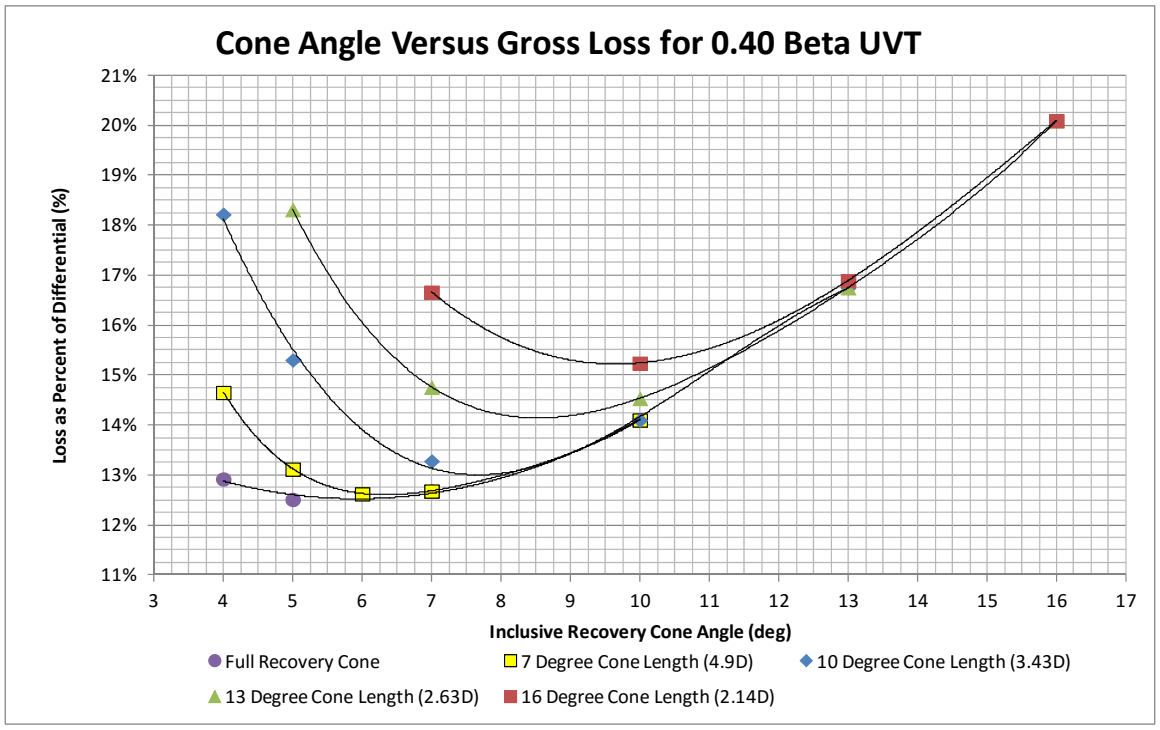


**Fig. 42. Head loss versus cone angle for a 0.40 beta ASME Venturi with different truncated recovery cones**

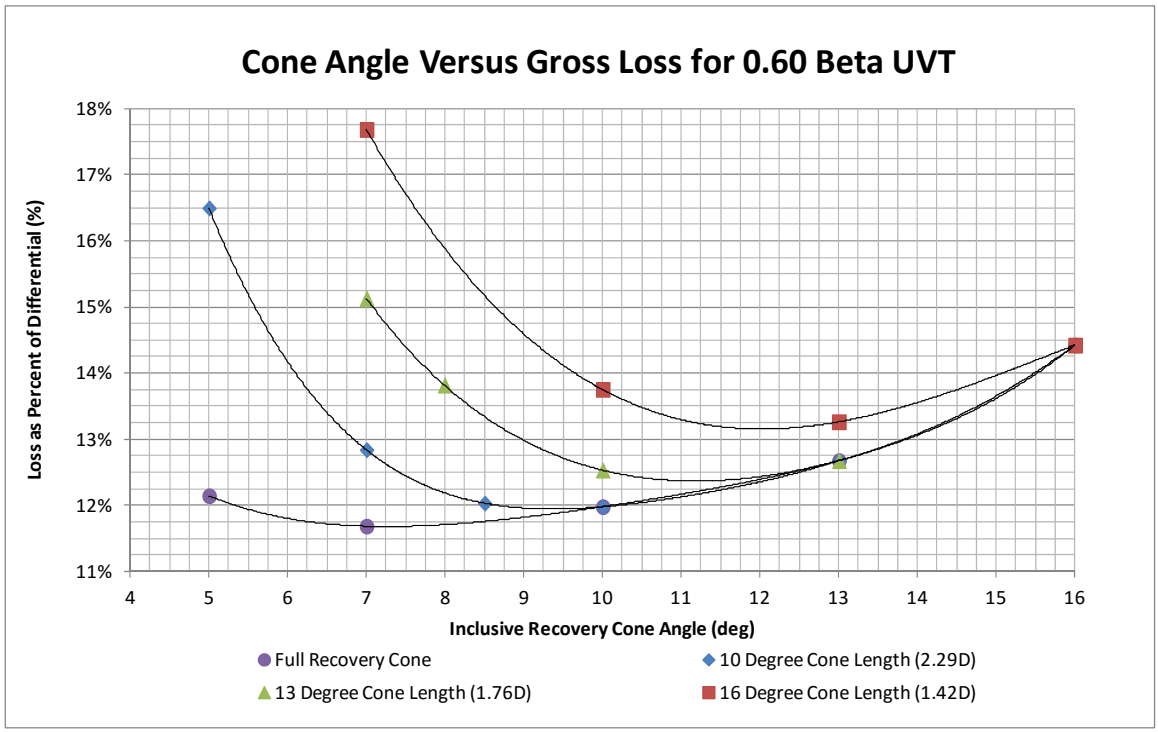


**Fig. 43. Head loss versus cone angle for a 0.6 beta ASME Venturi with different truncated recovery cones surface**

## Table 7. Summary of results for truncated recovery cone Venturi Designs

| Venturi Meter Design | Meter Beta Ratio | Diameter Ratio (%) | Recovery Cone Length Reduction (%) | Recovery Cone Length (Pipe Diameters) | Recovery Cone Optimum Angle (degrees) |
|---|---|---|---|---|---|
| | | | | | |
| ASME | 0.2 | 82.4% | 22.0% | 6.87 | 5.2 |
| ASME | 0.2 | 74.0% | 32.5% | 5.72 | 5.4 |
| ASME | 0.2 | 64.7% | 44.1% | 4.57 | 5.6 |
| ASME | 0.2 | 59.9% | 50.1% | 3.81 | 6 |
| ASME | 0.2 | 55.0% | 56.2% | 3.04 | 6.6 |
| ASME | 0.3 | 88.0% | 17.2% | 5.72 | 5.8 |
| ASME | 0.3 | 76.1% | 34.1% | 4.00 | 6.6 |
| ASME | 0.3 | 68.1% | 45.6% | 2.66 | 8.2 |
| ASME | 0.4 | 89.4% | 17.7% | 4.04 | 7 |
| ASME | 0.4 | 85.6% | 24.1% | 3.43 | 7.6 |
| ASME | 0.4 | 81.9% | 30.1% | 2.85 | 8.4 |
| ASME | 0.4 | 77.5% | 37.6% | 2.28 | 9.4 |
| ASME | 0.4 | 69.6% | 50.7% | 1.48 | 11.4 |
| ASME | 0.6 | 98.0% | 5.0% | 2.29 | 9.5 |
| ASME | 0.6 | 91.6% | 21.1% | 1.55 | 11.6 |
| ASME | 0.6 | 87.9% | 30.4% | 1.13 | 14 |
| ASME | 0.75 | 97.8% | 8.8% | 0.89 | 14.6 |
| ASME | 0.75 | 94.4% | 22.2% | 0.62 | 17.9 |
| | | | | | |
| HVT | 0.2 | 86.3% | 17.2% | 6.54 | 5.8 |
| HVT | 0.2 | 70.3% | 37.1% | 4.57 | 6.3 |
| HVT | 0.2 | 64.8% | 44.0% | 3.51 | 7.3 |
| HVT | 0.4 | 93.6% | 10.6% | 4.04 | 7.6 |
| HVT | 0.4 | 89.8% | 17.1% | 3.43 | 8.3 |
| HVT | 0.4 | 82.4% | 29.4% | 2.63 | 9.2 |
| HVT | 0.4 | 79.2% | 34.6% | 2.13 | 10.5 |
| HVT | 0.6 | 97.7% | 5.9% | 1.90 | 11.3 |
| HVT | 0.6 | 92.4% | 18.9% | 1.42 | 13 |
| HVT | 0.75 | 99.8% | 0.7% | 1.02 | 13.9 |
| HVT | 0.75 | 97.6% | 9.6% | 0.75 | 17.2 |
| | | | | | |
| UVT | 0.2 | 93.6% | 8.0% | 9.16 | 4.6 |
| UVT | 0.2 | 74.8% | 31.5% | 6.54 | 4.8 |
| UVT | 0.2 | 62.3% | 47.1% | 4.57 | 5.3 |
| UVT | 0.2 | 55.6% | 55.5% | 3.51 | 5.8 |
| UVT | 0.3 | 85.0% | 21.5% | 5.72 | 5.5 |
| UVT | 0.3 | 75.4% | 35.1% | 4.00 | 6.5 |
| UVT | 0.3 | 68.7% | 44.8% | 3.07 | 7.2 |
| UVT | 0.4 | 94.8% | 8.6% | 4.90 | 6.4 |
| UVT | 0.4 | 86.2% | 23.1% | 3.43 | 7.7 |
| UVT | 0.4 | 79.1% | 34.8% | 2.63 | 8.5 |
| UVT | 0.4 | 75.8% | 40.3% | 2.13 | 9.6 |
| UVT | 0.6 | 97.2% | 7.0% | 2.29 | 9.3 |
| UVT | 0.6 | 94.4% | 13.9% | 1.76 | 11.2 |
| UVT | 0.6 | 89.9% | 25.2% | 1.42 | 12 |
| UVT | 0.75 | 100.2% | -0.8% | 1.10 | 13.1 |
| UVT | 0.75 | 97.9% | 8.2% | 0.89 | 14.7 |
| | | | | | |
| Nozzle | 0.2 | 79.0% | 26.3% | 5.72 | 5.9 |
| Nozzle | 0.2 | 68.7% | 39.1% | 4.57 | 6.1 |
| Nozzle | 0.2 | 62.3% | 47.1% | 3.51 | 6.9 |
| Nozzle | 0.4 | 92.2% | 13.0% | 4.04 | 7.4 |
| Nozzle | 0.4 | 89.2% | 18.1% | 3.43 | 8.2 |
| Nozzle | 0.4 | 81.9% | 30.2% | 2.63 | 9.1 |
| Nozzle | 0.4 | 79.2% | 34.6% | 2.13 | 10.5 |
| Nozzle | 0.6 | 99.6% | 1.0% | 2.29 | 9.9 |
| Nozzle | 0.6 | 95.4% | 11.6% | 1.76 | 11.5 |
| Nozzle | 0.6 | 92.2% | 19.6% | 1.42 | 12.9 |
| Nozzle | 0.75 | 98.9% | 4.4% | 0.89 | 15.3 |
| | | | | | |
| As Cast ASME | 0.2 | 82.5% | 21.9% | 6.88 | 5.2 |
| As Cast ASME | 0.2 | 73.2% | 33.5% | 5.75 | 5.3 |
| As Cast ASME | 0.2 | 65.1% | 43.6% | 4.61 | 5.6 |
| As Cast ASME | 0.4 | 92.5% | 12.6% | 4.92 | 6.1 |
| As Cast ASME | 0.4 | 86.9% | 21.9% | 4.06 | 6.6 |
| As Cast ASME | 0.4 | 84.6% | 25.7% | 3.49 | 7.3 |
| As Cast ASME | 0.4 | 78.9% | 35.1% | 2.68 | 8.3 |
| As Cast ASME | 0.6 | 96.6% | 8.5% | 2.33 | 9 |
| As Cast ASME | 0.6 | 94.1% | 14.6% | 1.93 | 10.1 |
| As Cast ASME | 0.6 | 91.4% | 21.5% | 1.60 | 11.2 |
| As Cast ASME | 0.75 | 99.1% | 3.6% | 1.15 | 12 |
| As Cast ASME | 0.75 | 97.8% | 9.0% | 0.93 | 14 |

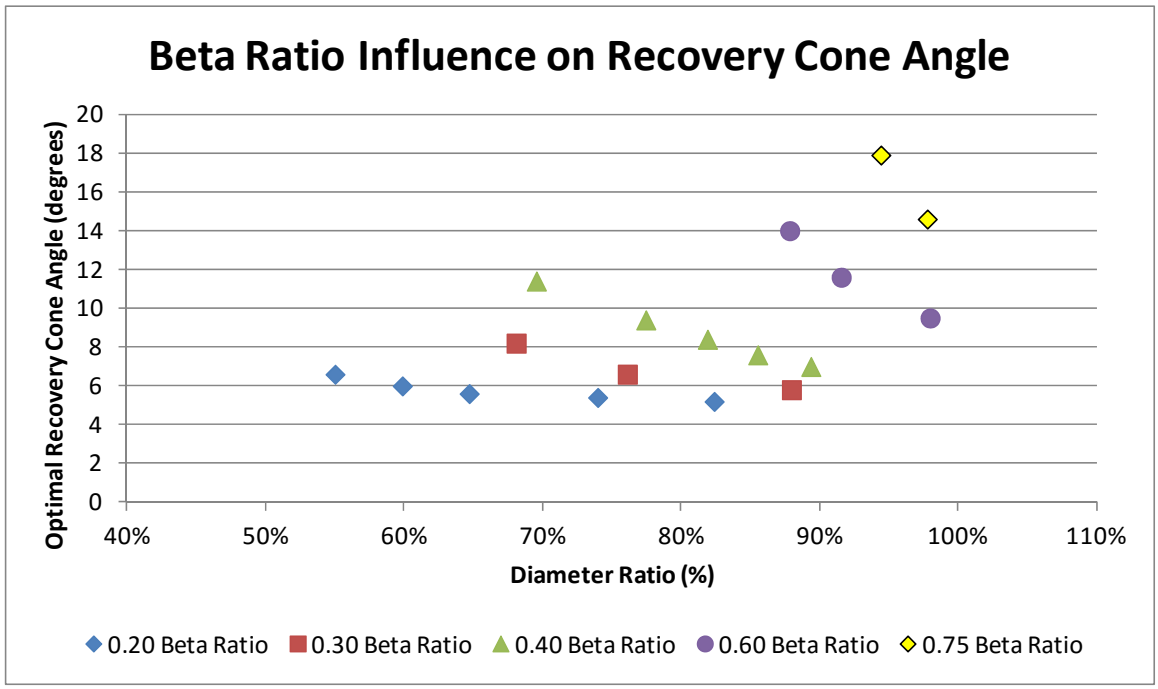


**Fig. 44. Plot of optimum cone angle versus diameter ratio for different beta ratios of an ASME Venturi**

Figure 44 shows a trend of the optimal recovery cone angle changing with diameter ration for different beta ratio meter designs. A 0.20 beta ratio can be truncated to a diameter ratio of 55% (nearly a 60% cone length reduction) and the optimal recovery cone angle changes by less than two degrees. Compare that to the 0.60 beta ratio design where the optimal angle changes by 4.5 degrees at an 88% diameter ratio (a 30% cone length reduction). This shows how much more susceptible large beta ratio meters are to slight geometry changes. This is because the magnitude of the pressure loss is so much less than that of smaller beta ratios.

The results of the study have been presented and contributing factors have been discussed. In order to bring value to the data the next section will discuss how the data

can be applied in practice. It is understood that changing meter designs is not an easy endeavor and the authors do not recommend changing all Venturi recovery cone designs. However when pressure loss through a Venturi needs to be minimized, the results of this study will be valuable in designing the recovery cone and should be implemented by meter manufactures and code manuals.

**Using the Results**

This study produced optimum RCAs for a broad range of Venturi designs and recovery cone lengths. In any Venturi application where head loss is of sufficient concern and a shortened Venturi is required, the data from this study will provide design guidance that was previously nonexistent. The study also confirms that CFD, coupled with experimental testing is a useful tool in optimizing the cone angle or other unique Venturi designs.

The ASME code calls for recovery cones angles of an ASME Venturi to be between 7 and 15 degrees inclusive. The code also states that a recovery cone can be by up to 35% of its length without affecting the meters discharge coefficient. The CFD results from this study however, showed Venturi recovery cone lengths can be truncated by as much as 60% with no effect on the discharge coefficient. The CFD results also showed that for ASME meter designs with a 0.30 beta ratio or smaller, the optimal recovery cone angle is less than 7 degrees. The optimal RCA for a 0.75 beta ratio ASME Venturi however, is at the other end of the spectrum and when the cone is truncated to be

22% shorter than the full cone of the same angle, the optimal RCA is as large 17.9 degrees.

Meter manufacturers commonly build ASME Venturi tubes with 15-degree recovery cones regardless of beta ratio because the meter still meets code, and is shorter and therefore less costly to build. The results of this study show that for a 0.30 beta ratio ASME Venturi, if the recovery cone is built the same length as the full 15 degree cone (2.66D), the head loss can be decreased by nearly 30% from the full 15 degree recovery cone if the optimal RCA of 8.2 degrees is used and the cone is truncated. The same case applies for a 0.40 beta ratio ASME Venturi. If the meter is constructed with the same recovery cone length as a 15-degree full recovery cone (2.28D), but the cone is built with the optimal RCA for that cone length and beta ratio which is 9.4 degrees, the head loss through the meter would be 21% less. The same case applies for a 0.60 beta ratio ASME Venturi where the head loss can be decreased by 8% if the recovery cone is truncated to the 15-degree full cone length (1.55D) and built with an 11.6-degree cone instead.

As shown in the previous discussion, the results of this paper can be very applicable and help meter manufactures build economical meters by reducing recovery cone lengths all while decreasing the permanent pressure loss and energy consumption. In order to graphically present the optimal RCA for each meter, plots of the optimum RCA versus the recovery cone length were created. This is also a convenient way to determine the optimum RCA for beta ratios that were not tested in this study. Figures 45 through 49 show these plots in the following order of Venturi design; ASME Venturi, HVT, UVT, Nozzle Venturi, and the as-cast ASME Venturi. The plots include many

data series including the optimal RCA for Venturi designs with full recovery cones, which were developed in previous research, and a series for each beta ratio tested for that Venturi design with truncated recovery cones. The plots also include two formulae to calculate the trend line for the optimum RCA curve. One formula is for all data with a 0.30 beta ratio and larger and the other is for the 0.20 beta ratio. Noteworthy is that the data for the 0.20 beta ratio meter designs do not trend well with the other beta ratios. This is why a 0.30 beta ratio meter design was tested for two meter types and as shown in the figures the 0.30 beta ratio designs trended very well with the larger beta ratios. This is also why there are two equations to calculate the optimal RCA with one of them being exclusively for the 0.20 beta ratio data. Since no data has yet been taken for beta ratios smaller than 0.20, it is assumed that the optimal angle could be determined using the 0.20 beta curves however the results should be validated in the laboratory or with CFD.

Surprisingly, the truncated recovery cone data closely matches the curve developed in previous research for the full recovery cones. This implies that recovery cone length has a stronger influence on the optimal RCA then the level of truncation or diameter ratio. In order to use these plots effectively for Venturi designs with truncated recovery cones, all that is needed is the recovery cone length in terms of the pipe diameter. This is the length from the exit of the throat to the location of the recovery cone truncation, or the end of the cone. In the case of full recovery cones this may be an iterative process, however when a meter length restriction is given, then lengths of truncated recovery cones are easily obtained since the geometry of the inlet cone and throat are fixed in meter deigns. As shown on the plots, some of the recovery cone

lengths required to optimize the recovery cone are extremely long, especially for small beta ratio meters. It is well understood by the authors that recovery cones as long as ten inlet diameters can be difficult and very costly to build. One of the reasons this research was undertaken was to be able to provide insight as to how shortening the meter by truncation will affect the head loss in the meter. Note that each data point on the plots in Figures 45 through 49 was determined from four or more CFD runs where the RCA was varied while other flow and geometric parameters remained constant.

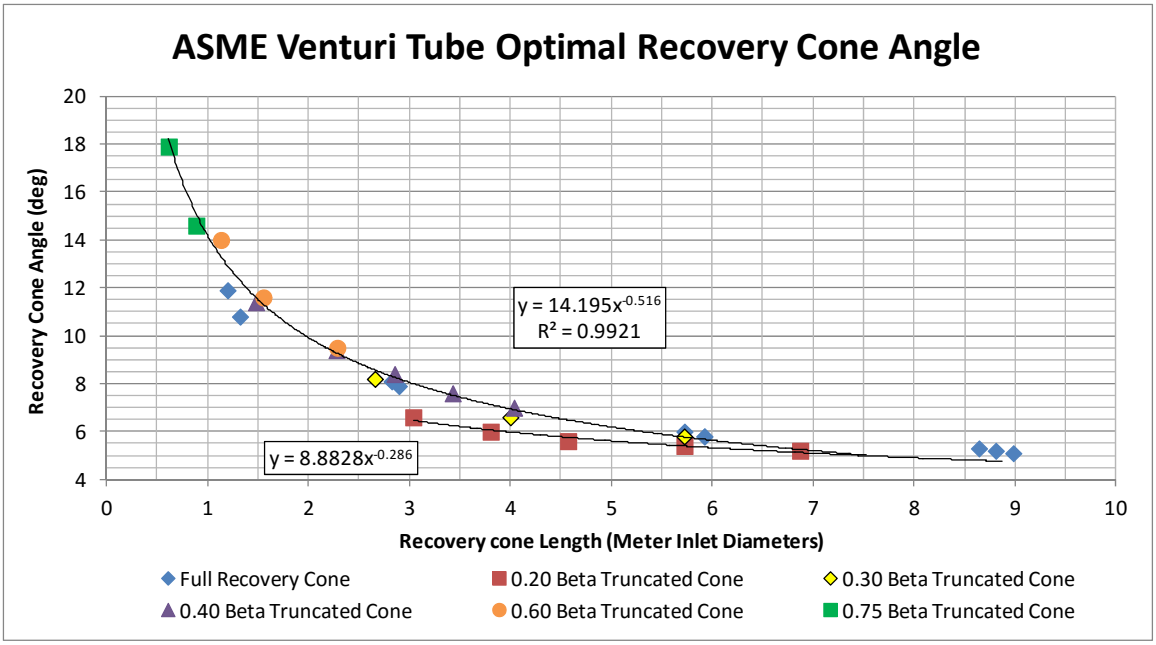


**Fig. 45. Optimum recovery cone angle versus recovery cone length for ASME Venturi**

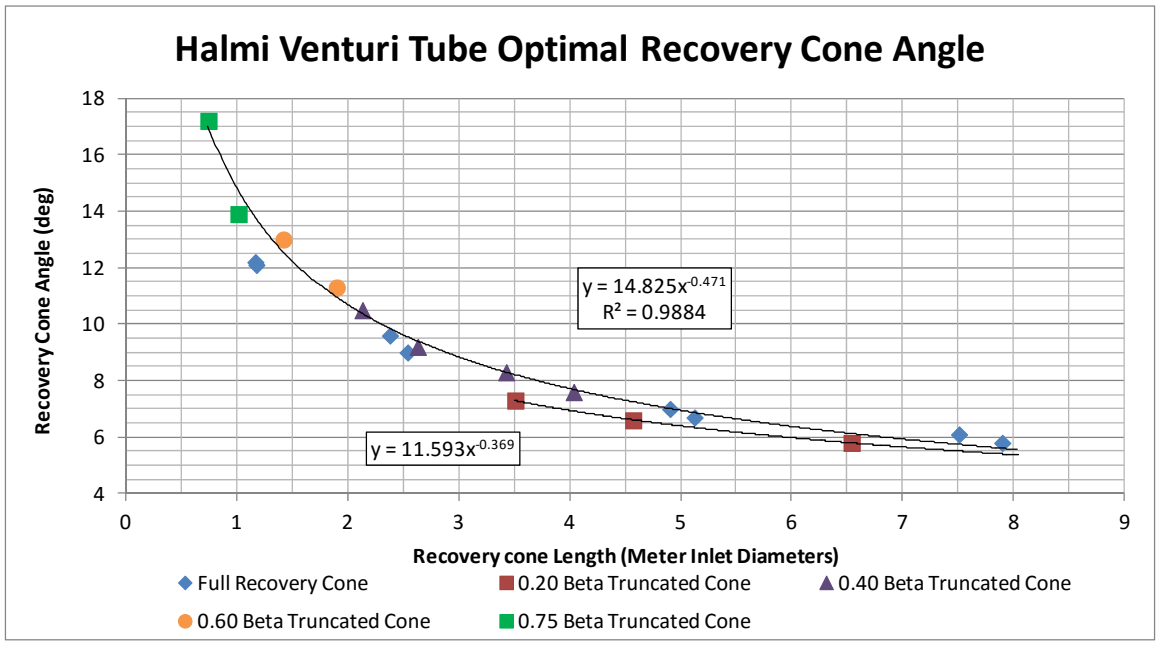


**Fig. 46. Optimum recovery cone angle versus recovery cone length for HVT**

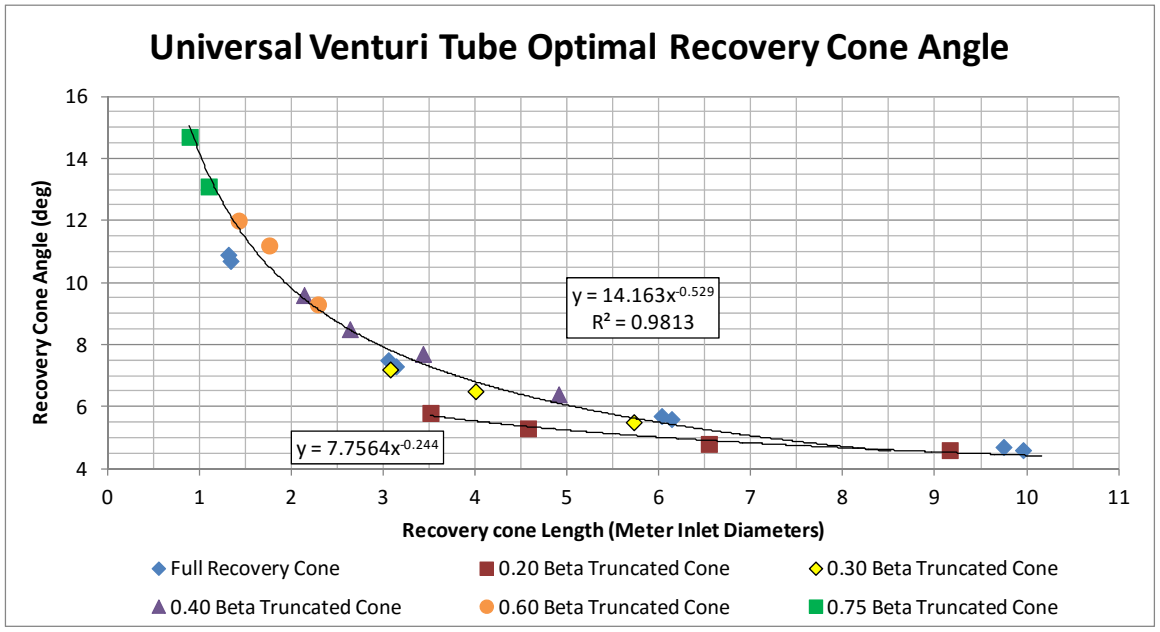


**Fig. 47. Optimum recovery cone angle versus recovery cone length for UVT**

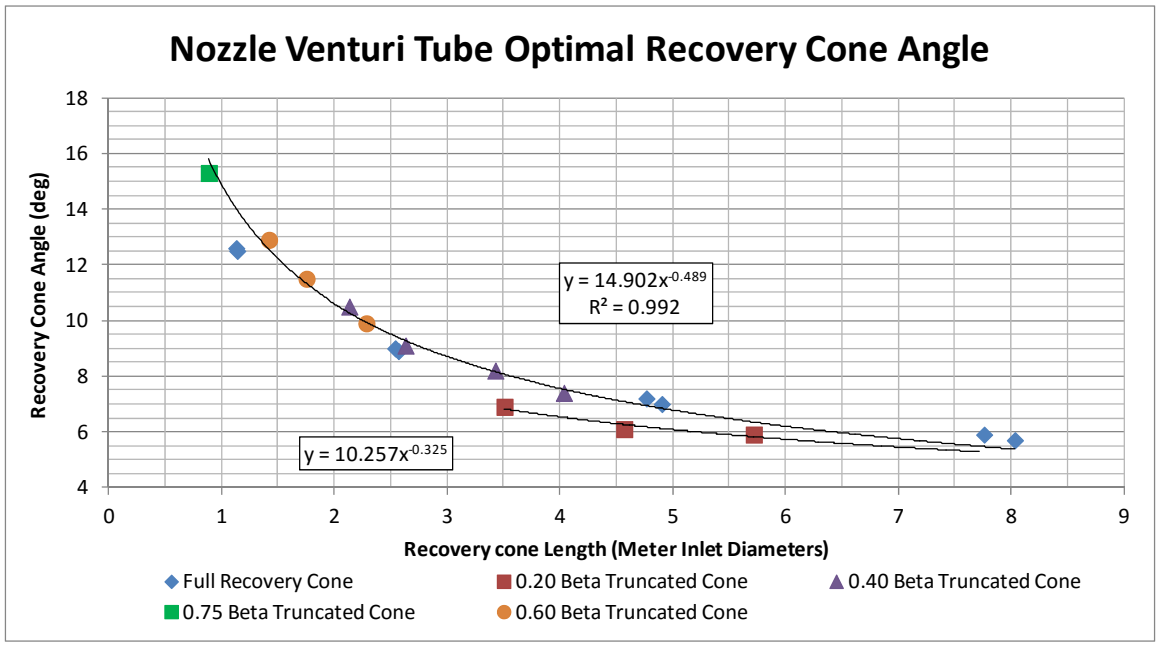


**Fig. 48. Optimum recovery cone angle versus recovery cone length for Nozzle Venturi**

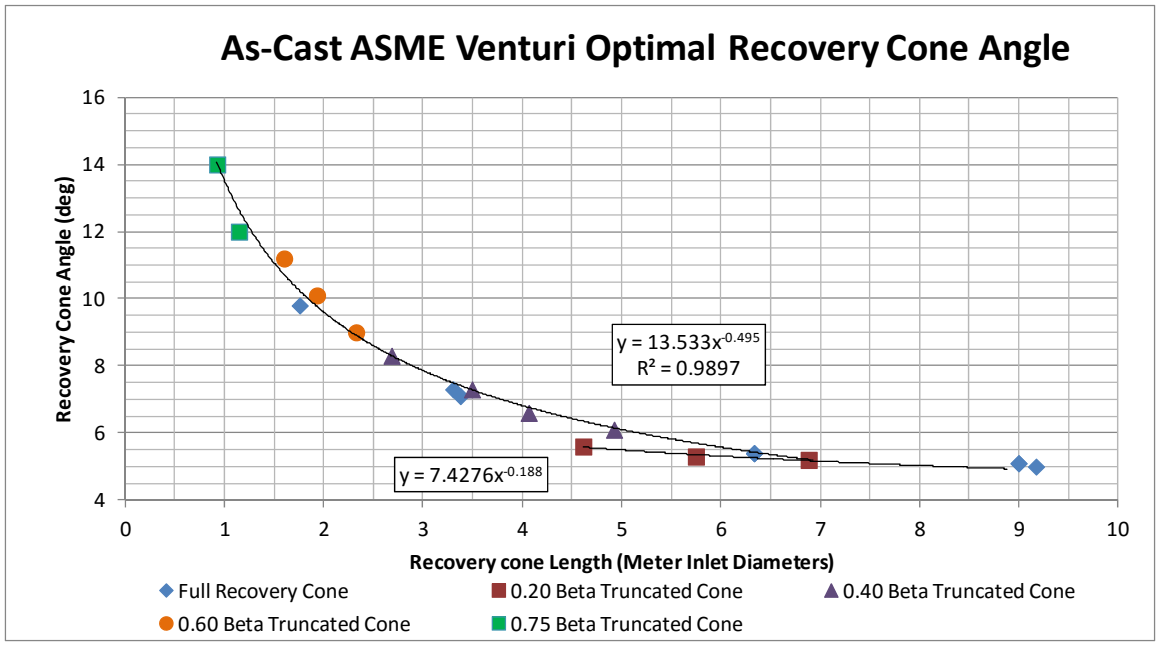


**Fig. 49. Optimum recovery cone angle versus recovery cone length for as-cast ASME Venturi**

**Discussion and Conclusions**

This study used physical and numerical data to determine optimum RCAs for five different truncated Venturi designs. Five different beta ratios of 0.20, 0.30, 0.40, 0.60, and 0.75 were analyzed with three different recovery cone lengths and multiple RCAs. The following describes some key findings of this study.

- CFD is capable of producing data predicting permanent pressure loss for many different Venturi designs including those with truncated recovery cones.
- Head loss measurements are sensitive both to the recovery cone angle and the location of the recovery cone truncation.
- Smaller beta ratio meter designs result in smaller optimal recovery cone angles and the truncation location does not have as much of an effect on the optimal recovery cone angle as it does with larger beta ratios.
- The more a recovery cone is truncated, the larger the optimal recovery cone angle needs to be. In other words the shorter the length of the recovery cone, the larger the optimal recovery cone angle.
- The change in the optimal recovery cone angle can vary widely for the same meter design and beta ratio as the truncation location changes. This is especially prevalent in meters with 0.60 and larger beta ratios.
- The optimal recovery cone without a truncation will always have less head loss than the optimal recovery cone with a truncation. This is also true for a full and truncated recovery cone of the same angle. There are however,

instances where for a given recovery cone length there is less head loss with a smaller recovery cone angle with a truncation than with a full recovery cone and a larger recovery cone angle.

- For small truncations, the increase in pressure loss is similar for each meter type tested. As the truncations get more extreme and approach the throat of the Venturis, the increase in pressure loss starts to vary by meter type.

It is anticipated that the data from this study will be used when a Venturi meter design is required to be shorter than recommended yet still have low head loss. When these conditions exist, as they often do, the meter length and design can be used with the data of this paper to determine the optimal recovery cone angle, and hence the truncation details of the Venturi recovery cone. It is not implied that all of the data in this study are absolute, as the numerical uncertainties have been listed; however, it provides much needed guidance previously unavailable in recovery cone design when limiting head loss is of importance. There may be circumstances where a particular meter application is outside of the scope of this paper. If this is the case, CFD has proven to be capable of assisting is recovery cone design when proper meshes and methods are used and the model is verified with experimental data.

# CHAPTER 6

## DISCUSSION AND CONCLUSIONS

The research presented in this dissertation show a small portion of the capabilities Computational Fluid Dynamics (CFD) has when applied to flow measurement and meter design. The research also presents the successes of CFD while being used in flow measurement when in reality there are some areas where CFD is not as applicable or accurate. For example, the flow simulations performed throughout this research calculated both the discharge coefficients and the head loss for multiple Venturi designs. As shown in the research, both the values of the discharge coefficients and head loss determined from CFD match experimental data. A good match for CFD could mean a one to two percent match with deviations as great as five percent considered acceptable by many CFD practitioners. While CFD accuracy might be good enough for head loss measurements and even for discharge coefficient in some applications, there are other applications where the flow measurements have required accuracies as low as 0.1 percent. This type of accuracy cannot be expected from CFD, and therefore, CFD should never be considered a replacement for a laboratory flow meter calibration on any type of meter.

In general when solving CFD problems in flow measurement, as the turbulence in the flow increases the accuracy of the CFD model decreases. For most Venturi meter designs the flow streamlines stay approximately parallel with the wall of the Venturi. This is how Venturi meters are designed, both to minimize head loss and have predictable

and stable differential pressure measurements. In meter designs where separation occurs, like an orifice plate or a wedge meter, it is more difficult for CFD to accurately predict discharge coefficients than with Venturi designs. This is because the zone of separation causes an increase in turbulence that CFD is not always able to accurately reproduce. While some turbulence models like the Reynolds stress and Large Eddy simulations do a better job of modeling the increase in turbulence from separation, they do not do as well as the K-epsilon turbulence model, which was used in this research, in predicting the discharge coefficients for any meter design tested by the author. When meter designs with separation are modeled in CFD, care needs to be taken to refine the mesh as needed where the separation occurs and, as with all CFD modeling, verification with laboratory data is invaluable.

Some other potential uses of CFD in flow metering include using CFD to predict the change in meter performance for particular piping arrangements. For many types of flow meters this kind of research has been performed for most piping scenarios (Baker 2000). The literature has many guidelines for meter installation distances from elbows, multiple elbows, expansions and reductions, and valves. There are still many meter installations, not researched due to the uniqueness of the installations, where CFD could successfully be used to predict the change in the meter discharge coefficients. Some of these could include multiple fitting combinations like elbows or manifolds coupled with control or isolation valves upstream of meters, or manifolds with flow to the meter and past the meter to another location. One of the strengths of CFD is being able to see differences in velocities and pressures in the flow domain resulting in geometry changes

like different piping scenarios. This type of analysis would not be have to be limited to differential producing meters alone, it could also work for magnetic, ultrasonic or turbine technologies as well. One of the keys to using CFD to predict flow measurement is to use it to make the same measurements as would be made with the meter technology. For example if using CFD to replicate a Venturi then the Venturi geometry needs to be appropriately modeled and then pressure measurement are taken in CFD at the same locations they would be taken physically if the meter were calibrated in a laboratory. If CFD is used to replicate an ultrasonic flow meter than the same steps should be taken as with the Venturi. The geometry needs to be modeled correctly, and then the velocity should be measured at the same locations in the CFD model as it would be by the ultrasonic meter in the field, which is in line with the transducers. Once these measurements are taken the flow rate can then be calculated in the same manner as with the ultrasonic meter in the field. While CFD may not accurately predict the absolute flow rates it will give the user a good idea of the change in flow reading the ultrasonic meter may see as a result of different piping arrangements.

The research presented used CFD to successfully solve three particular problems in flow measurement and provides information to both meter manufactures and users previously unavailable. The three problems are briefly described below:

1. Determine the effects of sudden pipe wall offsets on Venturi flow meters. This research included both the effects of the pipe wall offset on the meter discharge coefficient as well as the distance required between the offset and the Venturi so that there is no longer any effect on meter performance. This information is very

useful for laboratories calibrating meters of different diameters, end users who do not know the exact pipe diameter where the meter will be installed and instance when pipes are not perfectly round and the sudden expansion or contraction happens locally upstream of the meter.

2. Optimize the design of pressure recovery cones on different Venturi flow meter designs including determining the optimal angle of recover cone required to minimize permanent pressure loss. This information is valuable to committees writing codes and should be included in codes, meter manufactures, and any end user of a Venturi who needs the head loss to be as low as possible.
3. Optimize truncated recovery cone designs such that a meter can be manufactured using a shorter length. This research also included determining the best way to truncate the meter to minimize head loss while not changing the flow metering capability of the Venturi meter. This information is also valuable to committees writing codes and should be included in codes, meter manufactures, and any end user of a Venturi who needs the head loss to be as low as possible while having restraints in the meter length.

CFD coupled with laboratory data were used to solve these problems and present design information. The results of this research will be published in various peer reviewed journals. In closing, CFD can be and is used as a valuable tool in industry for solving flow problems related to flow measurement. The research presented opens some new avenues of research to be accomplished by using CFD to assist in flow metering and flow meter design applications which has rarely been done prior to this study.

# REFERENCES

Baker, R.C. (2003). *An Introductory Guide to Flow Measurement,* The American Society of Mechanical Engineers, New York.

Baker. R.C. (2000). *Flow Measurement Handbook: Industrial Designs, Operating Principles, Performance, and Applications,* Cambridge University Press, Cambridge.

BIF (Builders Iron Foundery) (2016). <http://www.bifwater.com> (Jan. 6, 2015).

CD-adapco (2016). "STAR-CCM+ User Guide Version 10.06." <http://stevedocs.cd-adapco.com/> (Jan. 20, 2016).

Celik, I.B., Ghia, U., Roache, P.J., Freitas, C.J., Coleman, H., and Raad, P.E. (2008). "Procedure for Estimation and Reporting of Uncertainty Due to Discretization in CFD Applications." *Journal of Fluids Engineering-Transactions of the ASME*, 130, 078001-3.

Crane, (1988). *Flow of Fluids through Valves, Fittings and Pipe. Crane Co. Technical Paper No. 410*, Crane Co., Joliet, Ill.

Finnemore, E. J. and Franzini, J.B. (2006). *Fluid Mechanics with Engineering Applications,* 10th Ed., McGraw-Hill, New York.

Gibson, A. H. (1908). *Hydraulics and its Applications*, 5th Ed., D. Van Nostrand Company, New York.

Hollingshead C.L., Johnson, M.C., Barfuss, S.L., and Spall, R.E. (2011). "Discharge coefficient performance of Venturi, standard concentric orifice plate, V-cone and wedge flow meters at low Reynolds numbers." *Journal of Petroleum Science and Engineering*, 78(3), 559-566.

Instrument Society of America (ISA) (1988). "Control Valve Capacity Test Procedure: An American National Standard", ANSI/ISA-S75.02-1988. Instrument Society of America, Research Triangle Park, N.C.

International Standard (ISO) (2003). "Measurement of fluid flow by means of pressure differential devices inserted in circular cross-section conduits running full — Part 4: Venturi tubes." ISO copyright office, Geneva, Switzerland. ISO 5167-4.

Miller, D.S. (1978). *Internal flow systems*, The British Hydromechanics Research Association (BHRA), Cranfield, United Kingdom.

Miller, R.W. (1996). *Flow Measurement Engineering Handbook,* McGraw-Hill, Boston.

Nayyar, M.L. (2000). “Introduction to Piping.” *Piping handbook*, McGraw-Hill, New York.

PFS (Primary Flow Signal Inc.) (2014). <http://www.primaryflowsignal.com> (May 20, 2014).

Pope, J.M., Barfuss, S.L., Johnson, M.C., and Sharp, Z.B. (2015). “Effects of Pipe Wall Offsets on Differential Pressure Meter Accuracy.” *Journal American Water Works Association*, 107(6), 313-320.

Prajapati, C.B., Patel, V.K., Singh, S.N., and Seshardi, V. (2010). “CFD Analysis of Permanent Pressure Loss For Different Types of Flow Meters in Industrial Applications.” *4th International Conference on Fluid Mechanics and Fluid Power*, Chennai, India.

Ramamurthy, A.S., Qu, J., and Zhai, C. (2006). “3D Simulation of Combining Flows in 90° Rectangular Closed Conduits.” *Journal of Hydraulic Engineering,* 132(2), 214-218.

Rapier, A.C. (1981). “The Effect of Upstream Flow Conditions on Flow Meters.” *Proc., Intl. Conf. on Advances in Flow Measurement Techniques,* Warwick, United Kingdom.

The American Society of Mechanical Engineers (ASME). (2005). “Flow Measurement: An American National Standard.” New York. ASME PTC 19.5-2005.

The American Society of Mechanical Engineers (ASME). (2007). “Measurement of Fluid Flow in Pipes Using Orifice, Nozzle and Venturi: An American National Standard.” New York. ASME MFC-3Ma-2007.

The American Society of Mechanical Engineers (ASME), 2006. “Test Uncertainty: An American National Standard.” New York. ASME PTC 19.1-2006.

# APPENDICES

# Appendix A: Optimization curves for Venturis with full recovery cones

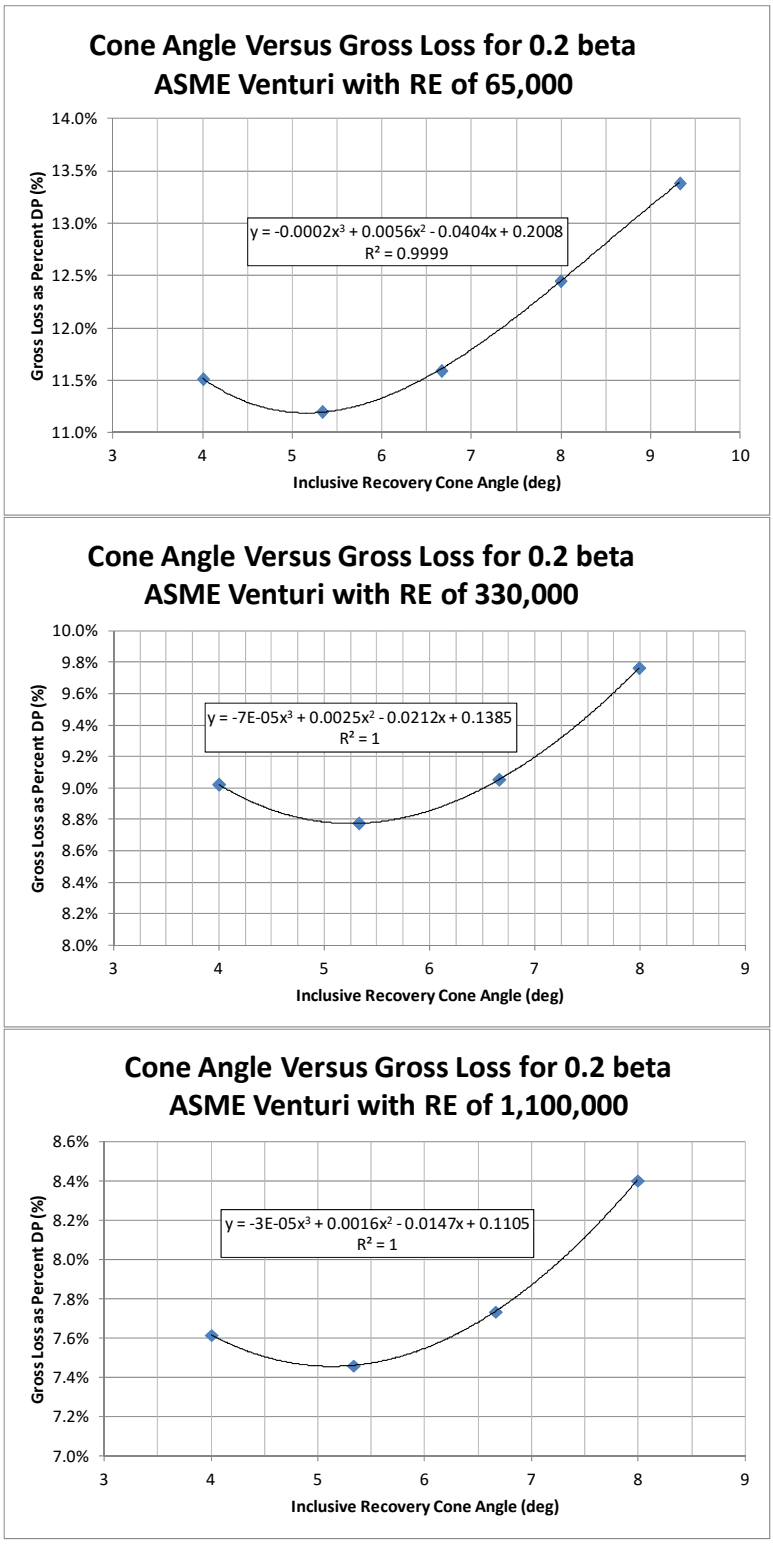


**Fig. A- 1. Head loss vs. cone angle for 0.20 beta ASME Venturi with smooth wall**

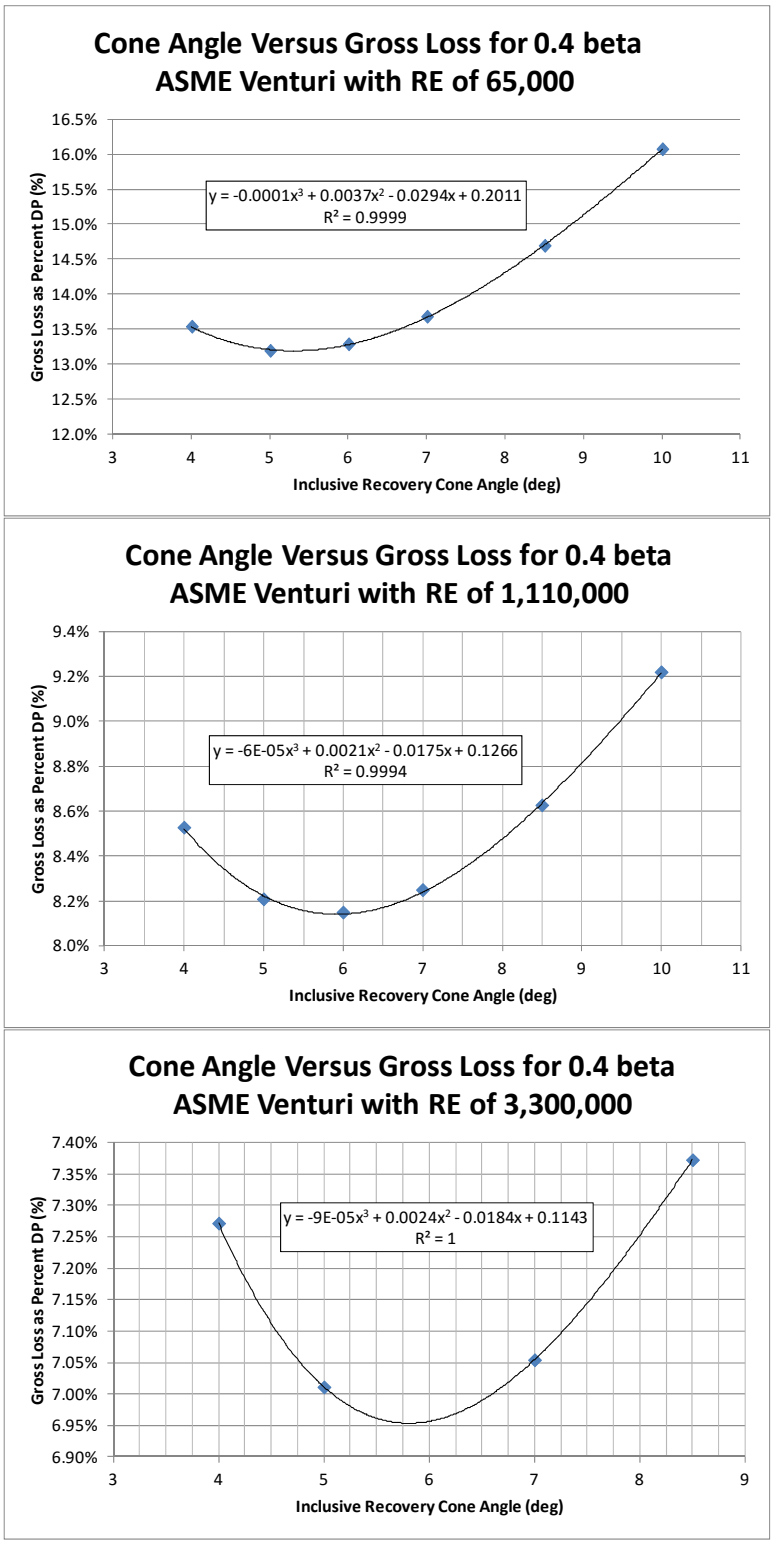


**Fig. A- 2. Head loss vs. cone angle for 0.40 beta ASME Venturi with smooth wall**

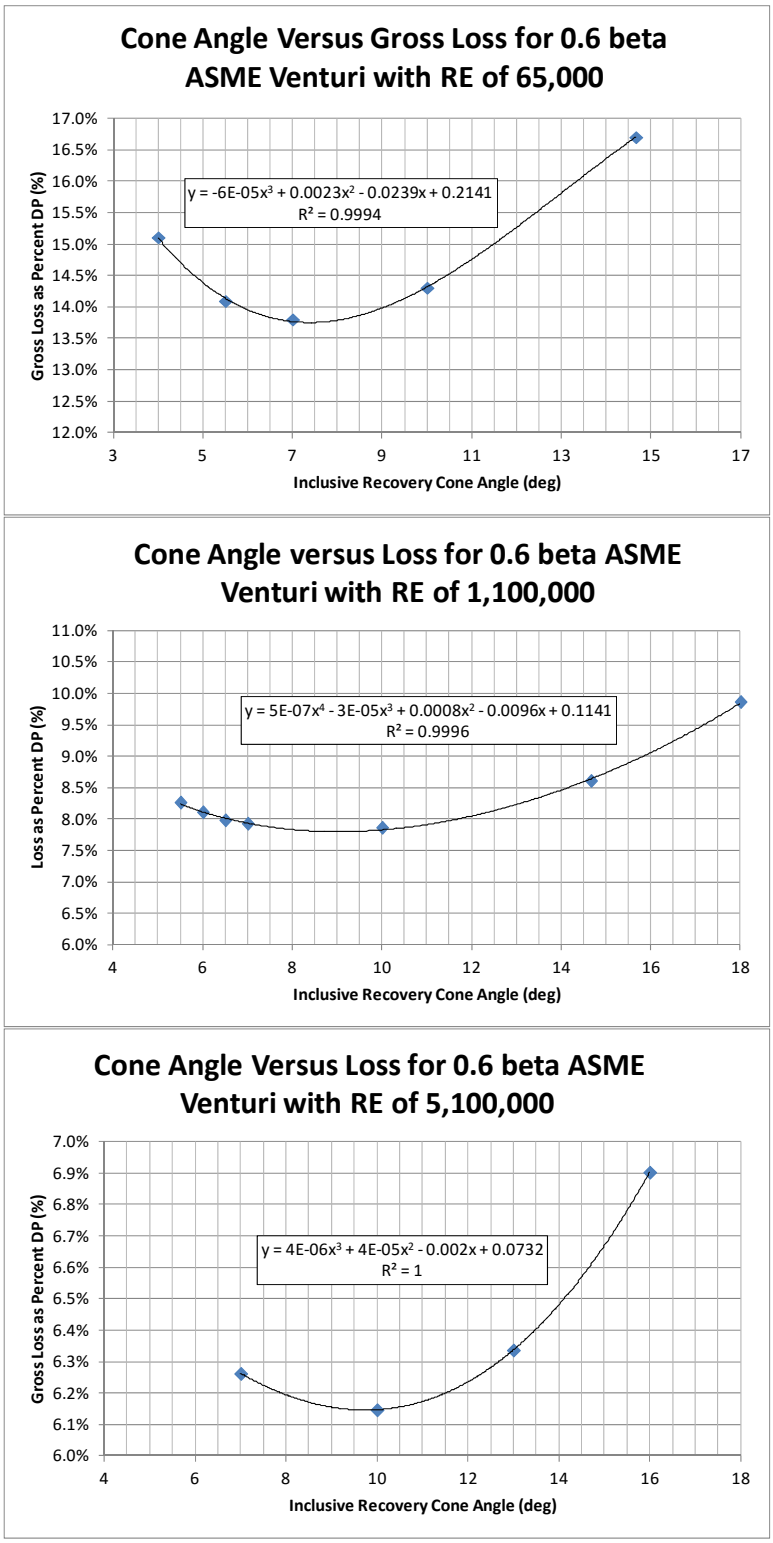


**Fig. A- 3. Head loss vs. cone angle for 0.60 beta ASME Venturi with smooth wall**

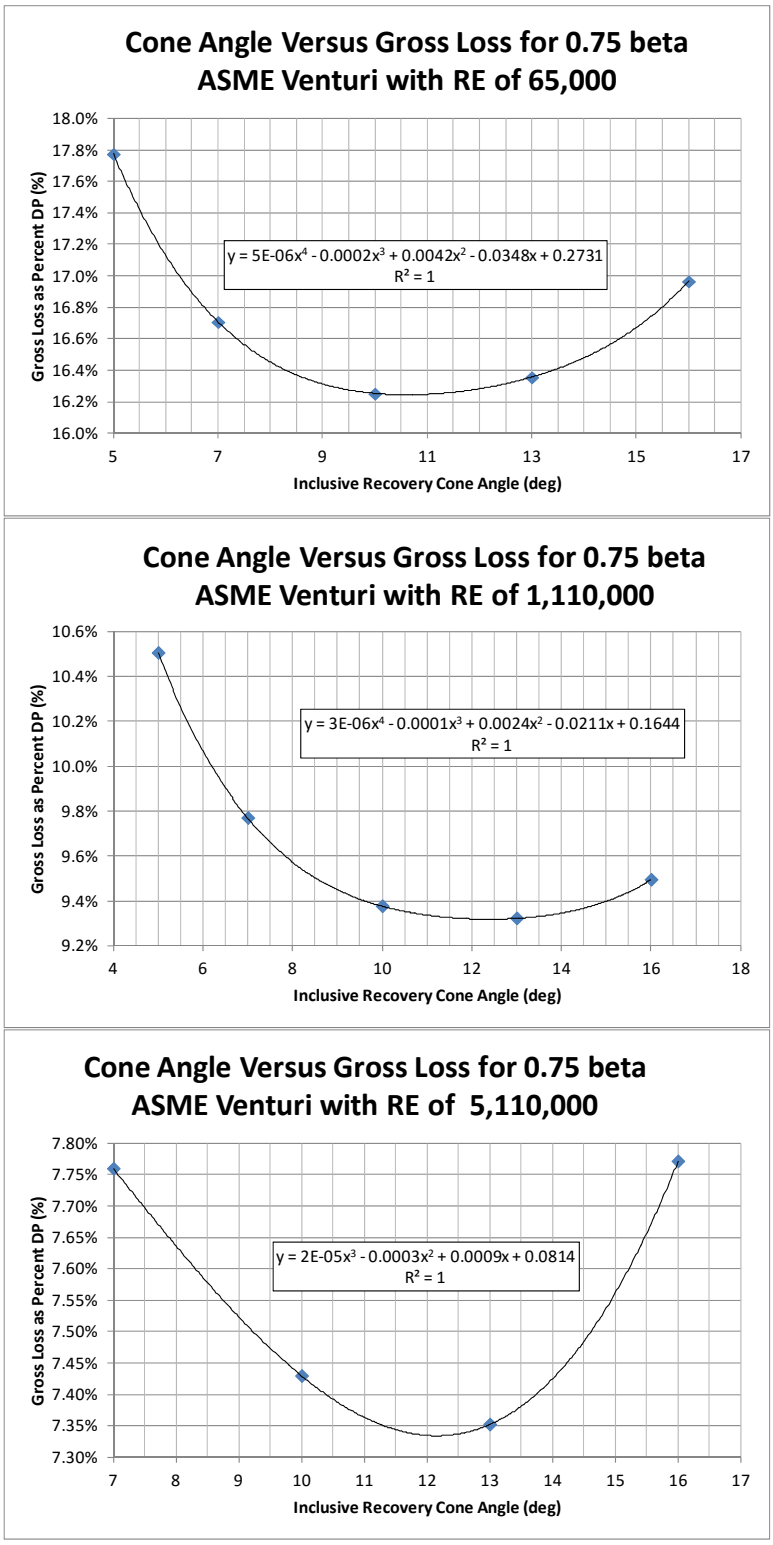


**Fig. A- 4. Head loss vs. cone angle for 0.75 beta ASME Venturi with smooth wall**

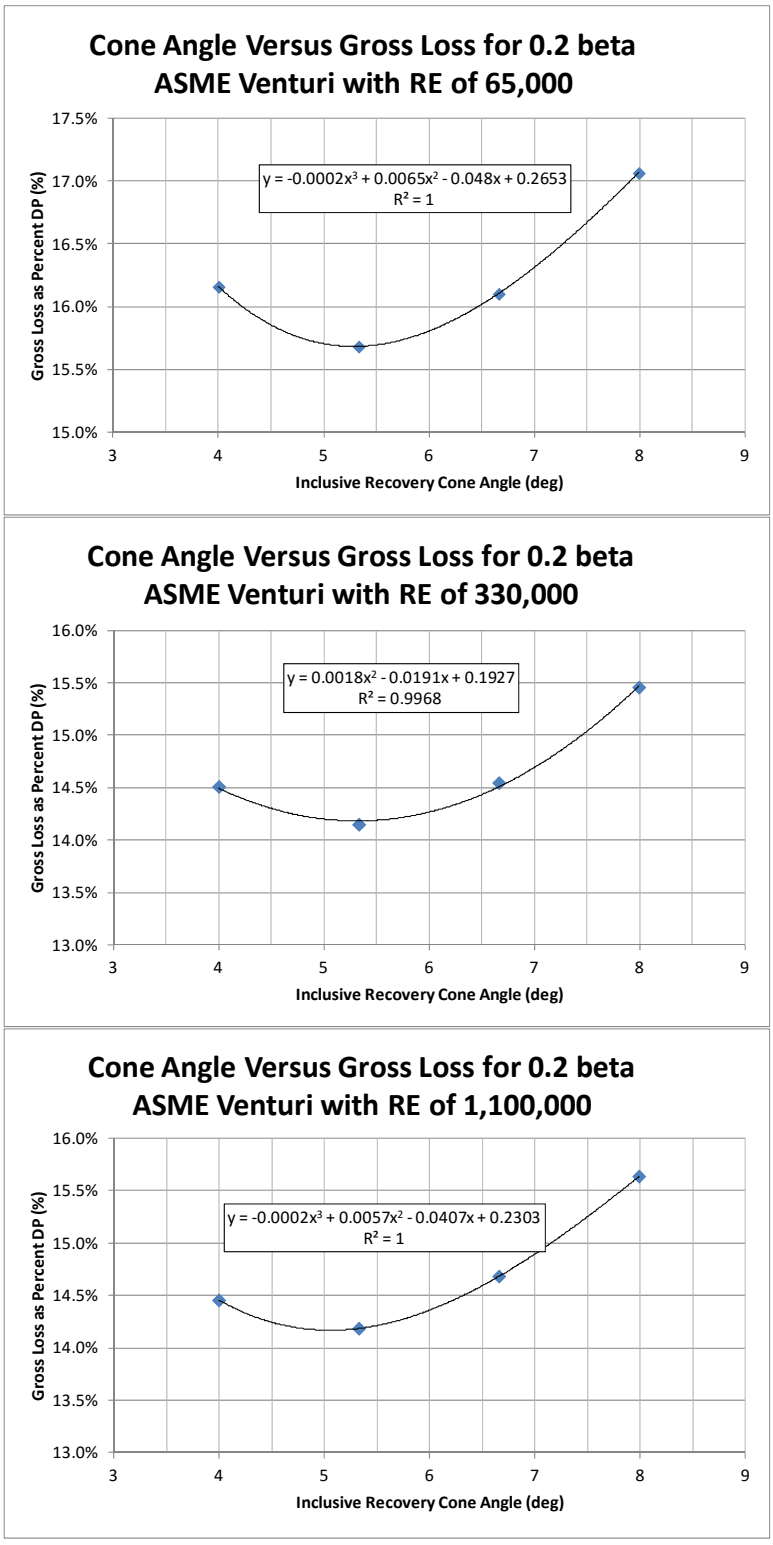


**Fig. A- 5. Head loss vs. cone angle for 0.20 beta ASME Venturi with rough wall**

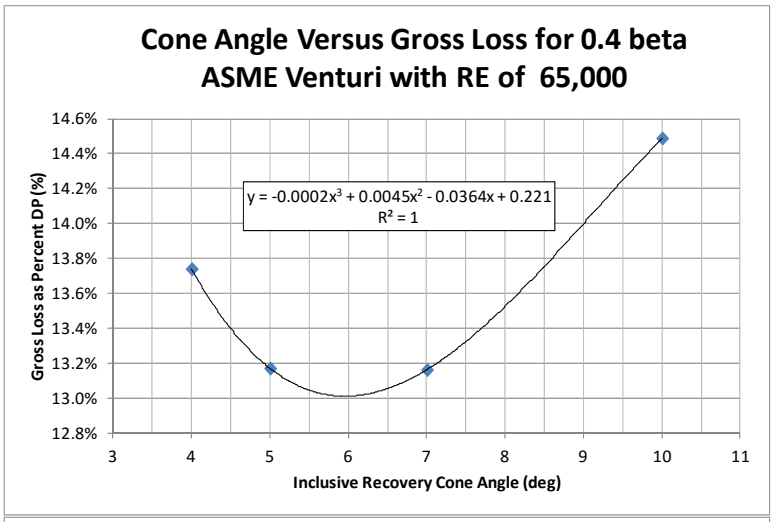


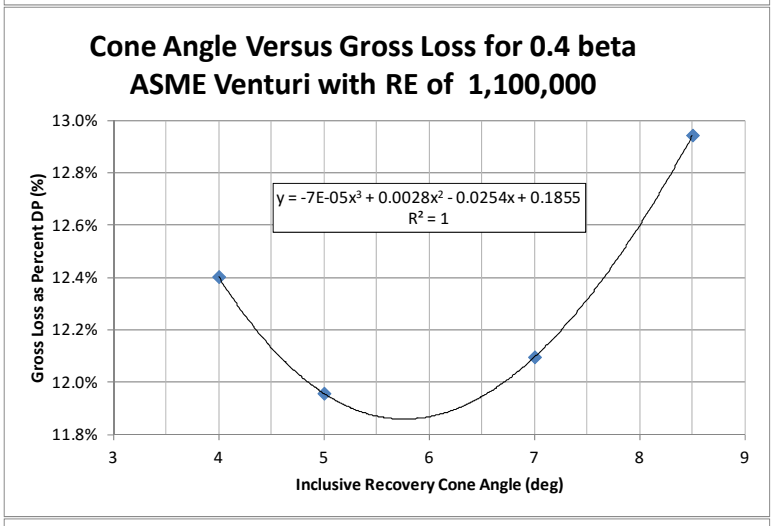


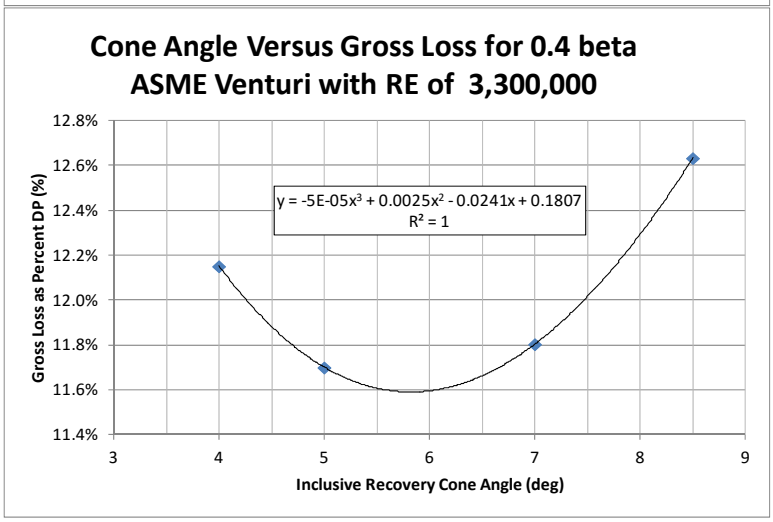


**Fig. A- 6. Head loss vs. cone angle for 0.40 beta ASME Venturi with rough wall**

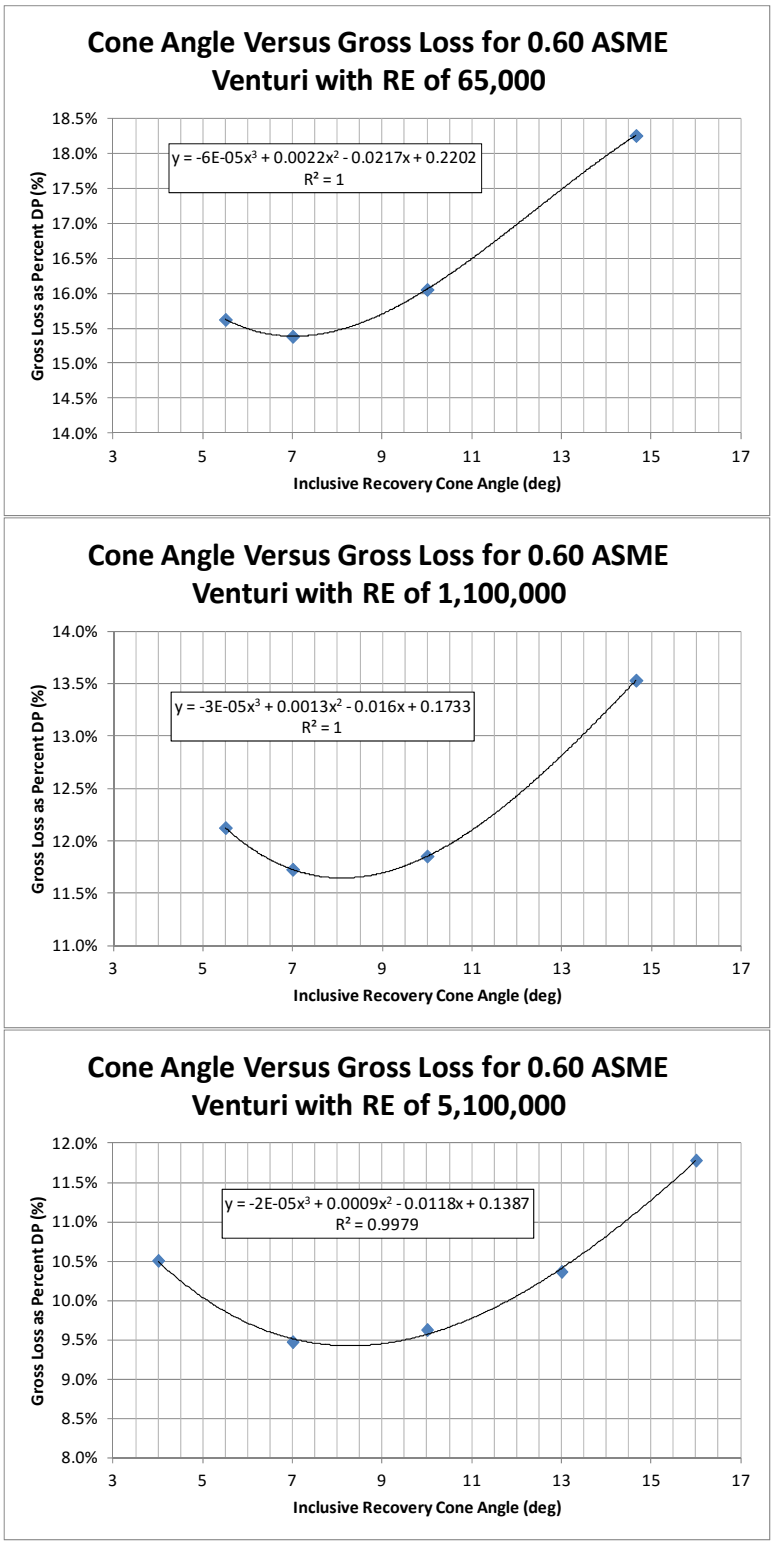


**Fig. A- 7. Head loss vs. cone angle for 0.60 beta ASME Venturi with rough wall**

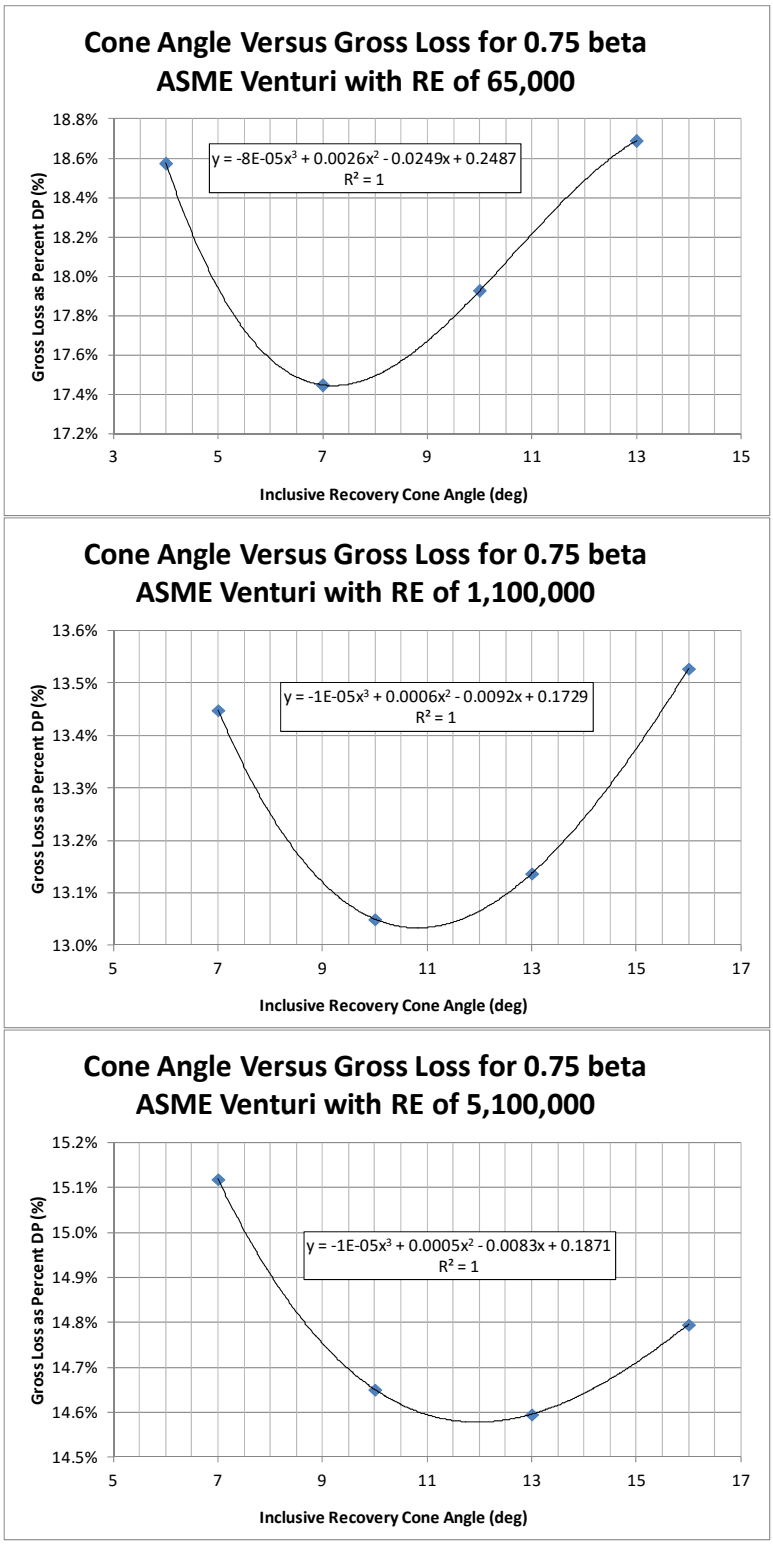


**Fig. A- 8. Head loss vs. cone angle for 0.75 beta ASME Venturi with rough wall**

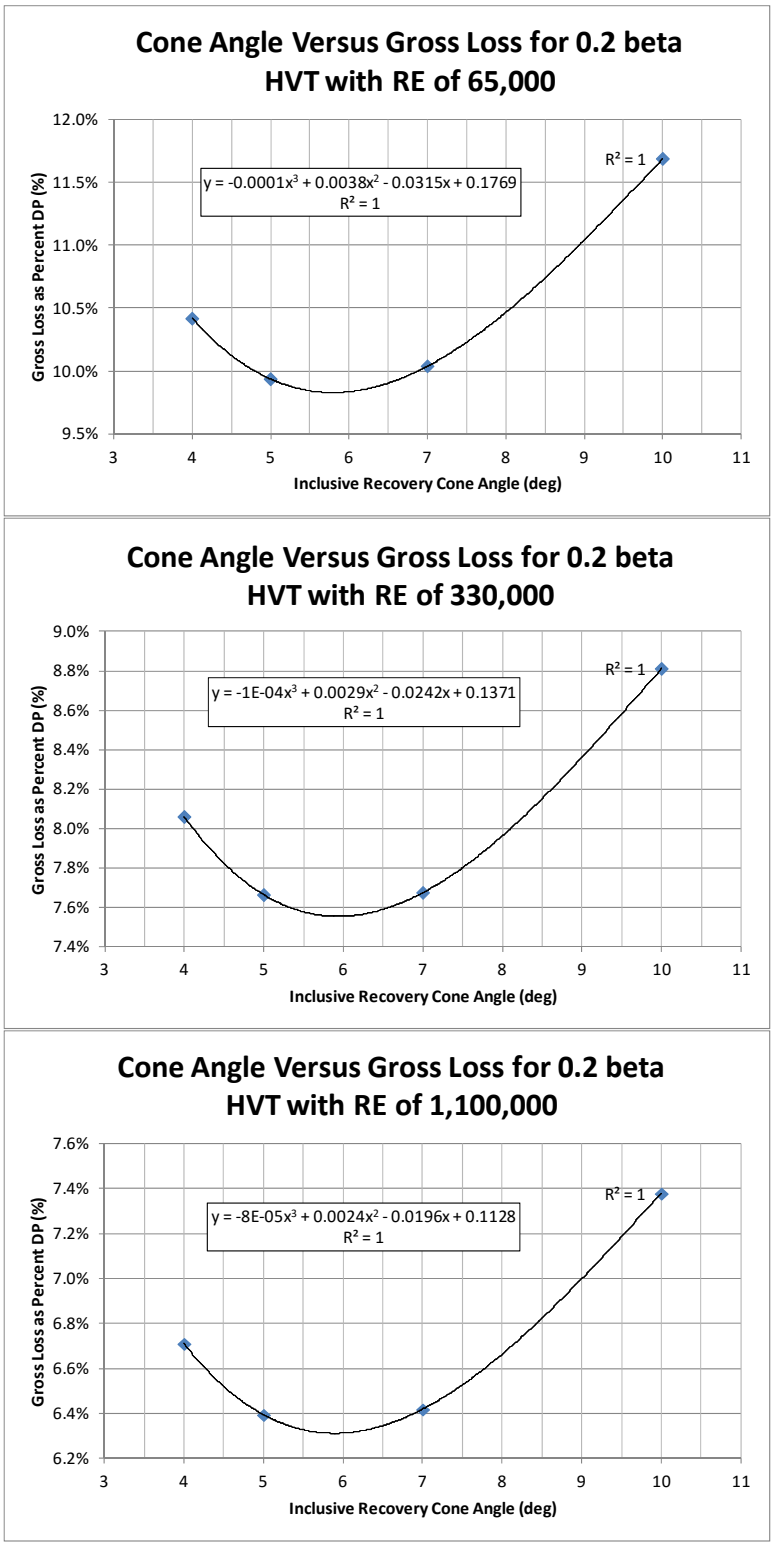


**Fig. A- 9. Head loss vs. cone angle for 0.20 beta HVT with smooth wall**

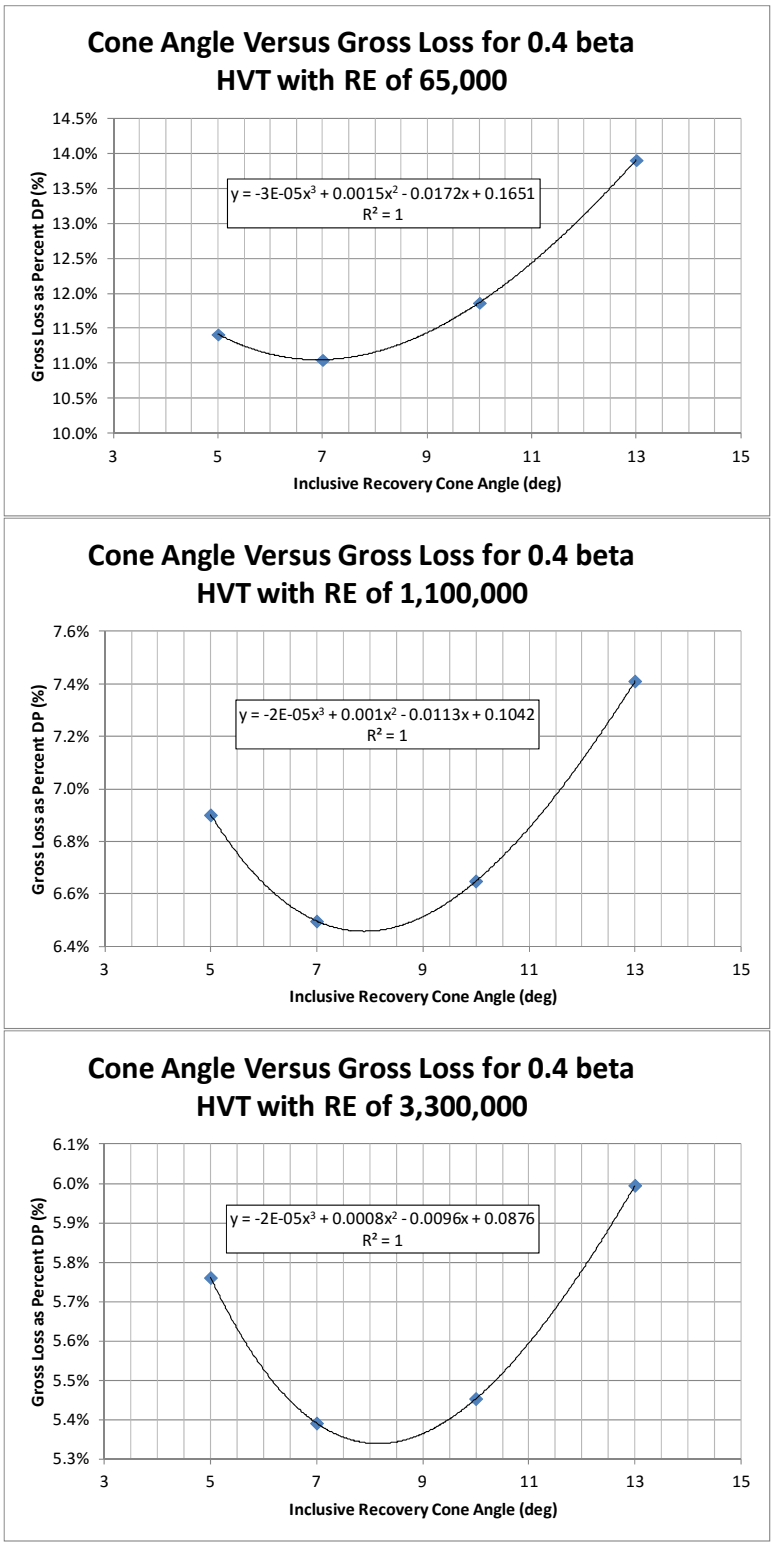


**Fig. A- 10. Head loss vs. cone angle for 0.40 beta HVT with smooth wall**

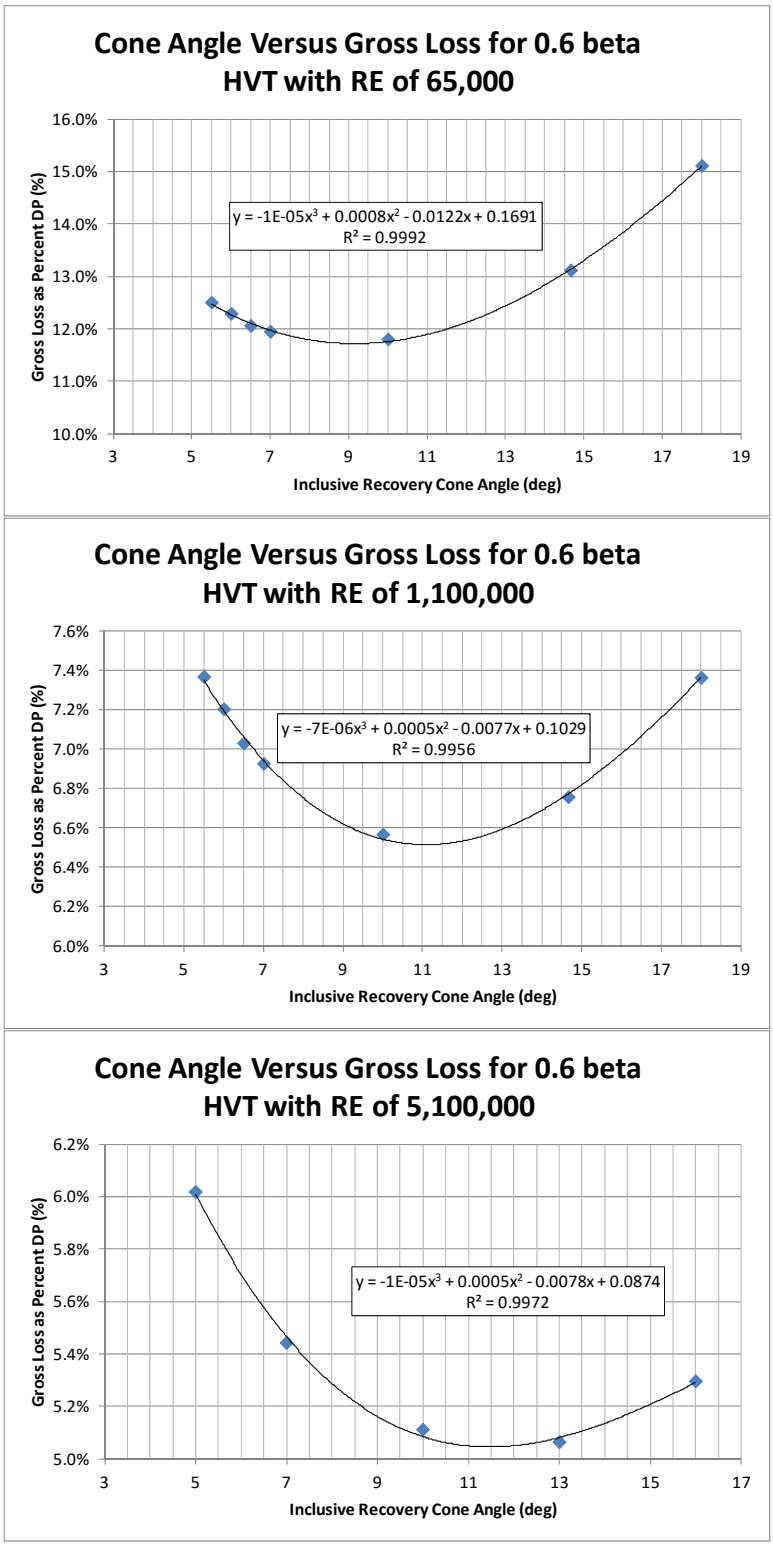


**Fig. A- 11. Head loss vs. cone angle for 0.60 beta HVT with smooth wall**

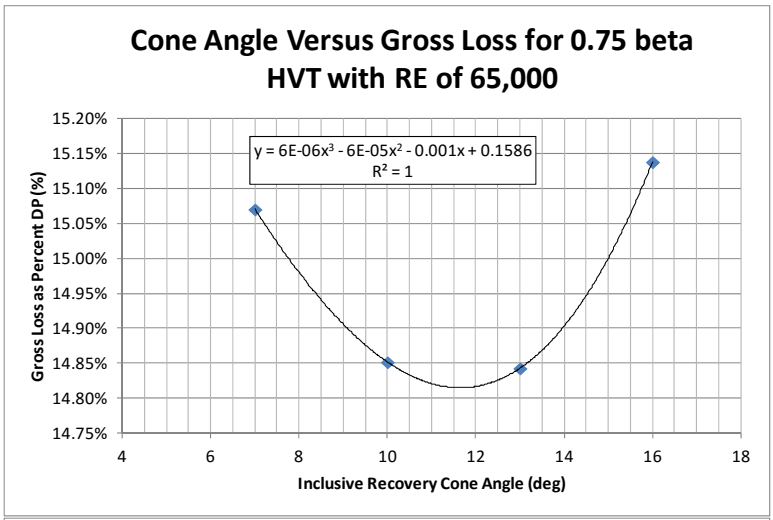


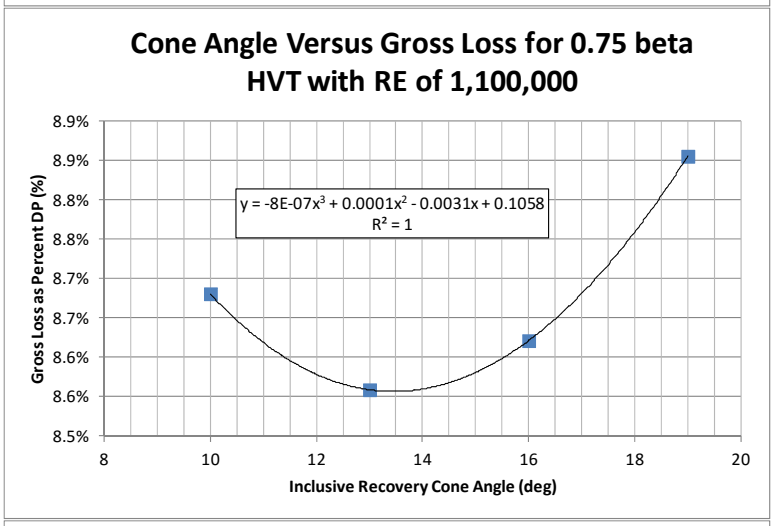


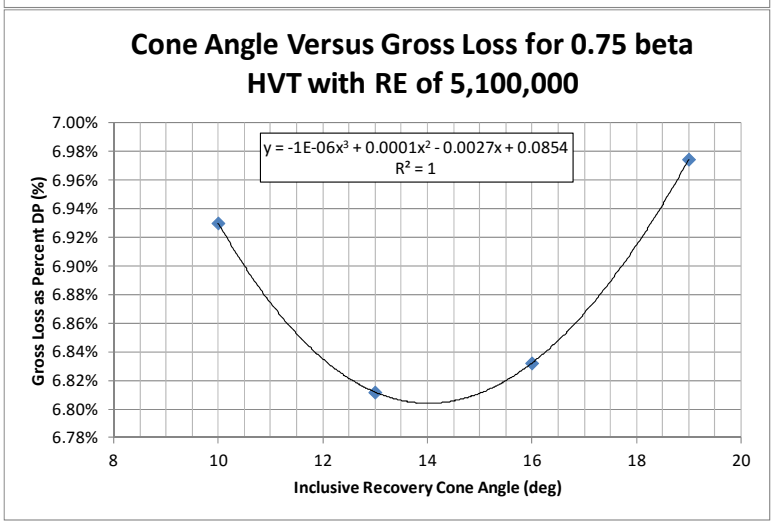


**Fig. A- 12. Head loss vs. cone angle for 0.75 beta HVT with smooth wall**

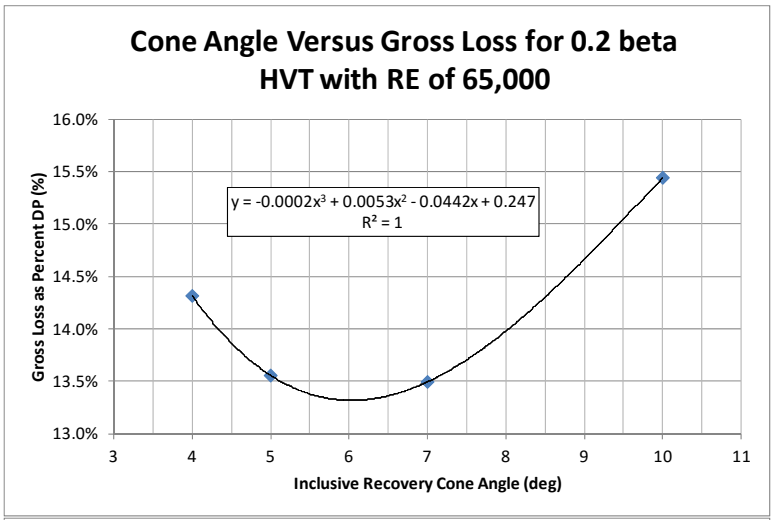


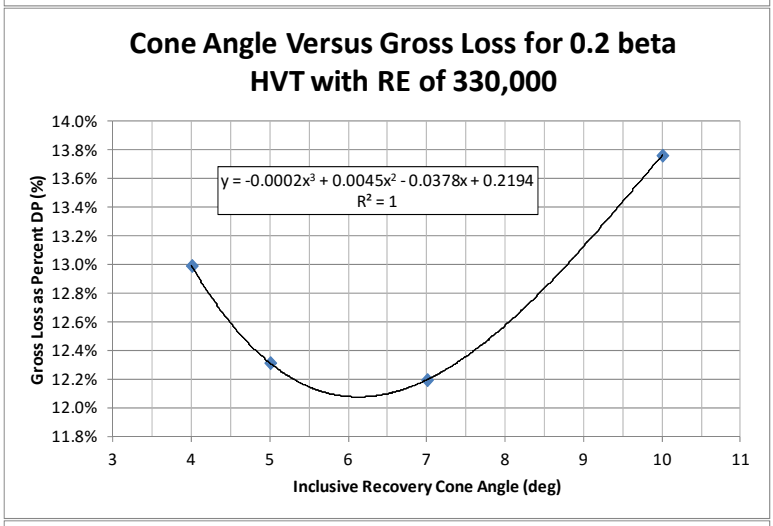


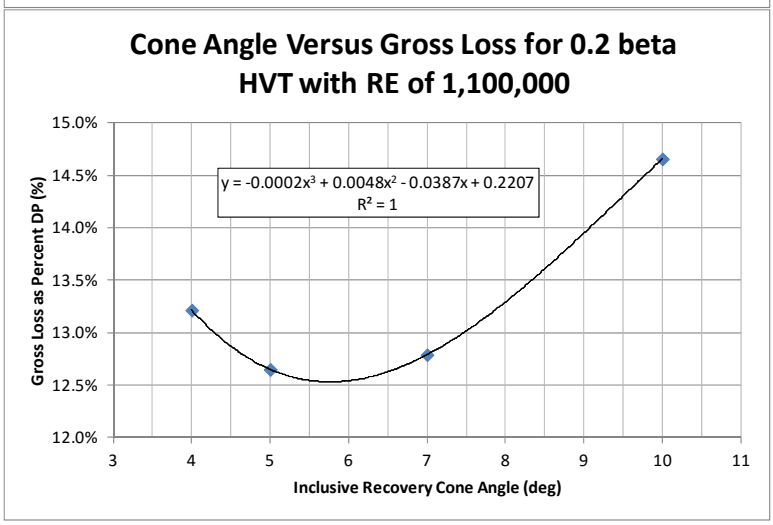


**Fig. A- 13. Head loss vs. cone angle for 0.20 beta HVT with rough wall**

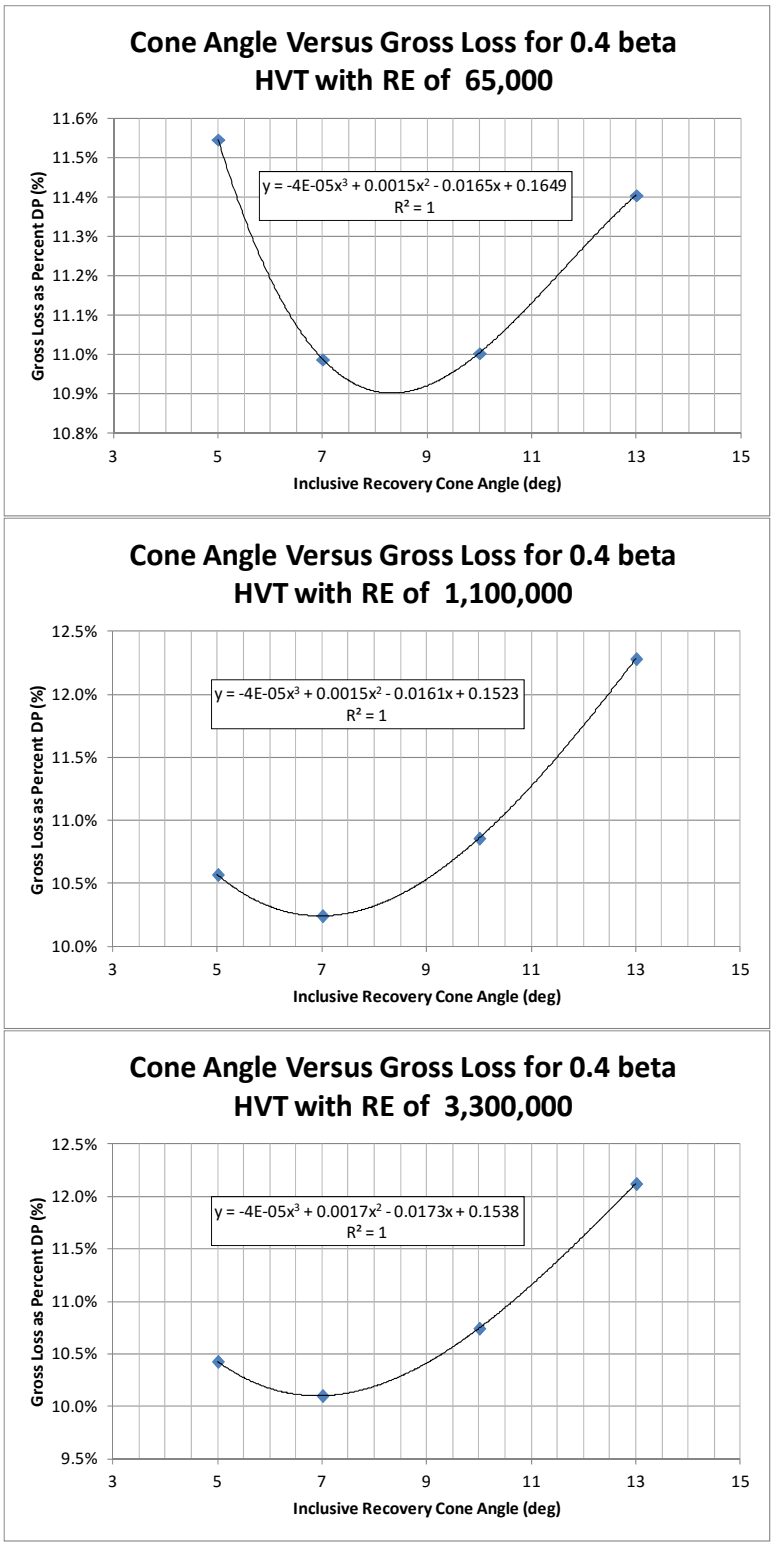


**Fig. A- 14. Head loss vs. cone angle for 0.40 beta HVT with rough wall**

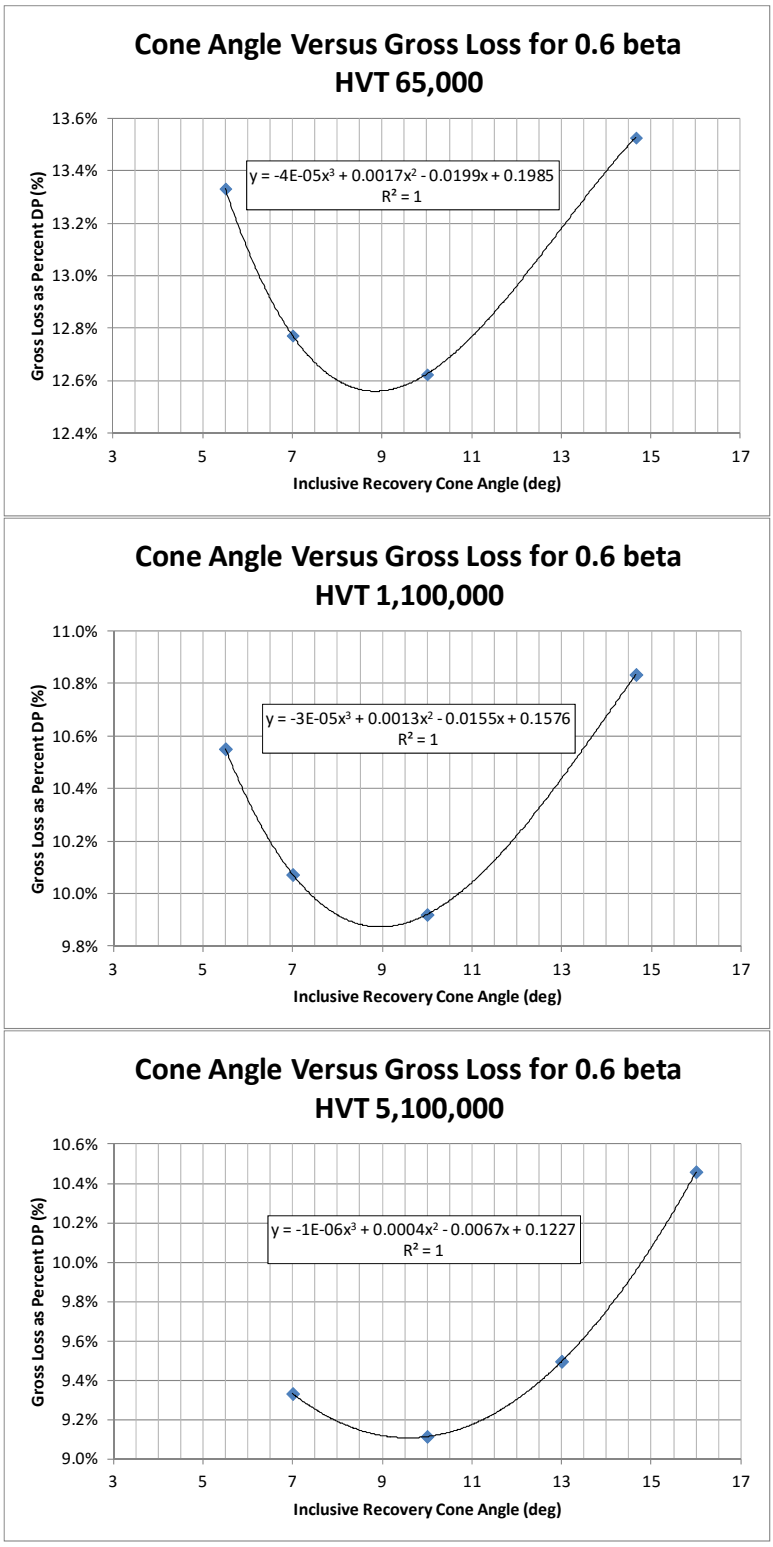


**Fig. A- 15. Head loss vs. cone angle for 0.60 beta HVT with rough wall**

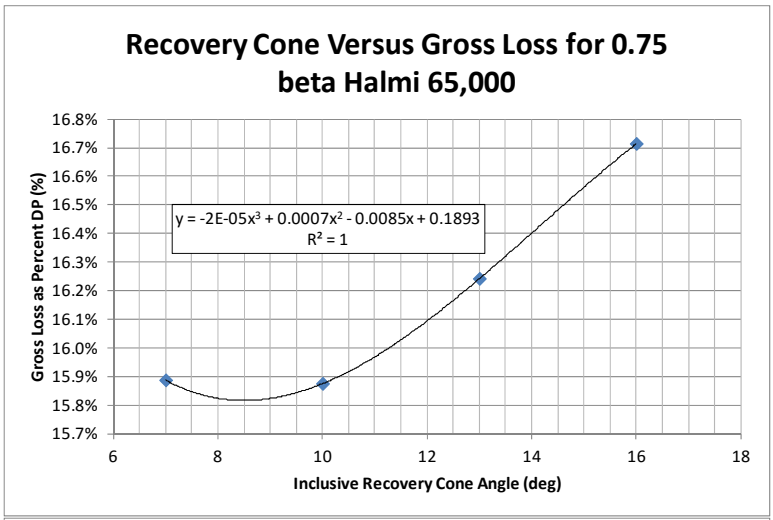


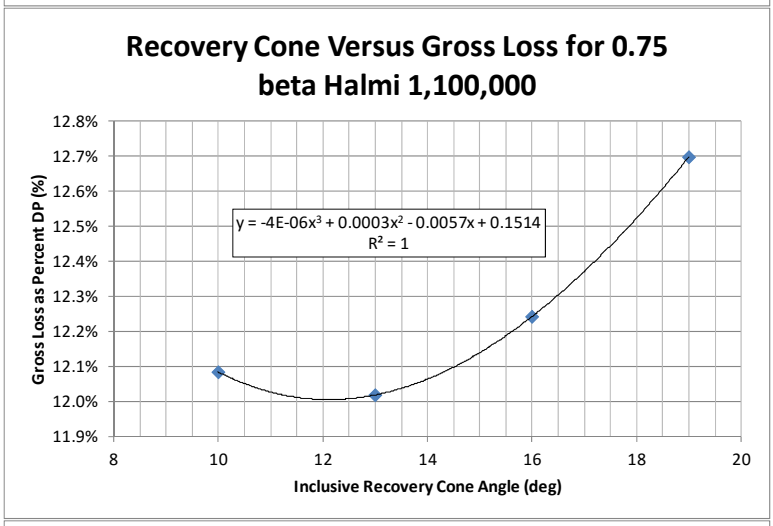


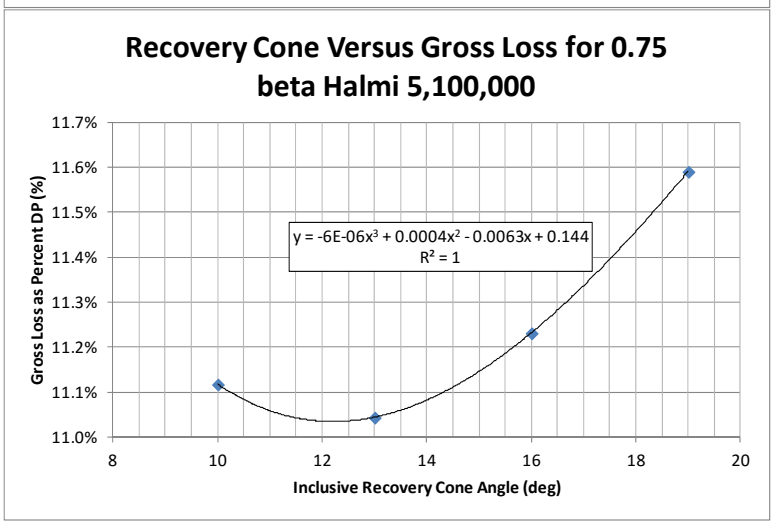


**Fig. A- 16. Head loss vs. cone angle for 0.75 beta HVT with rough wall**

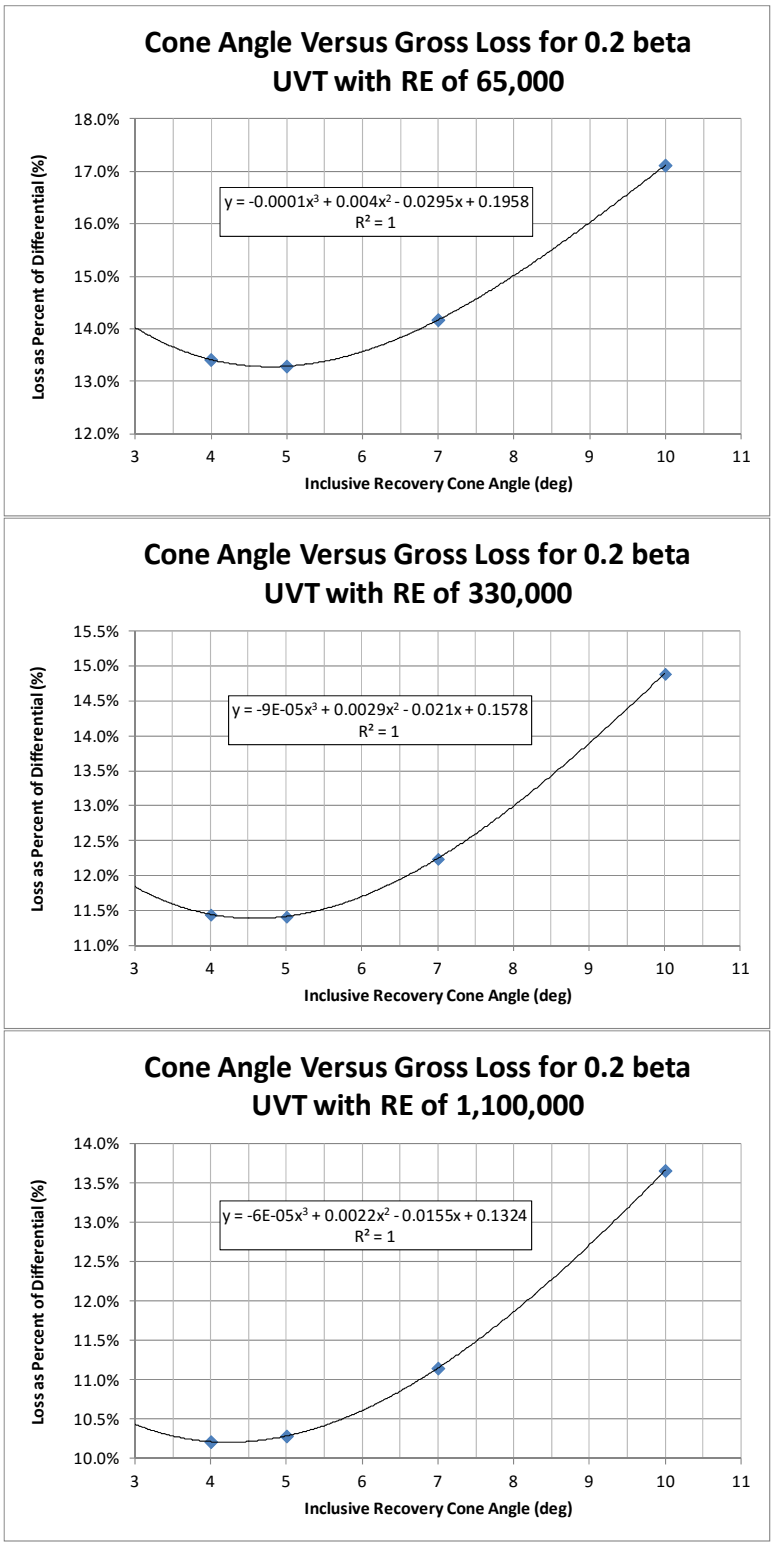


**Fig. A- 17. Head loss vs. cone angle for 0.20 beta UVT with smooth wall**

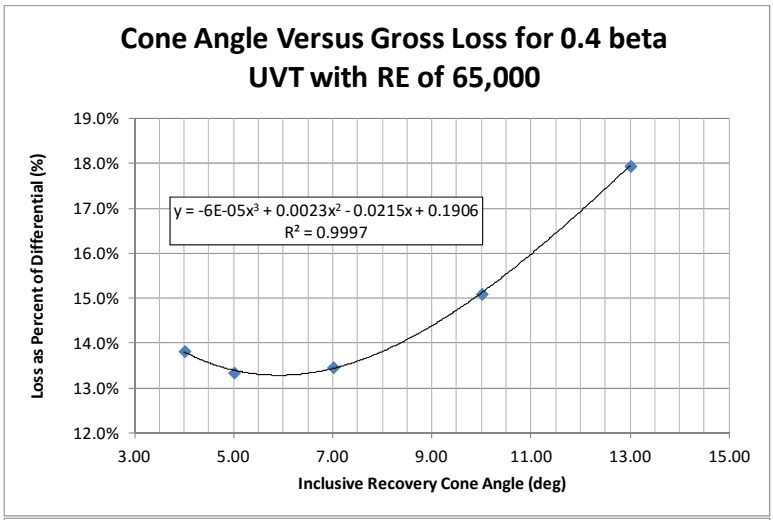


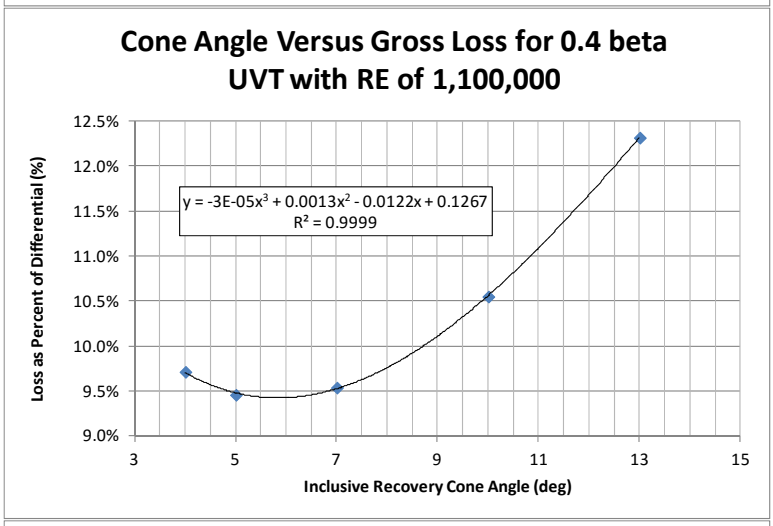


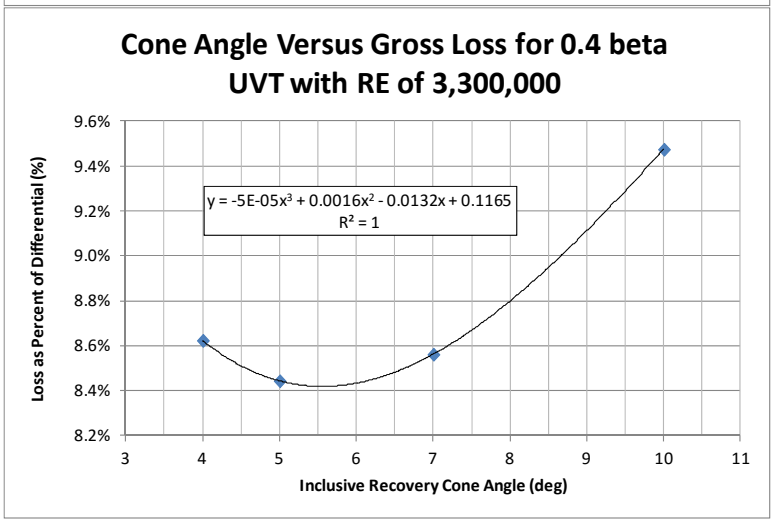


**Fig. A- 18. Head loss vs. cone angle for 0.40 beta UVT with smooth wall**

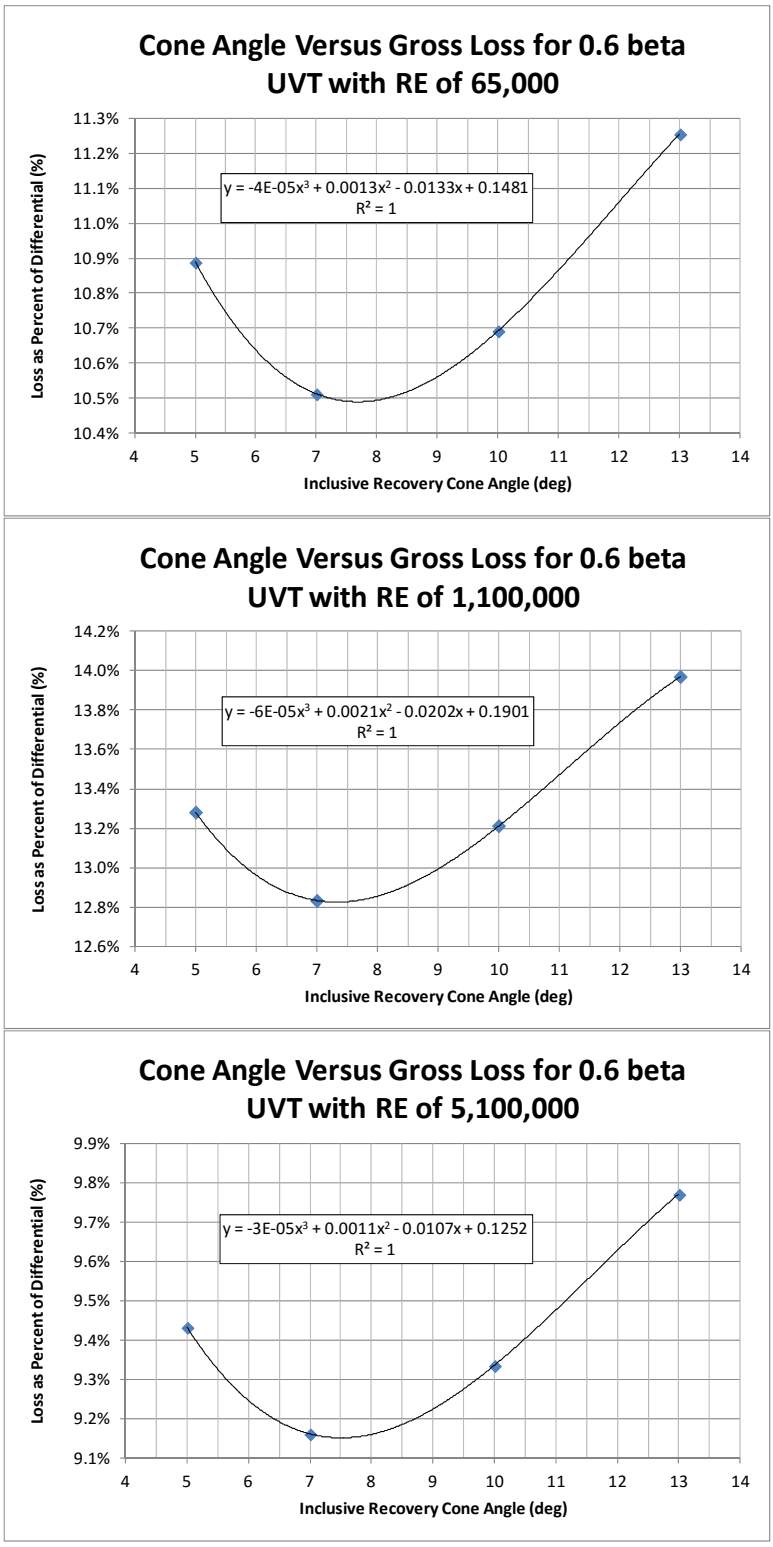


**Fig. A- 19. Head loss vs. cone angle for 0.60 beta UVT with smooth wall**

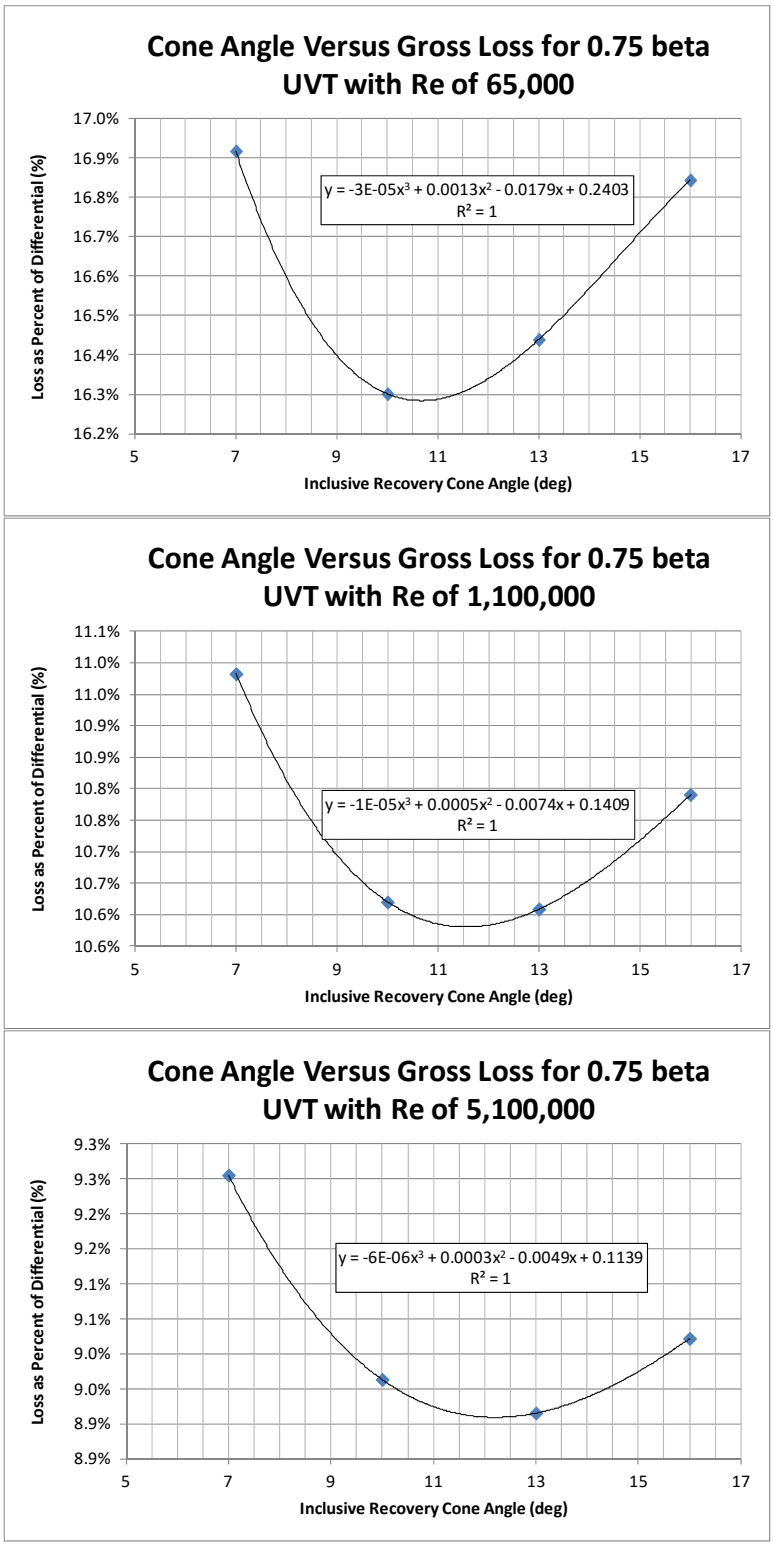


**Fig. A- 20. Head loss vs. cone angle for 0.75 beta UVT with smooth wall**

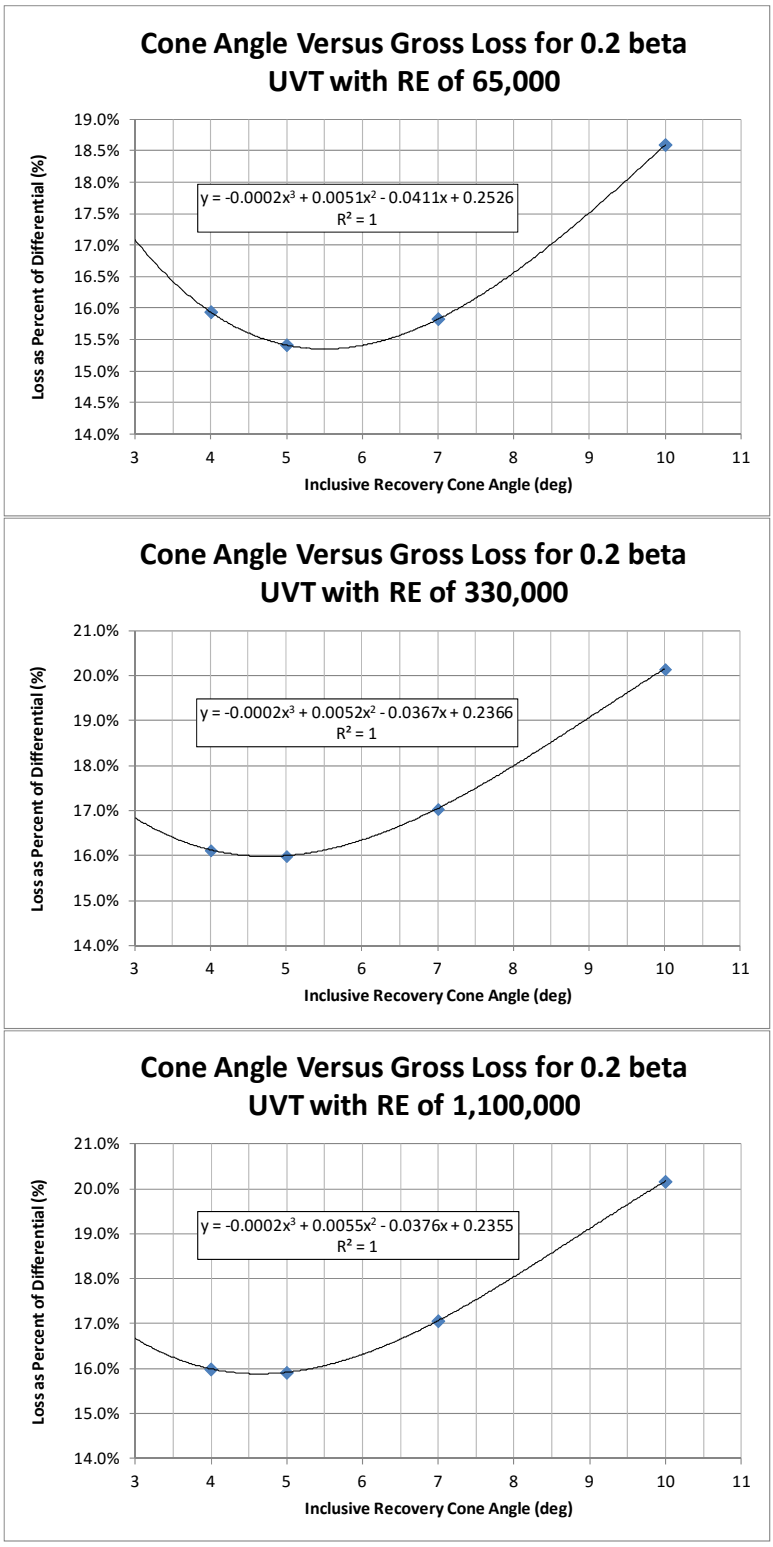


**Fig. A- 21. Head loss vs. cone angle for 0.20 beta UVT with rough wall**

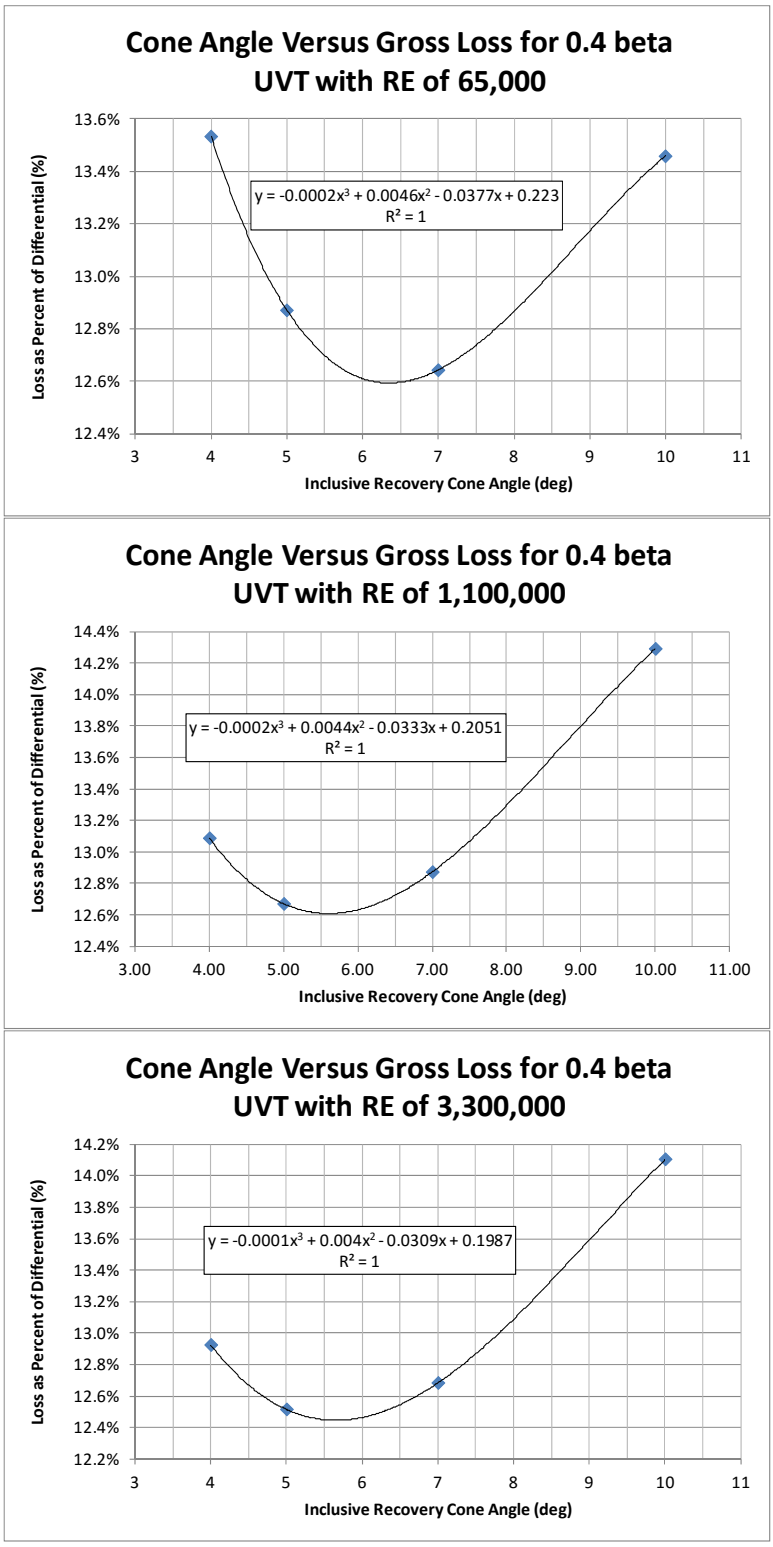


**Fig. A- 22. Head loss vs. cone angle for 0.40 beta UVT with rough wall**

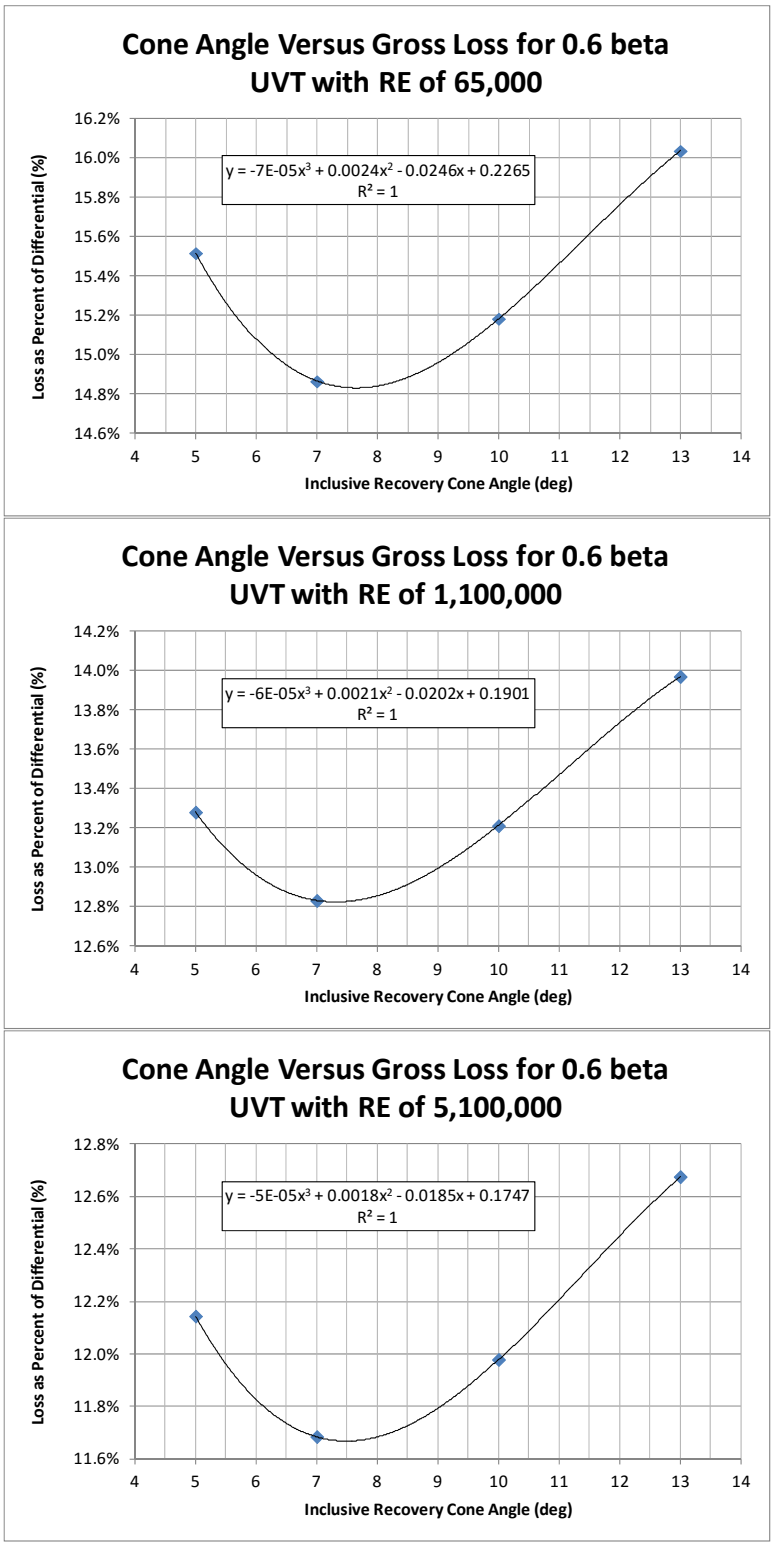


**Fig. A- 23. Head loss vs. cone angle for 0.60 beta UVT with rough wall**

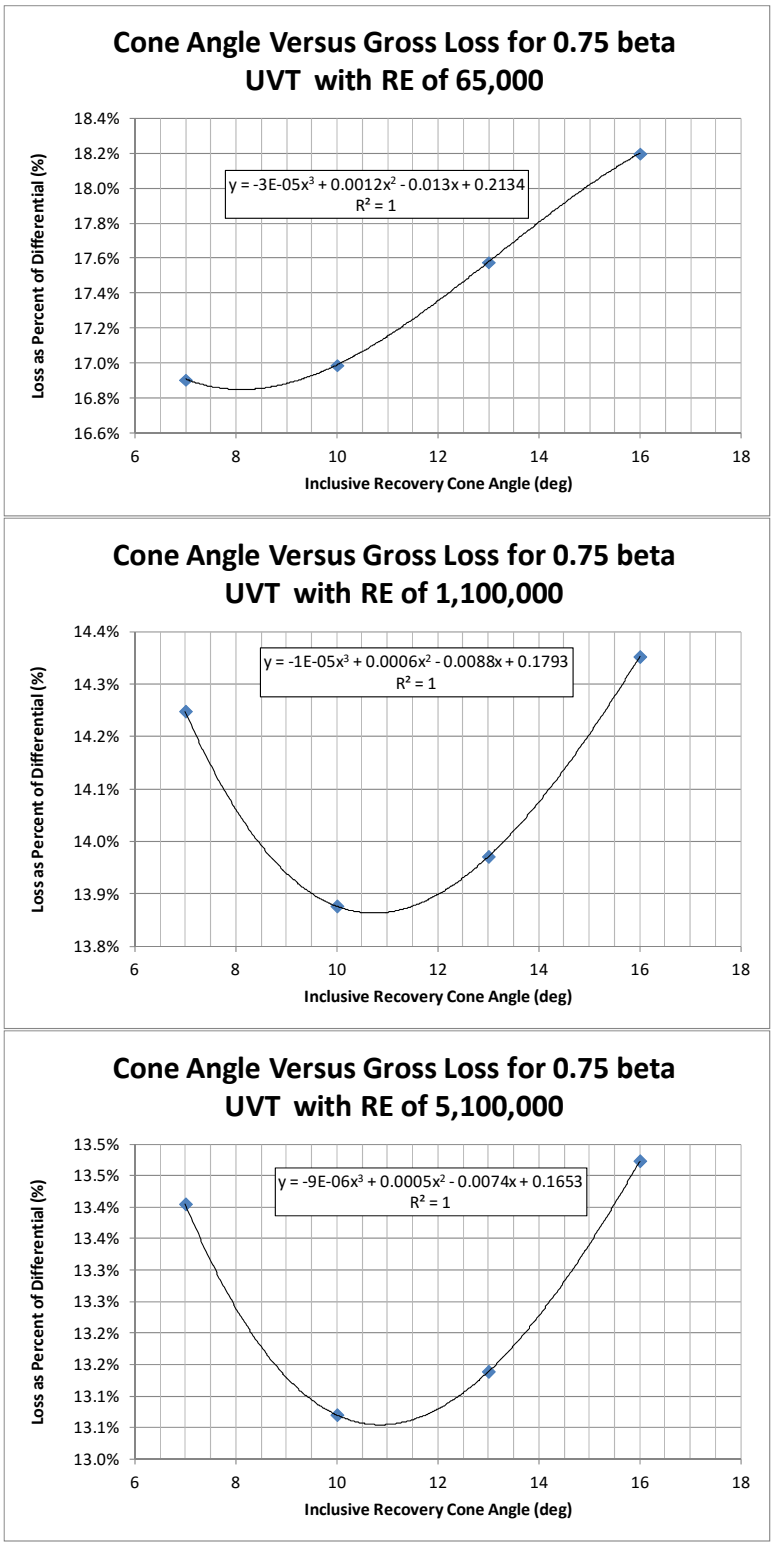


**Fig. A- 24. Head loss vs. cone angle for 0.75 beta UVT with rough wall**

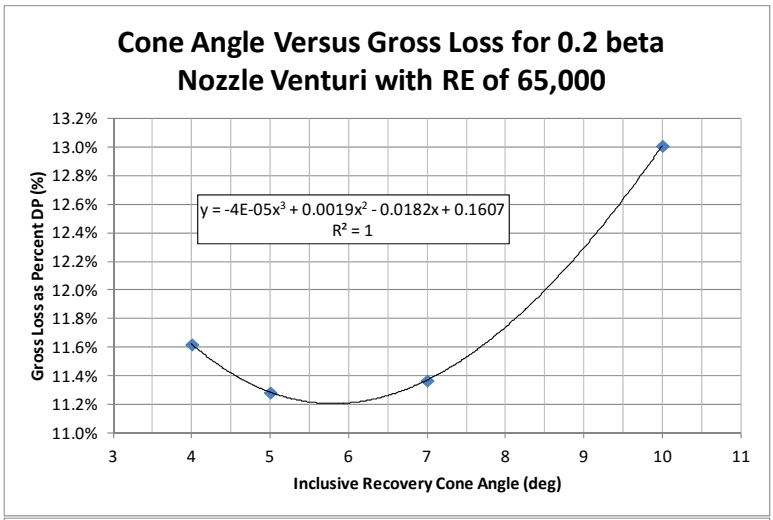


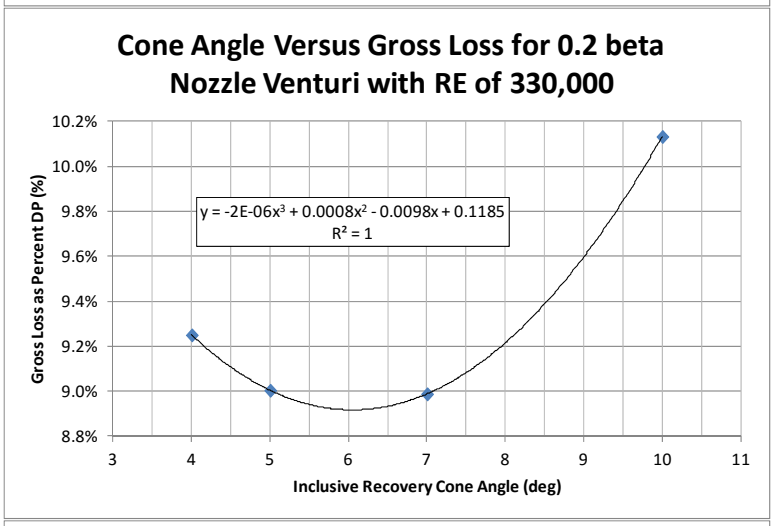


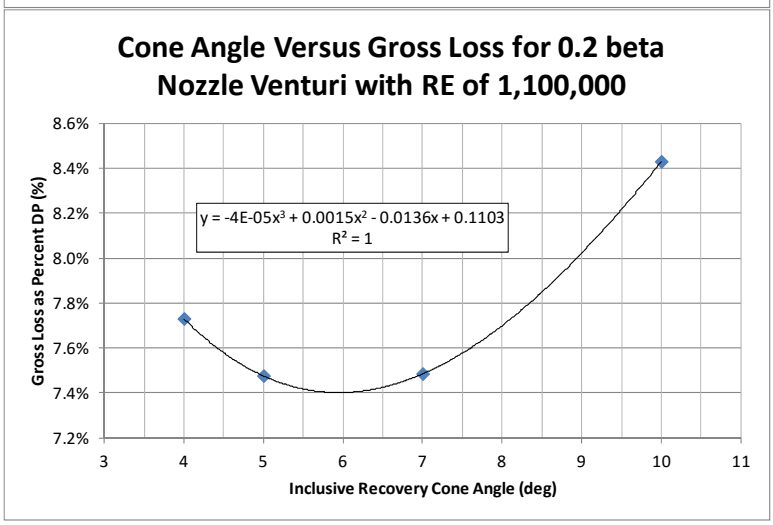


**Fig. A- 25. Head loss vs. cone angle for 0.20 beta Nozzle Venturi with smooth wall**

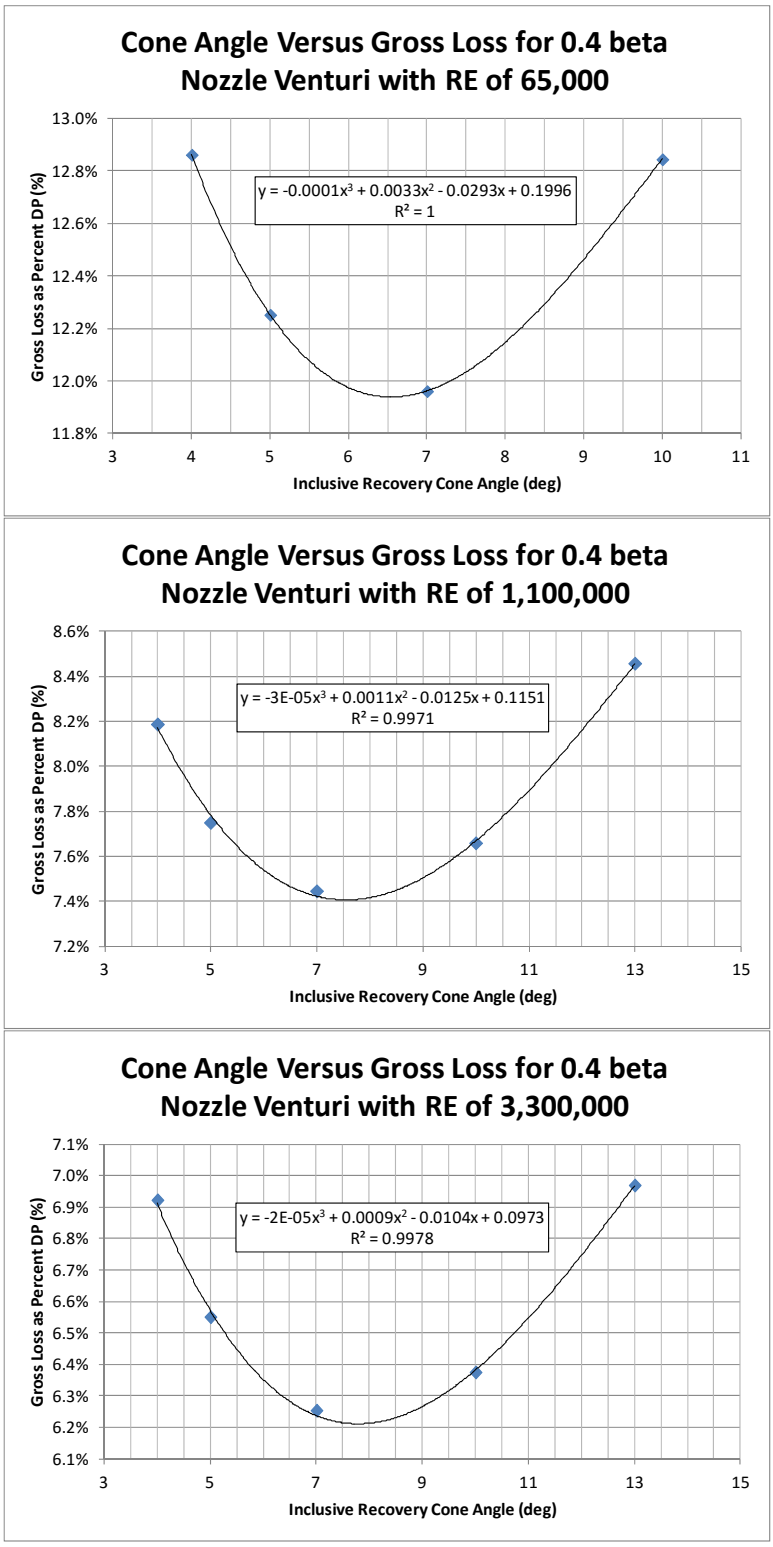


**Fig. A- 26. Head loss vs. cone angle for 0.40 beta Nozzle Venturi with smooth wall**

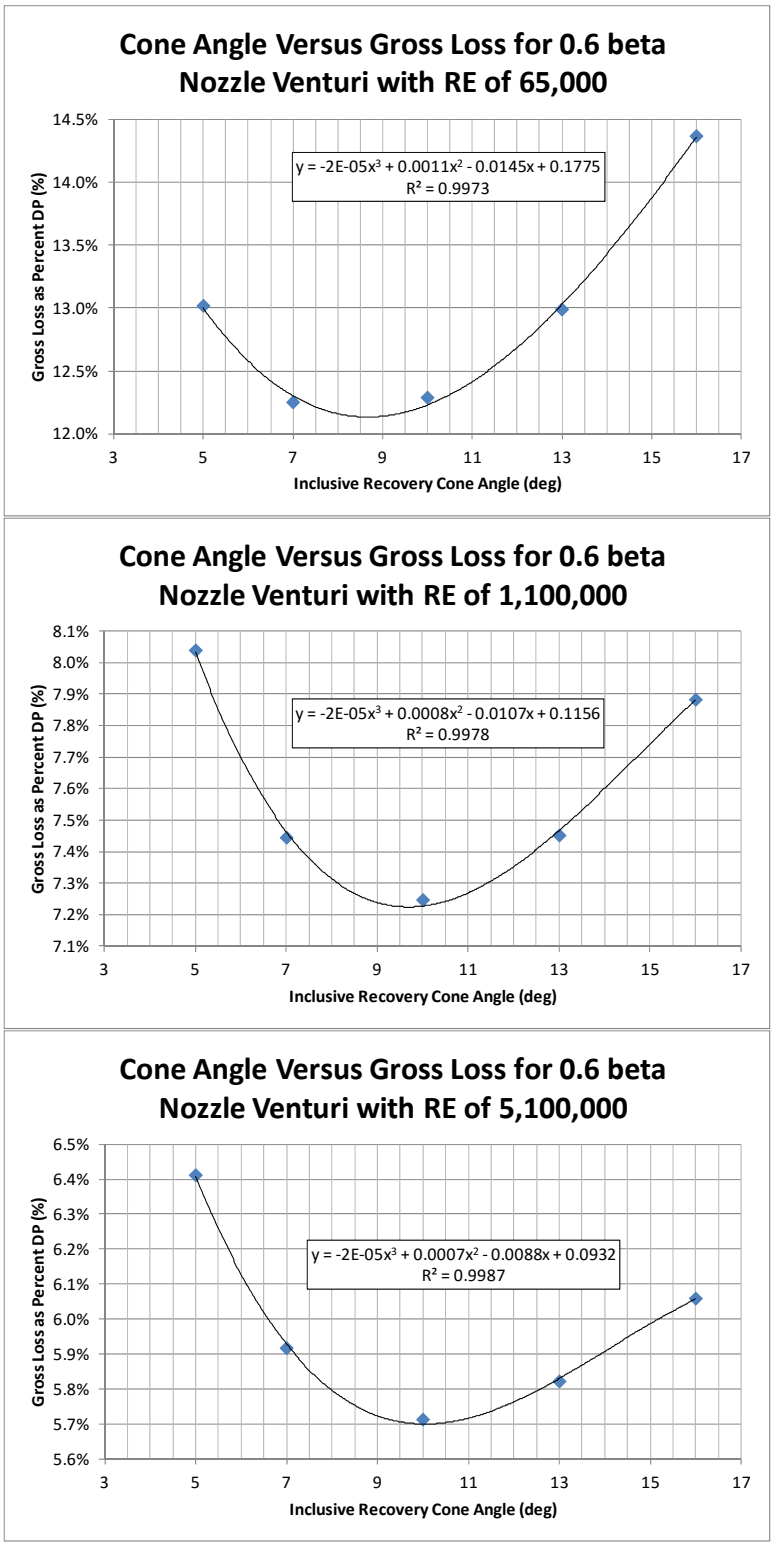


**Fig. A- 27. Head loss vs. cone angle for 0.60 beta Nozzle Venturi with smooth wall**

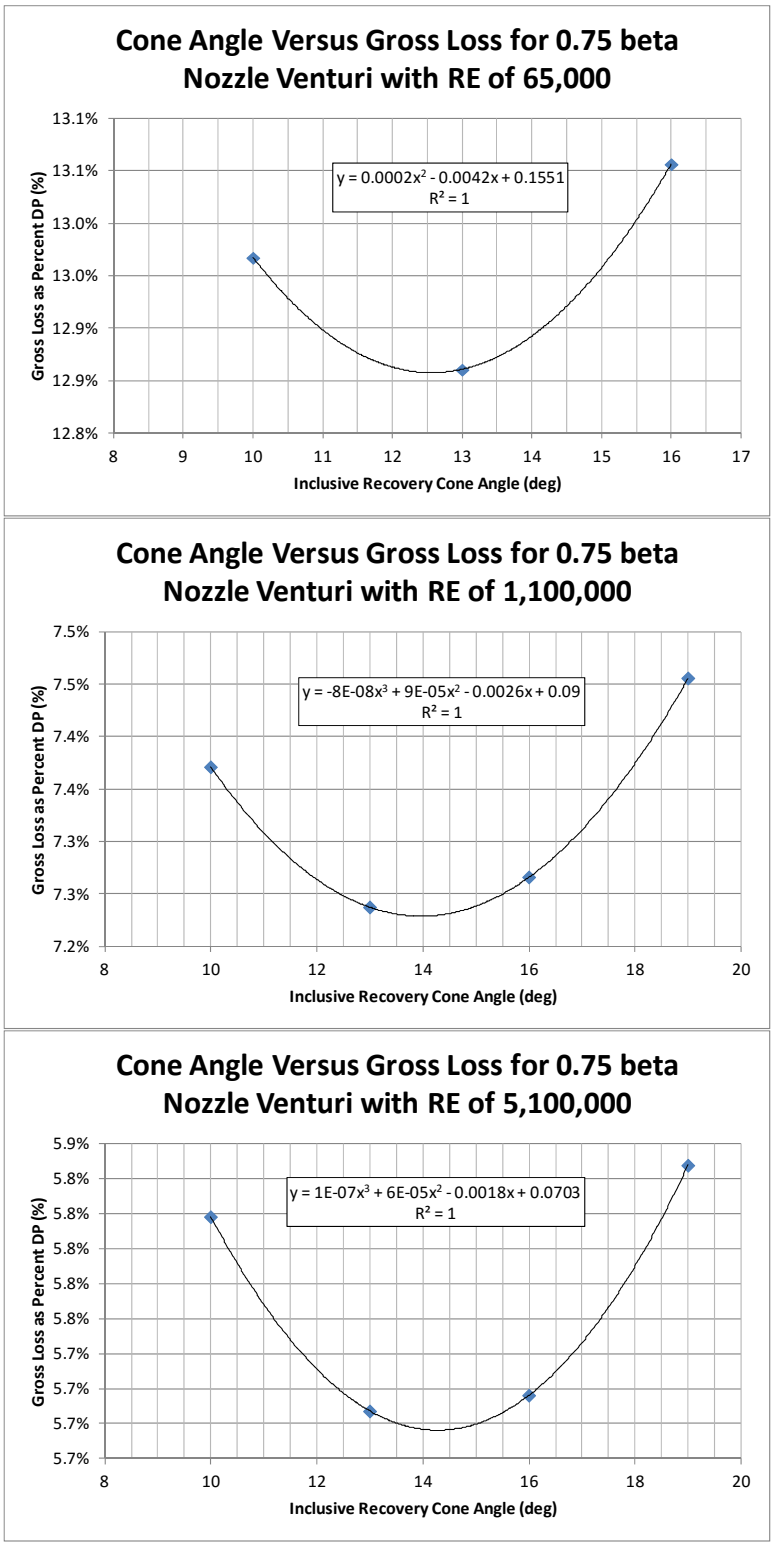


**Fig. A- 28. Head loss vs. cone angle for 0.75 beta Nozzle Venturi with smooth wall**

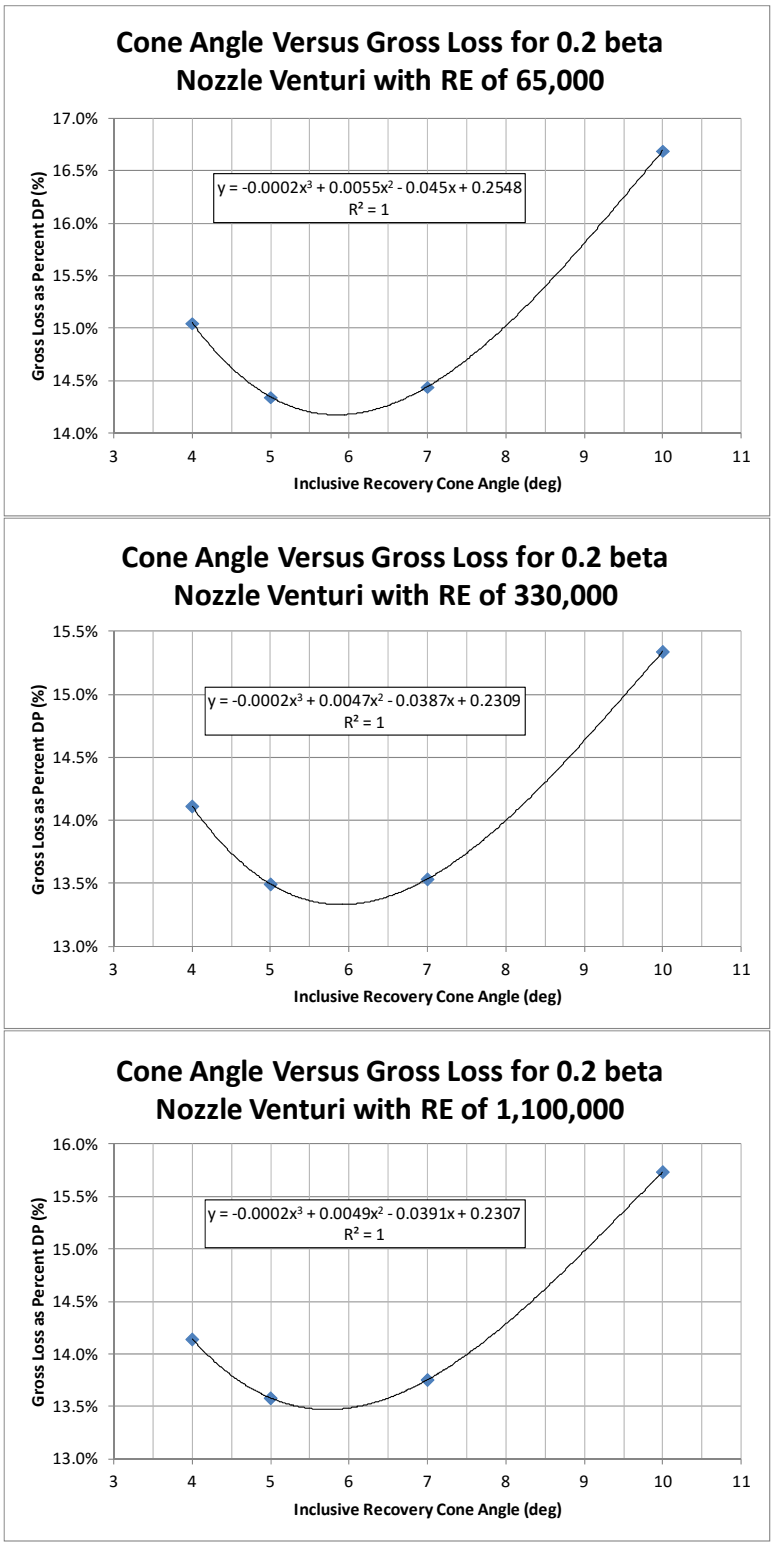


**Fig. A- 29. Head loss vs. cone angle for 0.20 beta Nozzle Venturi with rough wall**

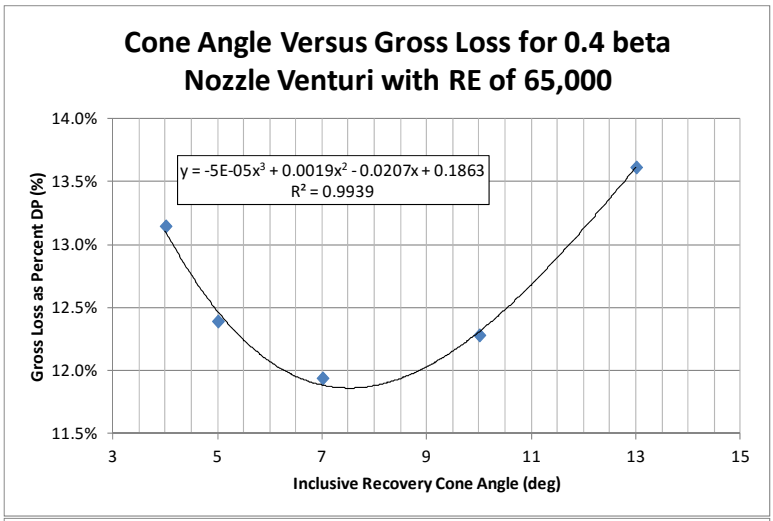


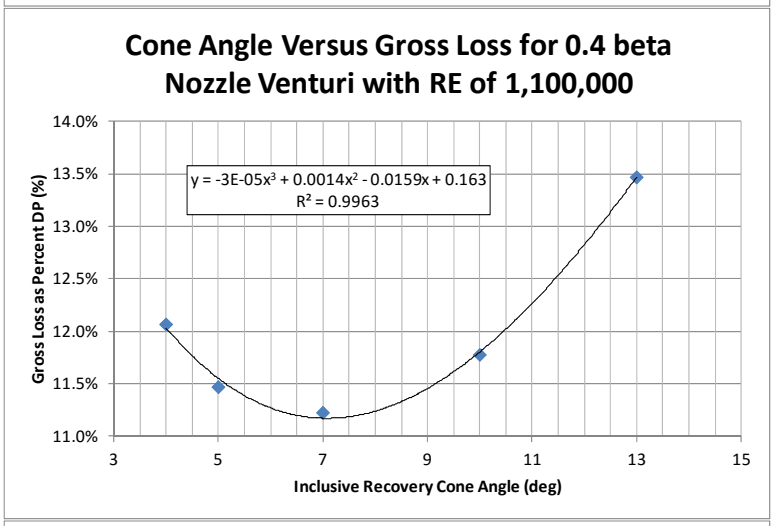


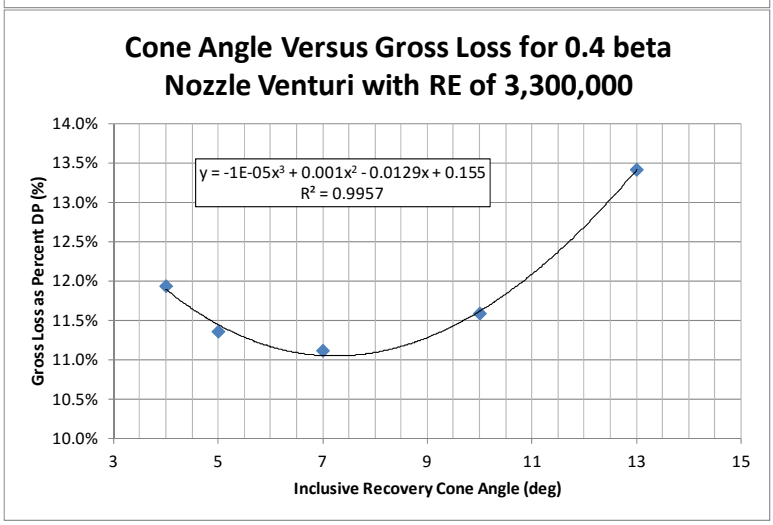


**Fig. A- 30. Head loss vs. cone angle for 0.40 beta Nozzle Venturi with rough wall**

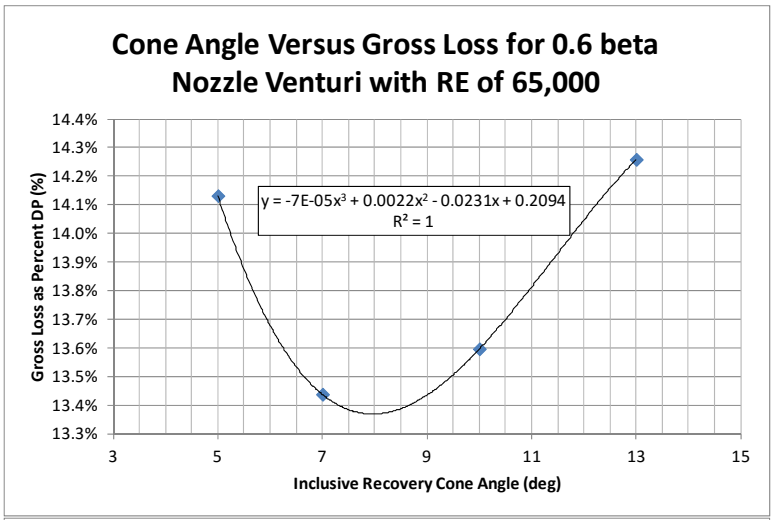


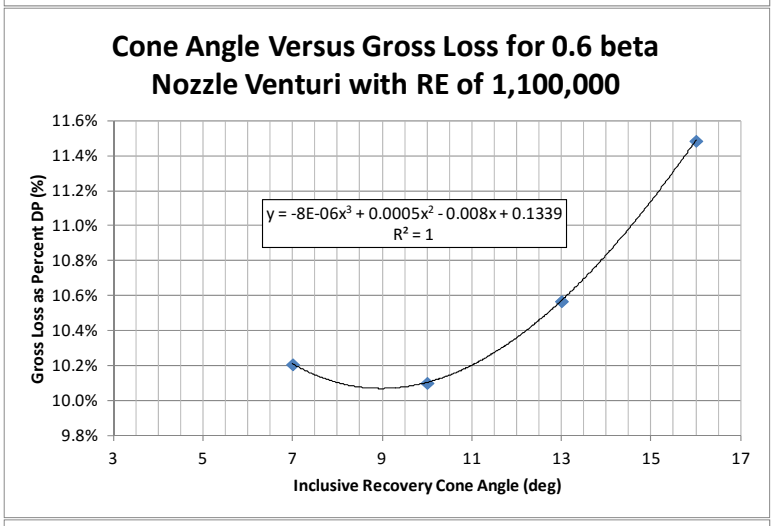


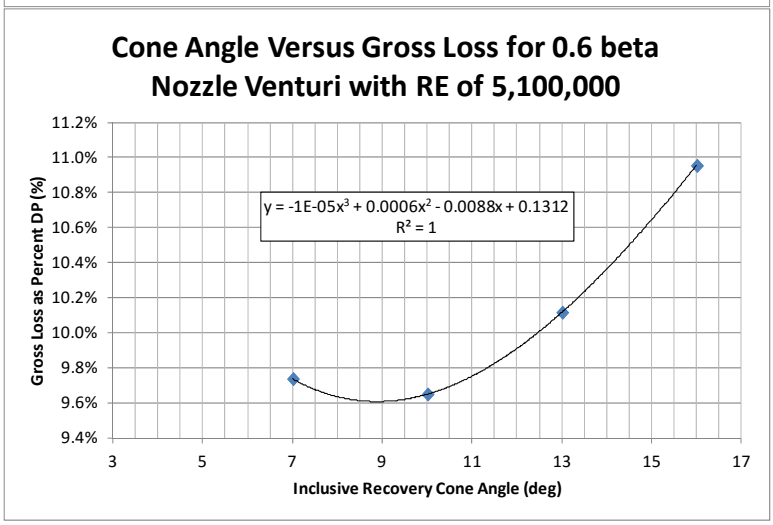


**Fig. A- 31. Head loss vs. cone angle for 0.60 beta Nozzle Venturi with rough wall**

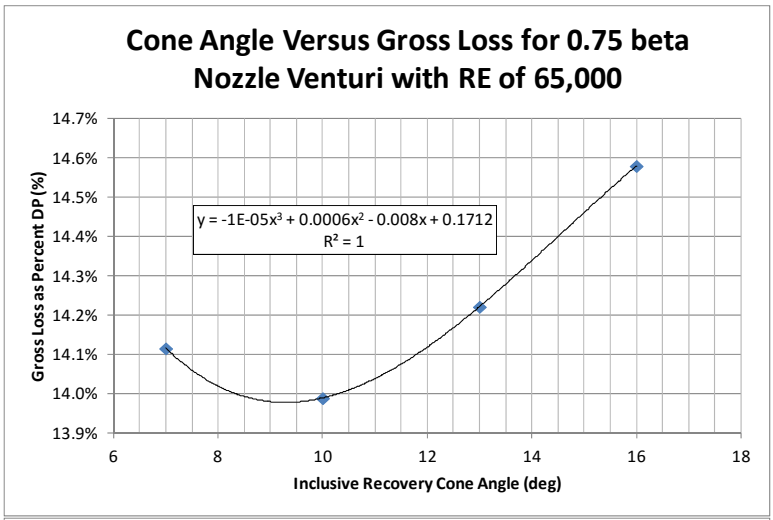


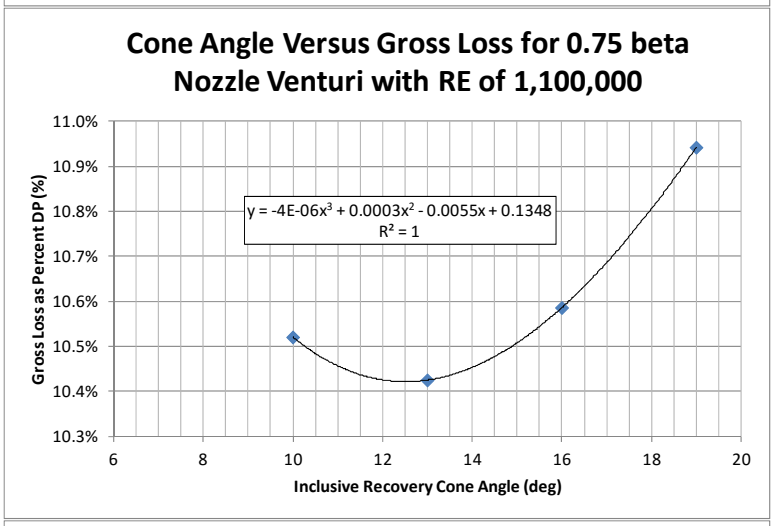


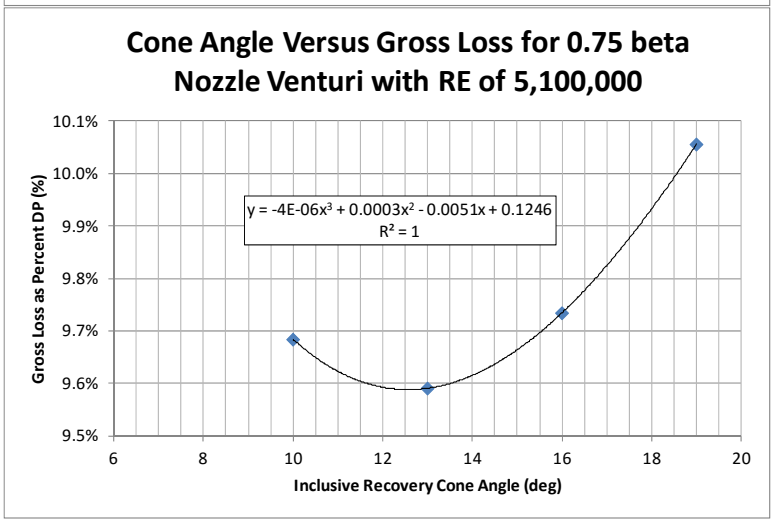


**Fig. A- 32. Head loss vs. cone angle for 0.75 beta Nozzle Venturi with rough wall**

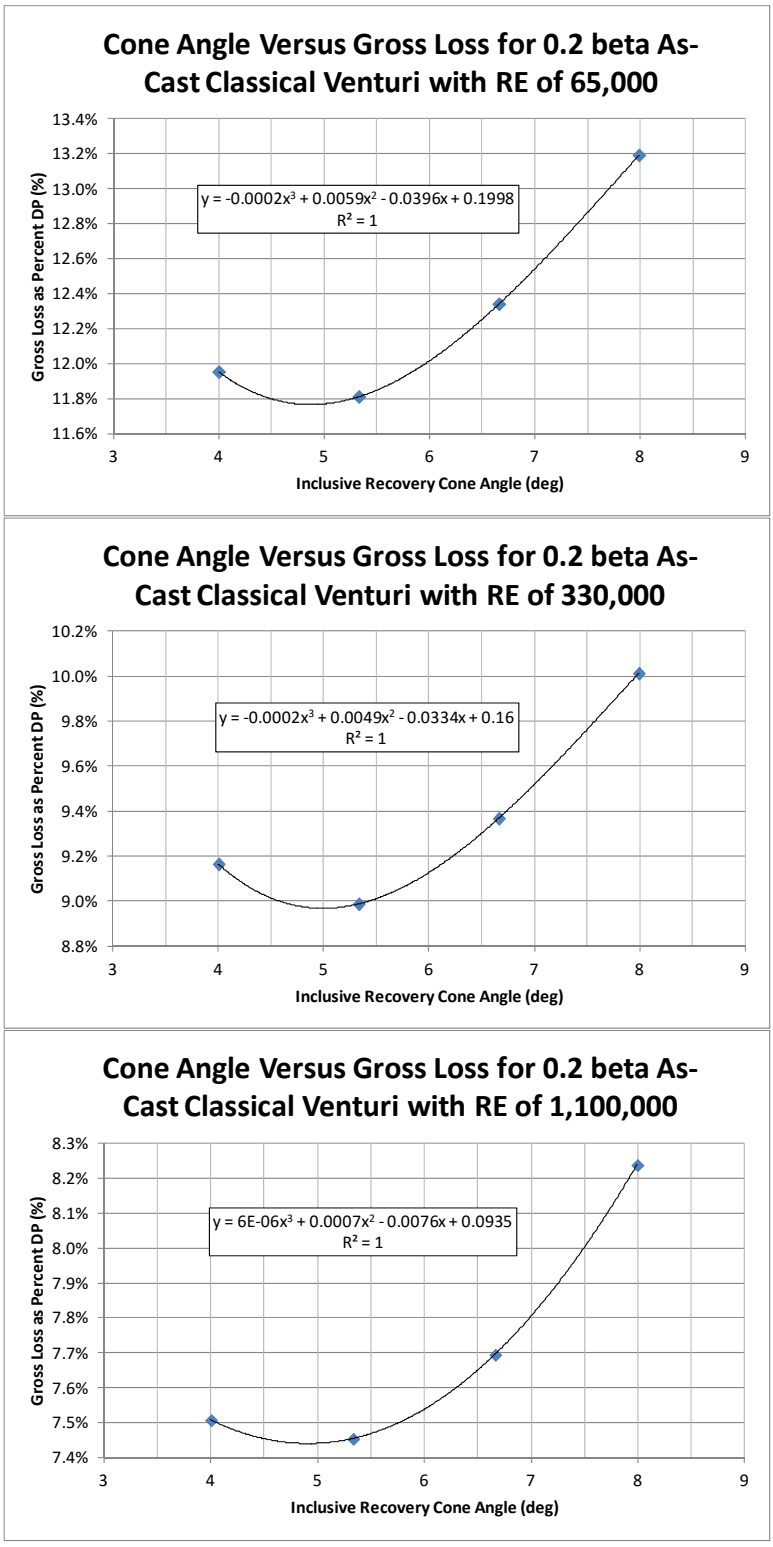


**Fig. A- 33. Head loss vs. cone angle for 0.20 beta As-Cast ASME Venturi with smooth wall**

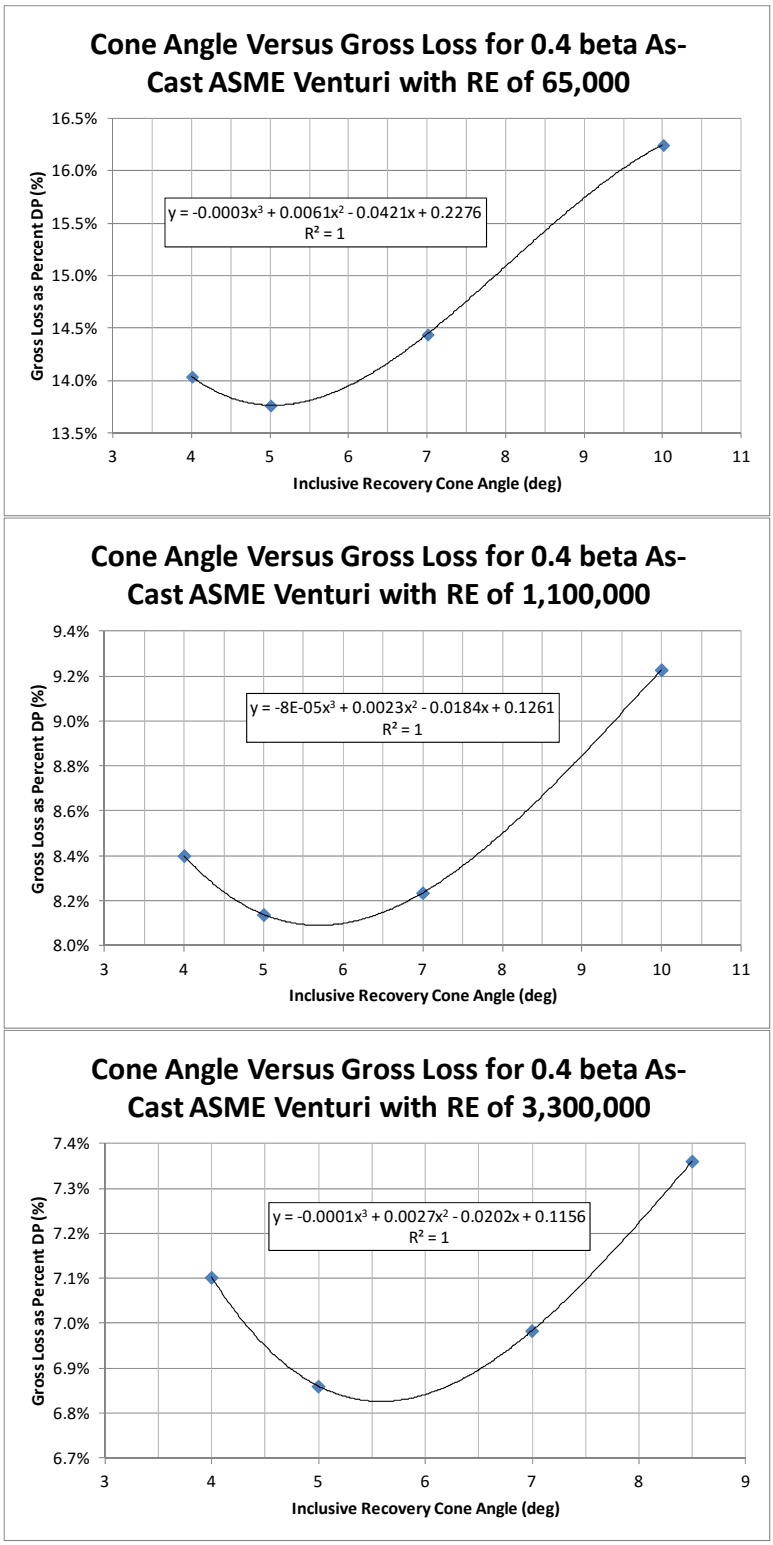


**Fig. A- 34. Head loss vs. cone angle for 0.40 beta As-Cast ASME Venturi with smooth wall**

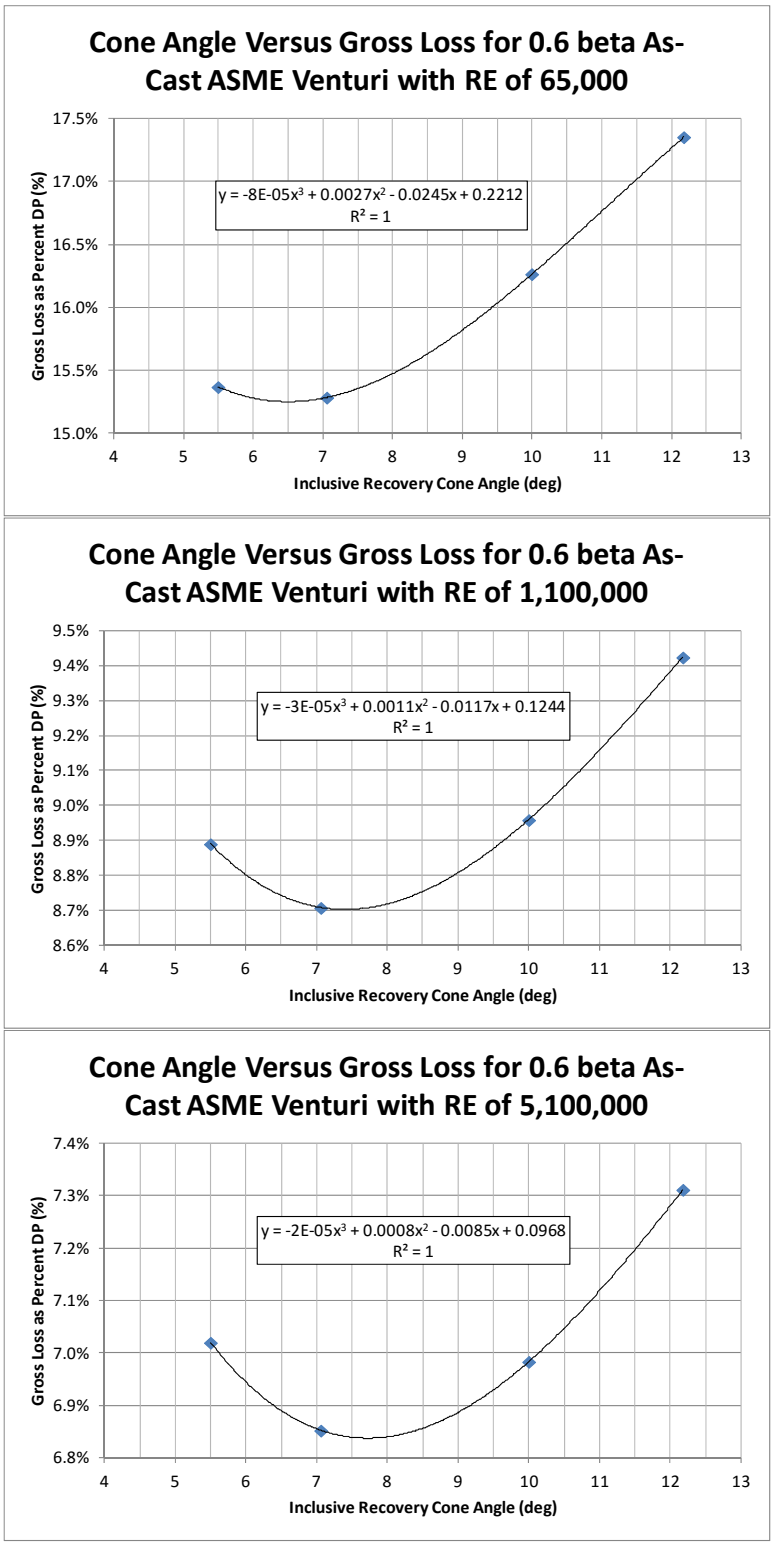


**Fig. A- 35. Head loss vs. cone angle for 0.60 beta As-Cast ASME Venturi with smooth wall**

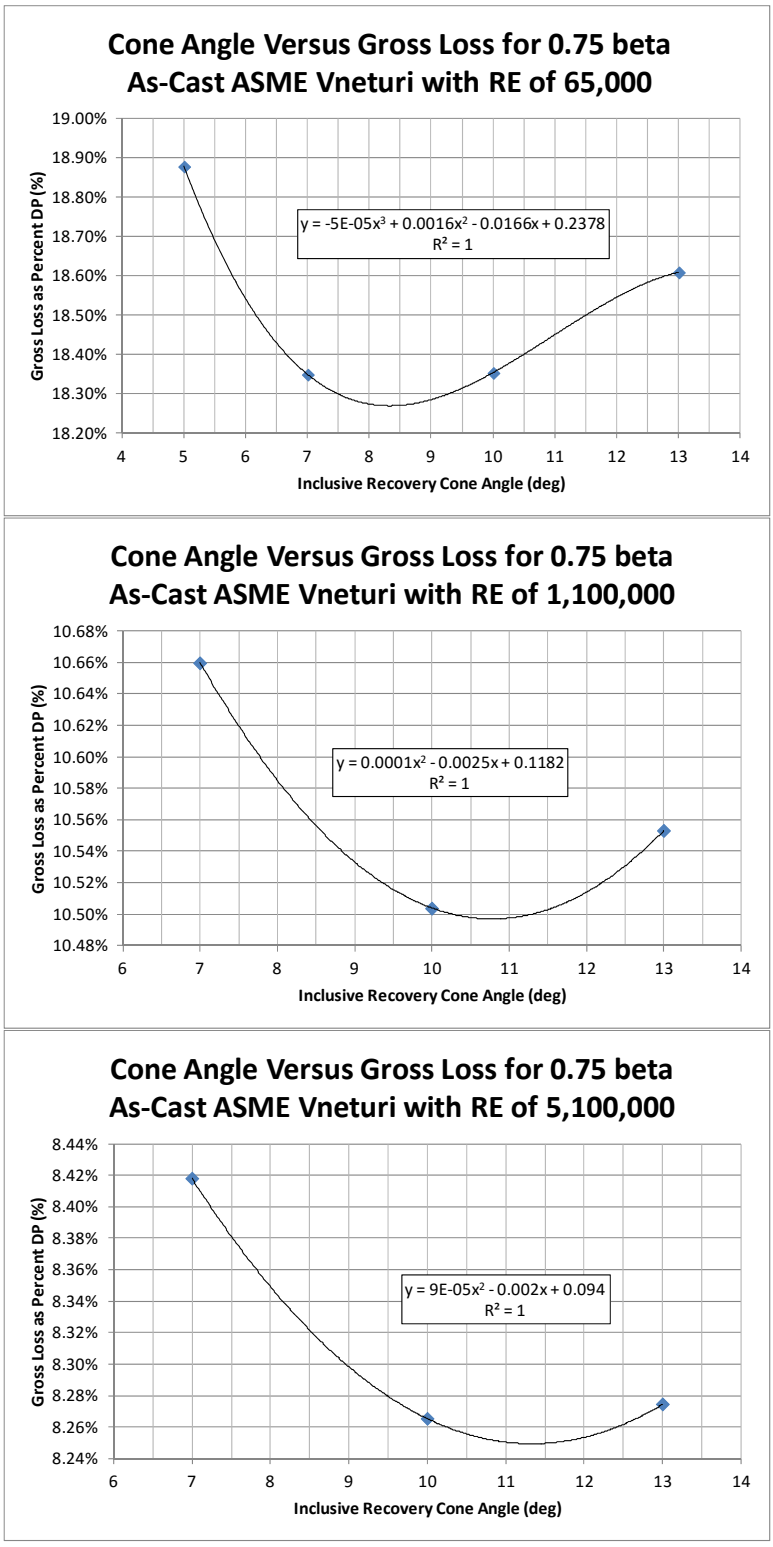


**Fig. A- 36. Head loss vs. cone angle for 0.75 beta As-Cast ASME Venturi with smooth wall**

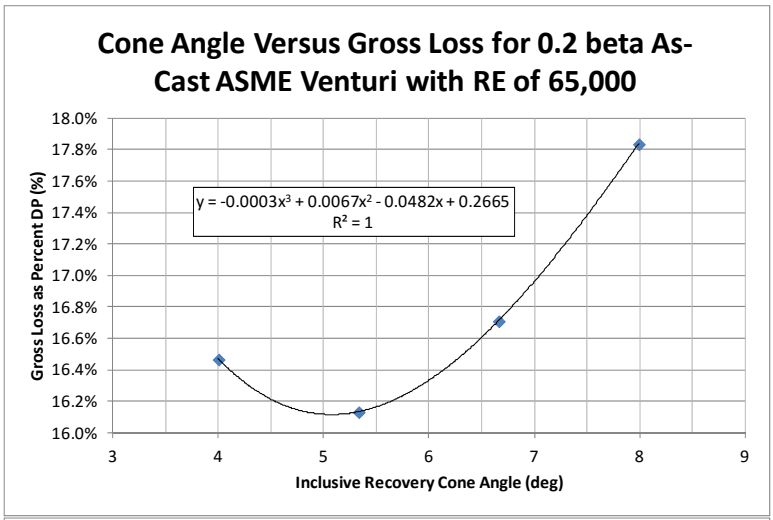


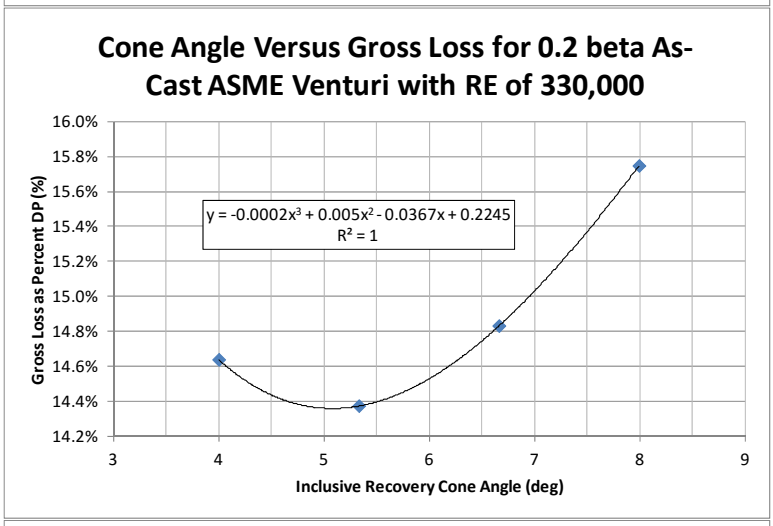


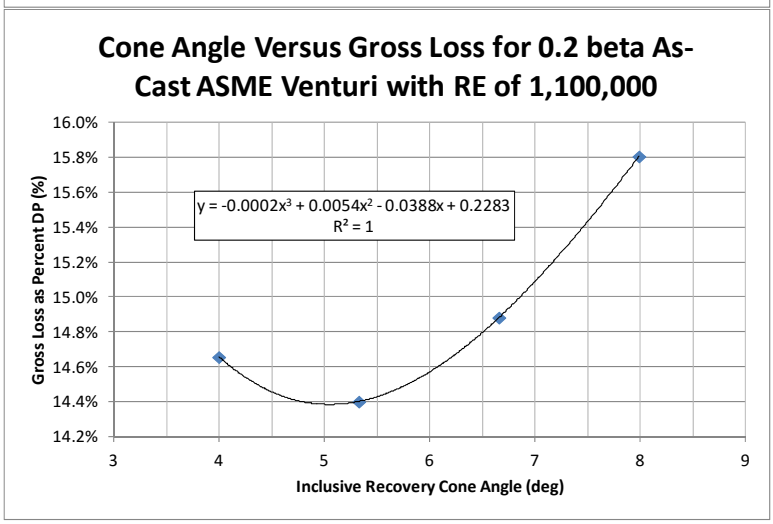


**Fig. A- 37. Head loss vs. cone angle for 0.20 beta As-Cast ASME Venturi with rough wall**

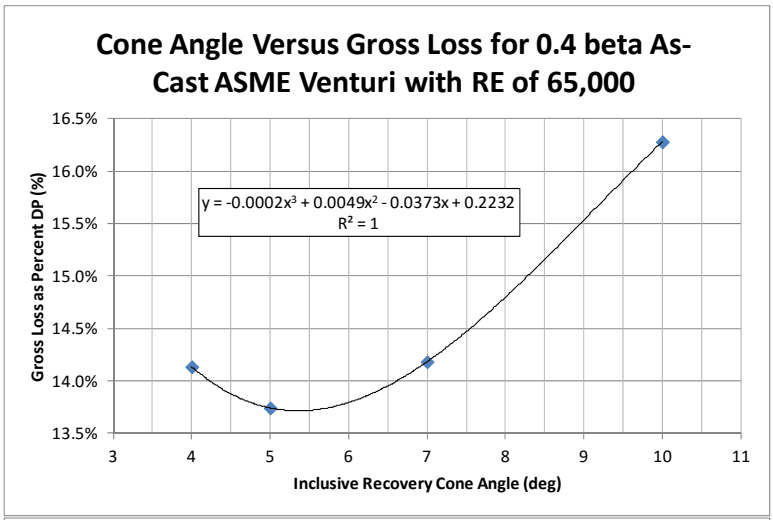


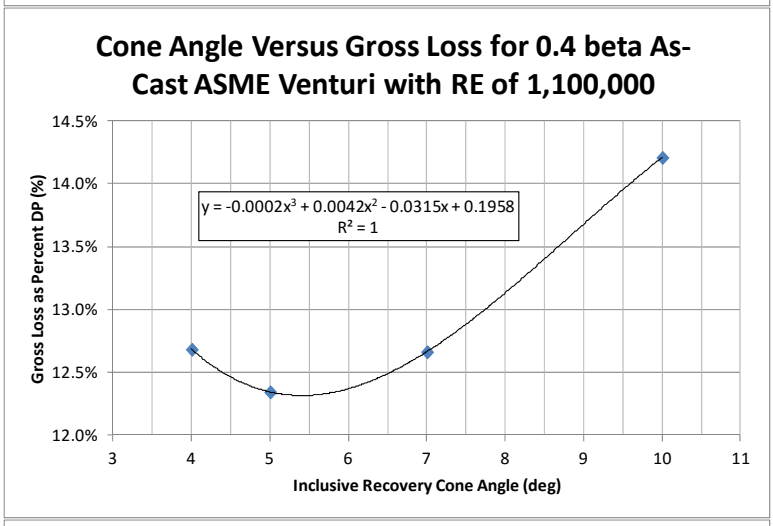


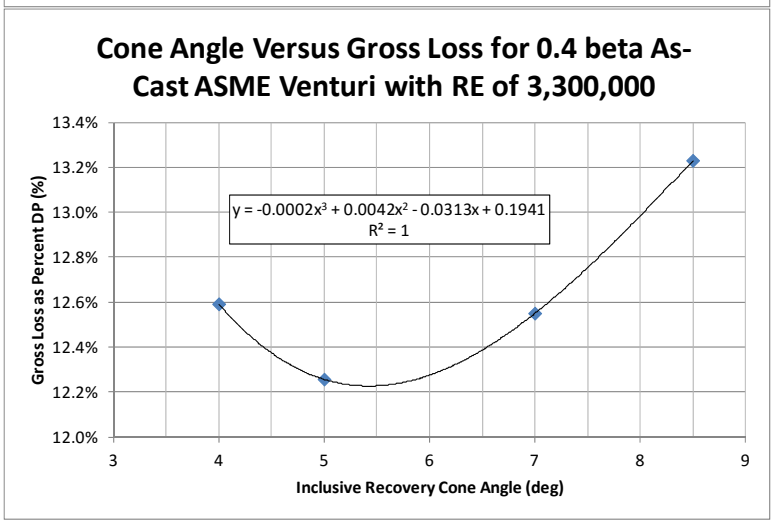


**Fig. A- 38. Head loss vs. cone angle for 0.40 beta As-Cast ASME Venturi with rough wall**

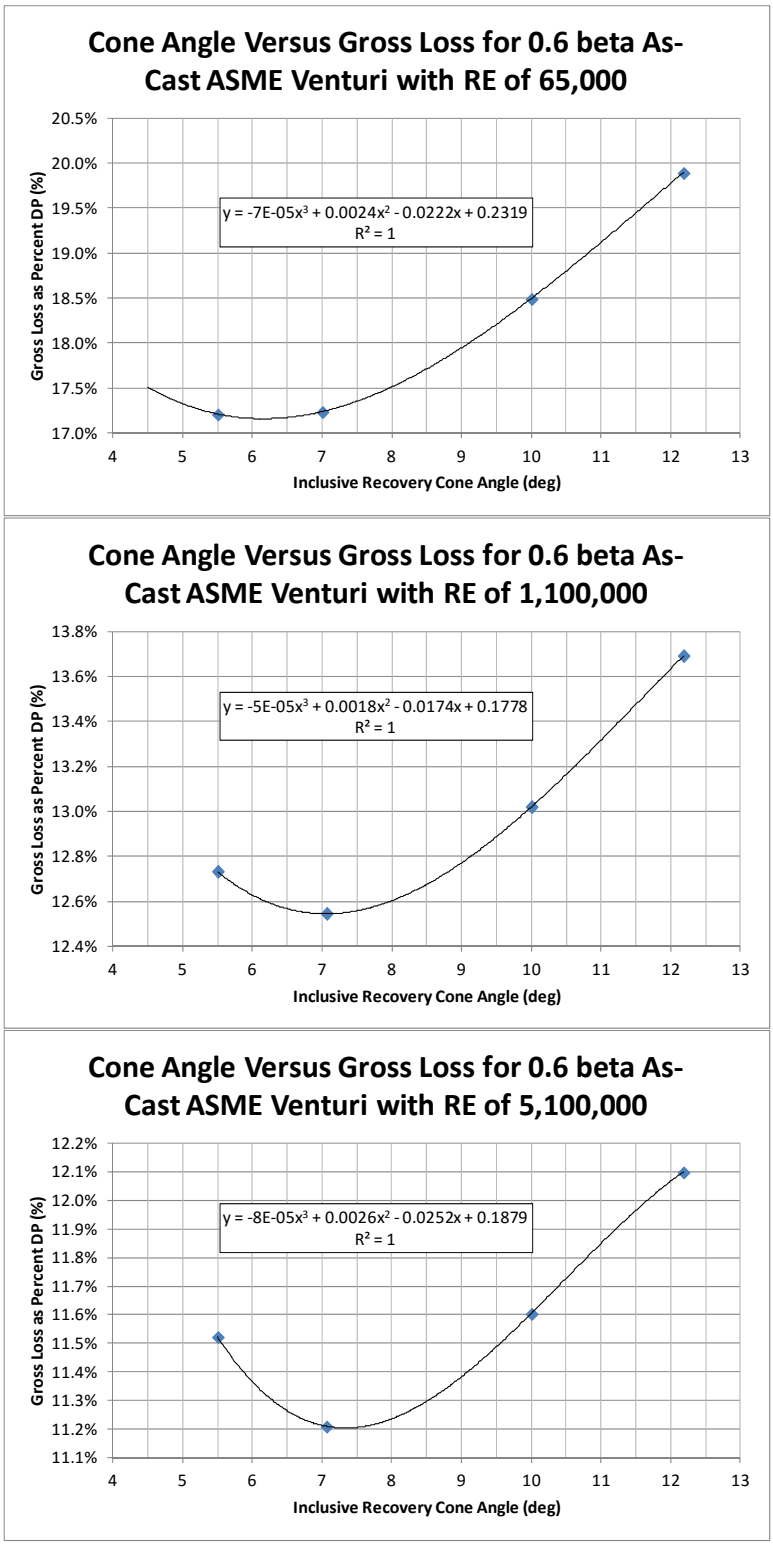


**Fig. A- 39. Head loss vs. cone angle for 0.60 beta As-Cast ASME Venturi with rough wall**

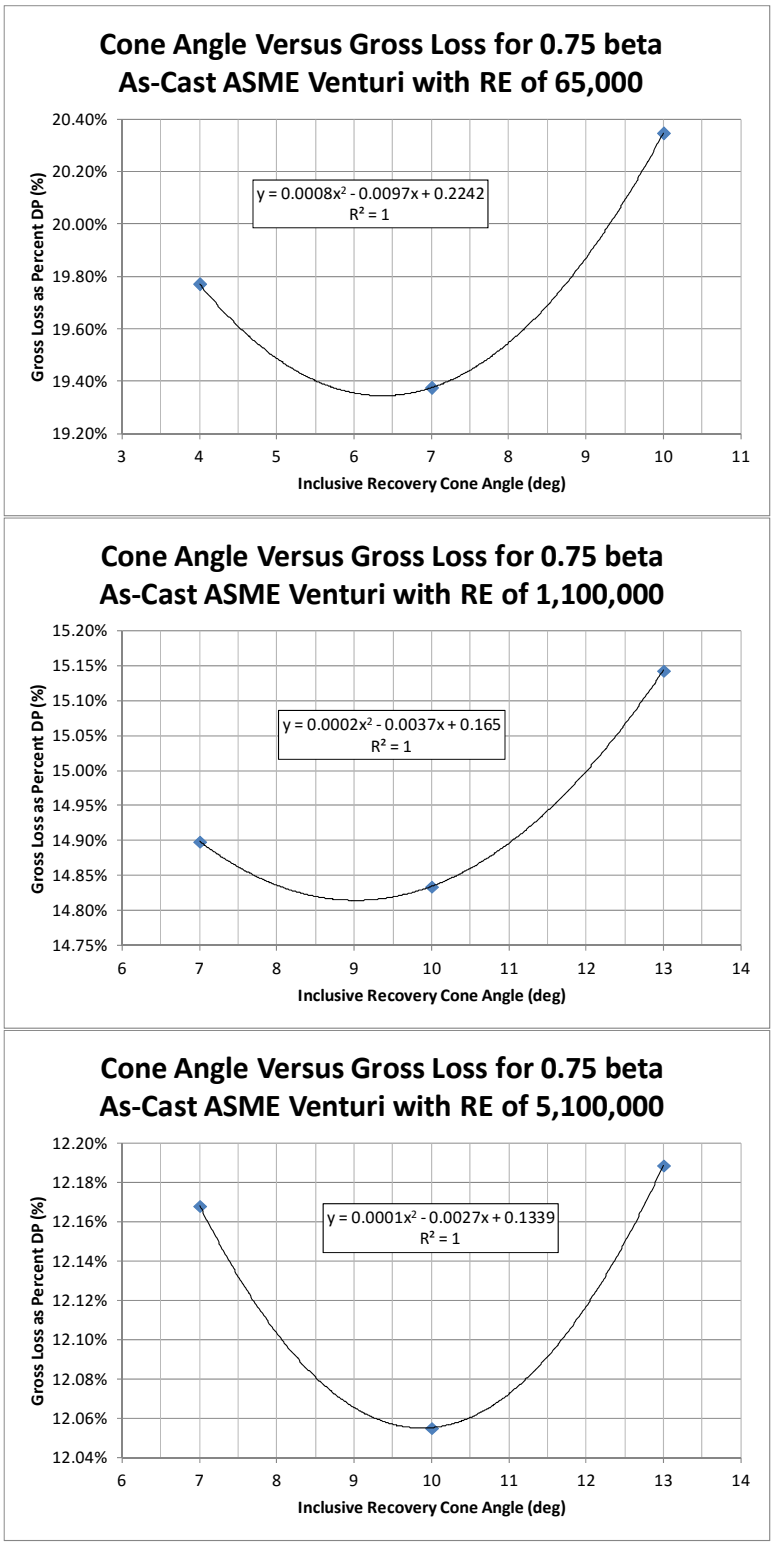


**Fig. A- 40. Head loss vs. cone angle for 0.75 beta As-Cast ASME Venturi with rough wall**

# Appendix B: Optimization curves for Venturis with truncated recovery cones

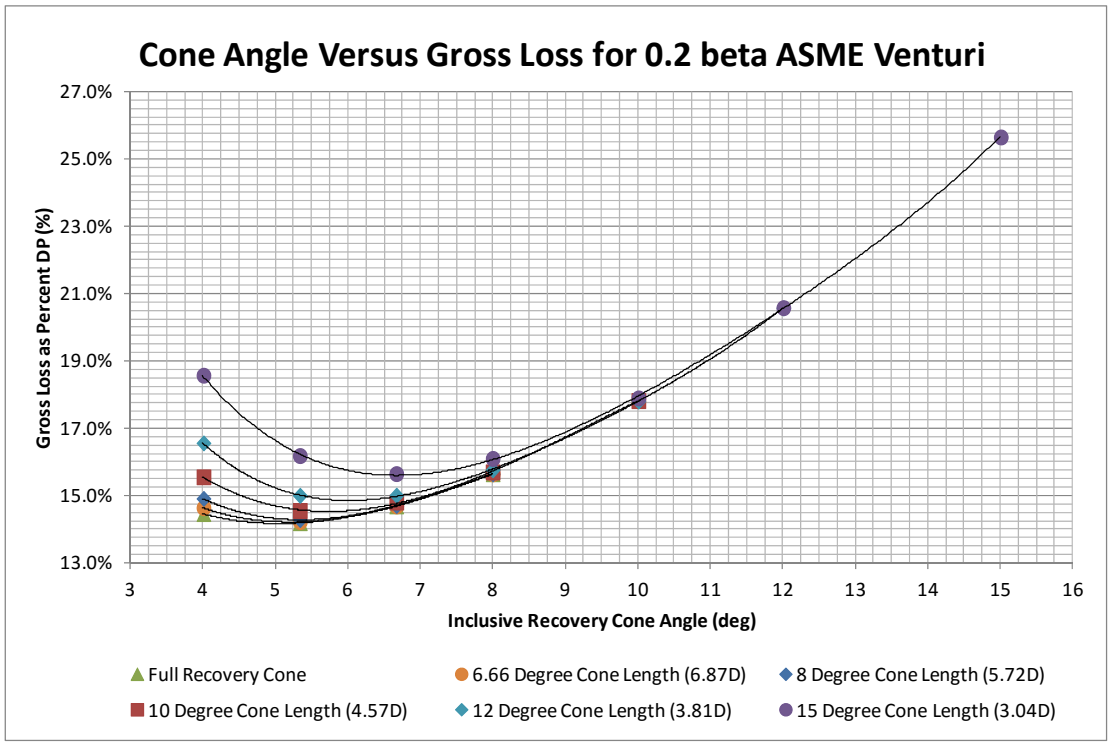


**Fig. B- 1. Head loss vs. cone angle for 0.2 beta Truncated ASME Venturi**

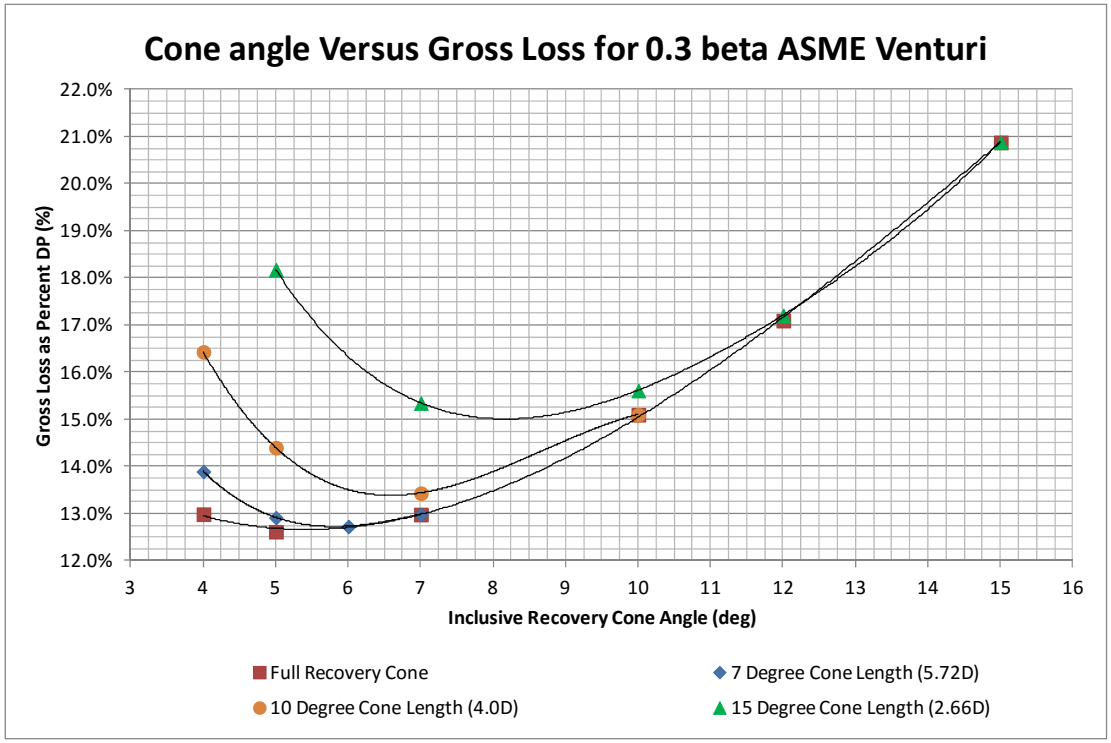


**Fig. B- 2. Head loss vs. cone angle for 0.3 beta Truncated ASME Venturi**

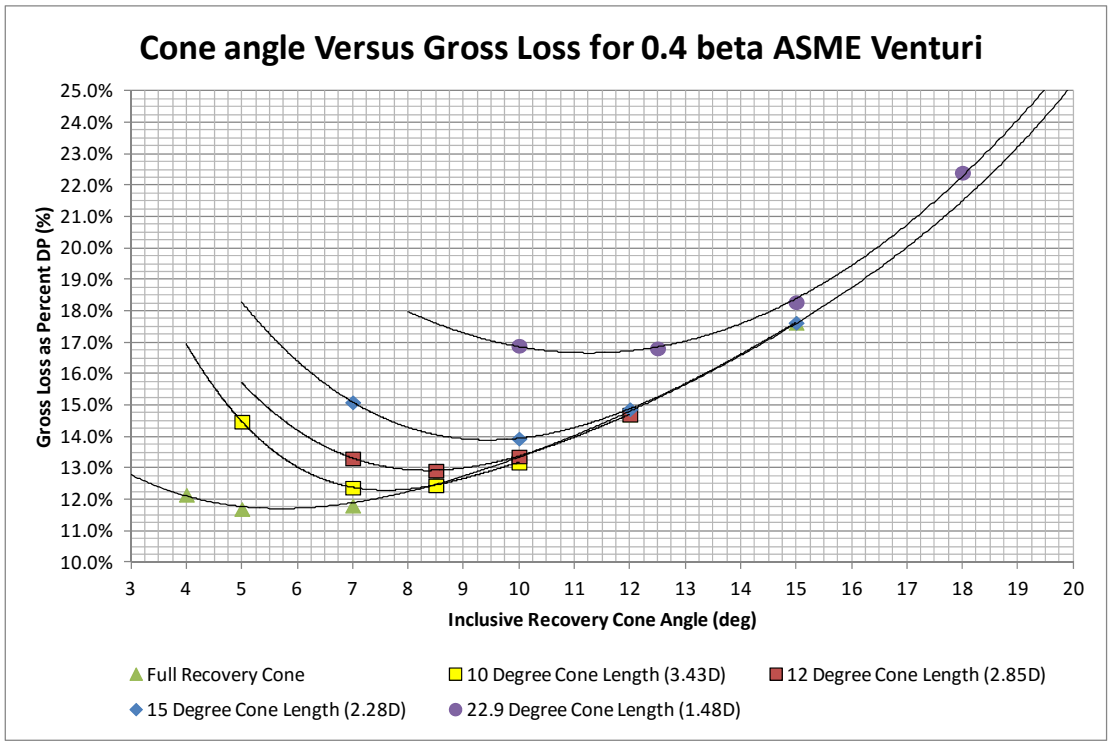


**Fig. B- 3. Head loss vs. cone angle for 0.4 beta Truncated ASME Venturi**

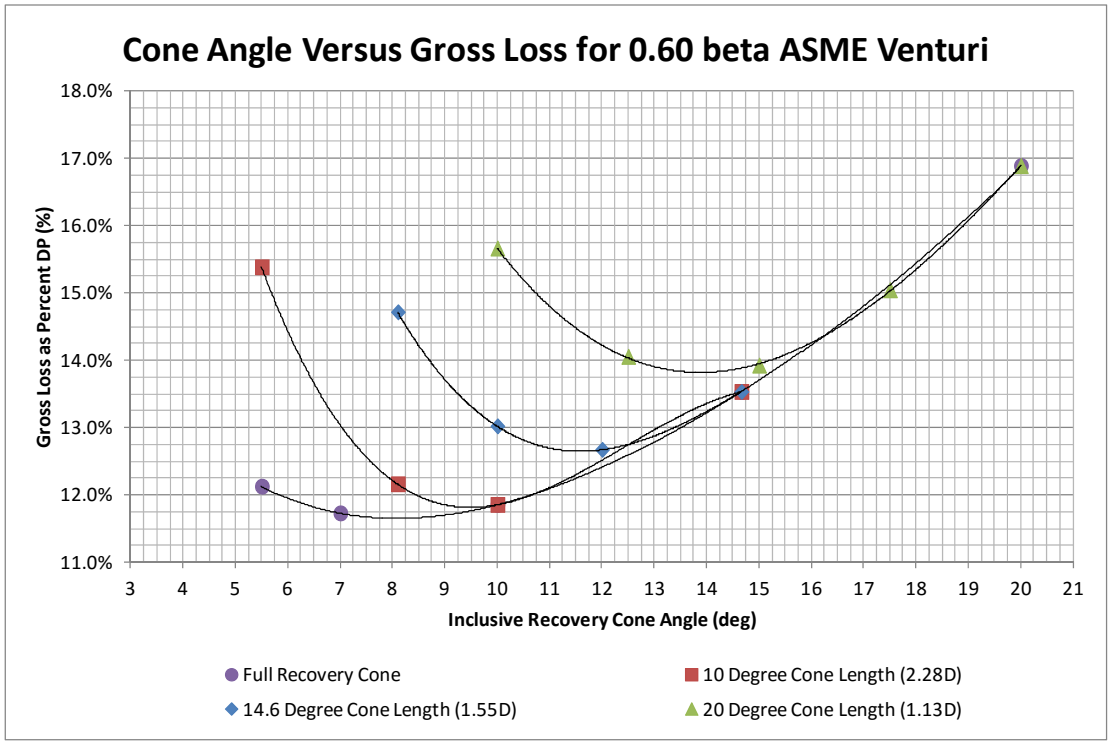


**Fig. B- 4. Head loss vs. cone angle for 0.6 beta Truncated ASME Venturi**

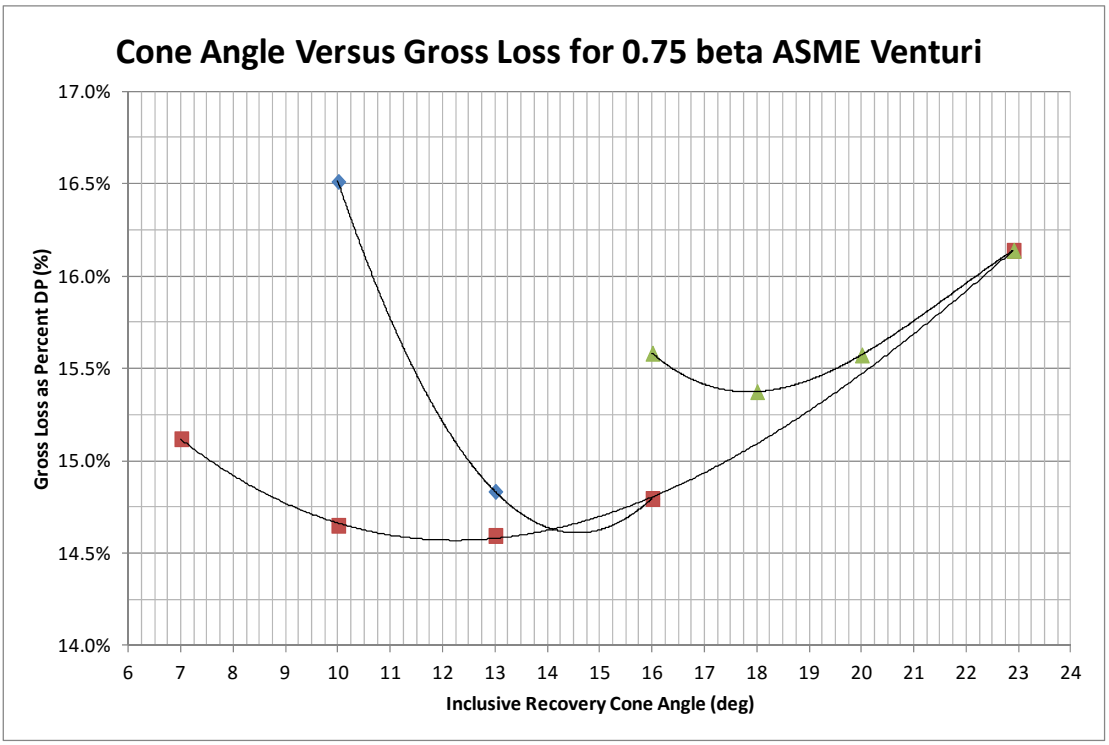


**Fig. B- 5. Head loss vs. cone angle for 0.75 beta Truncated ASME Venturi**

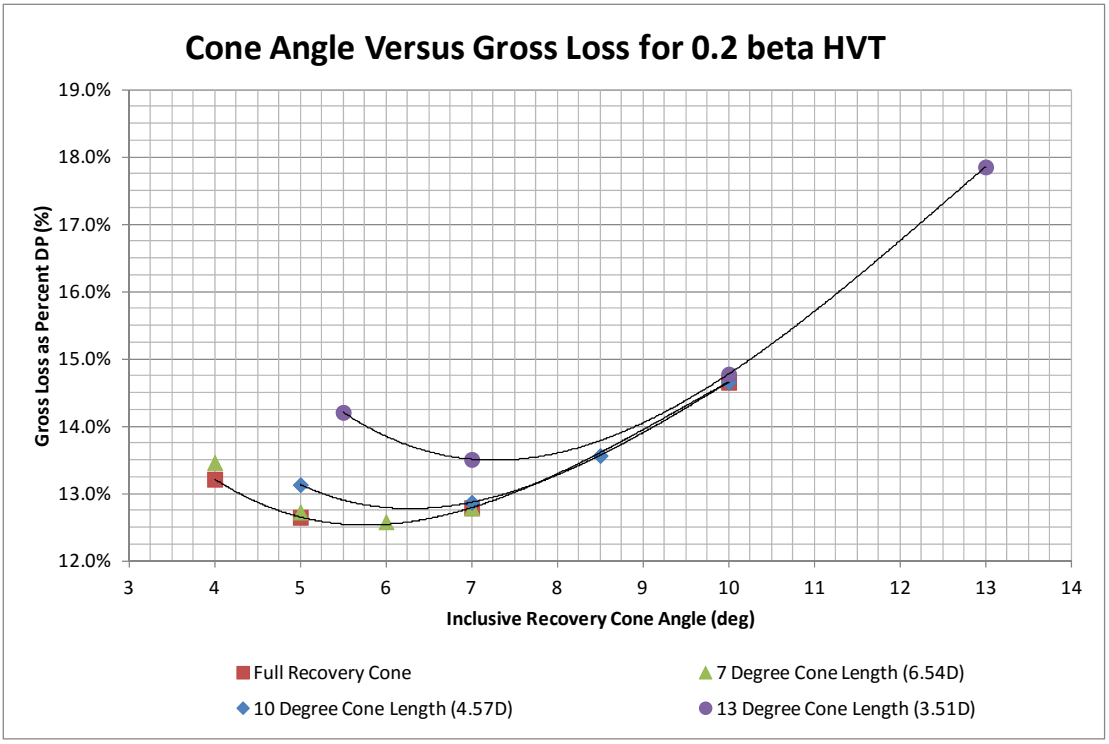


**Fig.B- 6. Head loss vs. cone angle for 0.2 beta Truncated HVT**

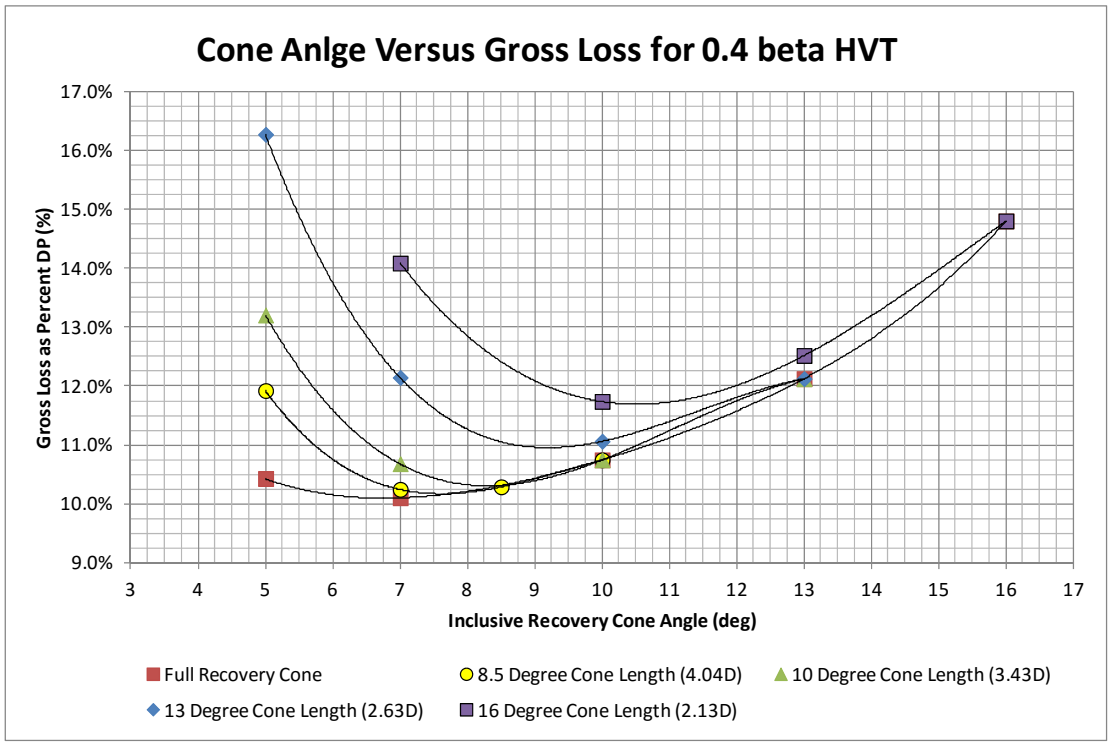


**Fig. B- 7. Head loss vs. cone angle for 0.40 beta Truncated HVT**

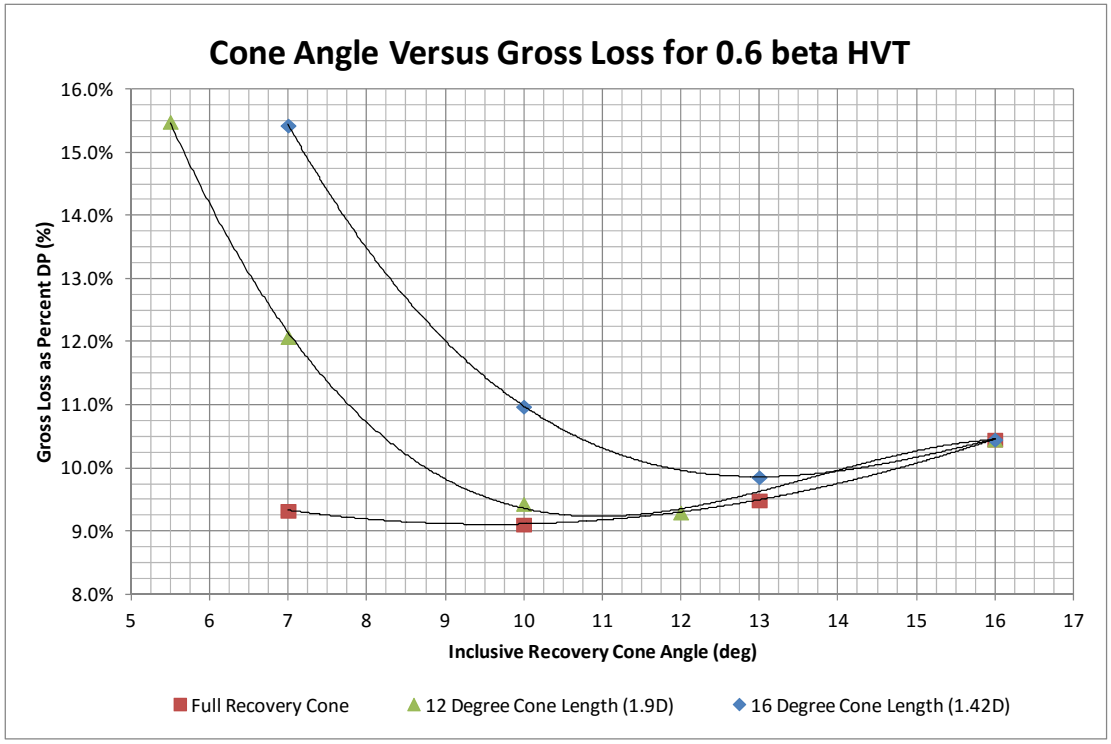


**Fig. B- 8. Head loss vs. cone angle for 0.60 beta Truncated HVT**

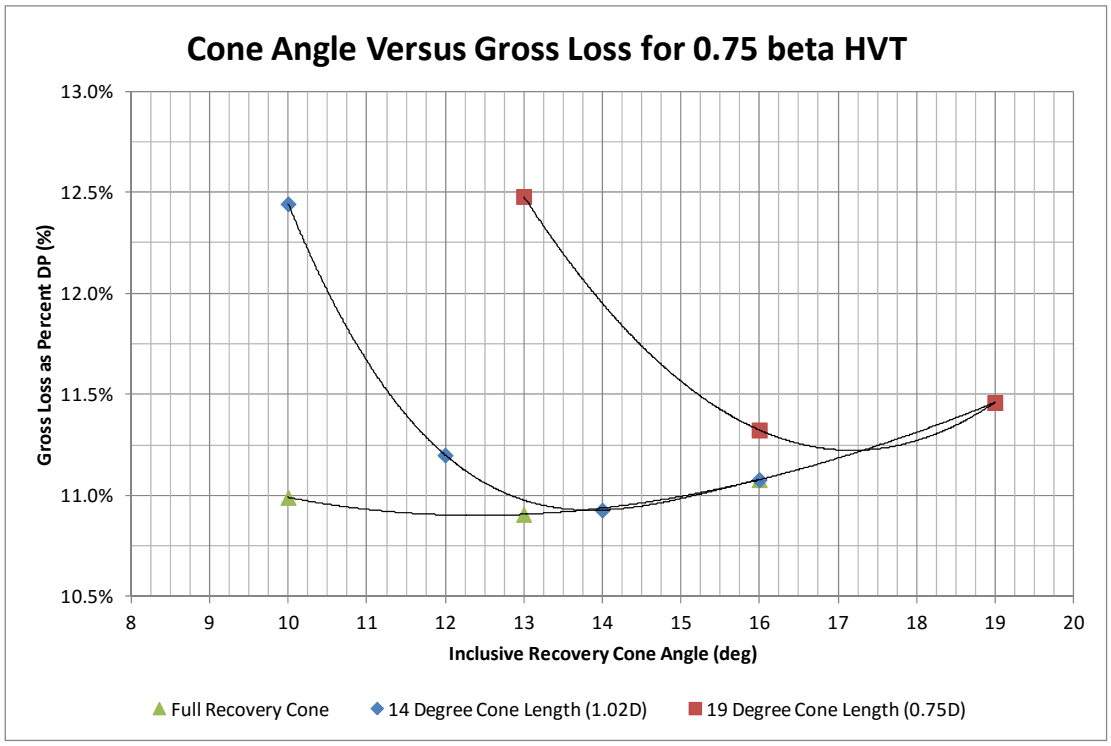


**Fig. B- 9. Head loss vs. cone angle for 0.75 beta Truncated HVT**

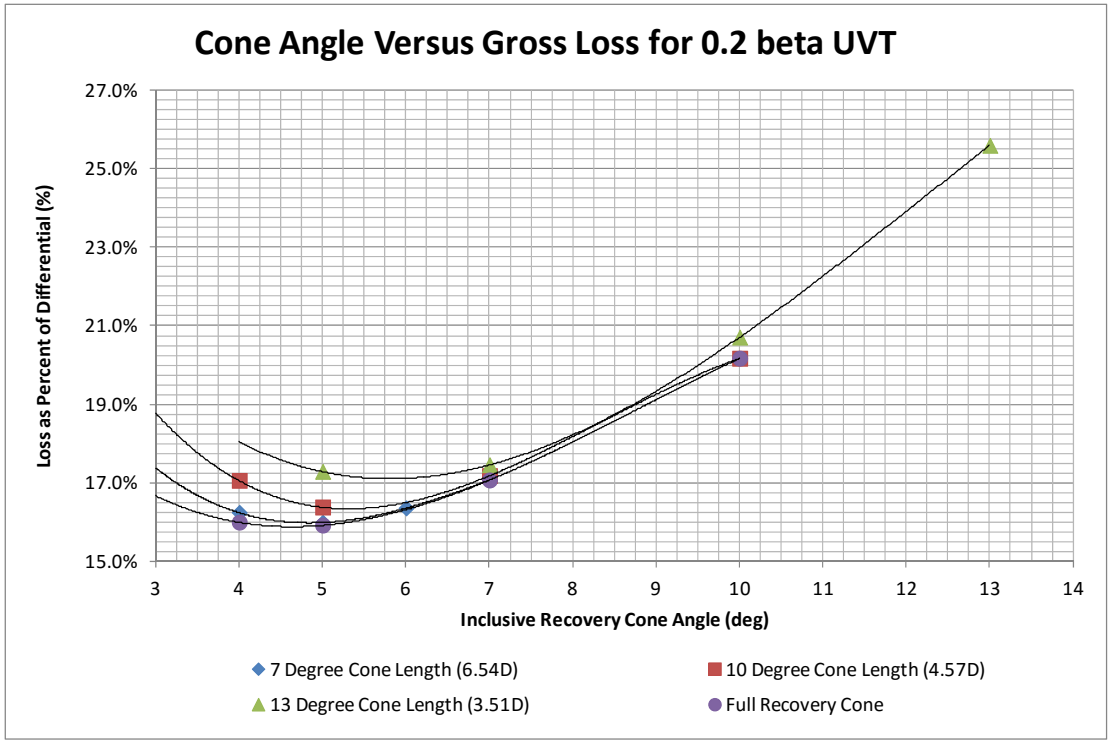


**Fig. B- 10. Head loss vs. cone angle for 0.20 beta Truncated UVT**

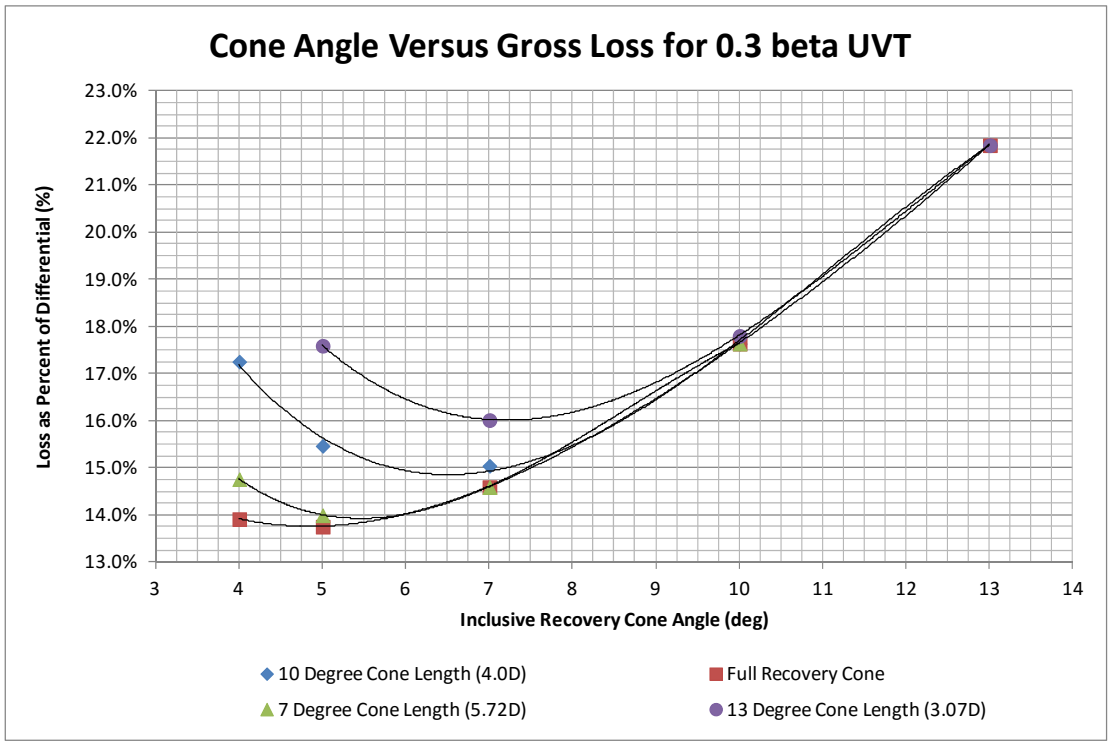


**Fig. B- 11. Head loss vs. cone angle for 0.40 beta Truncated UVT**

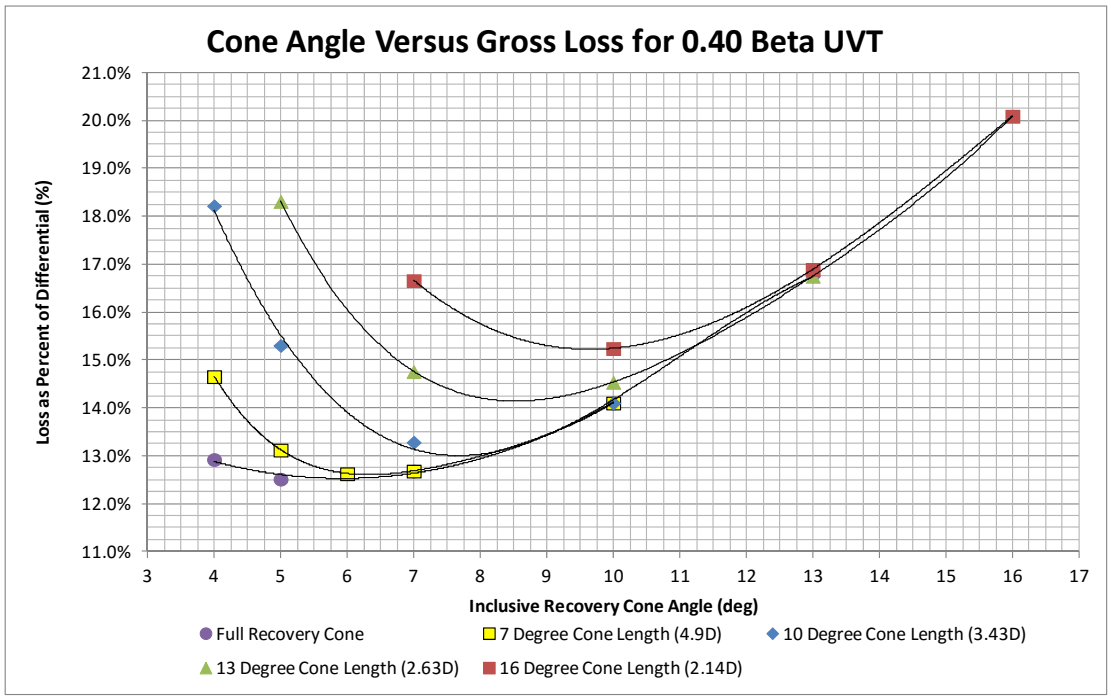


**Fig. B- 12. Head loss vs. cone angle for 0.40 beta Truncated UVT**

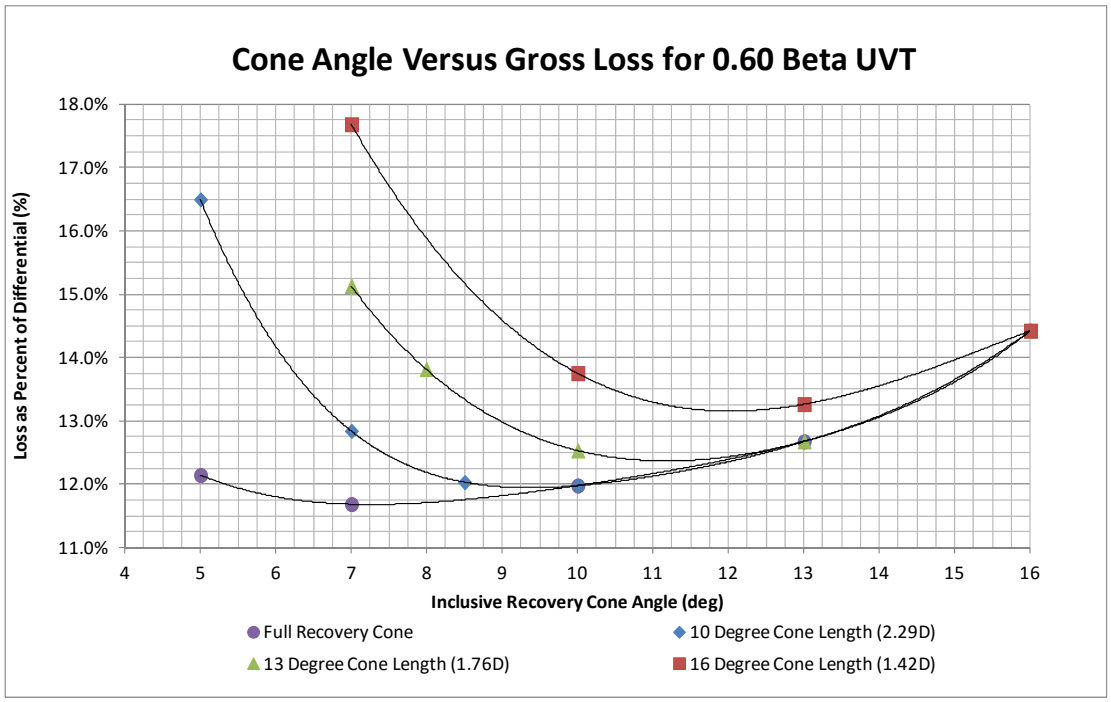


**Fig. B- 13. Head loss vs. cone angle for 0.60 beta Truncated UVT**

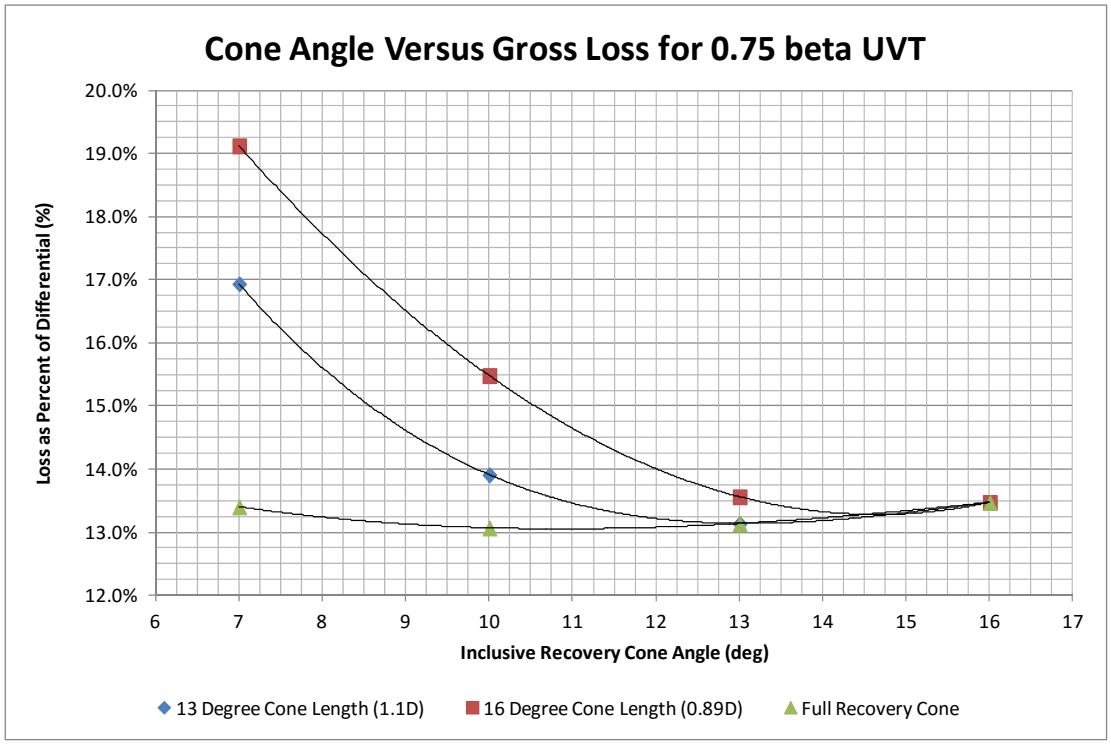


**Fig. B- 14. Head loss vs. cone angle for 0.75 beta Truncated UVT**

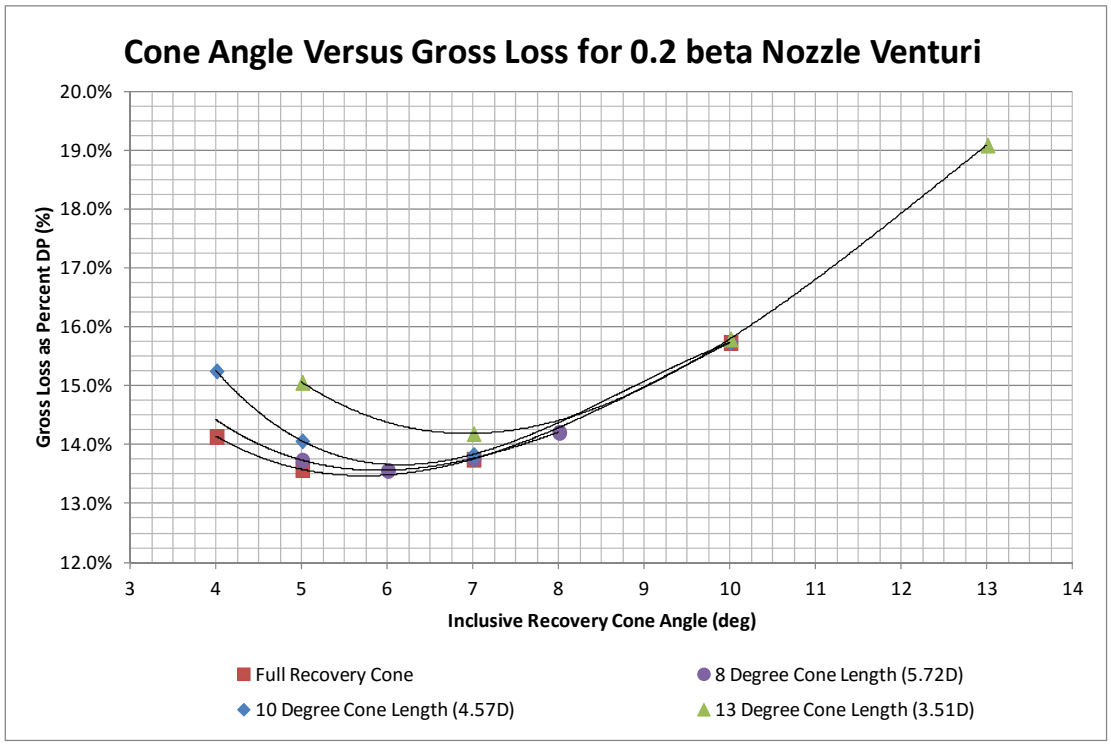


**Fig. B- 15. Head loss vs. cone angle for 0.20 beta Truncated Nozzle Venturi**

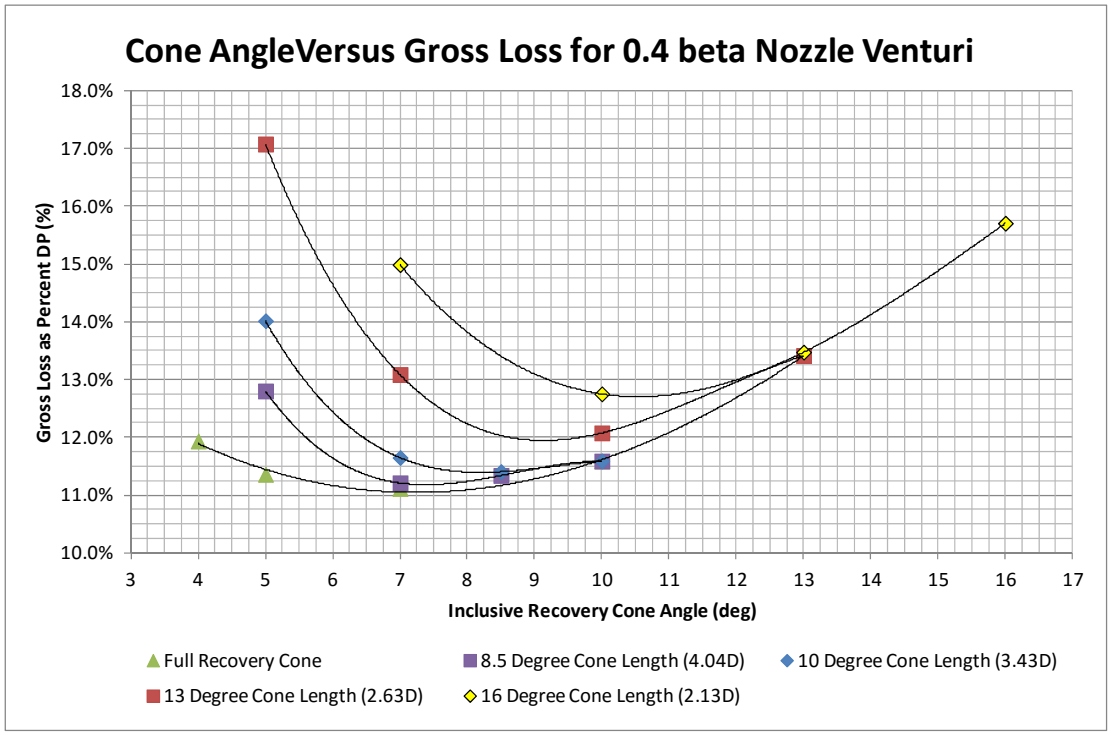


**Fig. B- 16. Head loss vs. cone angle for 0.40 beta Truncated Nozzle Venturi**

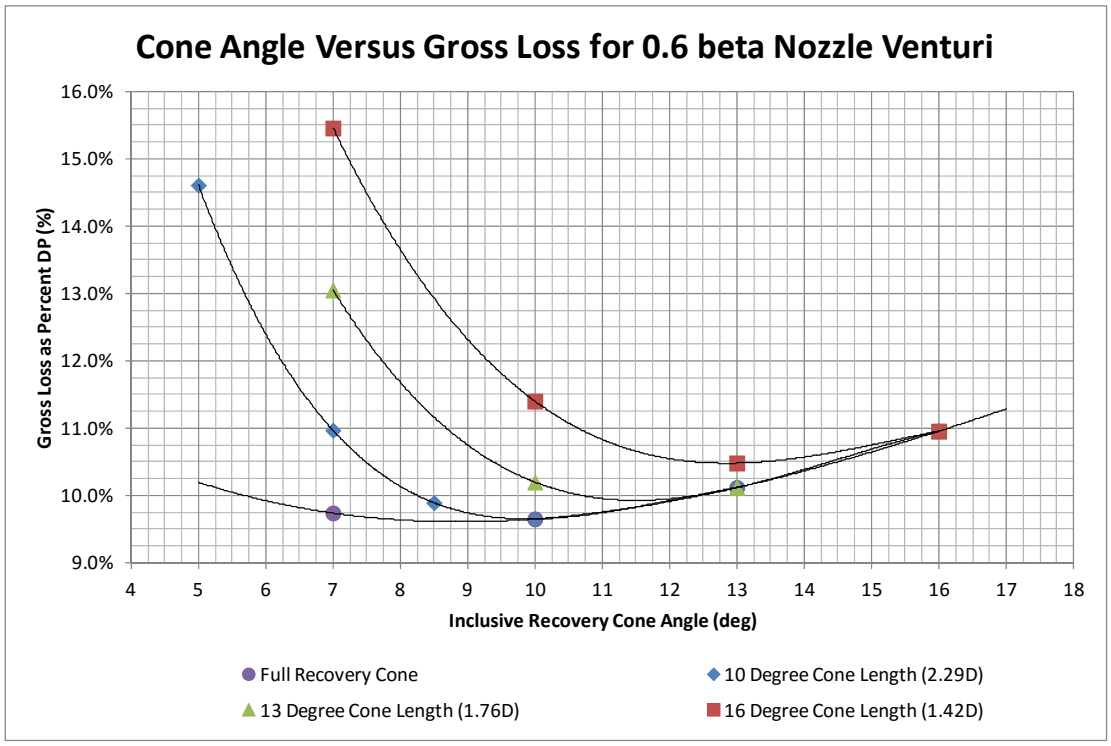


**Fig. B- 17. Head loss vs. cone angle for 0.60 beta Truncated Nozzle Venturi**

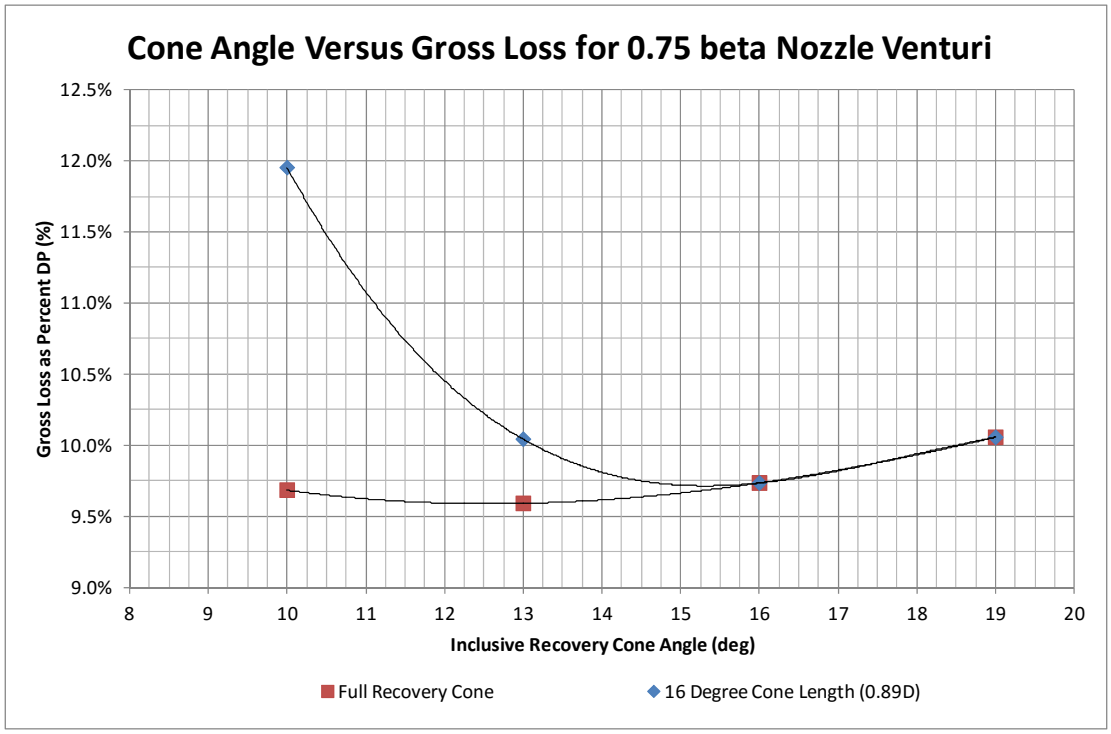


**Fig. B- 18. Head loss vs. cone angle for 0.75 beta Truncated Nozzle Venturi**

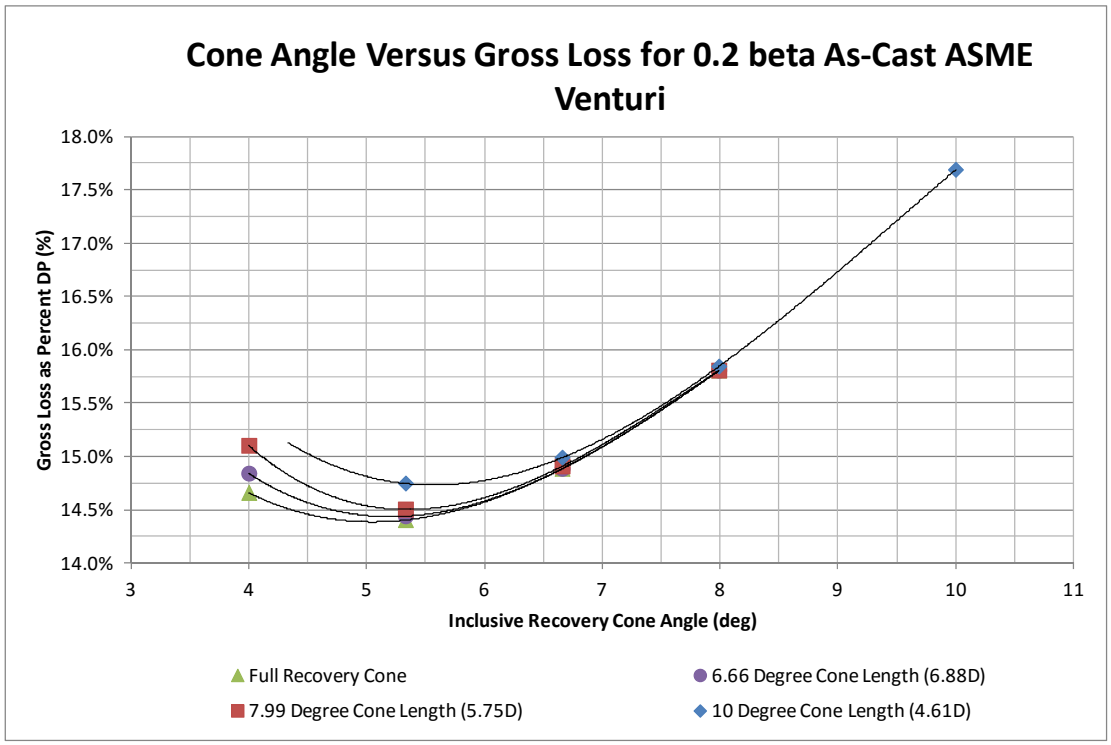


**Fig. B- 19. Head loss vs. cone angle for 0.20 beta Truncated As-Cast ASME Venturi**

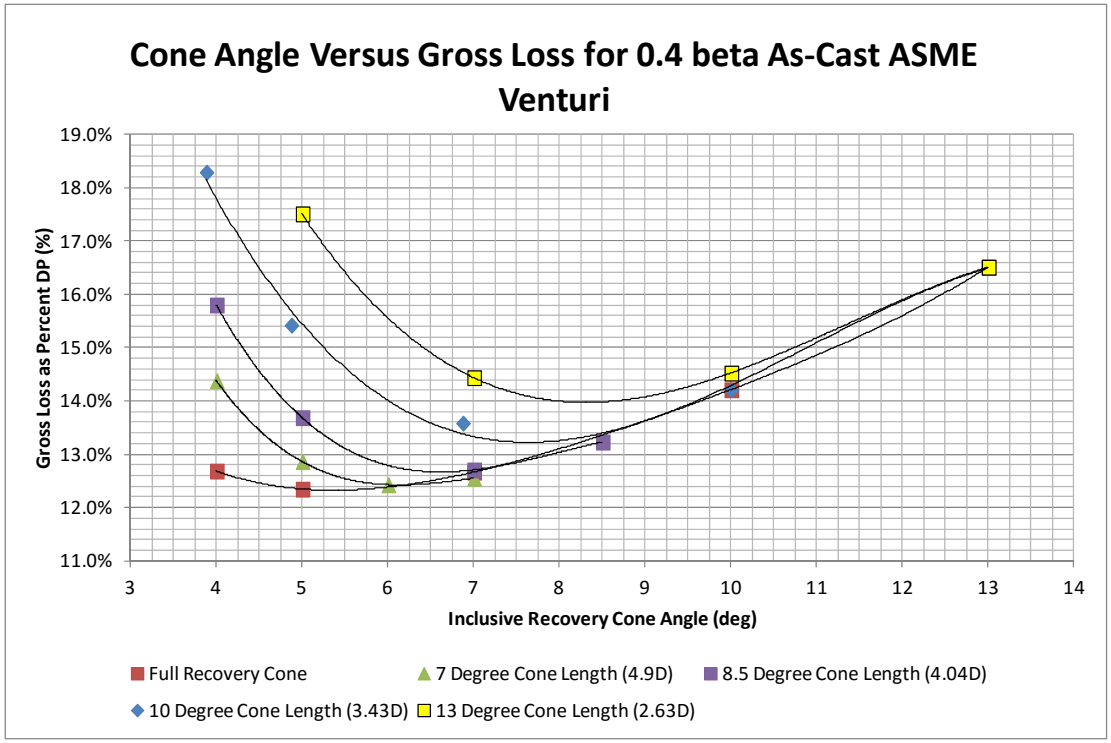


**Fig. B- 20. Head loss vs. cone angle for 0.40 beta Truncated As-Cast ASME Venturi**

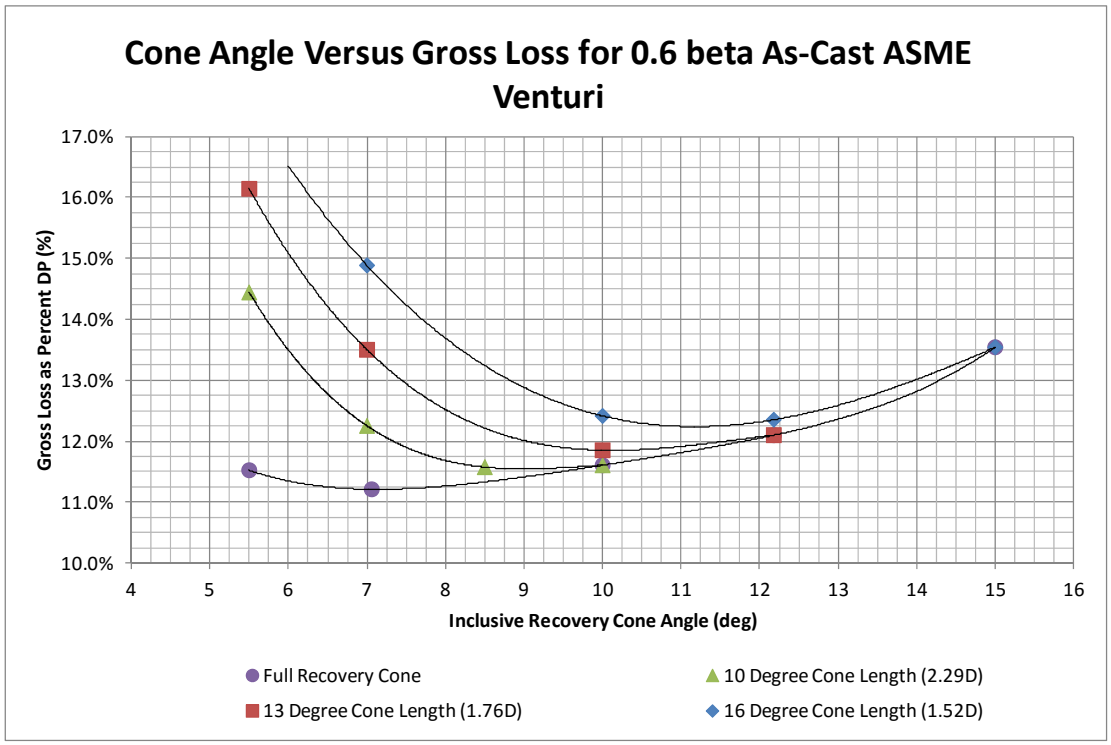


**Fig. B- 21. Head loss vs. cone angle for 0.60 beta Truncated As-Cast ASME Venturi**

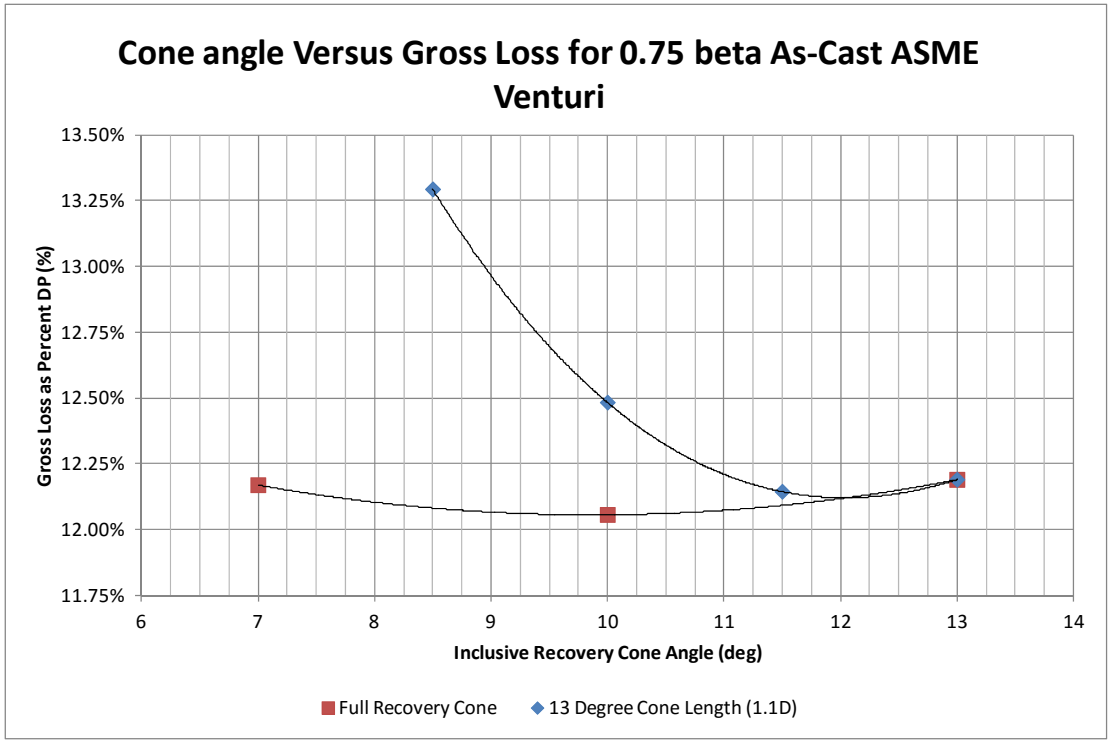


**Fig. B- 22. Head loss vs. cone angle for 0.75 beta Truncated As-Cast ASME Venturi**

# CURRICULUM VITAE

ZACHARY B. SHARP

***Research Engineer, Utah State University***

***435-797-3167 / zac.sharp@usu.edu***

## EDUCATION

PhD in Civil and Environmental Engineering, May, 2016

Major: Fluid Mechanics and Hydraulics. Dissertation: Applications of CFD in Flow Metering and Meter Design.

MS Civil and Environmental Engineering, Utah State University, 2009

Major: Fluid Mechanics and Hydraulics. Thesis: Energy Losses in Cross Junctions

BS Civil and Environmental Engineering, Utah State University, 2008

Major: Civil and Environmental Engineering.

## WORK SUMMARY

- 2009 - Present: **Research Engineer**, Utah Water Research Laboratory, Civil and Environmental Engineering, Utah State University, Logan, Utah
- 2009 - Present: **Independent Engineering Consultant**
- 2007 - 2009: **Research Assistant/Graduate Student**, Utah State University/Utah Water Research Laboratory
- 2004 - 2007: **Engineering Lab technician**, Utah State University/Utah Water Research Laboratory

- 1998 - 2004: **Construction Worker**, Various companies and responsibilities in residential and commercial construction

## EXPERIENCE

Extensive experience performing hydraulic structure physical model studies on dams and spillways, pumping pits, power plant intakes, erosion control issues, pipelines, channels, spillway basins, gated structures, control structures, outlet and energy dissipation structures, fish screens, bypasses, sewer and storm water systems.

Hydraulic Structures

- 2015, Physical Model Study of the 2nd Street Pump Station in Fargo North Dakota conducted for the Cascade Pump company.
- 2015, Physical Model Study of the John Hart Generating Station intake structure and operating gate conducted for SCN-Lavalin.
- 2014, Physical Model Study of the Lower Bois D'ark Dam spillway and energy dissipation basin conducted for Freese and Nichols.
- 2013, Physical Model Study of the Lake Isabella service and emergency spillways conducted for the U.S. Army Corp of Engineers.
- 2012, Physical Model Study of the Low level Outlet Work and Energy Dissipation Basin of the Susu Dam conducted for Snowy Mountain Engineering Consultants (SMEC).
- 2012, Physical Model Study of the Emergency and Service Spillways of the Susu Dam conducted for Snowy Mountain Engineering Consultants (SMEC).
- 2012, Physical Model Study of the Folsom Dam Emergency Outlet Gated Structure conducted for the U.S. Army Corp of Engineers.
- Nov 2011: Physical Model Study of the Utah Lake Pumping Station conducted for Bowen Collins & Associates of Draper, UT.
- Feb 2011: Physical Model Study of the I-84 overpass for the New York Canal conducted for Horrocks of Nampa, ID
- 2011, Computational Fluid Dynamics model study of the Clark Canyon Hydroelectric Project. Civil Science.
- Dec 2010: Physical model study of the Success Emergency Spillway conducted for HDR of Folsom, CA
- Dec 2010: Physical model study of the Success Dam Outlet Works conducted for HDR of Folsom, CA
- Computational Fluid Dynamics model study of the Upper and Lower Turnbull Turbine Bypass

System. Ted Sorensen and Associates, 2010.

- 2010, Physical model study of the Mammoth Pool Dam Low Level Outlet Energy Dissipater, Mesa and Associates.
- 2010, Physical model study of the Oroville Dam Low Level Outlet Energy Dissipater. Allied Engineering, California DWR.
- 2010, Physical model study of the Gilboa Dam Low Level Outlet Energy dissipater.
- 2009, Physical model study of Buchanan Dam Emergency Dewatering System. Freese and Nichols.
- May 2009: Physical Model Study of the SCOP Lake Mead Effluent Conveyance Discharge System conducted for MWH of Las Vegas, NV.
- Physical model study of the SCOP Lake Mead Effluent Conveyance System. MWH, Feb. 2009.
- Oct. 2008, Numerical model study of Summit Creek and Birch Creek 100-year Flood Analysis. City of Smithfield, Utah.
- Oct. 2008, Physical model study of the KCWA Section 4 Canned Pump. Dee Jaspar.
- Sep. 2008, Numerical model study of the Bear River Narrows Hydro Project. Schiess and Associates.
- Aug. 2008, Computational Fluid Dynamics model study of the Buchanan Dam Gated Spillway. Freese and Nichols.
- Aug. 2008, Physical model study of the Becks Run Suction Header. Gannett Fleming.
- Oct 2008: Physical model study of the Folsom Dam Auxiliary Spillway conducted for Owen Ayres and Associates, Inc. of Sacramento, CA
- Aug 2008: Physical model study of the IPS1 pump station for low lake level conditions conducted for Southern Nevada Water Authority of Las Vegas, NV
- Aug 2008: Physical model study of the Lake Mead Reservoir Intakes for pump stations No. 1 (IPS1) and No. 2 (IPS2) conducted for Southern Nevada Water Authority of Las Vegas, NV
- Mar 2008: Physical model study of the L.L. Anderson Dam Spillway modification conducted for
  MWH of Walnut Creek, CA
- Jan 2008: Physical model study of the IPS1 reservoir intake on Lake Mead conducted for Southern Nevada Water Authority of Las Vegas, NV
- Nov 2007: Physical model study of the IPS2 reservoir intake on Lake Mead conducted for Southern
  Nevada Water Authority of Las Vegas, NV
- Nov 2007: Physical model study of the Lake Mead intake pumping station NO. 3 (IPS3) conducted for MWH and CH2MHill of Las Vegas, NV
- Sep 2006: Physical model study of the Kentucky River Intake conducted for Gannett Fleming of
- Harrisburg, PA
- Nov 2005: Physical model study of the Nacimiento Dam Spillway conducted for Boyle Engineering of Lakewood, CO

- Oct. 2005, Physical model study of the Hickory Log Creek Dam. Schnabel Engineering
- Sep 2004: Physical model study of the Cooper Nuclear circulating water pump intake structure
  conducted for Nebraska Public Power District - Cooper Nuclear of Brownsville, NE
- Sep 2004: Physical model study of the Kern County Water Agency Cross Valley canal expansion
  project conducted for Boyle Engineering of Bakersfield, CA
- Hydraulic transient analysis of the Clark Canyon Dam Hydroelectric Project. Civil Science, 2011.
- Hydraulic transient analysis of the Dorena Hydroelectric Project. Bingham Engineering, Jan. 2011.
- Hydraulic transient analysis of the Brayton Point Nuclear Power Plant closed loop cooling project.
- Kiewit Power Engineers, May 2010.
- Pump and pipeline system design and development for the Utah Water Research Laboratory
  Hydraulics building, May 2009.
- Literature search and review of closed conduit air entrainment and dissolved air. MWH, Nov. 2008.

Valves and Flow Meters (partial listing)

- Personally responsible for over 400 large-sized flow calibrations since 2004, which culminated in the authorship of over 100 flow meter test reports. These calibrations included:
  ultrasonic, venturi, nozzle, turbine, orifice, insert probe, magnetic, v-cone, coriolis, pressure
  differential, open channel and velocity probe type flow meters. There are also numerous valve tests I am personally responsible for including butterfly valves, fixed-cone valves, globe valves, pressure reducing valves, sleeve valves, plug valves, gate valves, and numerous check valve designs. A list will not be included.

## JOURNAL PUBLICATIONS

**Sharp, Z.B.,** Johnson, M.C., Barfuss, S.L., "Using CFD to Optimize Venturi Recovery Cone Angles" to soon be submitted to the ASME Journal of Fluids Engineering.

**Sharp, Z.B.,** Johnson, M.C., Barfuss, S.L., "Using CFD to Optimize Venturi Recovery Cone Angles" Under Review with the ASME Journal of Fluids Engineering.

**Sharp, Z.B.,** Johnson, M.C., Barfuss, S.L., "Effects of Abrupt Pipe Diameter Changes on Venturi Flow Meters" to be published in Journal AWWA in August 2016 issue.

Stevens, D., Johnson, M.C., **Sharp, Z .B**. 2011. *Design Considerations for Fixed-Cone Valves with Baffled Hoods.* Journal of Hydraulic Engineering, Vol. 138, No. 2.

**Sharp, Z.B.,** Johnson, M.C., Barfuss, S.L., and Rahmeyer W.J. 2009. *Energy Losses in Cross Junctions.* Journal of Hydraulic Engineering, Vol. 136, No. 1, January 2010.

Nikfetrat, K., Johnson, M.C. and **Sharp, Z.B.**, *Computer Simulations Using Pattern Specific Loss Coefficients for Cross Junctions.* Journal of Hydraulic Engineering, Vol. 141, No. 9, September 2015.

Prettyman, B.J., Johnson, M.C. and **Sharp, Z. B.**, *Design Considerations for Stationary Hoods Used with Fixed-Cone Valves.* International Water Power & Dam Construction. Volume 21, No. 6, pp. 76-79, 2014.

Pope, J.M., Barfuss, S.L., Johnson, M.C and **Sharp, Z.B.,** *Effects of Pipe Wall Offsets on Differential Pressure Meter Accuracy*. Journal AWWA, 107(6):E313—E320.

Prettyman, B.J., Johnson, M.C. and **Sharp, Z. B.**, *Submerged Operation of a Fixed-Cone Valve with Baffled Hood.* International Water Power & Dam Construction. Volume 22, No. 4, pp. 74-77, 2015.

## OTHER PUBLICATIONS

Buck, B.S., Johnson, M.C. and **Sharp, Z.B.**, 2011. *Improving Concrete Containment Structures Associated with Fixed Cone Valves.* Engineering, 2011, 3, 145-151.